Title Page

AN INTEGRATED APPROACH TO UNDERSTANDING THE GEOLOGICAL CONTROLS ON GAS ESCAPE AND MIGRATION PATHWAYS IN OFFSHORE NORTHERN ORANGE BASIN, SOUTH AFRICA.

A Thesis submitted in fulfilment of the requirement for the Degree of Doctor of Philosophy in Earth Sciences of the University of the Western Cape.

By

Chris Adesola Samakinde

B.sc hons (Ilorin), B.sc hons (Western Cape), M.sc hons (Western Cape)

Supervisor

Prof. Jan Van bever Donker

March 2017

DECLARATION

I declare that "An Integrated Approach to understanding the Geological controls on gas escape and migration pathways in offshore northern Orange Basin, South Africa" is my own work, that it has not been submitted before for any degree or examination in any other university, and that all sources I have used or quoted have been indicated and acknowledged by means of complete references.

Chris Adesola Samakinde March 2017

Signature

DEDICATION

GRATEFULLY DEDICATED TO
My sister; Dr Bola Fayanju and Mum; Mrs Janet Samakinde
Whose encouragement inspired me.

ACKNOWLEDGEMENTS

The scholarship to pursue a PhD degree at the University was granted by the Inkaba yeAfrica and the National Research Foundation of South Africa. I would like to thank these two institutes for giving me tremendous financial support for the pursuance of this degree. Thanks is also giving to the Petroleum Agency of South Africa for providing the datasets used at a very affordable cost. Perhaps the most significant contribution was by Emeritus Professor Jan van Bever Donker for his unrelenting efforts to improve readability and writing of the chapters. In addition, his encouragement and commitment to such a difficult task does not go unnoticed. I equally thank Drs Seun Fadipe and Wasiu Sonibare, both of Schlumberger Corporation for critic and advice in structuring the thesis. I would like to express my sincere gratitude to Dr Silvia Lanes for her encouragement and support. Thanks is also giving to my Brother-in-law, Dr Lanre Fayanju for his moral and financial support, my colleagues, Monica Oghenekome, Oluwatoyin Ayodele and my friends; Seyi Omoniyi, Dr Dayo Ayoola, Deborah Biemo and Timilehin Okeowo .

I would like to thank my big cousin Yomi Akerele for his encouragement at all times. Thanks is giving to me nephews; Samuel and Emmanuel Fayanju, niece; Victoria Fayanju for proving me with needed theatrical relief at various times. Special regards to Israel Samakinde, for coming through when I least expected, and Feyisayo Fajana for being a sweetheart at all times.

Lastly, I thank my maker, way maker, my creator, the lifter of my head, my pillar, my strength for the amazing grace, unprecedented mercy, undying love and the divine strength to complete my studies—To god be the glory. Halleluyah!!!

BRIEF INFORMATION ON RESEARCH OUTPUT AND SKILLS.

PERSONAL INFORMATION

NAME: Chris Adesola Samakinde

RESEARCH OUTPUTS.

Clay Diagenesis effects on the Petrophysical properties of lower Cretaceous Sandstones, offshore Orange Basin. Article published in the Journal, Geological Society of South Africa Special Issue, 2016. 119, 1,187-202.

A Combination of Genetic Inversion and Seismic Frequency Attributes to Delineate Reservoir Targets in Offshore northern Orange Basin, South Africa. To be submitted to the American Association of Petroleum Geologists bulletin in 2017.

Paleo-stress patterns and its possible implications on hydrocarbon migration in offshore Orange Basin, South Africa. Conference Presentation at the Cape-Karoo Imbizo Conference in Port-Elizabeth, Eastern Cape South Africa 2015.

Clay Diagenesis Effects on the Petrophysical properties of lower Cretaceous Sandstones, offshore Orange Basin. Conference Paper at the Geological Society of London conference, Burlington House Piccadilly, London 2014.

An integrated approach to understanding the Geological controls on gas escape and migration pathways in offshore Northern Orange Basin, South Africa. Conference paper at the Global Climate Change Conference in Port-Elizabeth, Eastern Cape, South Africa 2016.

AWARDS RECEIVED AND SHORT COURSE ATTENDED

Inkaba yeAfrica scholarship for M.sc Research work candidate 2011.
Inkaba yeAfrica scholarship for PhD research in Geology, 2014.
National Research Foundation PhD Scholarship, 2015-2016.
Attendance of training and workshop on Field development, drilling techniques and procedure and reservoir engineering by Total Professors associate (TPA) 2012.
Presentation on the usage of Schlumberger Petrel software for reservoir and structural modeling 2012.
Attendance of Shell International training on seismic interpretations.2013
Attendance of Haliburton training on Petro physics and Geomechanics 2013
Field studies on clastic sedimentology in the Karoo foreland basin.2014.
Short course on Basin and Petroleum system modelling. Calgary, Canada 2016.

ELECTRONIC DATA PROCESSING KNOWLEDGE (EDP)

Windows based geological and geophysical software including; Surfer 8.0, Petrel 2013 and 2014©, Petromod 2014©, Move 2014©, Interactive Petrophysics 2012© and Techlog 2012©.

Table of Contents

Title Page ..... **ii**
DECLARATION ..... **i**
DEDICATION ..... **ii**
ACKNOWLEDGEMENTS ..... **iii**
BRIEF INFORMATION ON RESEARCH OUTPUT AND SKILLS. ..... **iv**
Table of Contents ..... **v**
List of Figures ..... **xi**
List of Tables ..... **xvii**
Extended Abstract ..... **xviii**
Chapter One **1**
1.1 Introduction and Scientific Background **1**
1.2 Brief Review of Research Approaches **3**
1.3 Location of the study Area **6**
1.4 Aim and Objectives **8**
1.5 Scope of Work **8**
1.6 Previous Studies on Hydrocarbon escape and migration in the Orange basin. **9**
1.6.1Problem Statement and Justification for the current study 10
1.7 Synopsis of Research **11**
1.8 Review of Keywords and concepts relevant to the current study. **12**
1.8.1 The basic concepts and applications of Seismic Stratigraphy 12
1.8.1.1 Seismic Sequence Analysis 13
1.8.1.2 Seismic Facies Analysis 14
1.8.1.3 Reflection Configuration Patterns of Seismic facies. 15
1.8.2 Summary of Seismic Facies Types and Reflection Configurations (Badley, 1985). 19
1.8.3 Seismic Lithology Analysis 23
1.9 Some Seismic Anomalies of gas presence and escape (evidences of Tertiary Migration). 24
1.9.1 Pockmarks 24
1.9.2 Bright Spot 25
1.9.3 Gas Chimneys 26
1.9.4 Mud Volcanoes 27
1.10 Pitfalls and Mitigations of DHI In Predicting Hydrocarbon presence 28
1.11 Seismic Attribute analyses 29
1.11.1Physical Attributes 29
1.11.2 Geometrical Attributes 29
1.11.3 AVO Analysis 30
1.11.4 Seismic Impedance and Frequency Inversion. 35

1.12 Hydrocarbon Migration modelling. 36
1.13 Geological controls on gas escape and migration pathways....38
1.14 Source Rocks Organic Maturation and Generation Potentials. 39
1.15 Forward Numerical Modelling Technique....40
Chapter Two Regional Geology 41
2.1 An Overview....41
2.2 Tectono-Stratigraphy 43
2.3 Brief description of the Orange Basin Petroleum Systems....46
2.3.1 Source Rock....46
2.3.2 Reservoir Rock....46
2.3.3 Traps 47
2.4 An Overview of Paleo Stress History and structural styles in the South Atlantic Margin and Orange Basin. 47
Chapter Three: Materials and Methodology 48
3.1Materials 49
3.1.1 Seismic Data used for this study. 49
3.2.1Seismic Data Loading. 52
3.2.2 Wells and Wireline Logs loading 53
3.2.3 Formation Tops and Check Shots Loading....53
3.2.4 Seismic Data Interpretation 54
3.2.5 Sonic Logs and Checkshots calibration. 56
3.2.6 Wavelet Extraction 57
3.2.7 Synthetic trace Generation....58
3.2.8 Creation of Time and Isopach Maps (Surfaces)....59
3.2.9 Velocity Modeling 60
3.2.10 Construction of Structural Framework....63
3.2.11 Seismic Impedance Inversion and Frequency Attributes....65
3.2.12 Seismic Stratigraphy interpretation Methods....67
3.2.13 Construction of Hydrocarbon Migration Modeling 69
3.2.14 Data Used for the Construction of a Hydrocarbon Migration model.....69
3.2.15 Importing of Depth Maps and Fault Model into Petromod 2014© Workstation. 71
3.2.16 Boundary Conditions 71
3.2.17 Age Assignment for Surfaces and Faults....74
3.2.18 Facies Assignment. 76
3.2.19 Petroleum System Elements and Kinetics 77
3.2.20 3D Simulation of Hydrocarbon Generation and Migration. 77
3.2.21 3D Forward Model Calibration....78
Chapter Four....81
MAPPING AND INTERPRETATION OF DEPOSITIONAL SUPER- SEQUENCES USING WELL LOGS SIGNATURES AND LITHO-FACIES MODELING OF SEDIMENTS IN BLOCK1, NORTHERN ORANGE BASIN, SOUTH AFRICA.....81
Keywords: Orange Basin- Well Logs- Depositional Sequences-Litho-Facies....81
4.1 Abstract....81
4.2 Introduction....82
4.3 Methodology 83

4.4 Results 84
4.4.1 Interpretation of Depositional Sequence from well logs Signature. **84**
4.4.1.1 Barremian-Aptian Sequence (13AT-1) AE-1 well. 84
4.4.1.2 Barremian / Aptian Sequence (13AT-1) Well AF-1. 86
4.4.1.3 Barremian-Aptian Sequence (13AT-1) AO-1 Well. 87
4.4.1.4 Summary of Barremian/ Aptian13AT-1 Sequence. 89
4.4.1.5 Early Aptian-Mid Aptian 13CT1 Sequence. 90
4.4.1.6 Early -Mid Albian 14 AT-1 Sequence AE-1 Well 92
4.4.1.7 Early -Mid Albian 14 AT-1 Sequence AF-1 Well 92
4.4.1.8 Early -Mid Albian 14 AT-1 Sequence AO-1 Well. 94
4.4.1.9 Summary of 14AT-1 Sequence. 95
4.4.1.10 Mid-Late Albian Sequence (14Bt-1, 14Ct-1, 14Et-1 and 14Gt-1 Unconformities) AE-1 Well (Southern part). 96
4.4.1.11 Late Albian/Cenomanian Sequence (14HT1 and 14JT1) AE-1 Well (Southern section). 97
4.4.1.12 Late Albian/Cenomanian Sequence (14HT1 and 14JT1) AF-1 Well (Central section). 98
4.4.1.13 Late Albian/Cenomanian Sequence (14HT1 and 14JT1) AO-1 Well (northern section). 99
4.4.1.14 Summary of Sequences Late Albian/Cenomanian (14GT1, 14HT1 and 14JT1). 100
4.4.1.15 Cenomanian-Turonian Sequences (14KT1, 15AT1 and 15BT1) AE-1 Well (southern section). 101
4.4.1.16 Cenomanian-Turonian Sequence (15AT-1) AF-1 Well (Central section). 102
4. 4.1.17 Summary of Cenomanian- Turonian Sequences. 102
4.4.1.18 Turonian-Coniacian-Maastrichtian Sequences. 103
4.4.2 Litho-Facies Modelling. **105**
4.4.2.1 Cenozoic and Maastrichtian Sequences 105
4.4.2.2 Turonian and Cenomanian Sequences 106
4.4.2.3 Late Albian and Albian Sequences 107
4.4.2.4 Barremian-Aptian Sequence 107
4.5 Conclusions 108
Chapter Five **111**
Seismic-stratigraphy, structural interpretations, mapping of Hydrocarbon escape features and their relationship to stratigraphic and structural features. **111**
Keywords: Seismic Sequence analysis-Seismic Facies- Gas escape features-Faults-Paleo-stress **111**
5.1 Abstract 111
5.2 Introduction 113
5.3 Methodology 114
5.3.1 Seismic Stratigraphy 114
5.3.2 Structural Interpretations and Structural Framework Modelling. 115
5.4.1 Results of Seismic Stratigraphy Analysis. **115**
5.4.1.1 Seismic Sequence Analysis around Well AO-1 (Northern Section). 115
5.4.1.2 Seismic Sequence Analysis around Well AF-1 (Central Section). 118

5.4.1.3 Seismic Sequence Analysis around Well AE-1 (Southern Section). 119
5.4.1.4 Seismic facies and Litho-facies Analysis of Maastrichtian –Cenozoic Sequence of well AO-1 (Northern section). 119
5.4.1.5 Seismic facies and Litho-facies Analysis of Maastrichtian –Cenozoic Sequence of well AF-1 (Central section). 120
5.4.1.6 Seismic facies and Litho-facies Analysis of Maastrichtian –Cenozoic Sequence of well AE-1 (Southern section). 121
5.4.1.7 Isopach variation (Thickness map) and Summary of seismic facies for Maastrichtian and Cenozoic sequences. 122
5.4.1.8 Seismic and Litho-facies Analysis of Cenomanian and Turonian Sequence (AO-1) (Northern Section). 123
5.4.1.9 Seismic facies and Litho-facies Analysis of Cenomanian and Turonian Sequence (AF-1) (Central Section). 124
5.4.1.10 Seismic facies and Litho-facies Analysis of Cenomanian andTuronian Sequence (AE-1) (Southern Section). 125
5.4.1.11 Isopach variation (Thickness Maps) and Summary of Seismic and Litho-Facies Analysis for Cenomanian and Turonian Sequences 126
5.4.1.12 Seismic facies and Litho-facies Analysis of Barremian/Aptian-Albian Sequence (AO-1) (Northern Section). 128
5.4.1.13 Seismic facies and Litho-facies Analysis of Barremian/Aptian-Albian Sequence in well AF-1 (Central Section). 129
5.4.1.14 Seismic facies and Litho-facies Analysis of Barremian/Aptian-Albian Sequence (AE-1) well (Southern Section). 131
5.4.1.15 Isopach variation and Summary of Seismic and Litho-facies Analysis for Barremian-Aptian/Albian Sequences. 132
5.4.2 Results of Structural Interpretations, Paleo stress Analysis and Structural Modelling. 136
5.4.2.1 Structural Interpretations (Inline 756) (Fault Mapping) 136
5.4.2.2 Structural Interpretations for Inline 1256. 138
5.4.2.3 Structural Interpretations for Inline 1326. 139
5.4.2.4 Structural Interpretations for (Inline 1426). 140
5.4.2.5 Structural Interpretations for (Inline 1586). 142
5.4.2.6 Paleo stress Analysis Review and Results. 143
5.4.2.7 Structural Inversion or Drag Fold 146
5.4.2.8 Structural Model/ Framework 147
5.4.3 Results of Gas escape features mapping and their relationship with faults and stratigraphy. 148
5.4.3.1 Pock mark (Inline 800) 149
5.4.3.2 Fault controlled Gas Chimney at Inline 2240 150
5.4.3.3 Fault Controlled Gas Chimney at Inline 2400 151
5.4.3.4 Acoustic Wipeout at Seismic Line 79-004 and 82-010. 152
5.4.3.5 Stratigraphically Controlled Chimney at Seismic Line K80-014. 154
5.4.3.6 Bright Spot at Inline 756 155
5.4.3.7 Mud Volcano at Inline 800. 156
5.5 Conclusions 157
Chapter Six 158

Application of Seismic Attributes Analysis for mapping of Faults and gas escape features, Identification of stratigraphic features and delineating hydrocarbon-charged sediments. 158
6.1 Abstract 158
6.2 Introduction 159
6.3 Methodology 159
6.4 Results 160
6.4.1 Application of Variance Attributes for Structural features and Sea Floor Imaging. 161
6.4.1.1 Inline756 and Time Slice 1140ms 161
6.4.1.2 Inline 2400 and Time Slice 1644ms 162
6.4.1.3 Inline 800 and Time Slice 180ms 164
6.4.2 Application of Seismic Impedance and Frequency for Stratigraphic Attributes 165
6.4.2.1 Time Slice 1160 for Seismic Impedance and Porosity Inversion 166
6.4.2.2 Time Slice 968(Late Cretaceous) for Instantaneous Frequency Inversion. 167
6.4.2.3 Time Slice 968ms for Iso-Frequency Attribute (Frequency Decomposition) 168
6.5 Conclusions. 170
Chapter Seven 171
3D Numerical Modeling of Hydrocarbon-generation and Faults control on Migration pathways. 171
7.1 Abstract 171
7.2 Introduction 173
7.3 Methodology 173
7.3.1Model Input 174
7.3.2 Boundary Conditions 175
7.3.3 Hydrocarbon Migration Modelling 175
7.4 Results 175
7.4.1 1D Numerical modelling of Hydrocarbon-generation and Burial history 175
7.4.1.1 1D modelling of Barremian/Aptian source unit and calibration with thermal and organic maturation data for well AE-1 (southern section). 176
7.4.1.1.1 Vitrinite Reflectance 176
7.4.1.1.2 Temperature 177
7.4.1.1.3 Burial History and Transformation Ratio. 177
7.4.1.2 1D modelling of Barremian/Aptian source unit and calibration with thermal and organic maturation data for well AF-1 (Central section). 178
7.4.1.2.1 Vitrinite Reflectance 178
7.4.1.2.2 Temperature 179
7.4.1.2.3 Burial History and Transformation Ratio. 180
7.4.1.3 1D Modelling of Barremian/Aptian source unit and calibration with thermal and organic maturation data for well AO-1 (Northern section). 181
7.4.1.3.1 Vitrinite Reflectance 181
7.4.1.3.2 Temperature 182
7.4.1.3.3 Burial History and Transformation Ratio. 183

7.4.2 Depth Maps of major super sequences. 185
7.4.2.1 Top of the Basement 185
7.4.2.2 Barremian/Aptian (Source Rock) 185
7.4.2.3 Mid-Albian (Reservoir Rock) 186
7.4.2.4 Late-Albian (Seal).....187
7.4.2.5 Cenomanian (Reservoir Rock).....188
7.4.2.6 Turonian Sequence.....189
7.4.2.7 Maastrichtian Sequence 190
7.4.2.8 Sea Floor 191
7.4.3 3D Primary Migration (Generation) Modeling. 193
7.4.3.1 Simulation Results for Barremian/ Aptian Source rock (120Ma) 193
7.4.3.2 Simulation Results for Barremian/Aptian Source rock (108Ma) 194
7.4.3.3 Simulation Results for Barremian/Aptian Source rock unit (95Ma) 196
7.4.3.4 Simulation Results for Barremian-Aptian Source rock at present day (0.0Ma).....198
7.4.4 Source Rock Hydrocarbon Generation Statistics.....200
7.4.4.1 Source Rock Generation Statistics at 105ma 201
7.4.4.2 Source Rock Generation Statistics at 0.0 Ma.....202
7.4.4.3 Source Rock Bulk Generation and Expulsion Statistics at 0.0Ma (Present day) 203
7.4.4.4 Timing of Hydrocarbon Generation and Expulsion.....204
7.4.4.5 Expulsion Efficiency.....205
7.4.5 3D Numerical Modeling of Hydrocarbon Migration Pathways. 206
7.4.5.1 Faults Model used in the study 206
7.4.5.2 Expulsion of Hydrocarbon from the Source Rock at 108 Ma 207
7.4.5.3 Evolution of Hydrocarbon Migration Pathways in Mid-Albian Reservoirs (Vectors) 208
7.4.5.4 Evolution of Hydrocarbon Migration Pathways in Cenomanian Reservoirs (Vectors) 210
7.4.6 Fault Controls on hydrocarbon Migration Pathways. 212
7.4.6.1 Faults Hydraulic Behaviours at 93Ma 213
7.4.6.2 Faults Hydraulic Behaviours at 91Ma 213
7.4.6.3 Faults Hydraulic Behaviours at 74Ma 214
7.4.6.4 Faults Hydraulic Behaviours at 65Ma 215
7.4.7 Evidence of Gas Escape at the Sea Floor.....216
7.4.8 Sensitivity Analysis 217
7.5 Conclusions.....218
Chapter Eight.....220
Summary of Findings, Main Scientific Contributions, Conclusions and Recommendations. 220
8.1: Summary of Findings.....220
8.2 Main Scientific Contributions and Economic Significance. 225
8.3 Conclusions and Recommendations.....226
References.....229
Appendix.....247

List of Figures

Figure 1.1: Locality map of Block 1(Red Square) with the three wells drilled so far, Offshore West Coast, northern Orange Basin (not to scale).....6
Figure 1.2: Map of study area showing the position of block 1 Orange Basin, with the wells drilled and seismic data used in this study. 7
Figure 1.3 ; Showing onlap surface geometry(blue circle) and other Erosional surfaces (Mitchum, 1977) 14
Figure 1.4: Showing Different Prograding Clinoforms (After Mitchum, 1977). 17
Figure1.5: Showing the occurrence of a pockmark in the Dutch North Sea. http://science.dodlive.mil/2013/06/16/nrl-reveals-absence-of-greenhouse-gas-emissions/.....25
Figure 1.6: A seismic section showing bright spot from Nile Delta, Egypt. Red amplitude represents the top of gas reservoirs and blue represents the base. Modified from Van Dyke (2011).....26
Figure 1.7: Highly localised gas chimneys in Yampi Shelf, Browse basin, O'brien et al (2005).....27
Figure 1.8: Different AVO trends occurring in an intercept-gradient cross-plot. Modified version of Avseth (2011).....32
Figure1.9: Reflection Coefficients versus Angle of Incidence Plot for different gas charged sands scenario (Castagna et al.,1998).....34
Figure 2.1: The rift phase in the Late Jurassic – Lower Valanginian showing the breakup of Africa, Madagascar and Antarctica (modified from Broad, 2007).....41
Figure 2.2: Chronostratigraphic and sequence stratigraphic diagram of the Orange Basin (Brown et al., 1996).....45
Figure 3.1: Methodology workflow.....51
Figure 3.2: Showing the merging process of Seismic data and Navigation. 52
Figure 3.3: Showing Well Tops Loader Interface on Petrel 2013 for this study. 53
Figure 3.4: Showing Checkshots Loader Interface on Petrel 2013. 54
Figure 3.5: Showing 2D lines mis-tie Analysis on Petrel 2013.....56
Figure 3.6: Showing Sonic Calibration step in the Seismic-Well tie Process. 57
Figure 3.7: Showing Wavelet Extraction Window for Well AO-1. 58
Figure 3.9: Showing an interface of Horizon conversion into a surface. 60
Figure 3.10 : Showing an Interface of velocity modelling parameters used in this study.....61
Figure 3.11: Showing a plot of Velocity-Depth functions for all wells used in this study.....62
Figure 3.12: Showing Structural Framework Construction Process.....64
Figure 3.13. Showing Horizon Modelling Techniques.....65
Figure 3.14: Showing the interface of Frequency Decomposition Process. 66
Figure 3.15: Lapout Surfaces from Bally, 1982. 68
Figure 3.16: Figure showing a plot of latitude and Global Mean Surface Temperature, after Wygrala (1989).....72
Figure 3.17: Showing variation of Paleo-water depth over geological ages used in this study.....73
Figure 3.18: showing the Heat flow model used in this study (After Mckenzie, 1978). 74
Figure 3.19: Showing Age Assignment process for Depth Surfaces and corresponding facies used in the study. 75
Figure 3.20: Showing Faults used in the study and their Assigned Ages.....76

Figure 3.21: Figure showing Facies Assignments for this study. 77
Figure 3.22: Figure showing hydrocarbon generation Simulation Report. 78
Figure 4.1: Locality Map of the study area and spatial distribution of the three wells drilled in Block 1, Orange Basin. The 3D seismic volume acquired in the centre covers well AF-1, while selected 2D lines within this study area cover the two other wells. 83
Figure 4.2A: Geophysical logs interpreted for the Barremian-Aptian Sequence. Facies, Gamma ray, Sonic, Acoustic impedance, Reflection Coefficients, Synthetic, Density and Porosity are in track 2, 3, 4, 5, 6,7,8,9 respectively in well AE-1. 85
Figure 4.2B: Geophysical logs interpreted for the Barremian-Aptian Sequence. Facies, Gamma ray, Sonic, Acoustic impedance, Reflection Coefficients, Synthetic, Density and Porosity are in track 2, 3, 4, 5, 6,7,8,9 respectively in well AF-1. 87
Figure 4.2C: Showing the geophysical logs interpreted for the Barremian-Aptian Sequence. Facies, Gamma ray, Sonic, Acoustic impedance, Reflection Coefficients, Synthetic, Density and Porosity are in 2, 3, 4, 5, 6,7,8,9 respectively in well AO-1. .89
Figure 4.3: Geophysical logs interpreted for the Early-Aptian-Mid Aptian Sequence. Facies, Gamma ray, Sonic, Acoustic impedance, Reflection Coefficients, Synthetic, Density and Porosity are in 2, 3, 4, 5, 6,7,8,9 respectively in well AE-1. 91
Figure 4.4A: Showing the geophysical logs interpreted for the Early-Mid Albian Sequence. Facies, Gamma ray, Sonic, Acoustic impedance, Reflection Coefficients, Synthetic, Density and Porosity are in 2, 3, 4, 5, 6,7,8,9 respectively in well AE-1…92
Figure 4.4B: The geophysical logs interpreted for the Early-Mid Albian Sequence. Facies, Gamma ray, Sonic, Acoustic impedance, Reflection Coefficients, Synthetic, Density and Porosity are in 2, 3, 4, 5, 6,7,8,9 respectively in well AF-1. 93
Figure 4.4C: The geophysical logs interpreted for the Early-Mid Albian Sequence. Facies, Gamma ray, Sonic, Acoustic impedance, Reflection Coefficients, Synthetic, Density and Porosity are in 2, 3, 4, 5, 6,7,8,9 respectively in well AO-1.....95
Figure 4.5: The geophysical logs interpreted for the Mid-Late Albian Sequence. Facies, Gamma ray, Sonic, Acoustic impedance, Reflection Coefficients, Synthetic, Density and Porosity are in 2, 3, 4, 5, 6,7,8,9 respectively in well AE-1. 97
Figure 4.6A: The geophysical logs interpreted for the Late Albian-Cenomanian Sequence. Facies, Gamma ray, Sonic, Acoustic impedance, Reflection Coefficients, Synthetic, Density and Porosity are in 2, 3, 4, 5, 6,7,8,9 respectively in well AE-1…98
Figure 4.6B: Geophysical logs interpreted for the Late Albian-Cenomanian Sequence. Facies, Gamma ray, Sonic, Acoustic impedance, Reflection Coefficients, Synthetic, Density and Porosity are in 2, 3, 4, 5, 6,7,8,9 respectively in well AF-1. 99
Figure 4.6C: Geophysical logs interpreted for the Late Albian-Cenomanian Sequence. Facies, Gamma ray, Sonic, Acoustic impedance, Reflection Coefficients, Synthetic, Density and Porosity are in 2, 3, 4, 5, 6,7,8,9 respectively in well AO-1.....100
Figure 4.7A: Showing the geophysical logs interpreted for the Cenomanian- Turonian sequence in well AE-1. Facies, Gamma ray, Sonic, Acoustic impedance, Reflection Coefficients, Synthetic, Density and Porosity are in 2, 3, 4, 5, 6,7,8,9 respectively in wel AE-1 101
Figure 4.7B: Geophysical logs interpreted for the Cenomanian–Turonian Sequence. Facies, Gamma ray, Sonic, Acoustic impedance, Reflection Coefficients, Synthetic, Density and Porosity are in 2, 3, 4, 5, 6,7,8,9 respectively in well AF-1. 102
Figure 4.8: Showing the geophysical logs interpreted for the Turonian- Coniacian-Maastrichtian sequence in well AF-1. Facies, Gamma ray, Sonic, Acoustic impedance, Reflection Coefficients, Synthetic, Density and Porosity are in 2, 3, 4, 5, 6,7,8,9 respectively. 104

Figures (4.9 A and B): Top view of Cenozoic (A) and Maastrichtian (B) sequences litho-facies model showing the distribution of Sandstones (Yellow) and Siltstones (Brown) across the study area. The geometry of sandstone deposit within the Maastrichtian.....106
Figures (4.9C and D): Top view of Turonian (C) and Cenomanian (D) sequences litho-facies model showing the distribution of Sandstones (Yellow), Shale (Green) and Siltstones (Brown) across the study area. The geometry of sandstone deposits occurs as possible mouth bar deposit in the Cenomanian sequence.....106
Figures (4.9E and F): Top view Late Albian (E) and Albian (F) sequences litho-facies model showing the distribution of Sandstones (Yellow), Shale (Green) and Siltstones (Brown) across the study area. The geometry of sandstone deposit within the Albian sequence.....107
Figures (4.9 G): Top view of Barremian-Aptian sequence litho-facies model showing the distribution of Siltstones (Brown) and Shale (Green) across the study area. The shale deposit here is the expression of the marine organic-rich shale deposit within this sequence. 108
Figure 4.10: Litho-chronostratigraphic correlation of Sedimentary Sequences mapped across the three wells in the study Area (northern Orange Basin), West Coast, South Africa. 109
Figure 5.1Aand B: Un-interpreted Seismic Line A84-007 and interpreted Seismic Line A84-007 showing apparent truncation caused by termination of Barremian-Aptian Sequences on down dipping basement.....116
Figure 5.2 Interpreted Seismic Line A80-002 showing termination of a reflector against an overlying reflector (Toplap).....117
Figure 5.3 A and B: Seismic line A86-002 showing a lowstand wedge of Mid- Albian age.....118
Figure 5.4: Seismic section showing the seismic Sedimentary Sequence of the study area and an occurrence of a half –graben (red circle) at Inline 2310.....118
Figure 5.5: Seismic section showing prograding sedimentary sequence in the Cenozoic around AE-1 well at Line SA 92-131in East-West transect. 119
Figure 5.6 A and B : Showing Seismic (Line A84-007) and Litho-facies Analysis of Cenozoic and Maastrichtian around well AO-1 respectively. The Gamma ray log shows a cleaning upward trend (black arrow). 120
Figure 5.8: Showing Seismic (Line SA-92-131) and Litho-facies Analysis of Maaschritian-Cenozoic sequence around well AE-1.....122
Figure 5.9 A and B: Figures showing the thickness variation maps for Cenozoic (A) and Maastrichtian (B) Sequences. There is thick sediment accumulation westward of Cenozoic sequence.....123
Figure 5.10: Showing Seismic facies (Line A79-003) (A) and Litho-facies Analysis (B) around well AO-1(northern section) respectively. 124
Figure 5.11 A and B: Showing Seismic facies (Inline 2370) for Turonian (A) and Litho-facies (B) Analysis around well AF-1(Central Section). 125
Figure 5.12 A and B: Showing Seismic facies (SA-192-131) (A) and Litho-facies Analysis (B) around well AE-1(Southern part). 126
Figures 5.13 A and B: Figures showing the thickness variation maps for Turonian (A) and Cenomanian (B) Sequences. Thick sediment accumulation Westward suggest progradation. 127
Figure 5.14A and B: Showing Seismic facies (Line A79-003) (A) and Litho-facies Analysis (B) around well AO-1(Northern Section).....129

Figure 5.15 A and B: Seismic facies (Inline 2370) and Litho-facies Analysis around well AF-1. Serrated logs at both Barremian/Aptian and Albian sequences suggest as storm dominated Shelf environment. 131
Figure 5.16 A and B: Showing Seismic facies (Line A79-003) and Litho-facies Analysis around well AE-1(southern section). 132
Figure 5.17A and B: Thickness variation maps for Albian (A) and Barremian/Aptian (B) Sequences. Erosion of this sequence occurs in the northernmost and southernmost part of the study area. 135
Figure 5.18 A and B: Figures showing un-interpreted and interpreted seismic section of Listric normal fault terminating at the Cenomanian Sequence respectively (Inline 756). Bright spot anomaly is noticed around the fault. 138
Figure 5.19 A and B: Un-interpreted (A) and interpreted (B) seismic sections of normal fault spanning from Cretaceous and stops just before the Tertiary Sequence respectively (Inline 1256). 139
Figure 5.20A and B: Un-interpreted (A) and interpreted (B) seismic sections of Antithetic normal faults of Cretaceous age for Inline 1326. 140
Figures 5.21A and B: Un-interpreted (A) and interpreted (B) seismic sections of Antithetic normal faults of Cretaceous age respectively for Inline 1426. 141
Figures 5.22 A and B: Un-interpreted (A) and interpreted (B) seismic sections of Antithetic faults of Cretaceous age. 142
Figure 5.23: Stereoplot of faults mapped in the study area. Plot shows three Bi-directional trends of deformation from the Fault Extraction Process using Petrel 2013. 145
Figure 5.24: Principal stress Orientation suggesting dominance of extensional Regime as the T-Pole (extension) lies within the mean principal plane. 146
Figure 5.25: A seismic section showing normal fault drag and fold due to Extensional regime. 147
Figure 5.26 (A-D): Figures showing the structural framework of the study area across the four quadrants. There is an evidence of Basin inversion in the late Cretaceous.Model size is 140km by 130km 148
Figure 5.27: Pock mark observed on the sea floor at Time slice 250ms (A) and inline 800ms(B) 150
Figure 5.28: Fault Controlled Gas Chimney observed at inline 2240. 151
Figure 5.29: Fault Controlled Gas Chimney observed at inline 2400 terminating within the Tertiary 152
Figure 5.30 A and B: Stratigraphically controlled Acoustic Wipeout at Lines 79-004(A) and A82-010(B) 153
Figure 5.31: Stratigraphically controlled Gas Chimney at line K80-014 154
Figure 5.32: Bright spot anomaly occurrence on both sides of a listric normal fault at inline 756. 155
Figure 5.33: Mud volcano occurrence on the sea floor at inline 800ms. 156
Figure 6.1 A and B: Figures showing a listric normal fault(blue circle in figure 6.1A and blue sticks in 6.1B) on Variance Time Slice intersection for an un-interpreted section (A) and interpreted Section(B) at Time Slice 1140 and Inline 756. 162
Figure 6.2 A and B: Horizontal Variance Time Slice intersection for an un-interpreted section (A) and interpreted (B) Section of Antithetic faults at Time Slice 1644ms and Inline 2400. 164
Figure 6.3 A and B: Figures showing Variance Time Slice intersection for an un-interpreted section and interpreted Section of mud volcano at Inline 800(A), and Pockmarks at Time Slice 180ms(B) at the Sea floor. 165

Figure 6.4 A and B: Figures showing Impedance Time Slice intersection and Porosity slice of braided fluvial channels at Time Slice 1160ms respectively. The porosity is high along the channels.....166
Figure 6.5A and B: Instantaneous Frequency Time Slice intersection (A) and Porosity inversion (B) of fault controlled gas-charged sediments at Time Slice 968ms. Frequency attenuation is observed on both side of the fault plane.....168
Figure 6.6A and B: Showing Time Slice intersection 968ms for Frequency Decomposition at 45Hz (A) and 8Hz (B) of fault controlled, gas-charged sediments. Low frequency attribute is suitable for the delineation of features for the seismic data. 169
Figure 7.1 A: Graph of calibrated measured Vitrinite data values (*) with the modeled Vitrinite values (straight line) for well AE-1, southern section of the study area. 176
Figure 7.1B: Graph of the calibrated Temperature data values (cross points+) with the modeled Temperature values (straight line) for AE-1 well (southern section). Figure shows a good match between the modelled temperature and calibrated temperature data.....177
Figure 7.1C: Well AE-1 burial plot showing the Transformation Ratio for the Barremian-Aptian Source rock Unit in this well. Figure shows transformation reached a peak in the upper Cretaceous. 178
Figure 7.2A: Well AF-1 shows the calibrated (asterisks) and predicted Vitrinite Reflectance values (straight line). There are high calibrated VR values in the Maastrichtian suggesting the possibility of basin inversion and more prominent in the central section. 179
Figure 7.2B: Well AF-1 showing the calibrated (cross points+) and predicted Temperature (straight line) values for the central section. Figure shows slight variation in predicted and temperature values in the Albian and Cenomanian periods and a perfect fit in the Maastrichtian 180
Figure 7.2C: Well AF-1 showing the Transformation Ratio of the Barremian-Aptian Source rock unit. 90% of the source rock unit has been transformed into hydrocarbon within the central part. 181
Figure 7.3A: Well AO-1 showing the calibrated Vitrinite Reflectance data (cross points+) and Modeled (straight line) of the Barremian-Aptian Source rock unit.....182
Figure 7.3B: Well AO-1 showing the calibrated measured Temperature (cross points+) and Modelled temperature (straight line) values. 183
Figure 7.3 C: Well AO-1 showing the Transformation ratio of the Barremian-Aptian Source rock unit. The transformation ratio shows the source rock is immature and none of the organic matter has been transformed into hydrocarbon in the northern part. 184
Figure 7.4A: Depth map of the top of the Basaltic Basement in the Study Area. 185
Figure 7.4B: Depth Map of the top of Barremian/Aptian sequence in the study Area. 186
Figure 7.4C: Depth Map of Mid-Albian sequence in the study area. 187
Figure 7.4D: Depth Map of Late-Albian sequence in the study area. 188
Figure 7.4E: Depth Map of Cenomanian sequence in the study area. 189
Figure 7.4F: Depth Map of Turonian sequence in the study area. 190
Figure 7.4G: Depth Map of Maastrichtian sequence in the study area. 191
Figure 7.4H: Depth Map of Sea Floor in the study area. 192
Figure 7.5. 3D Geological Model of the Study Area Comprising of different Unconformities Interpreted Above. 192

Figure 7.6 A and B: Figures showing the Temperature (A) and Vitrinite Reflectance (B) of Barremian-Aptian Source Rock at 120Ma. 194
Figure 7.7 A, B and C: Figures showing the Temperature (A) Vitrinite Reflectance (B) Transformation ratio (C) of Barremian-Aptian Source Rock 108Ma. Transformation into hydrocarbon started from the central portion at 108Ma. 196
Figure 7.8 A B and C: Figures showing the Temperature (A) Vitrinite Reflectance (B) Transformation ratio (C) of Barremian-Aptian Source Rock at 95Ma. 198
Figure 7.9 A B and C: Figures showing the Temperature (A) Vitrinite Reflectance (B) Transformation ratio (C) of Barremian-Aptian Source Rock at 0.0Ma. 200
Figure 7.10 (A and B): Figures showing Primary Cracking (A) and secondary cracking (B) of Barremian-Aptian Source Rock at 105 Ma. 201
Figure 7.11 A and B: Figures showing Primary Cracking (A) and secondary cracking (B) of Barremian-Aptian Source Rock at 0.0 Ma 202
Figure 7.12 A and B: Figure showing bulk oil and gas generated from the source Rock (A) and bulk hydrocarbon expulsion over time till present day. 204
Figures 7.13 A and B: Figures showing Timing of peak Hydrocarbon-generation (A), and Accumulation plus Expulsion for the Barremian/Aptian Source rock (B). 205
Figure 7.14: 3D View of Gridded Faults Model used in the study. 207
Figure 7.15: 3D generation of Hydrocarbon from the Barremian/Aptian Source Rock at 108 Mya. 208
Figures 7.15 A, B, C. 3D Hydrocarbon Migration Pathways (Red-Gas, Blue-Water, Green-oil) in Albian-aged Reservoir at 108mya, 92mya and 0.0mya respectively. The present day presence of oil vector distally of the Albian reservoir suggest migration of oil into deepwater by good carrier units within the reservoir rock. 210
Figures 7.16 A, B, C. 3D Hydrocarbon Migration Pathways (Red-Gas, Green-oil) in Albian-aged Reservoir at 108Ma, 92Ma and 0.0Ma respectively. Present day result shows Cenomanian reservoir to be gas-prone in contrast to the Albian reservoir unit which is oil and gas prone as seen in figure 7.15C above. 212
Figure 7.17A: Gas saturated Listric Fault (124-65mya) at 93mya at 625.186km by 6749.50km grid. 213
Figure7.17B: Partially saturated Listric Fault (124-65Ma) at 91Ma at 625.186km by 6749.50km grid.The listric fault has lost its saturation at 91Ma. 214
Figure 7.17 C: Partially saturated Listric Fault (124-65Ma) at 74Ma at 625.186km by 6749.50km grid. The listric fault has lost its saturation after reactivation while the younger fault which is an extension of the older listric fault, retains its sealing capacity. 215
Figure 7.17D: Gas saturated Listric Fault (124-65mya) at 65Ma at 625.186km by 6749.50km grid. The listric fault has almost lost lost all its saturation. 216
Figure 7.18: 3D Gas Migration pathways (Red) on the Sea Floor at 0.0mya.....217

Figure 7.19: 3D Hydrocarbon Migration Model of the study area at present day with the depth horizon maps and hydrocarbon components; Gas-Red, Oil-Green but Fault Pillars-in blue. Water component has been filtered. Model grid lies between, X., 520Km and 660km and Y., 6670km by 6800km . Model size is 140km BY 130km.

.....219

List of Tables

Table 1: Summary of different Seismic Facies. 18
Table 2 :Divergent and Parallel Reflection Configurations. 19
Table 3: Progradational Reflection Configurations. 20
Table 4: Mounded and Draped reflection configurations. 21
Table 5: Onlap and fill reflection configurations. 22
Table 6: Showing Wells used for this Study and Coordinates 50
Table 7: Table showing the output of velocity modelling process. 63
Table 8: A-B-C seismic facies technique of Ramsayer (1979). 68
Table 9: Table showing the data used in performing 3D forward simulation modelling. 70
Table 10: Showing data used for model Calibration excluding porosity data. 79

Extended Abstract

Introduction

The use of an integrated approach in science has gained more prominence recently because it is thorough and provides a dynamic perspective from which scientific problems can be investigated and solutions proffered. Here, an integrated approach (Litho and seismic stratigraphy, structural modelling, Seismic attributes analyses and 3D numerical simulation of hydrocarbon generation and migration) were used to investigate geological controls (faults and stratigraphic features) on hydrocarbon migration pathways and suggest prospective areas within the Block 1 of Orange Basin, South Africa.

Materials and Methods

The data sets used for this study include a total of 2430km 2D (SEG-Y) seismic lines, a 1500km^2 3D seismic volume, digital wireline logs, Geochemistry reports and Engineering well reports of three wells drilled so far in block 1. The 2D seismic lines were subjected to merging with their respective navigation files to ensure correct positioning within the block using PETREL 2013 and 2014©. Various digital wireline logs with different runs were spliced to ensure continuous runs throughout the wells. The wireline logs were calibrated with formation tops to identify different lithological sequences and classified into different super sequences based on the formation tops. Seismic–well tie was performed to ensure amplitude match between seismic and wells and synthetic was generated to enable proper mapping of different super sequences on the seismic sections.

Lithological sequences were defined based on python script (Gamma Ray (GR) Merged_new<60,0, If (GR_Merged_new>60 GR_Merged_new<100,1 ,2)), where 0

represents sandstone, 1 represent siltstone and 2 represents shale. Facies logs generated were upscaled for the three wells and facies modelling was performed using the Sequential Indicator Simulator on PETREL 2014©. Different super sequences on the seismic sections were mapped and Two -Way-Time maps were generated. A plane of discontinuity was mapped as a fault on the seismic sections. Subsequently, velocity modelling was done and depth maps generated were used to estimate thickness maps. A Structural model was constructed using different faults mapped and depth maps which represent chronology of supersequences (Top of the Basement to the sea floor) and a tectono- stratigraphic framework was generated. The faults were classified based on their dip directions and related to paleo-stress history of the South Atlantic margin which may have produced them. Seismic stratigraphy analyses were performed and correlated with litho-stratigraphy interpretations to infer depositional environment and suggest likely stratigraphic features (fluvial channels and mouth bars) present in the study area.

Seismic attributes analyses (Variance, Acoustic Impedance, Instantaneous and Iso-Frequency) were applied to investigate the presence of stratigraphic features that could be potential carrier beds for hydrocarbon migration, illuminate major faults that could serve as a seal or a leak for hydrocarbon migration, map gas escape features and identify likely hydrocarbon-charged sediments.

A 3D forward numerical simulation of hydrocarbon generation and migration was performed using the boundary conditions of Heat-flow (HF), Sediment Water Interface Temperature (SWIT) and Paleo-Water Depth (PWD) on PETROMOD 2014©. Numerical simulation of hydrocarbon generation was performed using the depth maps of the Barremian/Aptian source rock unit identified in the Orange Basin to know the timing of hydrocarbon generation. Prior to this, lithology mixing was performed for each super sequence; this represents the quantitative estimate of various lithologies within each supersequence. Later, the model results were calibrated with Vitrinite Reflectance of source rock samples and Temperature data from the three wells to ascertain its accuracy. An iterative numerical simulation process was adopted to factor- in episodes of uplift and erosion history in Southern Africa to ensure model accuracy. Consequently, 3D numerical simulation was performed for secondary migration process using the Hybrid flow path model to investigate the migration

pathways and saturation/ interactions with faults, and to understand how the faults could be controlling the migration pathways.

Results

The litho-facies analyses results revealed that coarsening upward Deltafront marine deposits and fining-upward fluvial sandstones are potential reservoir targets and possible carrier beds for a secondary migration process. 3D Stochastic Facies Modeling results reveal dominance of sandstones and siltstones in all depositional sequences and localized shale deposits prominent in the Barremian/Aptian and Albian sequences only. The depositional environments within these sequences range from fluvio-deltaic in the north to a marine pro-deltaic environment in the South. Seismic facies analysis revealed channel fill deposit in the northern section because of a chaotic reflection pattern observed in the late Cenozoic sequence. Also, there is a change in reflection amplitude from low in the Maastrichtian to high in the Cenozoic. Three seismic facies of parallel, chaotic and divergent patterns were seen within the Maastrichtian and Cenozoic sequence suggesting fluvial to fluvio- deltaic and shallow marine distributary point bars. In the Cenomanian and Turonian sequence, the seismic facies reveals the deposition of sedimentary sequences which exhibit, hummocky, wavy and parallel internal configurations. This architecture has been identified as deltaic deposits. Albian has low amplitude, sub parallel-wavy, discontinuous clinoforms, suggesting shallow marine shelf-edge prograding deposits.

The structural framework model indicates compressional events and possible uplift in the late Cretaceous, coupled with evidence of erosional terminations. Bright spot anomaly is noticed on both side of a listric normal fault suggesting possible leakage of gas across the fault. Results from seismic attributes analyses show that the Instantaneous Frequency (IF) attribute confirmed the likely presence of hydrocarbon charged Cenomanian reservoirs in close proximity to the listric normal fault, judging by the attenuation of frequency observed. Seismic acoustic impedance inversion calibrated with porosity inversion reveals the presence of meandering fluvial channels within the Cenomanian sequence.

3D numerical simulation of Barremian/Aptian source rock revealed that it is matured sufficiently enough, and has generated a lot of hydrocarbon but with lesser maturity in the northern part of the study area. The bulk generation and expulsion statistics as at present day shows 430.701,94Mtons of gas and 38.399,53Mtons of oil had been generated by primary and secondary cracking process, representing 91.81% and 8.19% of organic matter transformed into gas and oil respectively. The Hydrocarbon Migration model suggests that gas expulsion from the source rock unit started from the central part and southeastern part of the study area as early as 108Ma. There are evidences of vertical migration of gas into the Albian and Cenomanian reservoirs at this time, however at the present day, Albian-aged reservoir remains oil and gas – prone but with prone to oil westward (deep waters) of the study area. The Cenomanian reservoir unit is gas prone and displays hydrostatic pressure compartmentalization. Results also show a syn-rift listric fault to be 100% gas saturated as at 93 Ma and lost its saturation by 65Ma, suggesting a breakthrough path linked to fault reactivation could have caused it to lose its saturation. 1D calibration of modelled Vitrinite Reflectance and Temperature data revealed that the Barremian/Aptian source rock has matured well in the southern and central portion and not matured enough to generate hydrocarbon in the northern part, where well AO-1 was drilled. These observations validate the results from the 3D numerical simulation predicting lesser source rock maturity in the northern part of the study area.

Conclusions

It is concluded that braided fluvial channels and mouth bars might be serving as carrier beds (stratigraphic control) for hydrocarbon migration. The study is able to resolve, by integrating all methods applied, that a listric fault serves as the main structural control on gas escape and migration in the study area. This is based on:

- observed bright spot anomaly, and
- instantaneous frequency attenuation associated with gas compressible nature on both sides observed, and
- loss of its gas saturation at 65Ma.

Table of Acronyms

AVO- Amplitude versus Offsets
IF- Instantaneous Frequency
HF- Heat Flow
PWD-Paleo Water-Depth
SWIT-Sediment Water Interface Temperature
CCT-Cosine Correlative Transform
RMS-Root Mean Square
MFS-Maximum Flooding Surface

Chapter One

1.1 Introduction and Scientific Background

Hydrocarbon generation, migration, charge and escape processes are essential components of petroleum system modeling and basin reconstruction (forward modelling). More importantly, it has become an important area of study as the drive to discover more hydrocarbon reserves increases, especially in frontier areas, and thus form a major part of the exploration value chain. Petroleum system modelling is defined as the digital representation of interrelated processes between hydrocarbon source and other geological configurations that are essential for a pool of hydrocarbon accumulation to occur (Magoon and Dow, 1994). In most cases, petroleum system modelling and basin reconstruction processes are a synergy which involves the dynamic modelling of all geological processes including structural evolution, sedimentology and stratigraphy in a sedimentary basin over geological time span (Kauerauf and Hantschel 2009).

These geological processes do serve as a control on gas escape and migration. However, the controls of hydrocarbon migration do vary but are not limited to depositional events and tectonics only, it could also be caused by the absence and untimely formation of hydrocarbon traps. Globally, hydrocarbon seepages are a common occurrence in major sedimentary basins and have been well documented; Mayorga et al., (2012), Judd and Hovland (1992), Fader, (1991), Field and Jennings (1987), King and Maclean (1970). The modelling of hydrocarbon migration pathways from the source pod to the traps could mitigate the inherent uncertainty associated with hydrocarbon exploration by serving as a tool for predicting prospects and leads in sedimentary basins. Hydrocarbon migration may involve the generation and movement of hydrocarbon within a source rock unit (primary migration), or from the source rock through the carrier beds under the influence of subsurface pressure and geothermal gradient until it charges permeable rock layers capped with an impervious rock (secondary migration). The latter process is driven by vertical buoyancy forces due to density contrast between petroleum and formation waters.

The controls of hydrocarbon leakage and fluid escape have been well studied in sedimentary basins, this includes studies by Mayorga et al., (2012), Anka et al., (2009), Klerkx at al., (2006) and Qi-Pang et al., (2003). Similar studies carried out in the southern section of the Orange basin, South Africa documented the prominence of hydrocarbon escape features (Boyd et.al., 2011 and Hartwig et al., 2012). Specifically, seismic anomalies such as pockmarks and gas chimneys were reported. This suggests the presence of an active petroleum system and could be a pointer to deeper hydrocarbon reserves in the basin (Anka et al., 2009). The causes and controls of the gas escape have been established in the southern part of the basin where the Ibhubesi gas field was discovered; however, limited work has been done in the northern part of the basin to understand the controls on gas escape and the migration pathways. The northern part of the Orange basin South Africa is significant and strategic firstly because of its close proximity to the Namibia section of the Orange Basin where the huge Kudu gas deposit was discovered, and secondly because of the likely presence of gas hydrates in this area (Petroleum Agency South Africa, 2006). Gas hydrates have been identified as a future source of energy (Ramana, et al., 2007).

The study area is the most northern exploration block (Block1) in the South African section of the Orange Basin. The choice of Block 1 is premised on its trend with the discovered Kudu gas field in the North and Ibhubesi gas field in the South central part of the South African section. Therefore, the presence of gas charged sediments in block 1 is anticipated.

Previous work done on modelling hydrocarbon migration pathways often focuses on generation and expulsion of hydrocarbons with inadequate understanding of its interactions with geological controls such as faults. Also, the charge system is often poorly understood. This study will adopt a novel approach relating stress history of the South Atlantic margin to the timing of faults formation, timing of hydrocarbon generation and migration and interactions with faults and stratigraphy. In addition, an application of seismic stratigraphy and seismic attribute analysis to characterise stratigraphic features and hydrocarbon bearing reservoirs will be performed respectively. Seismic stratigraphy lays the foundation for sequence stratigraphy, seismic attribute analysis, volume interpretation and forward geological modelling

(Van Wagoner et al., 1990). Therefore, seismo-stratigraphy and structural interpretations, seismic attribute analysis and 3D petroleum system modelling will be integrated to provide a new perspective to hydrocarbon gas escape and migration studies.

1.2 Brief Review of Research Approaches

Seismic stratigraphy has been used in hydrocarbon exploration (Catuneanu and Eriksson, 2007); commonly based on utilising seismic reflection patterns to understand sea level changes, identify subtle stratigraphic traps, characterizing and predicting occurrences of source and reservoir rocks and determining fluid distribution in the subsurface (Cross and Lessenger, 1988).

Many workers have applied the principles of seismic stratigraphy, seismic attribute analysis and the utilization of source rock geochemistry data independently from each other to study gas escape and to model hydrocarbon migration pathways. However, the integration of these principles to achieve same objectives has rarely been performed. Seismic stratigraphy analysis has been used for the identification of unconformities within a sedimentary sequence and to provide detailed explanation on the distribution of sedimentary facies in time and space. Unconformities in sedimentary basins could serve as a conduit for gas migration and escape. Therefore, identification of patterns of truncation, onlap, topography and structural history of the area are key to understanding hydrocarbon migration processes (Visher, 1987). In seismic stratigraphy, an unconformity surface is commonly identified as an onlap surface which represents a basin-ward shift in sediment deposition (Christie-Blick et al., 1990). It is identified on seismic section profile as a progressive up-dip termination of strata against an underlying surface. Previously, unconformity surfaces have been used as a homogenous surface to divide the stratigraphic sequence and understand eustatic fluctuations but have recently become a hypothetical target for explorers studying controls on hydrocarbon migration processes (Kamp and Turner, 1990).

Increase in the global exploration drive for new hydrocarbon reserves has led to the emergence of unconformity as a vital exploration tool serving as a control on hydrocarbon migration and accumulation (Zhang and Fang, 2002). Apart from unconformity (stratigraphic control), hydrocarbon migration and seepages could also

occur as a result of other processes. These include direct contact of surfaces with source beds, surface seeps emerging from hydrocarbon bearing homoclinal beds and seeps emerging from hydrocarbon bearing formations which have been ruptured by faulting and folding (Khilyuk, 2000).

In the Baikal Rift Basin, an extensional regime area, there are reports of tectonically triggered fluid (gas hydrates) flow due to the displacement of a particular strike-slip fault coupled with high sediment compaction (Klerkx et al., 2006). Gas migration along the fault became evident in the shape of a vent structure on the sea bed identified on a seismic section. The interaction of fluids and faults has made detailed mapping of faults geometry crucial in hydrocarbon migration studies. Also, in the southern North Sea, there are reports of gas escape evidenced by gas venting structures observed on the sea floor (Schroot and Schuttenhelm, 2003). Many of the gas seepages are located just above of the salt domes in the Netherlands' section of the North Sea while an accompanying normal fault above the domes serves as the conduit for gas migration.

Hydrocarbon migration studies have also been enhanced by the utilization of the principles of seismic attributes. The common attributes applied are amplitude, frequency, and seismic impedance inversion. These attributes aid the mapping of subtle features on the seismic sections, and have been used in predicting quantitative and geometric properties including fluid content, lithology and porosity (Chambers and Yarus, 2002). However, like many geophysical techniques, they are associated with inherent uncertainty, notably the resolution. Nevertheless, their applications have been proven successful.

As mentioned above, there are varieties of seismic attributes that could be used in exploration; they are used depending on the type of geological hypothesis to be tested. In detecting fluids, AVO and acoustic impedance inversion are two of the common attributes in predicting fluids content in a formation. AVO was initiated by Knot (1899) and further development on AVO analysis was done by Zoeppritz (1919) .The application of AVO in fluids detection is based on increase in amplitude versus offset for a gas-charged reservoir and otherwise for brine–filled reservoirs (Ostrander,1984). The theory behind the application of AVO in fluids detection is on the sensitivity of

P-waves to change in pore fluids as a function of angle of incidence. The common AVO model used hydrocarbon indicators consisting of poorly consolidated gas filled sands enclosed in relatively impermeable shale, and brine filled-reservoirs enclosed in impermeable shale (Castagna et al., 1998). Gas charged reservoirs mostly display bright amplitude on stacked conventional seismic data but this is associated with uncertainty because a well compacted rock can display similar amplitude like hydrocarbon charged reservoirs, hence the adoption of AVO to mitigate the uncertainty. An increase of amplitude with offset will isolate a gas charged reservoir because it exhibits negative polarity while brine charged reservoir's amplitude decreases with offset with positive polarity (Chambers and Yarus, 2002). Seismic impedance inversion empirically involves the conversion of seismic trace in time-domain into harmonic-domain. It is a product of the compressional velocity and density. Also, the calibration of poison ratio with the synthetic impedance generated as a result of Fourier transform can give reliable information about gas presence in a reservoir. Seismic impedance inversion will be adopted for this study in the place of AVO because of the unavailability of pre-stack seismic data.

Having understood the possible controls on hydrocarbon migration, it is pertinent to establish faults-fluid interactions by simulating the generation and migration of hydrocarbon as a part of petroleum system modeling. Simulating the generation of hydrocarbon from source beds and construction of a hydrocarbon migration model is dependent on boundary conditions (Paleo-water depth, heat flow model and Sediment Water Interface Temperature). The output is conventionally calibrated with thermal, pressure and organic maturation data to ensure model accuracy. Hydrocarbon migration modeling is an iterative process and an integral part of petroleum system modelling from which other processes like generation and accumulation are modeled to reduce investment risk in drilling (Schlumberger, 2009).

The different approaches highlighted above offer a novel approach integrating petroleum system modeling, structural and stratigraphic evolution, paleo-stress history and seismic attributes analysis, to constrain the timing of hydrocarbon generation and expulsion, timing of the formation of major faults, and identification of hydrocarbon prospective areas respectively. In the Orange Basin, the prominence of a basin wide

lower Barremian-Aptian gas prone source rock has been reported (Van der spuy, 2003). Therefore, forward modeling of gas migration vectors is feasible.

1.3 Location of the study Area

The Orange basin, offshore South West Africa is located within the passive continental margin of the South Atlantic between 31^0 and 35^0 S. It was developed within a divergent plate setting in response to extensional tectonics of the lithosphere that is related to South America and Africa plates in the late Jurassic. This was followed by seafloor spreading and opening of the South Atlantic Ocean in the Early Cretaceous around 136 Ma (Macdonald et al., 2003, Reeves and de Witt, 2000). The seismic lines (SEG-Y) to be utilized in Block 1 have three wells control (Figure1.1), these are the wells drilled so far in block 1. The three wells were drilled far from one another, the distance between AE-1 and AF-1 is 74206m and the distance between AF-1 and AO-1 is 30747m from the south to the north direction (Figure 1.2). The AO-1 well is the northernmost well drilled in the South African section of the Orange basin. The exploration right is held by a joint arrangement of PetroSA and Carn India. Recently, there was a 3D seismic acquisition by Carn india; this has been made available for this study.

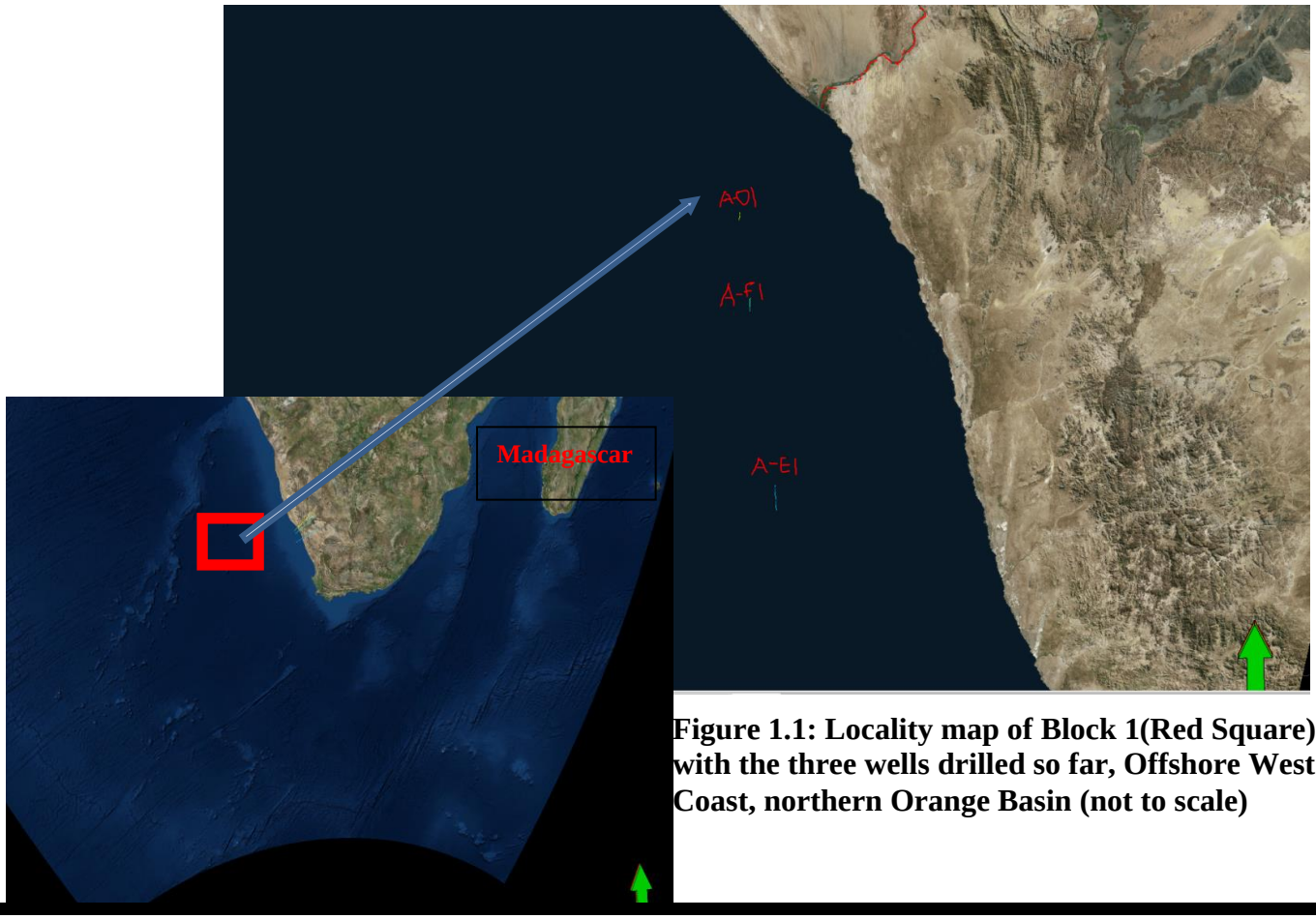

Figure 1.1: Locality map of Block 1(Red Square) with the three wells drilled so far, Offshore West Coast, northern Orange Basin (not to scale)

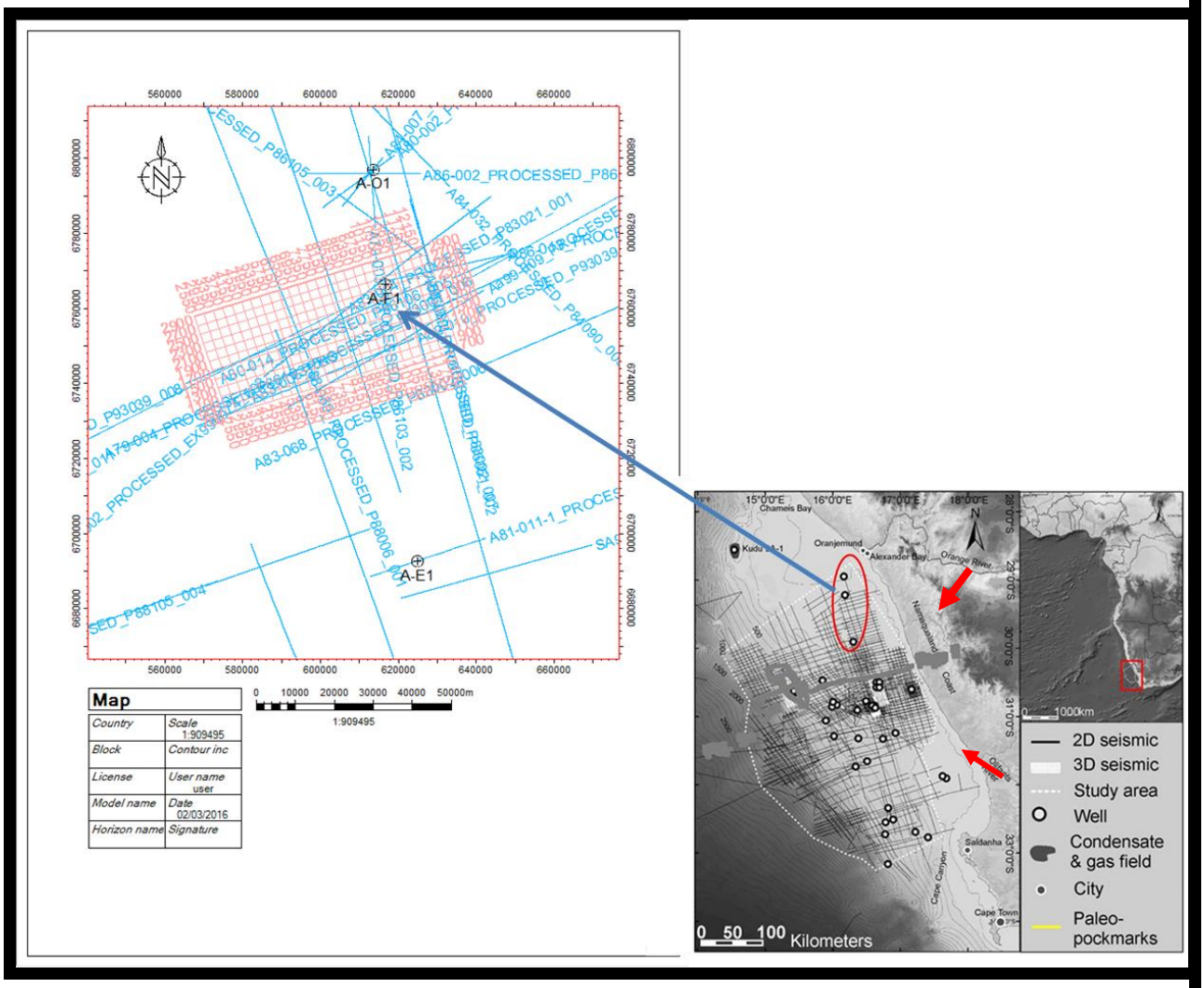

Figure1.2: Map of study area showing the wells and seismic data used for the study, the red arrows point to the input of Orange river in the North and the Olifant river in the South (modified from Hartwig et al., 2012).

1.4 Aim and Objectives

The main aim of this research is to understand the controls on gas migration pathways and construction of a 3D hydrocarbon migration model for block 1, Orange Basin. The objectives of the research are listed below;

- Geological interpretations of geophysical wireline logs of three wells drilled so far in the study area to infer depositional environments and performed litho-facies modelling.
- Detailed mapping of stratigraphic surfaces and features, faults, gas escape features and depositional systems using seismic stratigraphy concept. In addition, to understand the faults or stratigraphy controls on the gas escape features mapped.
- Detailed mapping of structural features present in the study area, and with references to the paleo-stress history of the South African margin.
- Application of acoustic impedance and frequency inversion technique as part of seismic attributes analysis to identify potential carrier beds, hydrocarbon-charged sediments, anomalies such as bright and dim spots. Also identification of gas chimneys, pock marks and mud volcanoes if present.
- 3D numerical Simulation of hydrocarbon generation and migration using boundary conditions and calibration with thermal and geochemical data to construct a 3-D hydrocarbon migration model. Also, to establish possible faults controls on hydrocarbon migration pathways.

1.5 Scope of Work

- Mapping of faults and stratigraphy surfaces and unconformities on seismic data.
- Identification of depositional systems using seismic facies concepts based on seismic reflection patterns and terminations.
- Identification of lithology, depositional environment and correlation of major surfaces using geophysical logs.
- Seismic data- well tie and generation of synthetic seismogram.

- Application of seismic impedance inversion and Iso and instantaneous - frequency attributes to predict direct hydrocarbon indicators and hydrocarbon bearing reservoirs.
- Correlation of wells in the study area based on depositional sequences.
- Establishment of any relationship between faults plus unconformity surfaces and direct hydrocarbon indicators (DHI'S).
- Velocity modelling and depth conversion of time maps.
- Exportation of faults and depth maps to Petromod 2014© workstation to model hydrocarbon generation and migration from source beds by incorporating heat flow model, and source rock geochemical data.
- Quantitative lithology mixing on depth maps which represent relative abundance of different lithologies deposited in each sequence.
- 3D modelling of hydrocarbon generation and migration using boundary conditions.

1.6 Previous Studies on Hydrocarbon escape and migration in the Orange basin.

Earlier studies in Blocks 3 and 4 by Kuhlmann et al., 2010 in the Orange Basin revealed the presence of stratigraphically-controlled gas chimneys on the shelf and upper slope (water depths up to 500m.) .Gas chimneys, pockmarks, seafloor mounds, and seismic anomalies associated with gas migration have been identified throughout the Orange Basin, South Africa.

Using a 2-D seismic dataset covering exploration blocks in the southern part of the basin (Paton et al., 2008 and Kuhlmann et al., 2010); various features probably associated with past or active natural hydrocarbon leakage have been identified both on the seafloor (pockmarks, mounds) and within the stratigraphic column (gas chimneys), as well as several seismic anomalies characteristic of gas presence (i.e. bright and flat spots). The gas chimneys either leak up to the seafloor ("active leakage") or are sealed within the Miocene (14 Ma). Depending on their origin, the gas chimneys have been classified as structurally and stratigraphically related (Kuhlmann et al., 2010).

The structurally controlled chimneys are mainly found in the outer margin the basin, between 500 to 1500 ms (TWT) whereas; the stratigraphically controlled chimneys are mostly located on shelf and seem to be linked to an onlap/pinch out of the Aptian shales. The structurally controlled chimneys are located on top of flower structures, mounds and extensional-fault clusters. The stratigraphically controlled chimneys end-up in seafloor as pockmarks or in seismic bright spots close to the sea floor.

Schmidt (2004), showed that the source of hydrocarbon desorbed from near surface sediments in the Orange basin, offshore South Africa is of thermal origin. This was supported by Wilhelms et al., (2001), who suggested that the depth and origin of gas chimneys in the Orange basin as well as their relationship to geological features indicates that a biogenic source of gas is unlikely, as microbial activity is considered to be inactive if not completely absent at a temperature greater than 80 degrees Celsius.

1.6.1 Problem Statement and Justification for the current study

The studies above considered, by observation, the association of structural features with gas escape features to draw inferences and establish that gas escape is either stratigraphically or structurally controlled in the southern part of the Orange Basin. This approach has its limitation, because it focused on mapping of gas escape features and speculative migration pathways without knowledge about the timing of regional faults formation, timing of hydrocarbon generation and faults interaction with hydrocarbon migration pathways. Also, 3D forward numerical modelling of hydrocarbon migration into reservoirs was not performed, hence migration processes were not properly articulated. Consequently, the current study adopts an integrated approach mentioned earlier to characterise primary and secondary migration processes and their interaction with faults and stratigraphy features in the northern Orange Basin. The outcome of this study will be invaluable for future exploration efforts in the Orange Basin.

1.7 Synopsis of Research

The components of this research has been identified and grouped into phases based on the general scope of study. Chapter one will give an overview of the study and its relevance, the aims and objectives, study location, and the detailed insight into relevant literature with regards to keywords of the research will be discussed.

In Chapter two, the regional geology of the Orange Basin will be discussed in detail with more focus on the stratigraphy and petroleum system. Also previous studies on the basin and the relevance of hydrocarbon migration studies will be highlighted.

Chapter three will focus on materials and methodology used in carrying out the research. Seismic data and well-logs received from the Petroleum Agency of South Africa will be listed and the merging of 2D seismic lines with the navigation data on Petrel 2013 will also be discussed. Procedures of each task completed on Petrel 2013 software will be explained. Also, relevant deliverables achieved on Petrel 2013 will be exported to Petromod© to model migration flow paths.

Chapter four will discuss all results from geophysical well logs, litho-facies and depositional systems interpretations of all super sequences. Also, results from litho-facies modelling of sediments encountered within the study area to understand the internal geometry and likely will be discussed.

In chapter five, results from seismic sequences analysis and seismic facies calibrated with litho-facies analysis will be discussed. Isopach maps will be generated to understand sediment thickness distribution across the study area. Depth surface maps created will be used for the construction of a structural framework to investigate faults-stratigraphy relationship. In addition, mapping of faults, gas escape features including direct hydrocarbon indicators anomalies will be performed to know the relationship between faulting and these escape features. Faulting systems in relation to the paleo-stress history of the South Atlantic Continental Margin will also be discussed to know the episodic evolution of different faulting systems and their orientations.

Chapter six will focus on results from the application of seismic attributes to complement observations made from chapter five. Genetic seismic impedance inversion calibrated with porosity attribute to investigate stratigraphic features within area of study will be performed. In addition, variance attribute will be employed as an imaging tool for faults and to identify sea floor expressions of gas escape features. Instantaneous and Iso–frequency attributes analyses results will be performed to investigate probable areas of frequency attenuation which could point to hydrocarbon-charged sediments.

Chapter seven will discuss all results from the 3D numerical simulation of hydrocarbon generation and migration pathways, establish timing of hydrocarbon generation, expulsion and hydraulic behaviours of faults to hydrocarbon. 1D Petroleum system modelling calibration will be performed with the 3D modelling results to ascertain model accuracy.

Chapter eight will detail summary of findings, main scientific and economic contributions, conclusions and recommendations.

1.8 Review of Keywords and concepts relevant to the current study.

1.8.1 The basic concepts and applications of Seismic Stratigraphy

Seismic stratigraphy has revolutionized stratigraphy studies because of increased reliance of the Petroleum industry on seismic data as exploration moved into frontier regions where well-control is lacking. While its continuous application has provided the conceptual framework for developing deterministic numerical models of stratigraphic architecture, sedimentary facies distribution and basin evolution, it has also helped in the discovery of source, reservoirs, traps and seals.

Applications of seismic stratigraphy cover a broad field of sedimentary processes and tectonics studies, which are targeted at improving the success of petroleum exploration and production. It was introduced as a revolutionary tool to the oil industry by Vail (1975), its continuous application in exploration has led to the

evolution of other aspects of stratigraphy analysis. These include allostratigraphy, magnetostratigraphy and sequence stratigraphy.

Seismic stratigraphy involves the use of seismic data to identify subtle stratigraphy traps, characterizing and predicting occurrences of source and reservoir rocks and determining fluid distribution in the subsurface (Cross and Lessenger, 1988). The application of seismic data in stratigraphy study is conceptualized on identifying concordant reflections (genetically related strata) and terminations which are separated by the surfaces of discontinuity (Cross and Lessenger, 1988). There are concepts that have been adopted in seismic stratigraphy studies and the order of study has been defined in chronology. These are seismic sequence analysis, seismic facies analysis and seismic lithology analysis (Mitchum et al., 1977).

1.8.1.1 Seismic Sequence Analysis

The concept of interpreting depositional sequence by employing seismic data is aimed at defining the regional stratigraphic framework and architecture and to recognise unconformity bounded depositional surfaces which are composed of genetically related strata (Vail, 1975). The philosophy behind separation of concordant reflections in packages is based on the assumption that strata of sedimentary basins were deposited in geographically and temporally confined episodes, separated by a period of erosion or non –deposition. This assumption was conceived based on earlier work of Sloss (1963), which recognised that the Phanerozoic strata of the North American craton are divisible into major depositional intervals and separated by periods of continental-scale erosion and non-deposition (unconformities). These depositional sequences bounded by unconformities represent the rock record of a major tectonic cycle (Krumbein and Sloss, 1963).

The fundamental precept on which the identification of unconformity surfaces on seismic section is based is how they generate a strong reflection because of acoustic impedance contrast between a rock stratum and the hiatus. Only reflections that are not stratigraphic in origin are excluded from this precept. The reflection emanating from an unconformity surface may vary laterally as different lithologies with different

impedances are superimposed across the surface. Therefore, unconformities separate strata of different lithologies and structural attitudes (Cross and Lessenger, 1988). Also the ages of bounding unconformities do give information about the temporal limits of a sequence often represented as an onlap sequence on the seismic section. It is an indicator of seaward shift in sites of sediment accumulation during a relative sea level fall and subsequent landward encroachment of deposition upon the unconformity surface as relative sea level rises. It is recognized by systematic oblique updip terminations of reflectors against an underlying seaward dipping reflection (Figure 1.3). Also, a period of non-deposition is defined as an oblique downdip reflection termination against an underlying horizontal or seaward dipping reflection. This is regarded as a surface of unconformity (downlap), figure 1.3.

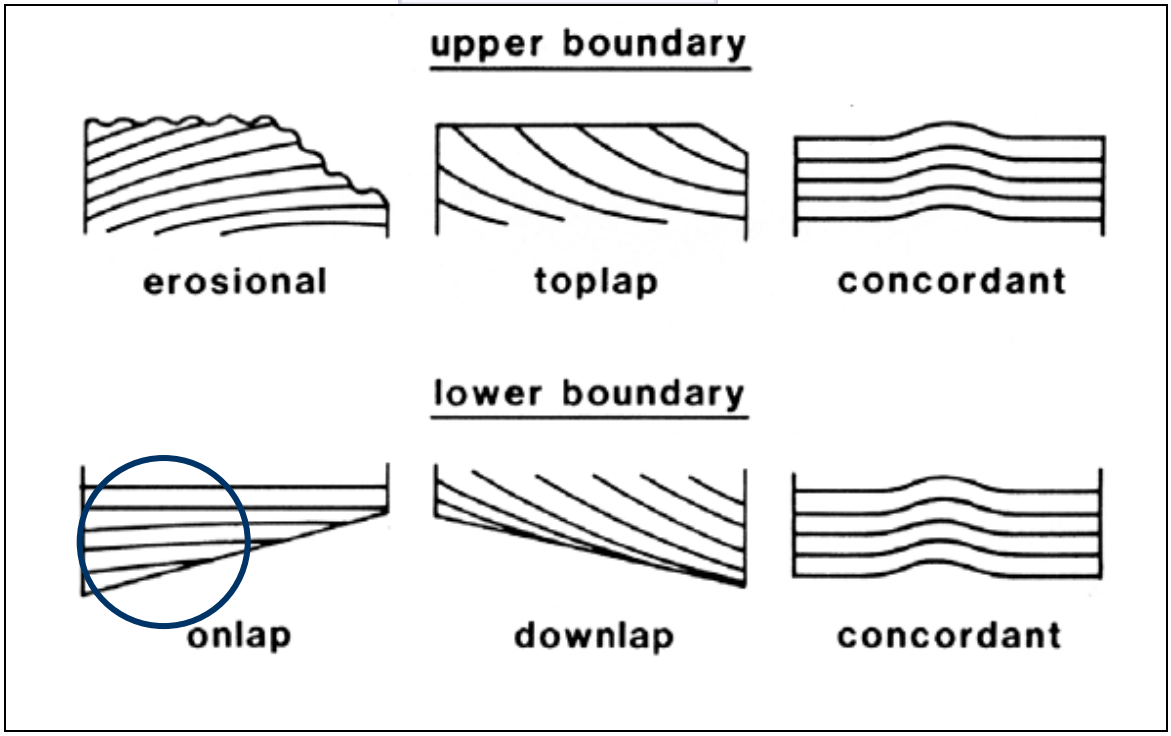

Figure 1.3 ; Showing onlap surface geometry(blue circle) and other Erosional surfaces (Mitchum, 1977) .

1.8.1.2 Seismic Facies Analysis

An integrated approach to understanding the geological controls on gas escape and migration pathways in offshore northern Orange Basin, South Africa.

The objective of seismic facies analysis is to predict and interpret the occurrence and distribution of specific lithologies, such as potential source or reservoir rocks. Whilst, also interpreting the depositional environments and geological history represented by strata in different positions within a sequence. A seismic facie consists of a group of seismic reflections whose character differs from adjacent groups within a sequence (Mitchum et al 1977a). Reflection characteristics used in distinguishing one seismic facie from another include geometry of reflections with respect to the two unconformity surfaces bounding the sequence. The external geometry of the facies and the internal configuration of the reflections which include the amplitude and frequency are also a distinguishable characteristic (Sangree and Widmier 1977). The two criteria that have been used in classifying seismic facies are; reflection terminations with respect to the two unconformities that bound the sequence, and reflection configurations which reveal pattern of stratification from which depositional processes can be inferred (Cross and Lessenger, 1988). According to Sangree and Widmier (1977) as well as Bubb and Hatlelid, (1978), there are four common reflection configurations used in seismic facies analysis. These include divergent patterns associated with alluvial plains, shallow marine shelf deposits, delta platforms and marine basin plains. Also, there is a progradational pattern associated with alluvial fans, prograding shelf platforms, pro-delta environments and the transition from outer shelf to slope environments. The reflection configuration that represents this, is an inclination of a strata with respect to an overlying or underlying reflection.

In addition to these, there is mounded and drape patterns which are a characteristic of reefs, banks or deltas in shallow marine shelf and platform environments, and could be of slumped submarine canyon fans or aprons and turbidites or hemipelagic deposits in deep marine settings. Lastly, there are onlap and fill patterns that are produced by onlapping strata of coastal-plain and paralic environments by deposits that fill the submarine canyons or drowned alluvial valleys. The variation in seismic facies reflections characters and configurations is best represented on a seismic facies map which may indicate some property of reflections like amplitude and phase.

1.8.1.3 Reflection Configuration Patterns of Seismic facies.

Seismic facies analyses are carried out to improve the geological interpretations of seismic data, the classification of each seimsic facies is based on the internal

configuration of reflections generated on the seismic section. The factors that define each seismic facies are amplitude, continuity and frequency and interval velocity. All the factors above define each seismic facies adjacent to one another. Specifically, lateral continuity and reflection patterns defines the stratigraphic patterns in a basin. The major seismic facies as classified by (Mitchum, et.al.,1977) are highlighted below.

1.8.1.3.1 Prograding Clinoforms

Prograding sedimentary pacakage generates different reflection configurations as a result of lateral outbuilding of sediment which forms a gently sloping depositional surface called clinoform (Figure 1.4.). The oblique prograding pattern is generally interpreted to represent high-energy conditions and some combination of relative high sediment supply, little or no basinal subsideience and relatively stationary sea level

The sigmoid prograding pattern (Figure 1.4)) represents a lower energy regime with a relatively low sediment supply, relatively rapid basin subsidience and increase in sea level. The sigmoid pattern is associated with predominantly argillaceous sediments. Shingled prograding clinoform is interpreted as reflectors stacked between two bounding reflectors with gentler dip. It is typical of shallow water environment conditions and can be further described depending on similar patterns as hummocky, wavy, contorted and lenticular patterns.

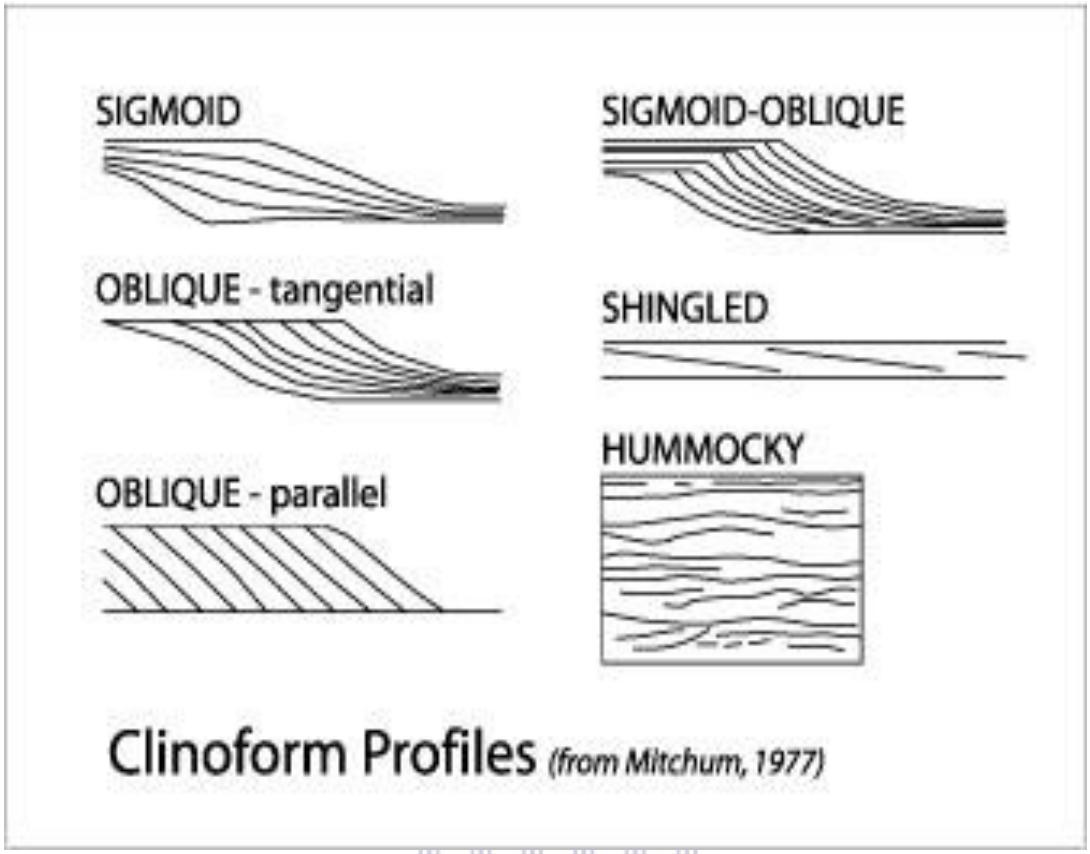

Figure 1.4: Showing Different Prograding Clinoforms (After Mitchum, 1977).

1.8.1.3.2 Parallel and subparallel reflection pattern

These are reflection configurations generated by strata that were deposited at a uniform deposition rates and at a uniform subsidience rates or in a stable basin. It susggests basin–fill of horizontally stratified reflectors controlled by dynamic ocean currents (Stoker, et al 1997).

1.8.1.3.3 Divergent Reflection Pattern

Divergent configurations are characterized by a wedge-shaped unit in which the entire sedimentary unit thickens as a result of thickening of an individual sub-unit within an entire unit. It therefore represents, lateral variation in rates of deposition or tilting of a sedimentary surface during deposition. It represents varying rates of deposition caused by tectonic tilting or changing rates of sediment input and varying rates erosion and sedimentation.

1.8.1.3.4 Chaotic reflection patterns

Chaotic reflection clinoform represents varying high energy environments during depsoitional processes and a disordered arrangement of reflection surfaces due to soft – sediment deformation.

Table 1: Summary of different Seismic Facies (Badley 1985).

Seismic facies	Reflection configuration	Reflection continuity	Reflection amplitude and frequency	Bounding relationship	Depositional environment interpretation	Example (Vertical scale bars represent 100 ms)
1 Parallel continuous high amplitudes	Parallel	Continuous	High amplitude and low frequency	Continuous and draping underlying topography	Pelagic or hemipelagic	
2 Semiparallel continuous high amplitudes	Semiparallel	Continuous to semicontinuous	High amplitude and high frequency	Restricted to the top of the regional anticline	Debris flows or hyperconcentrated density flows or turbidites	
3 Mounded discontinuous low amplitudes	Contorted to mound-shaped	Discontinuous	Low amplitude and high frequency	Onlap, downlap, toplap, and truncation	Debris flows or (hyper) concentrated density flows	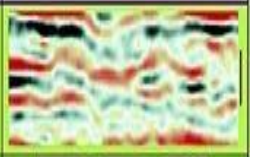
4 Blocky semicontinuous high amplitudes	Oblique	Semicontinuous	High amplitude and high frequency	Separated by linear vertical to oblique surfaces	Lower slope and slumps or large lithified collapse blocks	
5 Oblique semicontinuous high amplitudes	Oblique	Semicontinuous	High amplitudes	Thinning out toward the platform	Upper slope	
6 Chaotic amplitudes	Chaotic	Discontinuous	Low amplitude	Grading vertically to facies 7 and laterally to facies 5	Platform interior	
7 Mounded semicontinous high amplitudes	Contorted to mound-shaped	Semicontinuous	High amplitude and low frequency	Numerous diffraction hyperbolas	Karstified platform top	

1.8.2 Summary of Seismic Facies Types and Reflection Configurations (Badley, 1985).

Table 2 :Divergent and Parallel Reflection Configurations.

Properties of seismic facies	Depositional environments/Settings			
	Shelf/Platform	Delta platform: DELTA FRONT/DELTA PLAIN	Alluvial plain/ Distal fan delta	Basinal plain
Reflection configuration	Parallel/slightly divergent; highly divergent near rare growth faults	Parallel/slightly divergent on shelf; highly divergent near growth faults in deep-water deltas	Parallel, generally grades basinward into delta plain or into shelf/platform facies	Parallel/slightly divergent; may grade laterally into divergent fills or mounds
Lithofacies and composition	Alternating neritic limestone and shale; rare sandstone; undaform deposits	Shallow marine delta front sandstone/shale grading upward into subaerial delta plain shale, coal, sandstone channels; prodelta facies excluded except where toplap is absent; undaform deposits	Meanderbelt and channel-fill sandstone and floodbasin mudstone; marine reworked fan delta sandstones/profan shale; undaform deposits	Alternating hemipelagic clays and siltstone; calcareous and terrigenous composition; fondoform deposits
Geometry and structure	Sheetlike to wedge-shaped or tabular; very stable setting; uniform subsidence	Sheetlike to wedge-shaped or tabular on shelf-prismatic to lenticular basinward of subjacent shelf edge with growth faults and roll-over anticlines; relatively stable, uniform subsidence on shelf; rapid subsidence and faulting in deep-water delta	Sheetlike to wedge-shaped (individually elongate ribbons or lobes), commonly tilted and eroded	Sheetlike to wedge-shaped; may be slightly wavy or draped over subjacent mounds; generally stable to uniform subsidence; may grade laterally into active structural areas
Lateral relationships	May grade landward into coastal facies and basinward into shelf-margin carbonate facies; local carbonate mounds	May grade landward into alluvial systems and basinward into prodelta/slope clinoforms (on shelf) or growth-faulted prodelta/slope facies (deep-water setting)	Grade landward into reflection-free, high sandstone facies; alluvial facies grade basinward into upper delta plain; fan delta facies grade basinward into shelf/platform or into slope clinoforms	Commonly grades shelfward into mounded turbidites, or slope clinoforms; may grade laterally into deep-water mounds or fills
Nature of upper/lower boundaries	Concordant, coastal onlap and/or baselap over upper surface; upper surface may be eroded by submarine canyons; basal surface concordant, low-angle baselap or (rare) toplapped by subjacent clinoforms	Normally concordant at top but may be rarely onlapped or baselapped; upper surface may be eroded by submarine canyons; basal surface generally toplapped by prodelta/slope clinoforms (on shelf); rarely concordant with prodelta on shelf but common in deep-water, roll-over anticlines	Upper surface may be onlapped by coastal facies; top may be angular unconformity; base in generally concordant; fan deltas rarely overlie clinoforms (toplap)	Generally concordant at top and base; may onlap eroded slope clinoforms or eroded mounds; upper surface rarely eroded
Amplitude	High	High in delta front and coal/lignite or marine transgressive facies within delta plain; low/moderate in most delta plain and in prodelta where in continuity with delta front	Variable—low/high	Low to moderate
Continuity	High	High in delta front, coal/lignite and marine transgressive facies; low/moderate in remainder of delta plain and prodelta where in lateral continuity with delta front	Discontinuous; continuity decreases landward	High
Frequency (cycle breadth)	Broad or moderate; little variability	Variable; broader in delta front; coal/lignite and marine transgressive facies moderate; narrower in other delta plain and prodelta where in continuity with delta front	Variable; generally narrower cycles than shelf/platform	Generally narrower than shelf/platform; commonly very uniform breadth throughout

Table 3: Progradational Reflection Configurations.

Properties of seismic facies	Depositional environments/Settings	
	Slope: **ASSOCIATED WITH PROGRADING SHELF/PLATFORM**	Prodelta/Slope: **ASSOCIATED WITH PROGRADING SHELF DELTA OR SHELF-MARGIN DELTA; OR** Slope: **ASSOCIATED WITH PROGRADING NERITIC SHELF SUPPLIED PERIODICALLY BY SHELF DELTA/FAN DELTA**
Reflection configuration	Sigmoid clinoforms Progradational in dip profile; parallel to disrupted and mounded in strike profile	Oblique clinoforms Progradational in dip profile; hummocky, progradational to mounded in strike profile; mounds more common in deep-water slope than in prodelta/slope on shelf
Lithofacies and composition	Hemipelagic slope facies in upper/mid-clinoform; submarine fans common in lower clinoform; generally calcareous clay, silt and some sand (base of clinoform); clinoform deposited in deep water beyond shelf edge	*On shelf:* prodelta (upper) and shallow slope facies (mid-clinoform and lower clinoform); deposited on submerged shelf; composition generally terrigenous clay, silt and sand; sand concentrated in submarine fans at base of clinoform *Beyond shelf edge:* (1) prodelta and deep-water slope associated with shelf-margin delta; may be growth-faulted; clay, silt and sand (in basal submarine fans); and (2) deep-water slope associated with prograding neritic shelf supplied periodically by shelf deltas/fan deltas; clay, silt and sand (in basal submarine fans)
Geometry and structure	Lens-shaped slope system; poorly defined individual submarine fans and point sources; strike profile may intersect facies to define parallel to slightly mounded configurations; rarely affected by growth faults; represents low rate of sedimentation under relatively uniform sea level rise and/or subsidence rate	Complex fan geometry with apices at shelf-edge point sources; each submarine fan resembles a bisected cone; total slope system lens- to wedge-shaped; strike profiles intersect fans or cones to display complex mounds; seismic facies deposited rapidly relative to subsidence and/or sea level rise; highly unstable slopes associated with deep-water deltas (growth faults, roll-over anticlines)
Lateral relationships	Grades updip through shelf/platform edge facies into parallel/divergent shelf/platform (undaform) reflections; may grade downdip into basinal plain (fondoform) or mound/drape seismic facies; grades along strike to similar facies; may change landward to oblique facies	Terminates updip against base of delta platform or shelf/platform (undaform) facies and may grade downdip into basinal plain (fondoform), or mound/drape facies; may change basinward into sigmoid facies; grade along strike into mounded facies and locally submarine canyon-fill facies
Nature of upper/lower boundaries	Generally concordant at top and downlap (baselap) terminations at base; upper surface of outer or distal sigmoids may be eroded by submarine erosion and submarine canyons; eroded surface commonly onlapped by continental rise facies	Toplap termination at top and downlap (baselap) termination at base; may contain local or minor submarine erosion/onlap sequences; outer or distal oblique clinoforms commonly eroded by submarine erosion and submarine canyon cutting; eroded surface generally onlapped by continental rise facies
Amplitude	Moderate to high; uniform	Moderate to high in upper clinoform; moderate to low in lower clinoform; highly variable
Continuity	Generally continuous	Generally continuous in upper clinoform; discontinuous in mid-clinoform and lower clinoform; may exhibit better continuity near base
Frequency (cycle breadth)	Broadest in mid-clinoform where beds thickest; uniform along strike	Broadest at top and generally decreases downdip as beds thin; variable along strike

Table 4: Mounded and Draped reflection configurations.

Properties of seismic facies	Depositional environments/Settings: Reefs and banks: SHELF/PLATFORM MARGIN, BACK SHELF PATCH REEFS AND PINNACLE/BARRIER REEFS	Submarine canyon and lower slope: PROXIMAL TURBIDITIES, SLUMPED CLASTICS	Hemipelagic clastics: PROXIMAL BASIN AND LOWER SLOPE
Reflection configuration	Mounded, chaotic, or reflector-free; pull-up or pull-down common	Mounded; complex and variable	Parallel; mirrors underlying surface
Lithofacies and composition	Shallow-water carbonate biogenic buildups; may or may not exhibit reef-forming framework	Sand and shale submarine fans; complex gravity-failure fans or mounds; turbidity flow; other grain flows, submarine landslides/debris flows; clinoform/fondoform deposits	Terrigenous and calcareous clays (commonly alternating); pelagic oozes; deposition from suspension plumes and nepheloid clouds; fondoform deposits
Geometry and structure	Elongate lens-shaped (shelf/platform edge and barrier reefs); elongate to subcircular lens-shaped (patch and pinnacle reefs/banks); form on stable structural elements	Irregular fan-shaped to mounded geometry; common but not restricted to unstable basins	Sheet to blanket geometry exhibiting drape over underlying surface; common in deep, subsiding basins
Lateral relationships	Shelf/platform edge facies grade updip into parallel/divergent shelf/platform facies; grade downdip into talus and sigmoid clinoform facies; patch reef/bank facies grade updip and downdip into parallel/divergent shelf/platform facies; pinnacle and barrier facies grade downdip into talus clinoforms and to basinal plain (fondoform) facies	May grade shelfward into progradational clinoforms (normally oblique), canyon onlap fill, or pinch out against eroded slope; may grade basinward and laterally into basinal plain (fondoform); onlap fills or drapes	Commonly grades laterally or basinward into basinal plain (fondoform) facies; may grade shelfward into submarine canyon onlap fill; may onlap eroded slope
Nature of upper/lower boundaries	Upper surface concordant or may be onlapped by flank reflections; basal surface concordant, baselapping, or may overlie clinoform toplap; pull-up or pull-down of basal surface common	Upper surface commonly erosional and onlapped, baselapped, or concordant (with drape); basal surface irregularly baselapping; may appear concordant (low resolution), or may onlap (mounded onlap fill)	Upper surface commonly concordant, but may be onlapped or baselapped; basal surface generally concordant but may onlap eroded mound or slope
Amplitude	High along boundaries; may be moderate to low internally; commonly reflector-free	Variable; generally low; some higher internal amplitudes may be thin hemipelagic drapes	Low to moderate; some high-amplitude reflections (well defined on high-frequency, shallow data)
Continuity	High along boundaries; internally discontinuous to reflector-free	Discontinuous to chaotic	High
Frequency (cycle breadth)	Broad; cycle may diverge into massively bedded buildup	Highly variable; commonly narrow	Narrow, uniform

Table 5: Onlap and fill reflection configurations.

Properties of seismic facies	Depositional environments/Settings: Coastal (paralic) onlap facies	Continental rise: SLOPE-FRONT FILL AND ONLAP CLASTICS	Submarine canyon-fill deposits	Other deep-water fill deposits: MOUNDED, CHAOTIC, STRUCTURALLY ACTIVE BASINS
Reflection configuration	Parallel; coastal onlap	Parallel/divergent; platform or shelfward onlap	Parallel/divergent; landward and lateral onlap	Parallel/divergent; chaotic, mounded onlap
Lithofacies and composition	Delta/alluvial plain and medial fan delta sands and shales; supratidal clastic/carbonate facies; rarely beach/shoreface clastic facies	Sand and shale deposited in submarine fans by turbidity flows; hemipelagic terrigenous/calcareous clays; distal pelagic oozes	Sand and shale deposited by turbidity flow in submarine fans near base; hemipelagic and neritic shale/calcareous clays in middle and upper sequence, respectively; locally	Sand and shale deposited by turbidity flow in submarine fans; hemipelagic terrigenous/calcareous clays; pelagic oozes; locally proximal turbidites
	angular	eroded slope (and commonly outer shelf); may show baselap basinward against mounds or bathymetric highs	lapped by prograding prodelta and slope facies; basal surface onlaps updip and laterally; baselap onto basin floor rarely observed	forms; basal surface onlaps in all directions
Amplitude	Variable; locally high but normally low to moderate	Variable; hemipelagic facies moderate to high; clastics low to moderate	Variable; generally low to moderate	Variable; generally low to moderate
Continuity	Low in clastics; higher in carbonate facies; decreases landward	Moderate to high; continuous reflections in response to hemipelagic facies	Variable; generally low to moderate	Variable; poor in chaotic or mounded fill; high in low-density turbidites and hemipelagics
Frequency (cycle breadth)	Variable; generally moderate to narrow	Narrow; uniform	Variable but generally narrow may contain coarse proximal turbidites	Variable; commonly narrow; may increase breadth toward axis of fill
Geometry and structure	Sheetlike or tabular; uniform subsidence during deposition; periodic tilting and erosion; deposited near basinal hinge-line during subsidence and/or sea level rise	Wedge-shaped lens; may be fan-shaped or lobate in plan view; slow subsidence	Elongate; lens-shaped in transverse section; may bifurcate updip; pinches out updip; slow subsidence	Variable lens-shaped; commonly irregular; reflects bathymetric configuration of structural depression; slow to rapid subsidence
Lateral relationships	Pinches out landward; grades basinward into lower delta plain, distal fan-delta, or shelf/platform facies; may grade laterally into marine embayment facies	Pinches out updip; grades basinward into basinal plain or hemipelagic drape facies; continuous laterally for tens of kilometers	Pinches out updip and laterally; grades downdip into continental rise mounded turbidites, or large submarine fans	Pinches out in every direction
Nature of upper/lower boundaries	Upper surface commonly tilted, eroded, and onlapped by similar deposits; base of facies onlaps unconformity, commonly	Upper surface commonly baselapped by prograding clinoforms; basal surface onlaps updip against	Upper surface may be concordant with overlying shelf or platform reflections or commonly base-	Upper surface may be concordant with hemipelagic drape or baselapped by prograding clino-

1.8.3 Seismic Lithology Analysis

Geological concepts have been applied to seismic data by constructing a seismic cross section, calculating reflection divergences and discontinuities to map stratigraphic pinchouts and reefs (Jasinki, 1957, Cartwright et al., 1993). The application of seismic data in lithology identification is thus imperative; it is centered on extracting information about the properties, geometries and distribution of rocks and fluids, and the identification of geometries of reflection patterns, especially reflectors with a high angle geometry (offlap). While the offlap patterns suggest a shelf –break, seaward of the depositional coastal break is deeper water (Vail, 1987). The calibration of seismic reflection patterns with well-logs ensures accurate prediction of lithologies in sedimentary basins.

As a result of advancement in research centered on extracting information about lithology and fluid properties, analysis of variations in seismic reflection characteristics and amplitudes led to the concept of Direct Hydrocarbon Indicators (DHI'S). The bright spot principle is primarily dependent upon contrasts in acoustic impedance, whereby an impedance contrast along a particular reflector, specifically along the gas and water contact may result into a 'bright' spot, thereby suggesting a gas charged reservoir. Various empirical and deterministic models have been applied to model this subsurface anomaly; variations in angle of incidence of seismic on a reflector because of different offsets often lead to variations in amplitude and phase along the reflector.

The most prominent seismic attributes being used in lithology and fluid analysis are AVO, Impedance inversion and Frequency spectra decomposition (Iso-Frequency). AVO has been widely used to identify gas-bearing sands, an example of this is in Sacramento Valley, California (Ostrander, 1984). There are however limitations of AVO application: basalts could display as bright spots on a seismic section and could thus be misinterpreted as gas bearing sands in sedimentary basins. This ambiguity can be mitigated by the determination of poisson's ratio of the target of interest.

1.9 Some Seismic Anomalies of gas presence and escape (evidences of Tertiary Migration).

Gas presence in sedimentary basins may be due to the activities of bacteria on organic matter or the influence of pressure and temperature in the generation of gas from a matured source rock (Davis, 1992). Distinguishing between thermogenic gas and biogenic gas is complex as thermogenic gas could be encountered at a very shallow depth. There have been evidences of thermogenic gas trapped at shallow sedimentary layers after migration from deep seated sedimentary layers (Rice and Claypool, 1981). In this instance, controversy as to the source of the gas is solved by an application of isotope geochemistry to "finger print" the gas to determine the source of the gas. There are seismic anomalies associated with gas presence and escape in the subsurface. These are highlighted below.

1.9.1 Pockmarks

These are surface expressions on the sea bed of a sedimentary basin, mostly identified as rimmed circular expressions on seismic section where reflections are faint (Figure 1.5). It is very common at the Dutch section of the North Sea (McQuillin and Fannin, 1979). They are created by sudden or periodical continuous escape of gas and are commonly associated with the presence of carbonate-cemented sandstones (Judd, 1990). King and McLean (1970)., MacQuillin and Fannin (1979) argued that the most common sources of pockmarks are either from an underlying petrogenic source or formed by the decay of organic matter in the sediments as biogenic gas.

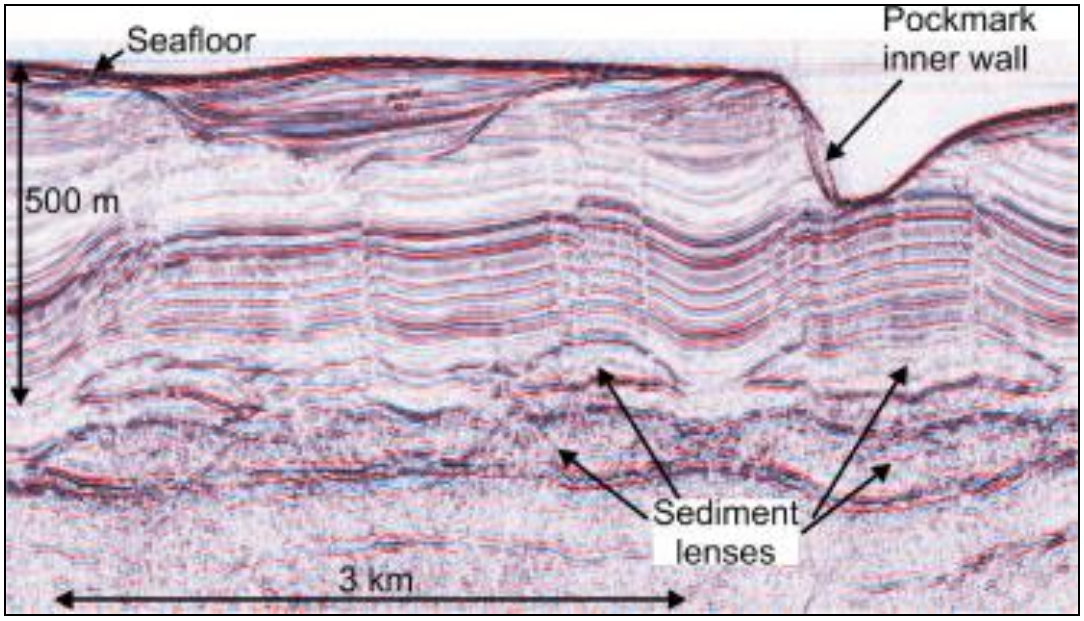

Figure1.5: Showing the occurrence of a pockmark in the Dutch North Sea. http://science.dodlive.mil/2013/06/16/nrl-reveals-absence-of-greenhouse-gas-emissions/

1.9.2 Bright Spot

An indicator of gas presence in the sedimentary basin is an occurrence of a bright spot on the seismic section. Bright spots are referred to as a phenomenon of strong increase in acoustic impedance contrast at the top of a reservoir filled with hydrocarbon and corresponding anomalously high amplitude (Figure1.6). If the reservoir is thick enough, it is usually accompanied by underlying high amplitudes of opposite phase caused by the impedance contrast at the oil-water interface (flat spot). The bright spot phenomenon of identifying gas presence in the reservoirs has been applied in the North Sea where bright spots identified above salt dome structures in the upper Pliocene-Pleistocene section are large enough to be of economic interest (Cross and Lessenger, 1988). This phenomenon is common in most clastic sedimentary basins, particularly in an unconsolidated clastic sedimentary rock.

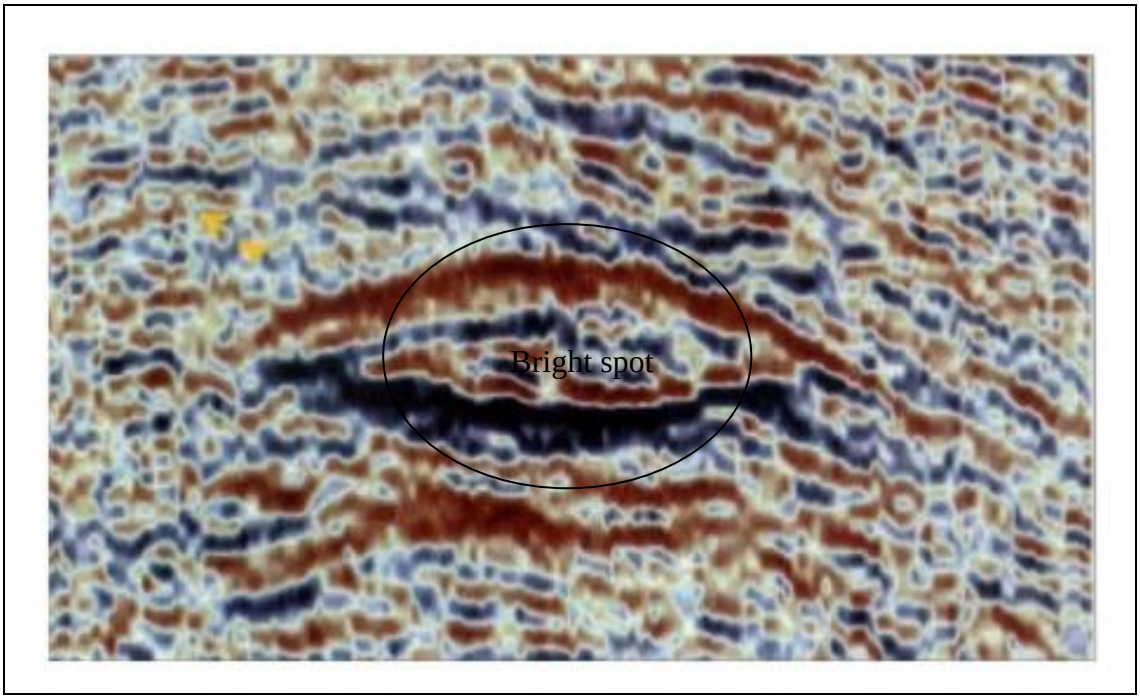

Figure 1.6: A seismic section showing bright spot from Nile Delta, Egypt. Red amplitude represents the top of gas reservoirs and blue represents the base. Modified from Van Dyke (2011).

1.9.3 Gas Chimneys

Gas chimneys in hydrocarbon migration are often described as an indication of gas escape and -leakage within the sedimentary column and are associated with vertical disturbances in seismic data that are interpreted as the upward movement of fluid or free gas. Most of the vertical disturbance is characterised by low seismic amplitudes (velocity push down) and low coherency because the presence of gas in pore spaces of sedimentary rocks changes the acoustic properties of the rock (Figure 1.7). Gas chimneys can be a pointer to hydrocarbon migration pathways when identified accurately on the seismic section, the presence of gas chimneys along faults particularly can indicate that the faults are open or have been opened for a time, in which case fluids can migrate through the faults. An example of this is in the 3D seismic survey in block F, Dutch section of the North Sea where observed gas chimneys are related to a fault running from an associated underlying salt dome up to the sea bed. This fault also serves as the migration pathway into shallow areas (Cross and Lessenger, 1988).

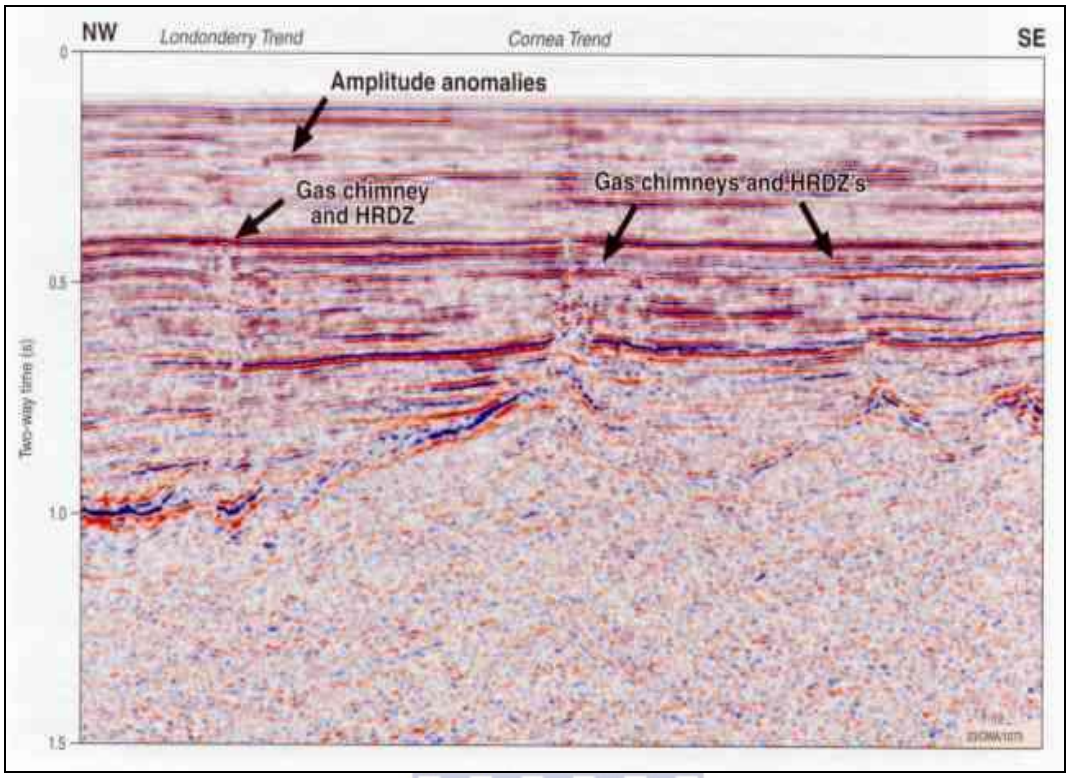

Figure 1.7: Highly localised gas chimneys in Yampi Shelf, Browse basin, O'brien et al (2005).

1.9.4 Mud Volcanoes

This is a common feature of gas escape on the sea floor alongside diapirs, pockmarks, pipe structure and gas hydrates (Kopf, 2003). It occurs as a mixture of argillaceous material, brine and gas which often builds up pressure and causes upward movements which are expressed as a vent on the sea floor; sizes range from millimetres to kilometres in diameter. The occurrence of mud volcanoes is controlled by many factors which include but are not limited to tectonic activity, sedimentary loading due to rapid sedimentation, the existence of thick, fine-grained plastic sediments and continuous hydrocarbon accumulation. A strong relationship has been established between the world-wide mud volcano distribution and industrial oil and gas concentrations (Tinivella and Giustiniani, 2012). Although this relationship is not valid for many mud volcano areas, in particular for modern accretionary complexes, it has been established that present-day or recent active oil and especially gas generation are characteristic features for all of them.

1.10 Pitfalls and Mitigations of DHI In Predicting Hydrocarbon presence

Bright, dim and flat stops are groups of seismic anomalies referred to as DHI's. The presence of gas is sometimes associated with the presence of high-amplitude reflections known as '' bright spots' and an indication of gas sands in a clastic basin (Allen and Peddy, 1993). A "Dim Spot" is a local decrease in reflection amplitude common in low porous sands while "Flat Spots" are indicators of fluid contacts due to acoustic impedance contrast emanating from changes in fluid density and lithology velocity (Van Dyke, 2011). The identification of flat spots is easier in a tilted reservoir (Allen and Peddy, *op.cit*), and is associated with fluid contacts in the reservoir. There are have been reports on the pitfalls on the application of DHI's as a tool for predicting possible drilling targets in clastic basins. This is because the presence of oil and gas in reservoirs can produce acoustic signals which are either obvious or subtle, depending on the rock physics, signal-noise ratio, accurate processing, and seismic data acquisition parameters. The major pitfall of bright spot is it similarity with the amplitude displayed by basaltic volcanics, therefore, the possibility of mis-identification is high. Dry holes drilled on bright spots have encountered wet sands, lignites, carbonates and volcanics (Allen and Peddy, 1993). One of the pitfalls of using flat spots in predicting hydrocarbon accumulation is the possibility of identifying diagenetically related flat spots for BSR (gas hydrates) and fluid contacts (flat spot) on the seismic section (Pegrum et al., 2001). These pitfalls as highlighted above, can be constrained by the applications of AVO analysis on pre-stack seismic data, seismic impedance inversion, instantaneous frequency or Spectra frequency decomposition. With these, deductions on the rock physics transforms of the seismic intervals can be made, consequently making prospects derisking feasible. With the application of these methods, the ambiguity of a true and false DHI could be resolved.

1.11 Seismic Attribute analyses

Seismic attributes are components of seismic data that can be computed, measured or implied from the seismic data (Subrahmanyam and Rao, 2008). The concepts of seismic attributes have developed over time as the technology of hydrocarbon exploration and production improves. With advancement in technology, especially 3D visualization, there have been increases in the number of attributes that can be tested on seismic sections. The varieties of seismic attributes have become tools for geologic prediction in recent years and thus, widely applied in the oil and gas industry (Chopra and Marfurt, 2006) .These attributes require systematic classification and analyses to determine the rock properties they can measure. Cosentino (2001) lists the properties that can be measured from analyzing seismic attributes as: structure (horizon depth, reservoir thickness, faults, etc.) internal architecture (heterogeneity), petrophysical properties (porosity, permeability, etc.) and hydrocarbon properties.

Analysis of seismic attributes is dependent on the properties to be computed or measured. Taner et al (1994), divide attributes into two main categories; which are physical and geometrical attributes. This can be further divided into pre-stack and post-stack attributes. The different classifications of attributes are discussed below.

1.11.1Physical Attributes

This is related to the attributes generated from seismic data as a result of the magnitude of the wave envelope (amplitude) and directly proportional to the acoustic impedance contrasts, which is a function of elastic rock properties of rock formations. Therefore, the quantitative and qualitative computation of sedimentary bed thickness, wave scattering and absorption, lithology and fluids present becomes feasible.

1.11.2 Geometrical Attributes

These are attributes that are computed based on the reflection and transmission patterns of the bedding surface, it gives specific information on the dip and azimuth of stratigraphic surfaces and can be used to establish a spatial and temporal relationship among other attributes like absorption, Root Mean Square (RMS), average and interval velocity, and dispersion. The concepts of AVO and seismic impedance,

frequency decomposition inversion, are classified as a geometrical attributes because they are dependent on the acoustic reflection of the bedding surface and attenuation by fluid contents respectively.

1.11.3 AVO Analysis

Amplitude **V**ersus **O**ffset analysis is one the most common seismic attributes used in understanding secondary migration mechanism because of its common application in identifying gas or brine charged sands. Its analysis is based on variation in seismic reflection amplitude with change in distance between the source and receiver of acoustic signals. The concept of AVO analysis was pioneered by Zoeppritz (1919), further linearization of Zoeppritz equation by Bortfield (1961), Aki and Richards (1980) enhanced the application of AVO in hydrocarbon exploration. AVO was proposed as a technique for validating seismic amplitudes anomalies associated with gas sands (Ostrander, 1984) and can also provide substantial exploration and development information; the concept of AVO is hinged on studying normal incidence reflection as a function of angle and the contrast in Poisson's ratio at the reflection interfaces. The Zoeppritz equation justifies the AVO analysis by illustrating that the energy reflected from elastic boundaries do vary with angle of incidence of incident wave.

Seismic data acquisition and processing are key to the principle of AVO analysis, the continuous acquisition of seismic data is based on changes made on the distance between the source and receiver (offset). These changes occur with corresponding changes in the angle of incidence of acoustic waves at the lithologic boundary. This is the concept which AVO is based on. The gathering of seismic traces from the receiver is sorted into pairs of source and receiver combinations that have different offsets but same common reflection points between each source-receiver pair. The collection of the traces is known as common mid-point (Chiburis, 1987). During seismic processing, stacking is performed to enhance structural and stratigraphic interpretation; these traces are summed to produce single average trace. However, stacking reduces gathering of information as regards amplitude variation with offsets because it causes different fluids and lithology to have identical amplitudes while

their AVO signatures are completely different. Therefore, utilizing processed seismic data limit the application of AVO in distinguishing between fluid content and lithology (Chiburis, 1987).

Explorationists have identified different characteristics and scenarios for gas sands reflections and that AVO can be useful for analyzing reflections that do not necessarily correspond to bright spots on seismic data. Rutherford and Williams (1989) introduced the three-fold classification of AVO based on reflection coefficient at the interface between shale and underlying gas sands. This classification is based primarily on the Poisson ratio values of encasing shale relative to gas sands. Therefore, the AVO response of all gas sand classes would be characterized by increase in negative reflection coefficient with increasing offset. Castagna and Swan (1997) also classified the gas sands scenario based only on graphical plots between AVO intercept and gradient. The classes and scenarios involved are high impedance sands (class 1), near-zero impedance contrast sands (class 2) and low impedance sands (class 3).

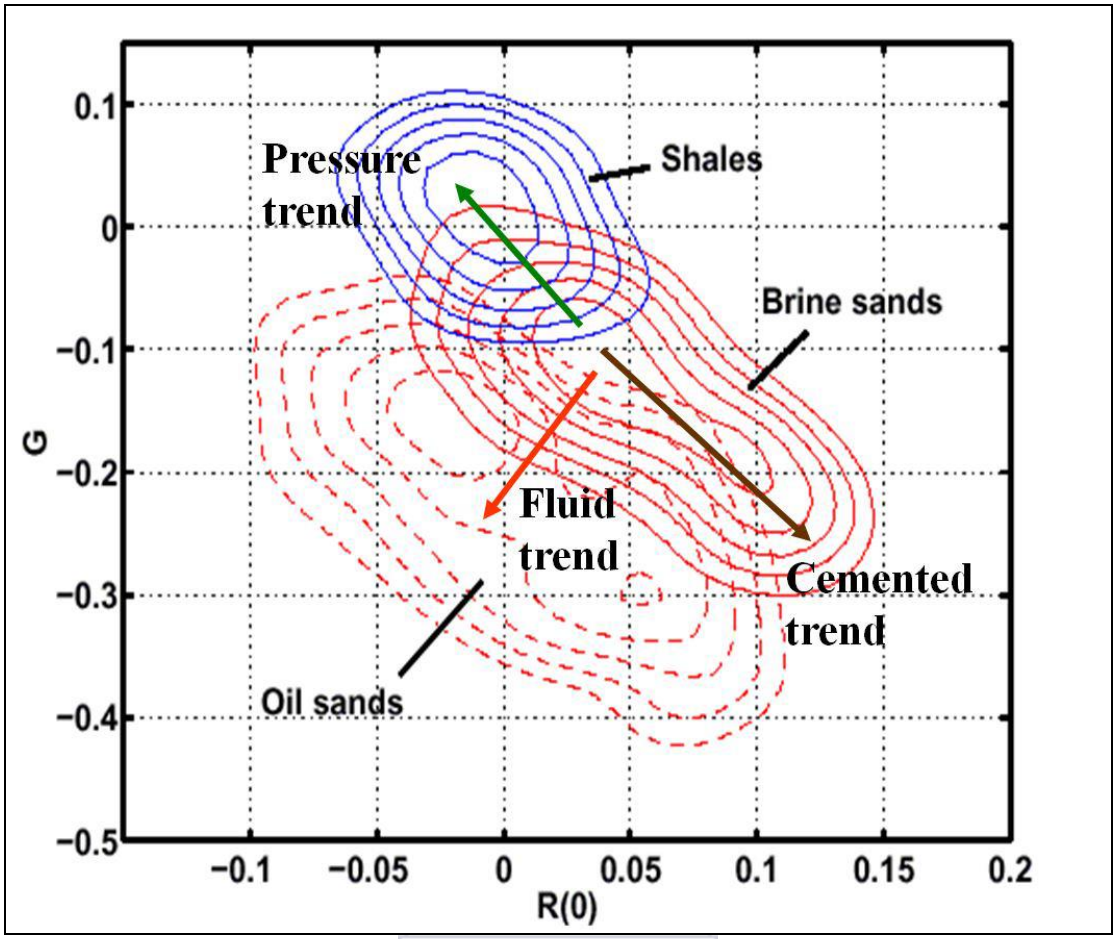

Figure 1.8: Different AVO trends occurring in an intercept-gradient cross-plot. Modified version of Avseth (2011).

1.11.3 .1 Class One

A class one sand has higher impedance than the encasing medium, usually shale. A shale-sand interface for these sands has positive reflection coefficient (Rutherford,1989). It is common in highly compacted sands. The positive reflection coefficient of high-impedance sand is positive at zero offset and initially decreases in magnitude with offset. The gradient for class 1 sand is usually greater than that of class two sands and class three. Gradient is the rate of change of magnitude with offset, it can decrease as reflection coefficient decreases and also, the poisson ratio. The gradient can change polarity if adequate angle/offset range is available (Figure 1.9).

1.11.3.2 Class Two

Class two sand has nearly the same impedance as the encasing material. Such sand is generally moderately compacted and consolidated. The zero offset reflection coefficients of class 2 sands are close to zero, significant fractional changes in reflectivity from near to far offset can occur, enhancing the identification of this sands, reflections do appear at large offsets when the reflection amplitudes rise above noise level (Figure 1.9.)

1.11.3.3 Class Three sand

Class three sands has a lower impedance than the encasing medium. Such sand is usually under compacted and unconsolidated with amplitude anomalies on stacked seismic data and have large reflectivity at all offsets. The gradients are usually significant but of lower magnitude than class 1 and class 2 sands since the normal incidence reflection coefficients are already negative. The amplitude do not change significantly from near to far offset. Therefore class three sands have a high amplitude that's is relatively flat with offsets (Figure1.9.)

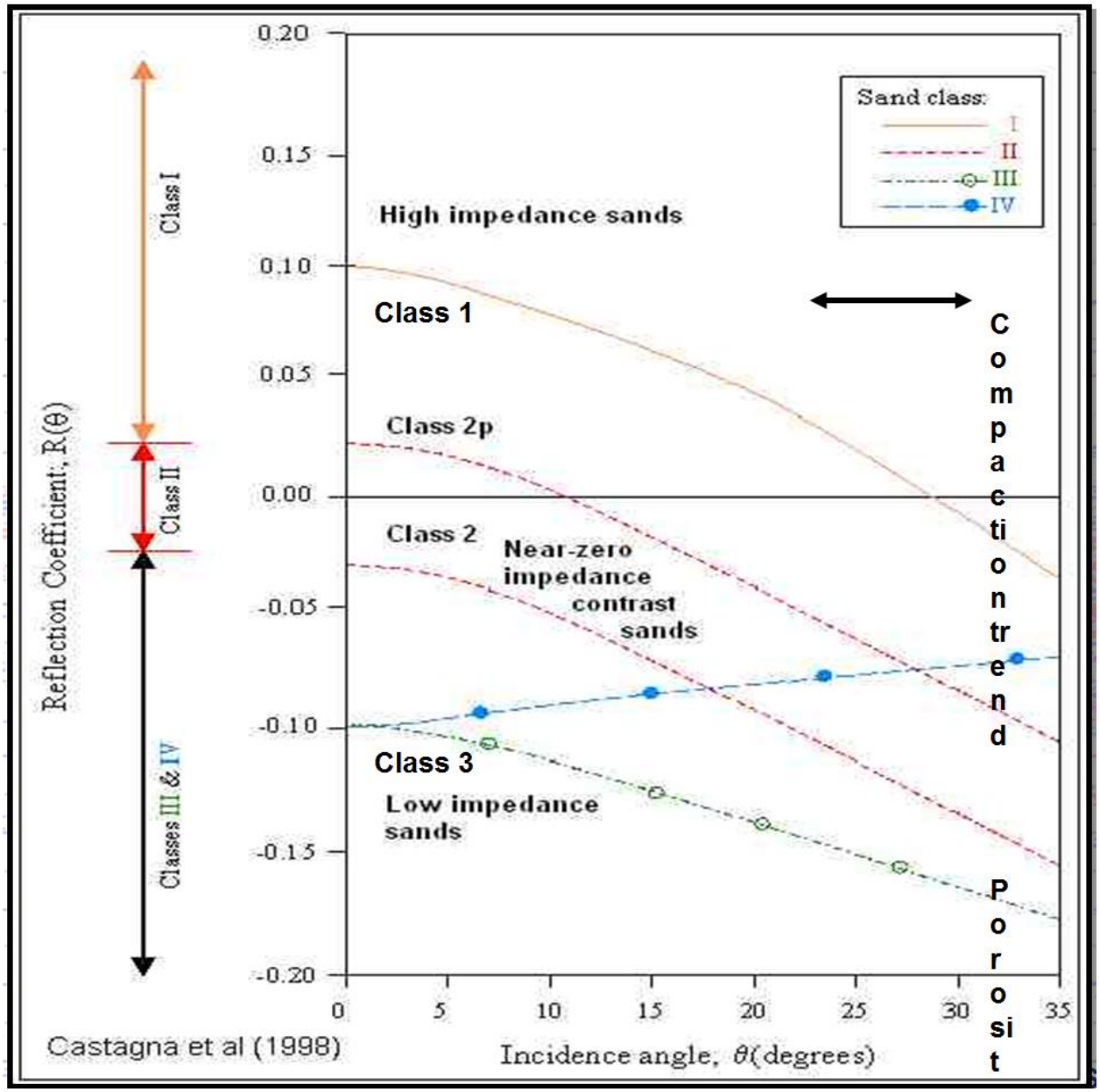

Figure1.9: Reflection Coefficients versus Angle of Incidence Plot for different gas charged sands scenario (Castagna et al.,1998).

1.11.4 Seismic Impedance and Frequency Inversion.

Inversion of seismic reflectivity data is aimed at converting conventional seismic reflectivity (interface property) into reflection coefficient and to impedance domain (Layered property) (Lindseth, 1979). It has developed over time as a complementary method in analysing conventional seismic datasets, and like other exploration concepts in the oil industry, seismic inversion has inherent uncertainties. Reducing these uncertainties meant the adoption of the seismic inversion concept should complement observations made from synthetics generated from well-logs.

The rationale behind this process was to build static reservoir models or establish the probability of hydrocarbon presence in the reservoirs (Cooke and Cant, 2010). The conventional seismic data has been used for structural and stratigraphic interpretations, however, the inversion of seismic data amplitudes is suitable for the description of internal properties of rocks (fluids type, porosity and lithology); therefore, it is an invaluable method for stratigraphic and reservoir characterisation. In contrast to AVO analysis which mostly utilizes pre stack seismic datasets for the delineation of hydrocarbon presence, the seismic inversion method utilizes pre-stack and post-stack seismic datasets.

The process of seismic inversion is complex without certain input models. For example, inverting seismic data into impedance domain will say less about the impedance change trends in the rocks, this is because seismic data do not record very low frequency data (Francis, 2006a). This inadequacy is addressed by the usage of different input models; Deterministic Inversion or Probabilistic Inversion. Stochastic Inversion, Forward Model and Geostatistical Model are all classified as either deterministic or probabilistic. The seismic trace is generated as a product of acoustic wavelet, earth's reflectivity and inherent noise. Deterministic model using AI property inversion concept on post stack datasets, is less complex than the pre stack seismic datasets (probabilistic model and stochastic inversion) because it outputs a blocky impedance layer model as opposed to the many-layered model output by probabilistic and stochastic inversion model. The genetic inversion model is constrained to a forward modelling process that estimates reflection coefficient from impedance contrast and subsequently convolved with the source wavelets. A limitation of seismic

inversion is that the genetic inversion/deterministic model utilizes high frequency and does not account for thin bed phenomenon in the subsurface, especially if the bed thickness is lesser than the tuning frequency (Cooke and Cant, 2010).

A deterministic model driven process involves inversion of post stack seismic data and subsequently tying up with well-logs. This enables the validation of the Seismic impedance model and establishes the relationship between the seismic wavelet and intrinsic properties of the rocks.

In addition, Frequency decomposition involves the decomposition of a seismic band into its individual frequency components by utilising **S**hort-time **W**indow **F**ourier **T**ransform (SWFT) or Continuous Wavelet Transform (Partyka et al., 1999; Sinha et al., 2005). These have proven to be successful in delineating zones of frequency variations caused by the presence of hydrocarbon (Castagna et al., 2003; Sinha et al., 2005). The major advantage of these methods is their unbiased application in detecting hydrocarbon presence on post-stack seismic data inversion, unlike AVO analysis which has bias for pre-stack seismic data.

1.12 Hydrocarbon Migration modelling.

The liberation of hydrocarbon from the source rock often moves vertically through the crust under the influence of subsurface pressure and geothermal gradient until it charges permeable rock layers capped with an impervious rock. Hydrocarbon migration through the carrier beds could also escape through the spill point and subsequently seeps to the surface. Hydrocarbon migration remains one of the least understood component of a Petroleum system, yet is very crucial in assessing both conventional and unconventional resources. Three major hydrocarbon migration mechanisms that have been documented include the generation and migration of hydrocarbon within a source rock unit which is termed primary migration. This mechanism is aided by pressure build - ups due to generation capacity of the source pods and subsequent fracturing of the rock. Another mechanism is the secondary migration process; this involves the movement of hydrocarbon from an active source rock pod into the reservoir unit or traps. The main driving force for secondary

migration is the vertical buoyancy force due to density contrast between petroleum and formation water, and according to Eppelbaum et.al., (2012),also the stratigraphic character of the carrier beds also plays a role. The third type of hydrocarbon migration mechanism is tertiary migration and is attributed mostly to effects of tectonics. It commonly occurs as a result of uplifting created by tectonic activities; this may cause the migration of already trapped hydrocarbon in a sedimentary basin to another area within the basin. The evidence of which is commonly in the form of gas escape features in the subsurface and the sea floor.

In modelling a primary hydrocarbon migration or charge system, the technology of Hybrid or flow Darcy model on the Schlumberger PETROMOD 2014© software environment is invaluable. It utilizes boundary conditions, thermal and maturation geochemical data of a source rock unit to simulate the generation and migration of hydrocarbons. The methodology involved in modelling primary and secondary migration processes is different. While primary migration processes could be modelled or characterised through simulation of hydrocarbon generation by using boundary conditions, secondary migration process is better studied by integration with the application of geophysical seismic attribute concepts because of the latter success in characterising fluid and rock properties. Modelling of secondary hydrocarbon migration process and its interaction with faults and stratigraphy is feasible by the application of seismic impedance inversion of frequency attributes. Therefore, the application of the seismic impedance deterministic approach and frequency attributes in modelling hydrocarbon presence in reservoirs or along faults should be complementary to simulation of hydrocarbon generation process.

The application of seismic attributes has been proven successful in characterising hydrocarbon migration and presence in carrier beds (Fatti et al., 1994, Madiba and Mcmechan, 2003, Farfour et al., 2015). In offshore Colombia, application of a seismic attribute (spectral frequency decomposition) has proven successful to understanding the extent of gas chimneys and the hydrocarbon migration pathways (Mayorgal et al., 2012). The integration of these approaches in modelling hydrocarbon migration pathways offers an alternative approach in constructing a hydrocarbon migration model with a better precision.

1.13 Geological controls on gas escape and migration pathways

Geological controls as mentioned in this study are classified into structural and stratigraphic features. The influence of geological controls on hydrocarbon migration pathways is well documented in the literature (Boyd et al., 2011, Lampe et al., 2012). Different rock units deposited as a result of influence of tectonics and stratigraphy could control hydrocarbon migration pathways; while a well compacted rock could serve as a barrier to migration, an unconsolidated rock unit could influence migration paths. An example of this is found in Bohai Basin, China, where sandy and conglomeratic facies mostly present in the northern graben flank area of the basin serve as stratigraphic conduits and provide possible migration pathways in the basin (Lampe et al., 2012).). Also over most of Bohai basin, faults - active at different times throughout basin evolution - add important additional conduits for petroleum migration, as well as acting locally as seals, depending on their surrounding lithology and their respective sealing or leaking properties through time (Lampe et al, 2012).

In addition, unconformity surfaces could be categorised as a stratigraphic feature and thus have been identified as a conduction system that controls lateral migration of oil and gas, provided the seals exists above the unconformity surfaces (Wu et al., 2012.The influence of structural features on hydrocarbon migration is documented by Eppelbaum, et.al., (2012). They suggested that faults can play a role within the phase of migration, acting as both conduit or seal, with some individual faults acting as both, along the fault trace through time.

Faults do play an important role by influencing the hydraulic property of the rocks, thus making the rocks a permeable carrier bed. Hydrocarbon migration in the subsurface does follow certain pathways which are determined by maturation of source rocks, stratigraphy of reservoir beds and structural configuration of the basin (Tainter, 1984). The understanding of these controls can be used as a predictive tool to understanding the distribution of hydrocarbon in a basin or within an exploration block (Tainter, 1984).

1.14 Source Rocks Organic Maturation and Generation Potentials.

Source rocks are organic-rich fine-grained sedimentary rocks which can produce hydrocarbons at the attainment of thermal maturity. Geochemical characterisation of source rocks to evaluate their organic and thermal potentials remains an important workflow in hydrocarbon generation and migration modelling. Therefore parameters like Total Organic Carbon (TOC), Temprature, Vitrinite Reflectance, Maximum temperature for pyrolysis (Tmax), Hydrogen Index (HI), Pressure (P), and Oxygen Index (OI) are evaluated and put into perspective to determine the hydrocarbon generation potential of source rocks.

Source rocks are deposited through time and are affected by factors such as structural evolution, heat flow, paleo-temperature, depositional environment and stratigraphy of sedimentary basins. These factors have direct relationship with the parameters evaluated for determining hydrocarbon and generation potentials of source rocks and as a ‘rule of thumb’ are adequately considered when modelling of hydrocarbon generation and migration is carried out. Depositional environment affects source rock quality and potentials because different environments preserve organic matter differently. For example, organic matter in a lacustrine environment is likely to be oil prone because organic matter is well preserved in such environment. The preservation is caused by the halocline nature of lacustrine environments which allows bottom waters to be undisturbed by sediment transports and preserves organic matter better than other environments. This type of source rock is often richer in hydrogen than marine-prone source rocks, and depending on the thickness and geometry, will have more generation potential than source rocks found in other environments.

Also, by considering the effect of structural evolution, for instance, in rift basins, source rock quality is affected by unprecedented increase in thermal events and could contribute to maturity or over-maturity of source rocks. Furthermore, the effect of stratigraphy is defined by basin geometry and subsequent increase or slow rate of sediment burial and erosion. In addition, impact of geothermal gradient and thermal conductivity also plays a role in thermal maturation of source rocks.

There are different models of simulating hydrocarbon generation and migration. However, Hybrid Flowpath Migration Modelling on Petromod 2014 core system is most reliable because it has a unique numerical algorithm designed to factor in lithological facies, pressure gradient and basin topography and -geometry in the simulation process. Hence, it is a ray-tracing method to analyse simple buoyancy-driven flow to characterise the generation potentials and migration pathways of source rocks using parameters mentioned earlier to calibrate the prediction.

1.15 Forward Numerical Modelling Technique

Forward modelling involves the use of seismic data and well logs to produce geological models and simulate events in the earth subsurface. Inverse modelling, back-stripping modelling, stochastic modelling and forward modelling are techniques used in studying tectonics, and stratigraphic configurations of the earth subsurface. Depending on the event to be simulated, a particular modelling technique is applied. Inverse modelling has been used for thermal subsidence analysis of periods of lithospheric stretching in extensional basins and passive margins (McKenzie, 1978; Barton and Wood, 1984). Backstripping modelling is applied in decompaction; a process whereby older sediments are "removed" and younger sediments "restored" to allow burial history reconstruction (Peters et al., 2012). The current study adopts a forward modelling approach to simulate thermal histories of rocks and behaviours of petroleum system elements in space and time by constraining numerical data from the past to present day to represent evolution of rock properties through time. Uncertainties are associated with forward modelling techniques because of geological assumptions made, especially in frontier areas where there is sparse data (Kopf, 2003). Its application in frontier areas becomes a high risk because of limited data, hence observations and decisions cannot be made solely on it without integration with other approaches or techniques.

.

Chapter Two Regional Geology

2.1 An Overview

The Orange basin is situated along the South Atlantic margin and straddles the borders of Namibia and South Africa, and as a classic divergent passive continental margin, is an ideal recorder of detailed sedimentary deposit evolution (Barton et al., 1993). The tectonic evolution was as a result of the break-up of Gondwanaland, rifting and subsequent drifting apart of South American and African plates in the late Jurassic and early Cretaceous period (Figure 2.1). The breakup of Gondwanaland was initiated by extensional forces that started in the early Mesozoic. (Petroleum Agency Brochure, 2006).

Figure 2.1: The rift phase in the Late Jurassic – Lower Valanginian showing the breakup of Africa, Madagascar and Antarctica (modified from Broad, 2007).

This separation divided the South African offshore basins into three tectono-stratigraphic zones. The narrow passive margin with protracted rift phase history along the east coast is as a result of the drifting away of Madagascar and Antarctica. Due to limited sediment influx, only the Durban and Zululand basins contain denser sediments. To the S-E, the African plate is bounded by the Agulhas marginal fracture zone (Visser, 1998), a dextral transform margin that formed during the movement of the Falkland Plateau. Movement began in the early Cretaceous at the onset of drifting

and caused the truncation of structural trends such as the Permo-Triassic fold belt on the Jurassic- early Cretaceous graben and half graben complexes of the Bredasdorp, Pletmos and Gamtoos basins. The western coast of South Africa has the orange basin which is a tensional transverse fractured marginal zone that has undergone local displacement and displays major structural attributes; the columbine-Agulhas arch and adjacent continental margins. The divergent passive Orange basin is characterized by graben structures trending sub parallel to the coast line (Jikelo, 1999).

The basin is highly underexplored with relative ratio of 1 well drilled per 400km square. The sediment supply into the basin was sourced from a river system (Orange river) with a rivaling Okavango delta to the north of basin, the sediments are a mix of continental and volcanic sediments (Fatti et al., 1994). Olifant and Berg river systems have also sourced sediments for the Orange basin, but with a major influence in the Southern part of the basin (Brown et al., 1996).

The Orange River was responsible for the deposition of sand-rich sediments at high rates in the northern part of the region after 103Ma. The Olifants drainage system to the south (near Lamberts Bay) also contributed sediments along the Agulhas-Columbine Arch, between 117.5 and 103 Ma. The principal passive margin drifting phase in the southern proto-Atlantic Ocean was restricted in the basin by open marine conditions at 112Ma. The main drift phase begins and was marked by an unconformity recorded at 112Ma. There was deposition of at least 30 third-order postrift sequences during the Cretaceous (Brown et al., 1996). The total thickness of drift sequence is at least 8000 m within the Orange Basin depocentre.

Sedimentation probably started in the Kimmeridgian and Tithonian (152-154 Ma). The Cretaceous sediments in this basin range from continental in the East to deep marine in the West while the Tertiary succession of sediments mainly comprises of calcareous oozes and chemical sediments with a characteristically deformed thick wedge of sediment due to sediment loading and slope instability (Petroleum agency SA, 2006). Sand deposition was mainly as a result of a reworked delta front and marine storm channel bars, as well as wave action. The sands are generally well-sorted ranging in grain size from very fine to medium grained. Dominant occurrence of well laminated and massive, greenish sandstones are a major pointer to the presence of detrital glauconite which serves as an indication of prevailing marine conditions. The source rocks identified in the Orange basin include the late

Hauterivian- synrift source rock, Barremian to early Aptian source rock units and the source rock unit associated with the global Cenomanian-Turonian anoxic events (Barton et al., 1993). Campher (2009) modelled the maturity of the three source rock units in the Orange basin, and observed that the three source rock units can be linked to the three phases of development of the Orange basin: Pre rift, Synrift and Post rift. The Barremian-Aptian source rock units are thermally matured and currently producing gas with potentials for oil in the deeper part of the basin. The model also indicates that the younger Cenomanian- Turonian source rock is not over-mature and is presently in the oil window as inferred from the lower values derived from vitrinite reflectance.

The wells drilled in the Orange basin so far have targeted the reservoir units of the lower Cretaceous syn-rift fluvial and post-rift coastal and deltaic post depositional systems.

The sequence stratigraphy of sediments deposited in the Orange basin as documented by Dingle et al., (1983) suggested most siliciclastic sediments were continuously deposited during the Cretaceous and decreased gradually till Cenozoic. The Cenozoic depositional processes have not been well understood but it was dominated by mixed carbonates, siliciclastic and authigenic sediments. Shelf progradation was dominant in the early cretaceous, this was terminated during the upper Cretaceous when aggradation prevailed. The Cenozoic was characterised by basinward prograding sedimentary wedges.

2.2 Tectono-Stratigraphy

The tectonic evolution of this basin is characterized by north-south trending grabens, filled with late Jurassic siliciclastics, lacustrine sediments and volcanics marking the syn-rift evolution stage. The overlaying transitional stage (Cretaceous) above the late Jurassic succession is characterized by infill of fluvial red beds and is itself overlain by marine sediments. The drift succession contains mainly siltstones and clays with few sandstone interbeds (Gerrard and Smith, 1982). The three major tectonic phases that characterize this area are classified into Pre -, Syn- and post-rifts (Gerrard and Smith, 1982). Significant compressional tectonism occurred in the pre rift phase where high grade and low grade metamorphites dominate the southern part while the occurrence of granitic and alkaline intrusives dominates the northern part (Broad et al;

2007). The pre-rift rocks are overlain by a succession of Pre-Barremian synrift basic lavas within the central rift sequence and coarse continental clastic, fluvial and lacustrine sediments along with volcanics within the marginal rift basins (Barton et al., 1993). This is in turn overlain by a Barremian to Aptian succession of Post rift alternating fluvial and marine rocks that are deposited as a result of transgression and regression of sea level (Van der Spuy, 2003).

The sequences of sedimentary succession in the Orange basin are highlighted below;

- Barremian to early Aptian sediments are occasionally interbedded with basaltic lavas together with shales and sandstones of marine origin. Sandstones of Aeolian origin have been intersected in the Namibia portion of Orange basin, (Barton et al., op.cit).
- In the early to middle Aptian, there was extensive deposition of organic shale which may have been due to the prevalence of an anoxic environment which was caused by basin margin sag and rapid sedimentation rate.
- The Albian to Cenomanian time witnessed the deposition of fluvio-deltaic sandstones while the Cenomanian to Turonian period was characterized by aggradational deposits. Progadational deposits as a result of sea level regression were also found but to a lesser extent than the aggradational deposits (Broad et al., 2007).
- The Tertiary to recent successions of sediments are predominantly organic in nature containing chemical sediments with minimal presence of terriginous materials (Barton et al op.cit).

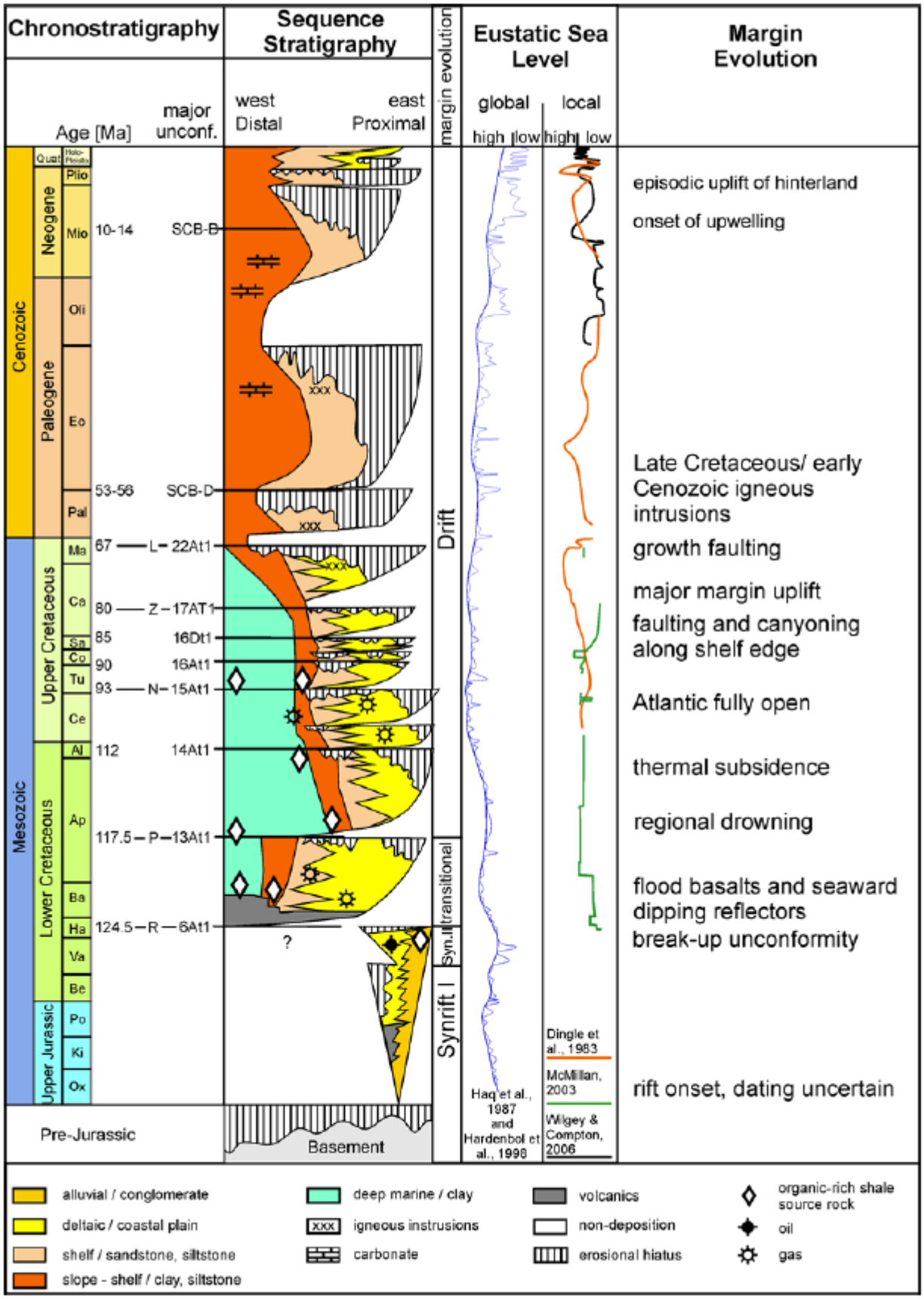

Figure 2.2: Chronostratigraphic and sequence stratigraphic diagram of the Orange Basin (Brown et al., 1996).

2.3 Brief description of the Orange Basin Petroleum Systems

A Petroleum system is defined as the systemic interaction of some geological configurations that could lead to commercial accumulation of hydrocarbons; it is a unifying concept that encompasses all of the disparate elements and processes of petroleum geology (Magoon and Beaumont, 1999). The appropriate timing of generation or formation of these elements is crucial to the accumulation of hydrocarbon in pools. The essential elements of petroleum systems that will be discussed about the Orange basin are source, reservoirs and traps.

2.3.1 Source Rock

Exploration activities so far in the Orange basin have suggested that there is evidence of active Barremian- Aptian wet gas source rocks and more recently Cenomanian and Turonian source facies (Aldrich et al., 2003).The strongest petroleum system is sourced from lower Aptian and Barremian source shales located at the depocentre of the Orange basin (Petroleum agency report 2008).There is occurrence of synrift oil-prone Hauterivian shale located within a half graben structure and trapped stratigraphically within lake shoreline sandstones interbedded with shale. An active petroleum system has been speculated to be present within the deep water areas of the basin, as seismic gas chimneys, seismic wipe-out zones, seafloor gas-escape features, bottom-simulating reflectors, flat and bright spot are all pointers to the likelihood of an active petroleum system (Jikelo, 1999).

2.3.2 Reservoir Rock

Fluvio-deltaic and lacustrine sandstones are the major reservoirs observed within the marginal rift basin while post rift successions of fluvio deltaic to deep marine turbiditic sandstones are also target reservoirs. In the Kudu area, Barremian Aeolian sandstones act as reservoirs while the reservoirs in the Ibhubesi area is of Albian – Cenomanian age. Sandstones deposited in the late Permian were dominantly volcanoclastic with poor reservoir qualities; Triassic sandstones tend to be more matured (Petroleum agency report, op.cit).

2.3.3 Traps

Compactional drape anticlines, stratigraphic pinch-out traps and inversion related closures are found within the synrift sequence and can act as major traps. Possible structural traps occur in the earlier sedimentary succession; structural plays have been identified in the deeper waters comprising of roll over-anticlines in the growth fault zone (Van der Spuy, 2003). A large number of possible traps, in the form of channel deposits and basin floor fans were in the basin in the Cretaceous and Tertiary (Roux et al., 2004).

2.4 An Overview of Paleo Stress History and structural styles in the South Atlantic Margin and Orange Basin.

Continental break-up and orogeny are tectonic events which are accompanied by specific stress fields. Therefore, different tectonic events with their specific stress orientations, yield different structural environments which have their specific implications for hydrocarbon prospectivity of sedimentary basins. These could be in terms of trapping mechanism, sealing mechanism or conduits for hydrocarbon migration pathways. The Orange basin is a rifted passive margin with volcanic activity and its evolution is well documented (Seranne and Anka 2005; Light et al., 1993 and Menzies et al., 2002). The evolution was characterized by a late Jurassic break up which was probably induced by the Tristan da Cunha hot-spot and followed by widespread flood basalt volcanism (Morgan, 1971). The evidences of which are prevalent in the voluminous Parana-Etendeka continental flood basalt provinces in Namibia. Continental rifting often follows flood basalt volcanism (Richards et al., 1989), this could have triggered the rifting of the continent which resulted into the opening of the South Atlantic Continental Margin. It is expected that the rifting of the continent leaves evidences of its faulting styles, most especially in the syn-rift sequences of the Orange Basin.

The presence of seaward dipping reflectors (SDRs) characterized with increased seismic amplitude could point to the volcanic nature of the Orange Basin (Menzies et al., 2002,). At the ceasing of rifting and subsequent deposition of post-rift sediments, there may be reactivation of existing syn-rift faults due to sediments loading which

may cause the propagation of their geometry into the Post-rift sequence. Faulting systems in the post- rift sediments are expected to have various orientations because of the different episodes of uplift and the consequent margin instability which happened in the late Cretaceous and Cenozoic. Aside from the faulting that may occur from stress release after uplift, there may be the occurrence of gravity tectonics induced faulting as a result of margin instability. The causes of uplift in major sedimentary basins are commonly related to a transient mantle plume associated with rifting (Menzies et al., 2002). The late Cretaceous uplift is believed to constrain extensional faulting to NE-SW orientation (Salomon et al., 2014), coupled with margin instability punctuated by gravitational failure in the post-rift sediments (de Vera et al., 2010).

There was an episode of a South-East compressive stress regime in the Late Santonian and Late Maastrichtian that affected Northern and Central Africa (Guiraud and Bosworth, 1997). While the Late Santonian compression may be related to the first generational compressional episode registered in the African-Arabian plate during the Alpine orogeny, the Late Maastrichtian episode may be due to counterclockwise rotational northward drift of Africa-Arabia into Eurasia (Guiraud et al., 2005; Guiraud and Bosworth, 1997). As a result of the compressive regimes highlighted above, there could be evidences of compressional faulting in southern Africa as a result of far field-stress transfer from northern and Central Africa. Consequently there could be evidence of faulting styles associated with both extensional and compressive stress regimes. This study will elucidate more on the stress regimes and the resultant faulting system and its implications on the hydrocarbon prospectivity of the Orange Basin.

Chapter Three: Materials and Methodology

3.1Materials

The datasets used for this study were obtained from the Petroleum Agency of South Africa (PASA), which is the agency charged with archiving all exploration data as it pertains to both onshore and offshore South Africa. Thirty-seven 2D seismic lines of different vintages were gathered based on strike and dip direction, and on their coverage of existing exploration wells (AE-1 and AO-1). Also, the only 3D seismic volume in block 1 with an estimated area of 1500km^2, was purchased and integrated with the 2D- lines by constructing a polygon on a PETREL 2013© workstation to define the study boundary. The 3D volume covers well AF-1. Digital geophysical wireline logs of Gamma ray, density, neutron and sonic were also collected for the three wells. Also the geological well-completion report, formation tops, geochemical well-reports, Engineering well-reports as well as velocity data were collected for the three exploration wells. Seismic data will be used to map major unconformities, mapping of faults and construction of a structural model. In addition, a suite of Geophysical logs will be used for lithology identification, correlation and estimation of rock properties such as porosity and impedance in the three wells. Source rocks organic maturation data and Pressure/ Temperature data will be extracted from the geochemical and engineering well-reports respectively for simulation and calibration purpose using PETROMOD 2014©.

3.1.1 Seismic Data used for this study.

Line Name	KM
A79-003	25
A80-002	23.2
A80-005	27.15
A80-014	16.2
A81-006	20
A81-008	23
A81-009	23
A82-008	68
A82-010	61
A83-068	20
A83-069	34
A84-007	17

A84-032	39
A86-002	30
A86-013	31
A86-014	39
A88-069	87
AA99-001	108
AA99-002	75
AA99-004	103
AA99-009	59
K80-001	137
K80-007	141
K80-009	123
K80-011	111
SA92-131	48
SA92-106	182.80
A83-004	16.47
AA99-002	75.40
A81-011	1360.00
A81-014	27.56
A78-001	118.00
A78-002	64.00
A78-006	92.00
K80-014	62.67
A83-006	33.73
A79-004	40.00
AF-2009 (3D)	1500KM^2

Table 6: Showing Wells used for this Study and Coordinates.

Wells	Long.	Lat.	Kb(m)	Water Depth(m)	Total Depth(m)
AE-1	16^o 17′ 37.244″ E	29^o 53′ 18.155″ S	25	180	4776
AF-1	16^o 11′ 58.4″E	29^o 11′ 27.7″ S	25	166	4003
AO-1	16^o 09′ 56.37″ E	28^o 56′ 54.59″ S	25	180	4605

3.2 Methodology workflow

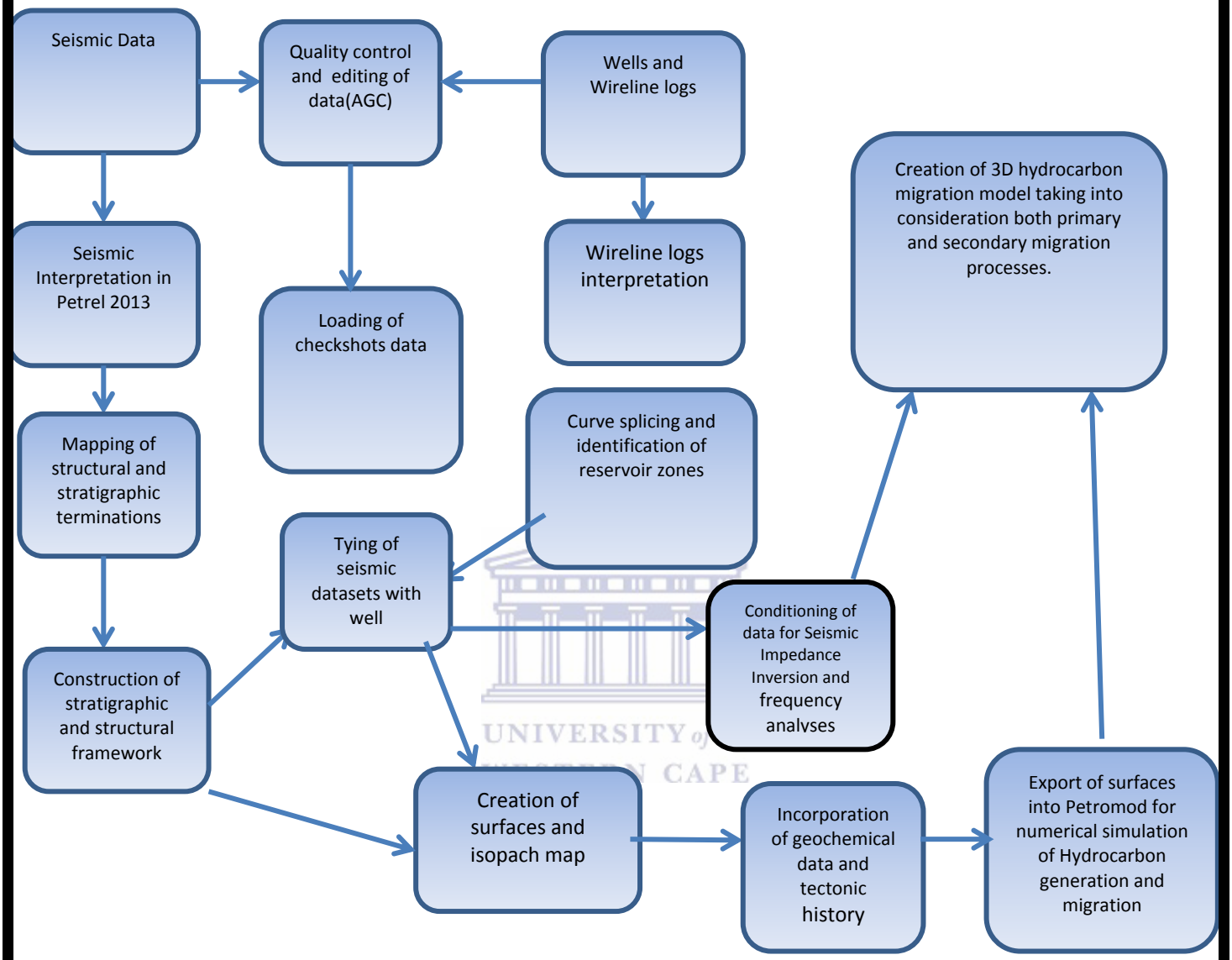

Figure 3.1: Methodology workflow.

3.2.1Seismic Data Loading.

Seismic data acquired and stored on electromagnetic tapes, is commonly saved in SEG-Y format, an universal saving standard created by the Society of Exploration Geophysicist to save seismic data on magnetic tapes. Prior to saving in SEG-Y format, acquisition of acoustic signals had to have been performed on either offshore basins or continental basin. Also, the mode of acquisition could have been in 2D or 3D and recently 4D depending on the spacing and arrangements of acoustic sources and receivers. The raw seismic signals acquired are then processed and saved in the SEG-Y format. Loading of seismic data and subsequent interpretation have been aided by advancement in technology; softwares have been developed to reduce projects' completion time, also to reduce risks associated with petroleum exploration. Kingdom (SMT) © and Petrel© are two of the most accepted industry softwares used for seismic data loading.

2D and 3D seismic data were received from PASA, the thirty-seven 2D seismic lines had different navigation files, hence merging the 2D lines with the navigation data is important. The SEG-Y utility tool box located in the utility tab of Petrel 2013© was used to achieve this (Figure3.2). All the project settings were done by using Universal Transverse Mercator (UTM) of WGS UTM 84 33S. This is the UTM for the Orange basin South Africa.

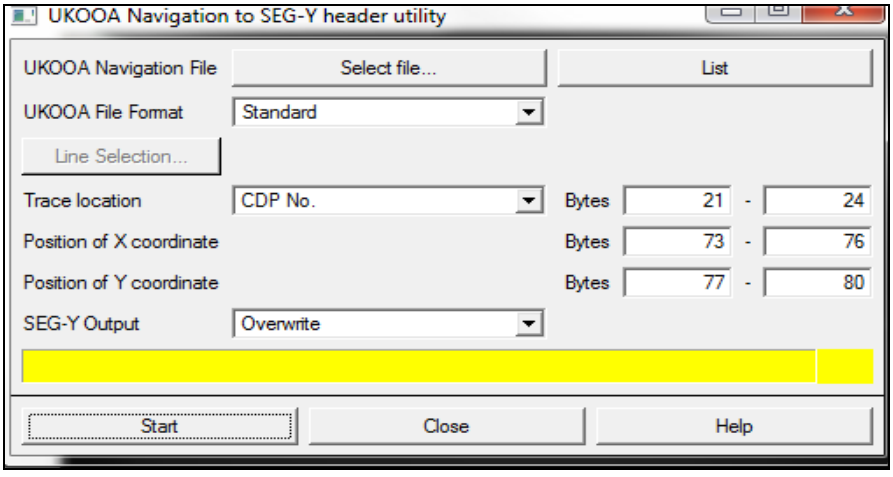

Figure 3.2: Showing the merging process of Seismic data and Navigation.

The 3D volume AF-2009 and thirty-seven 2D lines were loaded into Petrel 2013© workstation. The 3D volume has one well (AF-1) within its coverage while the two other wells falls within the 2D lines coverage.

3.2.2 Wells and Wireline Logs loading

The three wells drilled so far in block 1 were loaded into Petrel 2013© workstation by setting longitude and latitude coordinate parameters in x and y values. Subsequently, the different logs (in LAS format) available for each well were loaded into the global well-logs folder. Furthermore, editing of the logs (de-spiking) was performed in order to join different log runs together to make a complete run for each well (splicing). The well-intersection window on Petrel 2013© was used to display the wells and different geophysical logs associated with them.

3.2.3 Formation Tops and Check Shots Loading.

Formation tops are major chronostratigraphic tops of different formations encountered in the three wells. They were loaded through the spreadsheet option on Petrel 2013© in the format shown in Figures 3.3 and 3.4 respectively.

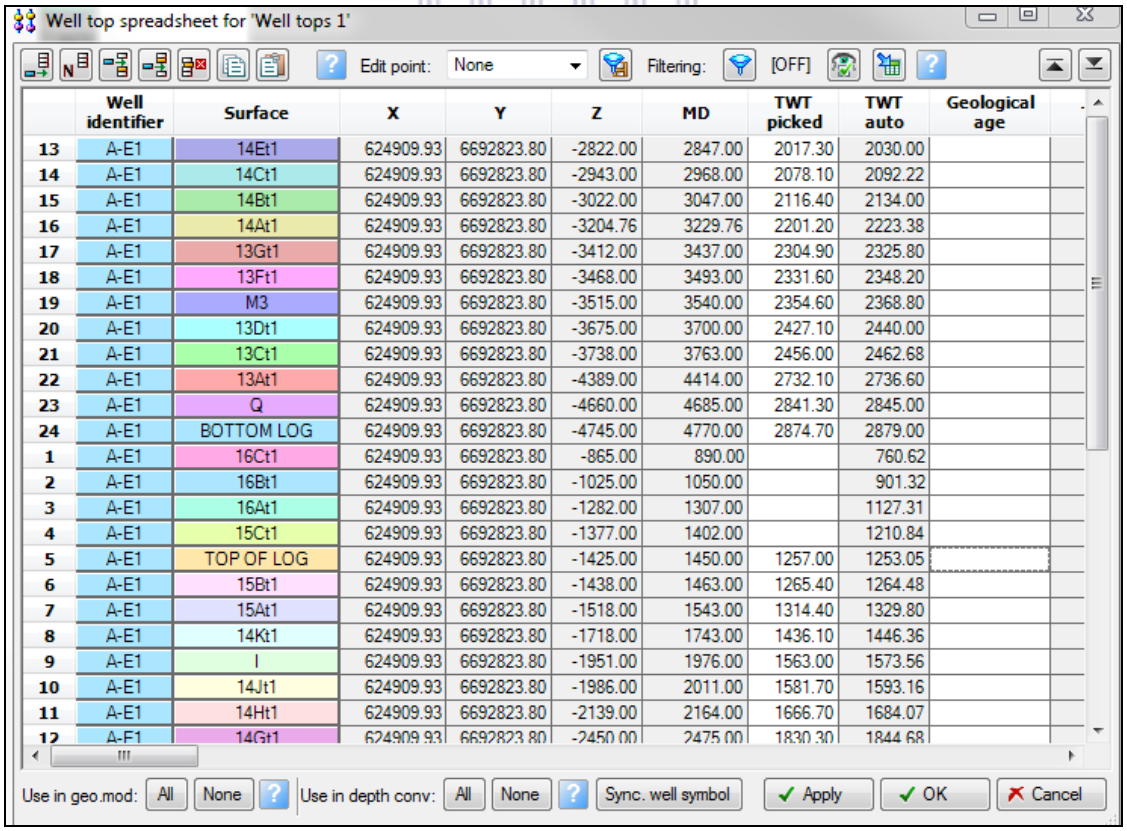

	Well identifier	Surface	X	Y	Z	MD	TWT picked	TWT auto	Geological age
13	A-E1	14Et1	624909.93	6692823.80	-2822.00	2847.00	2017.30	2030.00	
14	A-E1	14Ct1	624909.93	6692823.80	-2943.00	2968.00	2078.10	2092.22	
15	A-E1	14Bt1	624909.93	6692823.80	-3022.00	3047.00	2116.40	2134.00	
16	A-E1	14At1	624909.93	6692823.80	-3204.76	3229.76	2201.20	2223.38	
17	A-E1	13Gt1	624909.93	6692823.80	-3412.00	3437.00	2304.90	2325.80	
18	A-E1	13Ft1	624909.93	6692823.80	-3468.00	3493.00	2331.60	2348.20	
19	A-E1	M3	624909.93	6692823.80	-3515.00	3540.00	2354.60	2368.80	
20	A-E1	13Dt1	624909.93	6692823.80	-3675.00	3700.00	2427.10	2440.00	
21	A-E1	13Ct1	624909.93	6692823.80	-3738.00	3763.00	2456.00	2462.68	
22	A-E1	13At1	624909.93	6692823.80	-4389.00	4414.00	2732.10	2736.60	
23	A-E1	Q	624909.93	6692823.80	-4660.00	4685.00	2841.30	2845.00	
24	A-E1	BOTTOM LOG	624909.93	6692823.80	-4745.00	4770.00	2874.70	2879.00	
1	A-E1	16Ct1	624909.93	6692823.80	-865.00	890.00		760.62	
2	A-E1	16Bt1	624909.93	6692823.80	-1025.00	1050.00		901.32	
3	A-E1	16At1	624909.93	6692823.80	-1282.00	1307.00		1127.31	
4	A-E1	15Ct1	624909.93	6692823.80	-1377.00	1402.00		1210.84	
5	A-E1	TOP OF LOG	624909.93	6692823.80	-1425.00	1450.00	1257.00	1253.05	
6	A-E1	15Bt1	624909.93	6692823.80	-1438.00	1463.00	1265.40	1264.48	
7	A-E1	15At1	624909.93	6692823.80	-1518.00	1543.00	1314.40	1329.80	
8	A-E1	14Kt1	624909.93	6692823.80	-1718.00	1743.00	1436.10	1446.36	
9	A-E1	I	624909.93	6692823.80	-1951.00	1976.00	1563.00	1573.56	
10	A-E1	14Jt1	624909.93	6692823.80	-1986.00	2011.00	1581.70	1593.16	
11	A-E1	14Ht1	624909.93	6692823.80	-2139.00	2164.00	1666.70	1684.07	
12	A-E1	14Gt1	624909.93	6692823.80	-2450.00	2475.00	1830.30	1844.68	

Figure 3.3: Showing Well Tops Loader Interface on Petrel 2013 for this study.

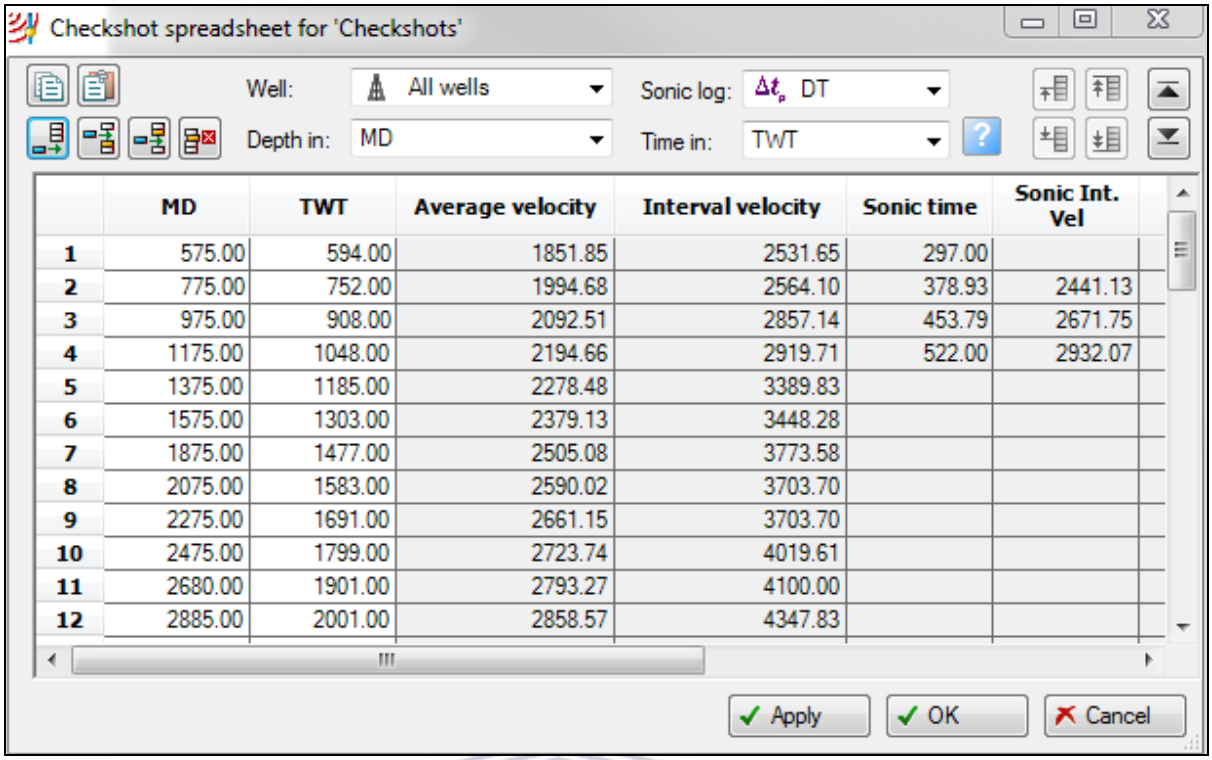

	MD	TWT	Average velocity	Interval velocity	Sonic time	Sonic Int. Vel
1	575.00	594.00	1851.85	2531.65	297.00	
2	775.00	752.00	1994.68	2564.10	378.93	2441.13
3	975.00	908.00	2092.51	2857.14	453.79	2671.75
4	1175.00	1048.00	2194.66	2919.71	522.00	2932.07
5	1375.00	1185.00	2278.48	3389.83		
6	1575.00	1303.00	2379.13	3448.28		
7	1875.00	1477.00	2505.08	3773.58		
8	2075.00	1583.00	2590.02	3703.70		
9	2275.00	1691.00	2661.15	3703.70		
10	2475.00	1799.00	2723.74	4019.61		
11	2680.00	1901.00	2793.27	4100.00		
12	2885.00	2001.00	2858.57	4347.83		

Figure 3.4: Showing Checkshots Loader Interface on Petrel 2013.

3.2.4 Seismic Data Interpretation

Identification of data phase and polarity is the first step in seismic interpretation. As phase and polarity determine seismic characters that are mapped during interpretation, it is imperative to condition seismic data to the choice of polarity (American or European Polarity) to be used. This mitigates the inherent pitfalls in picking high amplitudes as low amplitudes and vice-versa. The exact amplitudes of the seismic data may be scanned, and often Amplitude Gain Control (AGC), a seismic processing method, is applied to boost the amplitude of seismic data when the quality of resolution is low. In this study, AGC was applied to improve seismic data resolution. Various workflows used in carrying out detailed seismic interpretations are discussed below.

3.2.4.1 Fault Mapping

By using the insert option on the toolbar in Petrel 2013© workstation and activating the seismic interpretation tab under the process pane, the stage for faults mapping was set. The seismic section was displayed on the interpretation window and “inline” was used for the fault mapping. An inline is the section of a 3D seismic data that was acquired parallel to the direction of the marine streamer during the 3D seismic survey, therefore an inline represents a strike line of the seismic volume. In addition, a cross

line is the section that is acquired perpendicular to the direction of the marine streamer, therefore represents the dip line of the seismic volume. Each fault was picked along the inline section progressively across the survey (from 700 to 2990ms), also detailed mapping was carried out on the X-line section. Faults are planes of discontinuities where there is a movement of one fault block in relation to the other. These planes of discontinuities were identified and mapped at different inline and crossline positions until they were truncated. Faults were picked individually across the area polygon containing all the seismic datasets. In total, Eighty-six faults were mapped.

3.2.4.2 Seismic Horizon Mapping.

Mapping of seismic horizons requires a thorough process when compared to mapping of faults because seismic amplitudes could give false geological markers as a result of diagenetic modifications and the Basin's stratigraphy. Therefore, it is imperative that seismic data is tied to well-markers, which represent the ground truth. For a qualitative interpretation of major seismic horizons, the workflow highlighted below explains the process involved in mapping seismic horizons. The tasks highlighted below were completed to adequately map major seismic horizons, which by implications are major basin unconformity markers.

3.2.4.3 Seismic mis-tie analysis.

Mis-tie analysis of all 2D seismic lines was performed for vertical, phase and gain ties in this study (Figure 3.5). The importance of mis-tie analysis is to enable the balancing of phase and gains of seismic amplitude across different vintages of 2D seismic lines. Different vintages of seismic data are acquired by different methods at different times. Therefore, for a qualitative interpretation of seismic horizons, tying of seismic data acquired at different times should be performed to analyse phase and gain mis-tie.

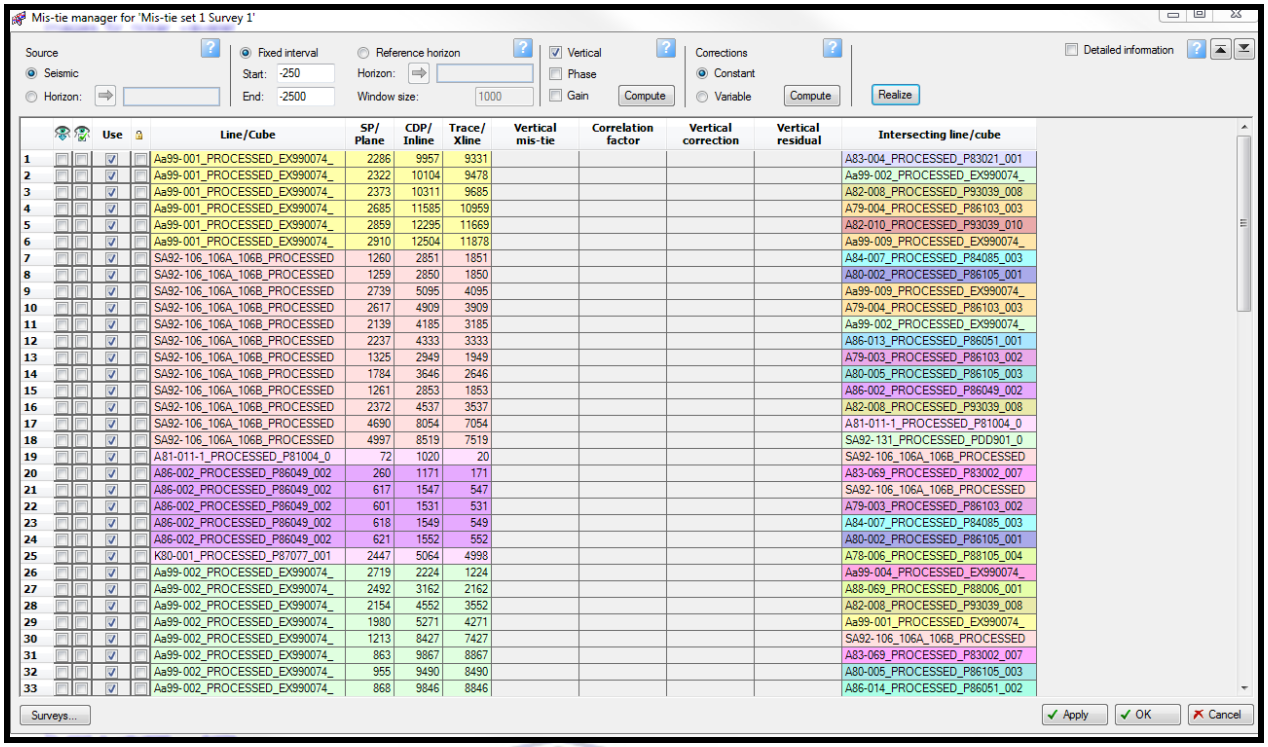

	Use	Line/Cube	SP/ Plane	CDP/ Inline	Trace/ Xline	Vertical mis-tie	Correlation factor	Vertical correction	Vertical residual	Intersecting line/cube
1	✓	Aa99-001_PROCESSED_EX990074_	2286	9957	9331					A83-004_PROCESSED_P83021_001
2	✓	Aa99-001_PROCESSED_EX990074_	2322	10104	9478					Aa99-002_PROCESSED_EX990074_
3	✓	Aa99-001_PROCESSED_EX990074_	2373	10311	9685					A82-008_PROCESSED_P93039_008
4	✓	Aa99-001_PROCESSED_EX990074_	2685	11585	10959					A79-004_PROCESSED_P86103_003
5	✓	Aa99-001_PROCESSED_EX990074_	2859	12295	11669					A82-010_PROCESSED_P93039_010
6	✓	Aa99-001_PROCESSED_EX990074_	2910	12504	11878					Aa99-009_PROCESSED_EX990074_
7	✓	SA92-106_106A_106B_PROCESSED	1260	2851	1851					A84-007_PROCESSED_P84085_003
8	✓	SA92-106_106A_106B_PROCESSED	1259	2850	1850					A80-002_PROCESSED_P86105_001
9	✓	SA92-106_106A_106B_PROCESSED	2739	5095	4095					Aa99-009_PROCESSED_EX990074_
10	✓	SA92-106_106A_106B_PROCESSED	2617	4909	3909					A79-004_PROCESSED_P86103_003
11	✓	SA92-106_106A_106B_PROCESSED	2139	4185	3185					Aa99-002_PROCESSED_EX990074_
12	✓	SA92-106_106A_106B_PROCESSED	2237	4333	3333					A86-013_PROCESSED_P86051_001
13	✓	SA92-106_106A_106B_PROCESSED	1325	2949	1949					A79-003_PROCESSED_P86103_002
14	✓	SA92-106_106A_106B_PROCESSED	1784	3646	2646					A80-005_PROCESSED_P86105_003
15	✓	SA92-106_106A_106B_PROCESSED	1261	2853	1853					A86-002_PROCESSED_P86049_002
16	✓	SA92-106_106A_106B_PROCESSED	2372	4537	3537					A82-008_PROCESSED_P93039_008
17	✓	SA92-106_106A_106B_PROCESSED	4690	8054	7054					A81-011-1_PROCESSED_P81004_0
18	✓	SA92-106_106A_106B_PROCESSED	4997	8519	7519					SA92-131_PROCESSED_PDD901_0
19	✓	A81-011-1_PROCESSED_P81004_0	72	1020	20					SA92-106_106A_106B_PROCESSED
20	✓	A86-002_PROCESSED_P86049_002	260	1171	171					A83-069_PROCESSED_P83002_007
21	✓	A86-002_PROCESSED_P86049_002	617	1547	547					SA92-106_106A_106B_PROCESSED
22	✓	A86-002_PROCESSED_P86049_002	601	1531	531					A79-003_PROCESSED_P86103_002
23	✓	A86-002_PROCESSED_P86049_002	618	1549	549					A84-007_PROCESSED_P84085_003
24	✓	A86-002_PROCESSED_P86049_002	621	1552	552					A80-002_PROCESSED_P86105_001
25	✓	K80-001_PROCESSED_P87077_001	2447	5064	4998					A78-006_PROCESSED_P88105_004
26	✓	Aa99-002_PROCESSED_EX990074_	2719	2224	1224					Aa99-004_PROCESSED_EX990074_
27	✓	Aa99-002_PROCESSED_EX990074_	2492	3162	2162					A88-069_PROCESSED_P88006_001
28	✓	Aa99-002_PROCESSED_EX990074_	2154	4552	3552					A82-008_PROCESSED_P93039_008
29	✓	Aa99-002_PROCESSED_EX990074_	1980	5271	4271					Aa99-001_PROCESSED_EX990074_
30	✓	Aa99-002_PROCESSED_EX990074_	1213	8427	7427					SA92-106_106A_106B_PROCESSED
31	✓	Aa99-002_PROCESSED_EX990074_	863	9867	8867					A83-069_PROCESSED_P83002_007
32	✓	Aa99-002_PROCESSED_EX990074_	955	9490	8490					A80-005_PROCESSED_P86105_003
33	✓	Aa99-002_PROCESSED_EX990074_	868	9846	8846					A86-014_PROCESSED_P86051_002

Figure 3.5: Showing 2D lines mis-tie Analysis on Petrel 2013.

3.2.5 Sonic Logs and Checkshots calibration.

Sonic logs measure the interval transit time of acoustic signals within the borehole and its calibration with checkshots were carried out as shown in figure 3.6. Datuming setting was done and the value was set at zero because the data for this study was acquired offshore. The importance of checkshots is to establish a Time-Depth-Relationship between seismic data and wells. A Time-Depth-Relationship was established between seismic data and the three wells present in the area of study.

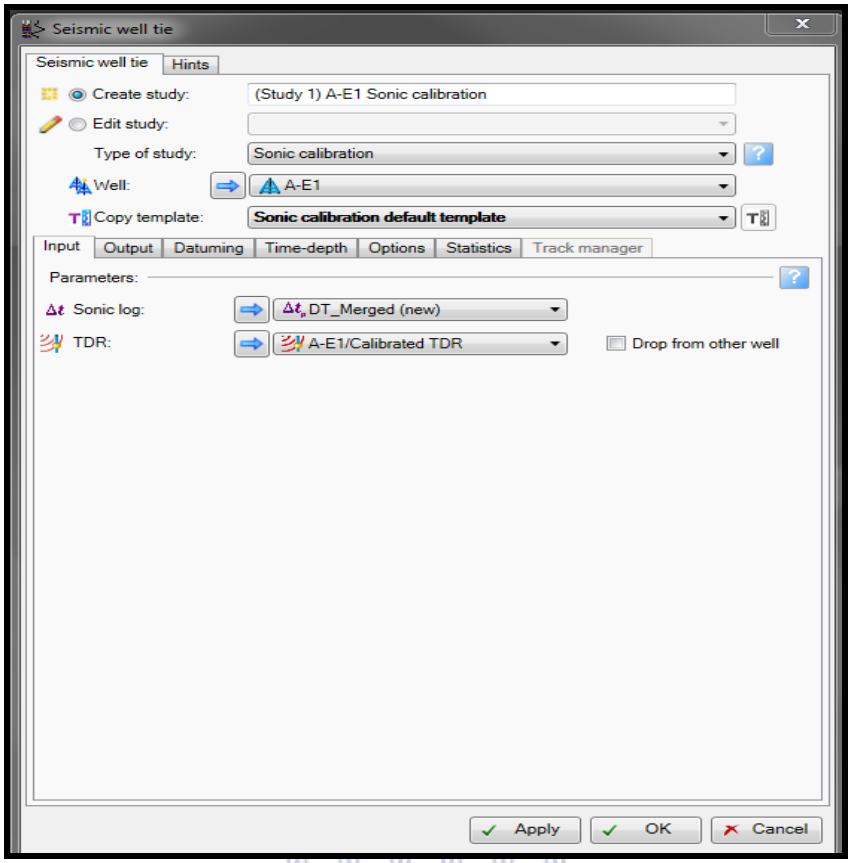

Figure 3.6: Showing Sonic Calibration step in the Seismic-Well tie Process.

3.2.6 Wavelet Extraction

Seismic data acquired from the field are asymmetrical with respect to time variation, and for a better representation of seismic signals, the frequency and characteristics should be defined systematically as fractional derivatives of a Gaussian function (Wang, 2015).

The significance of wavelet extraction is to specify the seismic data to be used to generate a wavelet that will be used as a tie with a wavelet generated from the reflection coefficient convolved from impedance logs. AF-2009 3D seismic volume was used to match the wavelet generated for AF-1 well; A81-011 seismic line (Figure 3.7) was used as a match to generate a wavelet for AE-1 and A79-003 seismic line for AO-1 well. Ricker wavelet, a zero-phase wavelet was used as a Gaussian function to extract wavelet from the field seismic data. Ricker or Ormsby wavelets are two major wavelet extraction functions that could be used but Ricker wavelet was used for this study.

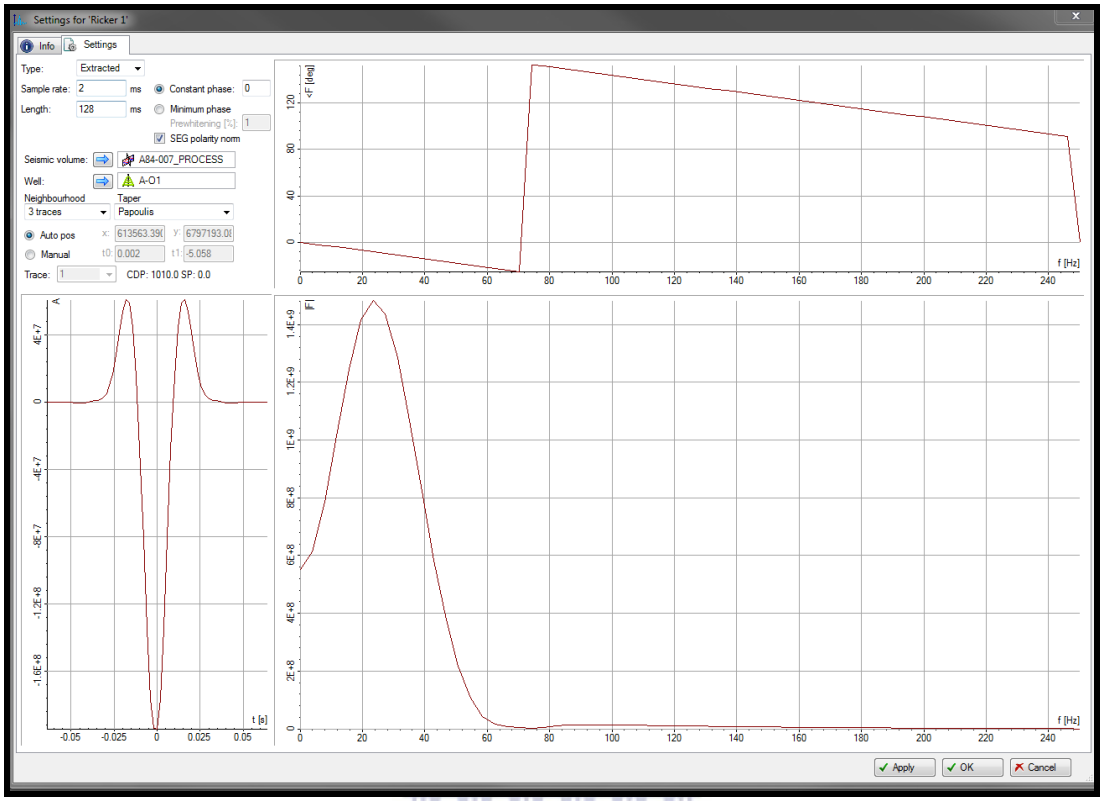

Figure 3.7: Showing Wavelet Extraction Window for Well AO-1.

3.2.7 Synthetic trace Generation

Tying up of the synthetics from the well with the seismic section ensures amplitude balancing and positioning of different formation tops to simplify seismic horizon mapping process. As shown in Figure 3.8, the well synthetic, the formation tops and the seismic data are tied to enure that a particular formation top in the well is matched accurately with its position on the seismic section. Synthetic trace is generated by generating acoustic impedance from sonic log, checkshots and density log. Thereafter, the reflection coefficient is estimated from acoustic impedance. In addition, the convolution of reflection coefficient gives a synthetic trace. After the generation of the synthethics, bulk shifting which is a process of adjusting the amplitude on the synthetic to match the seismic amplitude, was performed to ensure the wells and seismic are well tied.

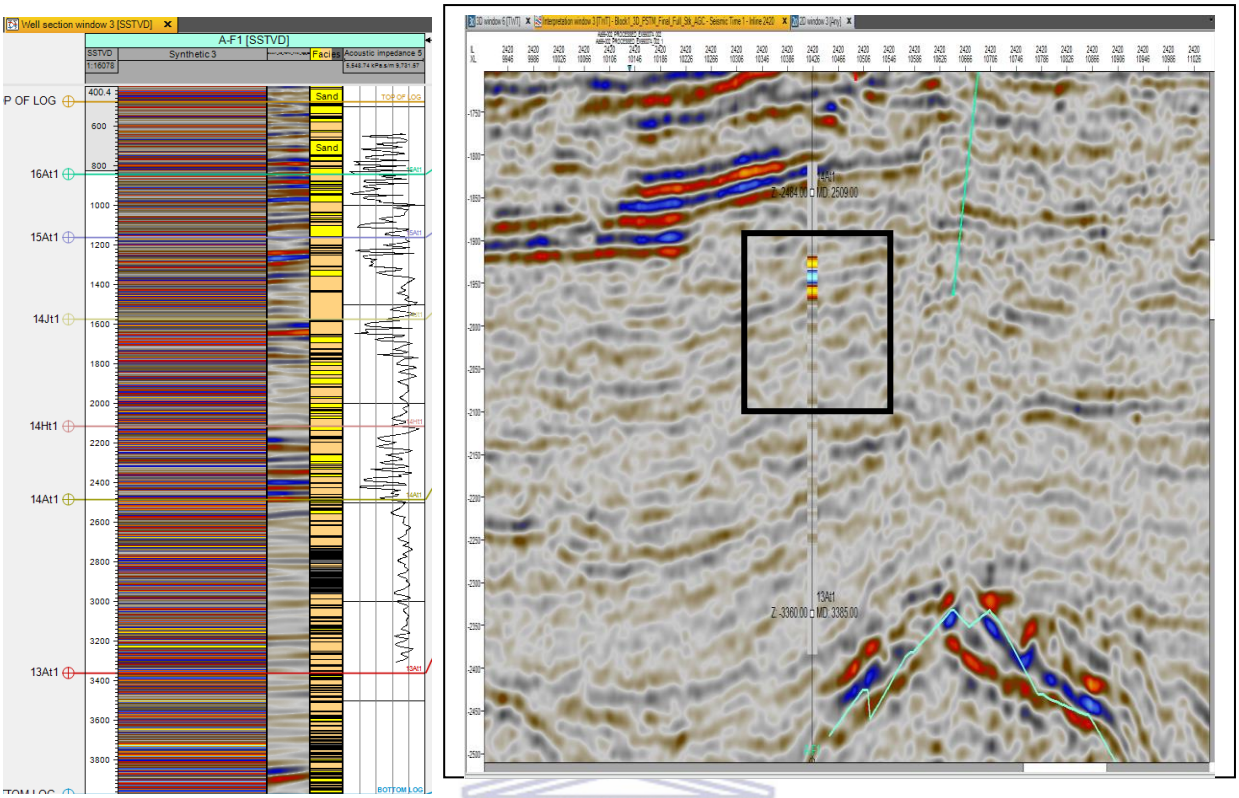

Figure 3.8: Showing the synthetic generation and balancing of the seismic amplitude and a well for this study.

3.2.8 Creation of Time and Isopach Maps (Surfaces)

Sequel to the creation of chronostratigraphic time maps, mapping of seismic horizons was carried out after completion of the seismic –well tie processes highlighted above. The mapping of seimsic horizons was done from the position of formation tops which represent the major chronostratigraphic markers of block 1, Orange Basin. Time maps were generated from seismic horizons by setting up a boundary (Polygons 2) as seen in Figure 3.9, on the coverage of seismic data and taking into consideration the three wells in the study area. The time maps represent the two -way time map of acoustic waves as it reflects off different formation tops. The time taken by acoustic waves to reflect at major horizon markers is dependent on the lithology, diagenesis and the variations in stratigaphic evolution across the basin. Subsequently, Isopach thickness maps were generated from the suraces maps

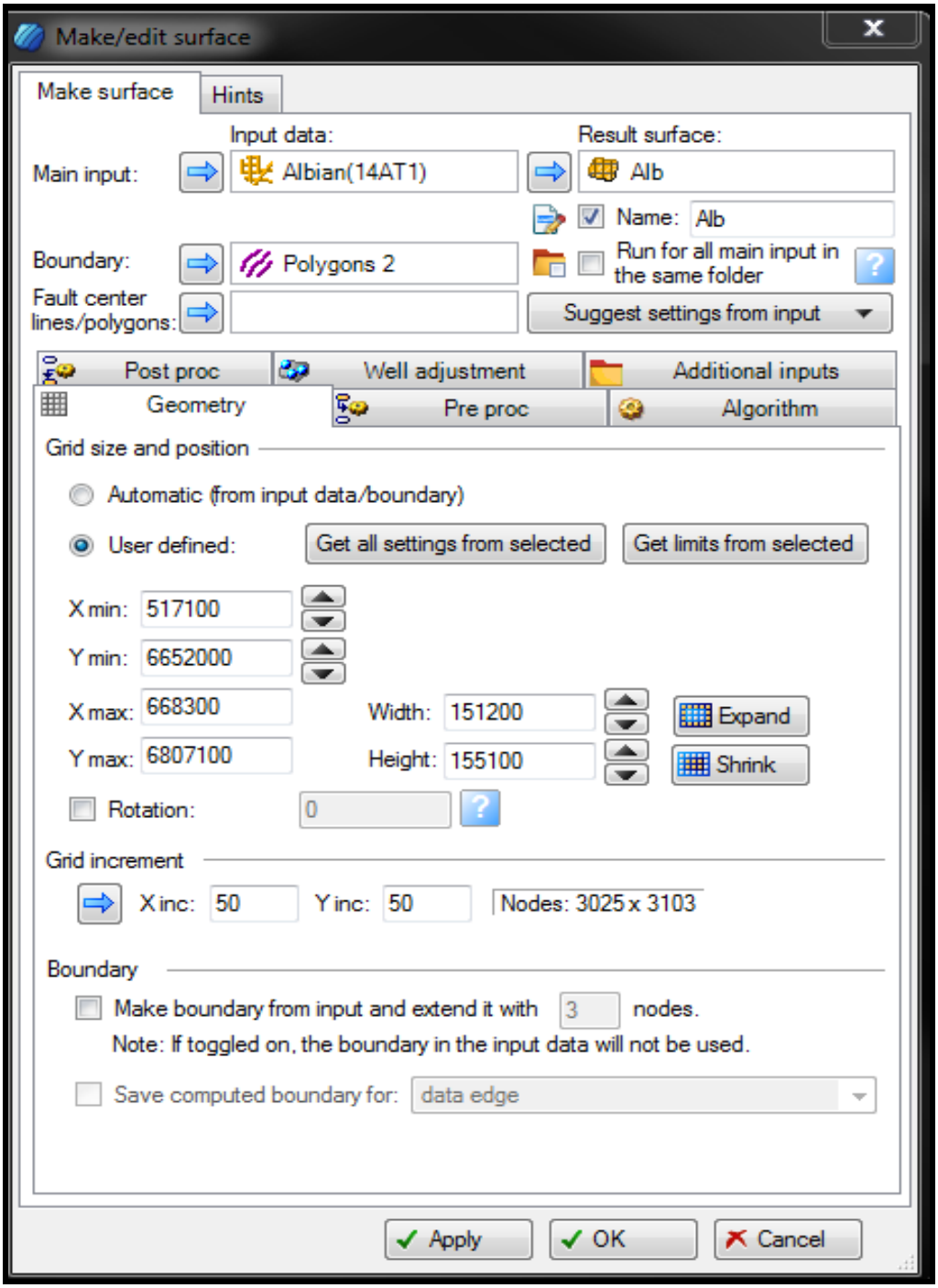

Figure 3.9: Showing an interface of Horizon conversion into a surface.

3.2.9 Velocity Modeling

Velocity modeling is key in the execution of depth imaging workflows of seismic data. The essence of which is to predict with a good level of certainty, the depth of prospects for drillers' targets. Therefore, it aids the mapping of depth and thickness of subsurface formations, identification of sweet spots and mapping of subtle

stratigraphic features. In this study, velocity modeling was carried out for all the time maps of major chronostratigraphic markers using the formula, V=V0+K*Z with the velocity values estimated from the calibration of sonic log and checkshots data. V0 represent the interval velocities between the formations in a chronostratigraphic order. K represents the gradient of the velocity increase with depth, while Z represents depths established as a result of Time –Depth-Relationship (Figure 3.10). Figure 3.10 below shows the interface of velocity modeling parameters.

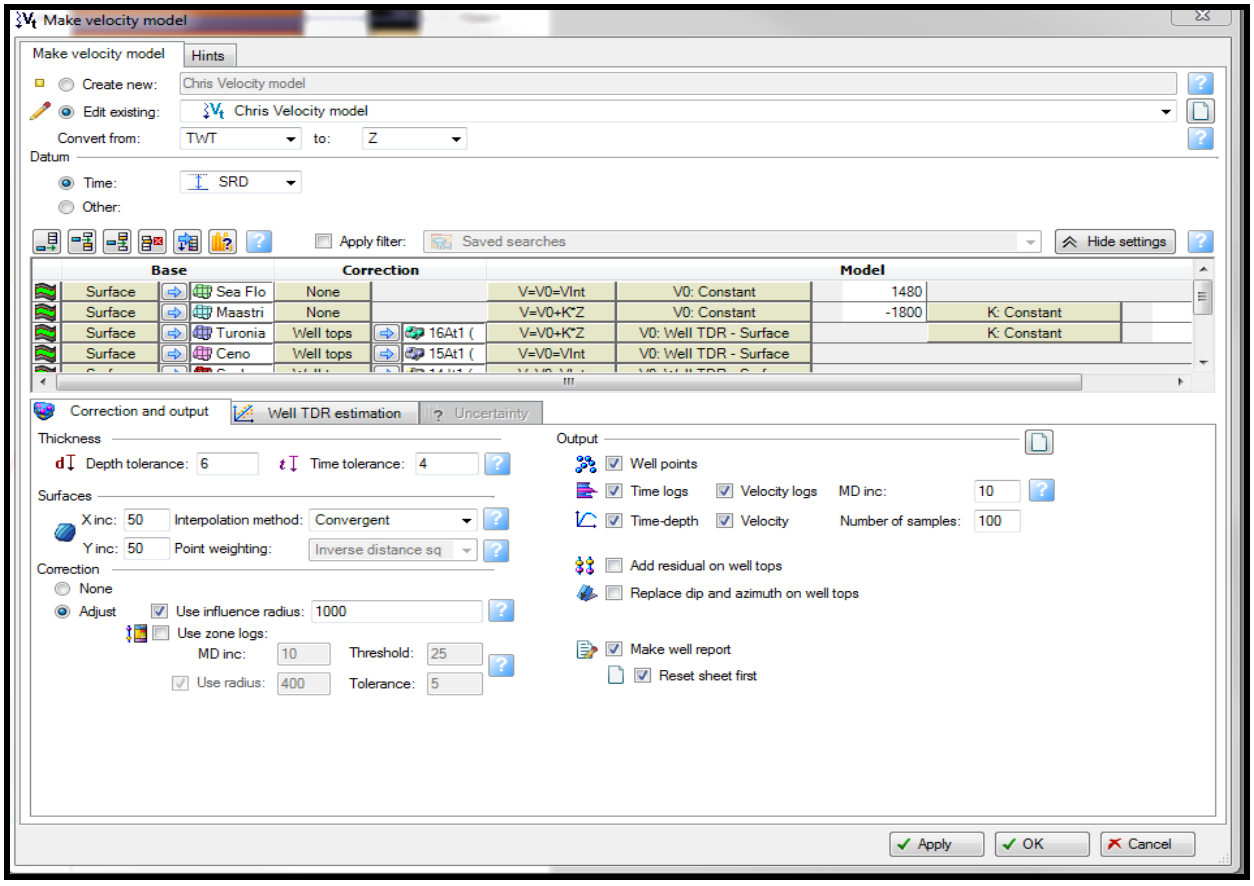

Figure 3.10 : Showing an Interface of velocity modelling parameters used in this study.

The rule of the thumb as regards velocity of subsurface layers is that it increases with depth (Figure 3.11), however, there could be anomalies. Anomalies emanating from diagenetic modification could include mechanical compaction (steady subsidence) or chemical compaction such as an excessive precipitation of calcite cements could be anomaly factors. Excessive cementation by calcite could increase the velocity of rocks at specific depths. In Figure 3.11, the interval velocity used in this study was plotted against the depth. Expectedly, it increases with depth but not without some outliers.

The occurrence of the outliers may be attributed to the presence of diagenetic cements as mentioned above.

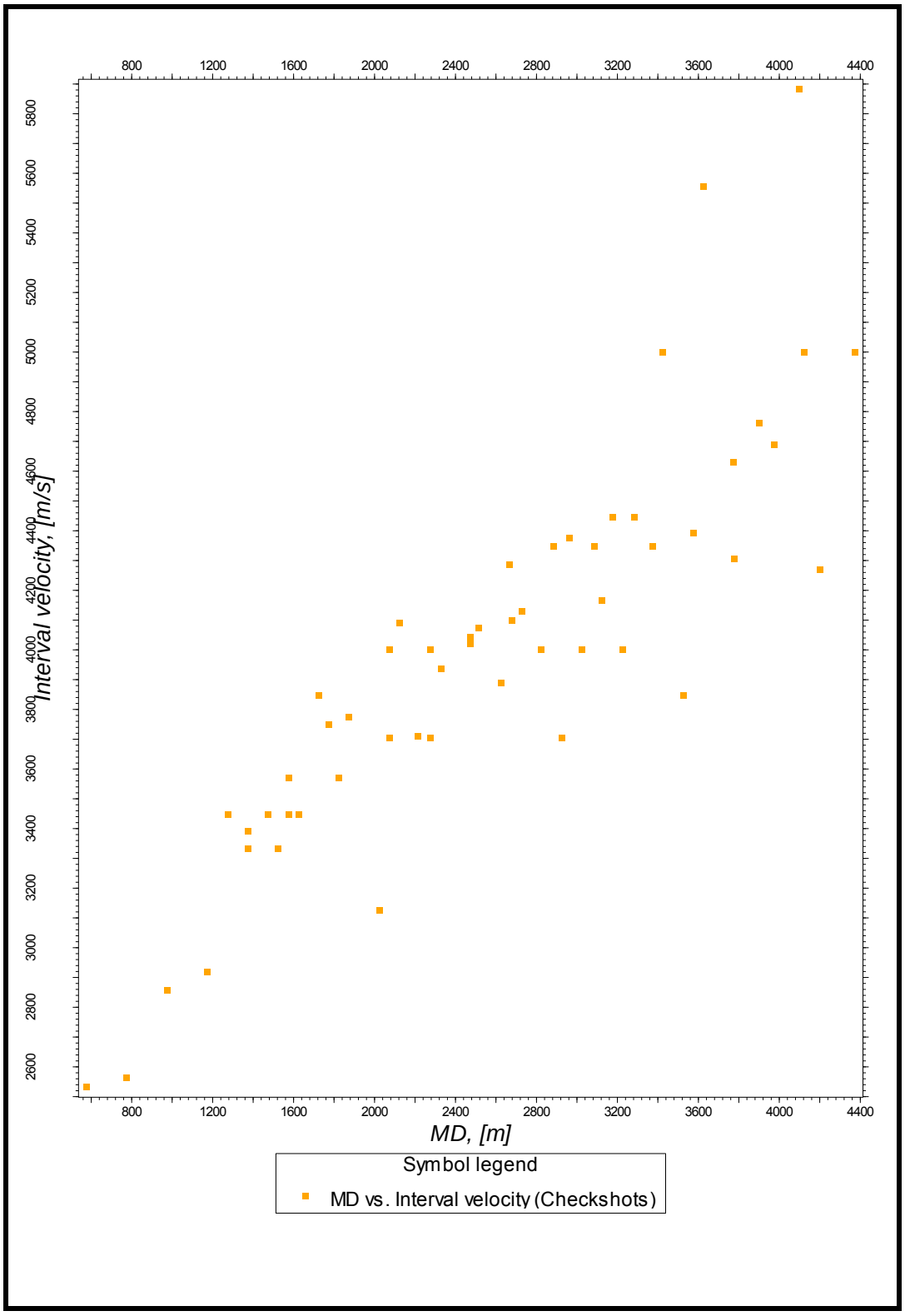

Figure 3.11: Showing a plot of Velocity-Depth functions for all wells used in this study.

In order to test the accuracy of the velocity model, it was corrected with the formation tops. The model tends to fit the velocity model with the exact positions of the well-tops. Once this is done, to a large extent, the velocity model is deemed to be accurate. The results of the correction as shown in Table 7, shows there is no discrepancy in the depths after applying the corrections.

Table 7: Table showing the output of velocity modelling process.

Velocity n	Chris Velocity model								
User name	user								
Project	SAMAKS3.pet								
Date	Wednesday, May 06 2015 12:06:23								
From:	TWT [ms]								
To:	Z [m]								
XY:	[m]								
Sea Floor	Well	X-value	Y-value	Z-value	Horizon af	Diff after	Corrected	Information	
Maastrich	Well	X-value	Y-value	Z-value	Horizon af	Diff after	Corrected	Information	
Turonian/	Well	X-value	Y-value	Z-value	Horizon af	Diff after	Corrected	Information	
	A-O1	613595.5	6797161	-765	-765	0	Yes		
	A-E1	624909.9	6692824	-1282	-1282	0	Yes		
	A-F1	616587.9	6766561	-842	-842	0	Yes		
Ceno	Well	X-value	Y-value	Z-value	Horizon af	Diff after	Corrected	Information	
	A-O1	613595.5	6797161	-1135	-1135	0	Yes		
	A-E1	624909.9	6692824	-1518	-1518	0	Yes		
	A-F1	616587.9	6766561	-1161	-1161	0	Yes		
Seal	Well	X-value	Y-value	Z-value	Horizon af	Diff after	Corrected	Information	
	A-O1	613595.5	6797161	-1473	-1473	0	Yes		
	A-E1	624909.9	6692824	-1986	-1986	0	Yes		
	A-F1	616587.9	6766561	-1575	-1575	0	Yes		
Alb	Well	X-value	Y-value	Z-value	Horizon af	Diff after	Corrected	Information	
	A-O1	613595.5	6797161	-2178	-2178	0	Yes		
	A-E1	624909.9	6692824	-3195	-3195	0	Yes		
	A-F1	616587.9	6766561	-2484	-2484	0	Yes		
Barremian	Well	X-value	Y-value	Z-value	Horizon af	Diff after	Corrected	Information	
	A-O1	613595.5	6797161	-2953	-2953	0	Yes		
	A-E1	624909.9	6692824	-4389	-4389	0	Yes		
	A-F1	616587.9	6766561	-3360	-3360	0	Yes		
Top of Bas	Well	X-value	Y-value	Z-value	Horizon af	Diff after	Corrected	Information	

3.2.10 Construction of Structural Framework

Based on the geological observations made from the seismic and logs, it becomes important to model faults and formation surfaces to understand the effects of faulting,

folding and erosion on the stratigraphic evolution of the study area. This task was initiated by carrying out editing of fault pillars and smoothing of formation surfaces (a quality control tool) to tune the accuracy of the model. After this, fault modeling was performed; seventy-six regional faults were loaded into the structural framework interface and were resolved into a fault model. Fault modeling constitutes the foundation for the construction of a structural framework, as seen below in Figure 3.12 .

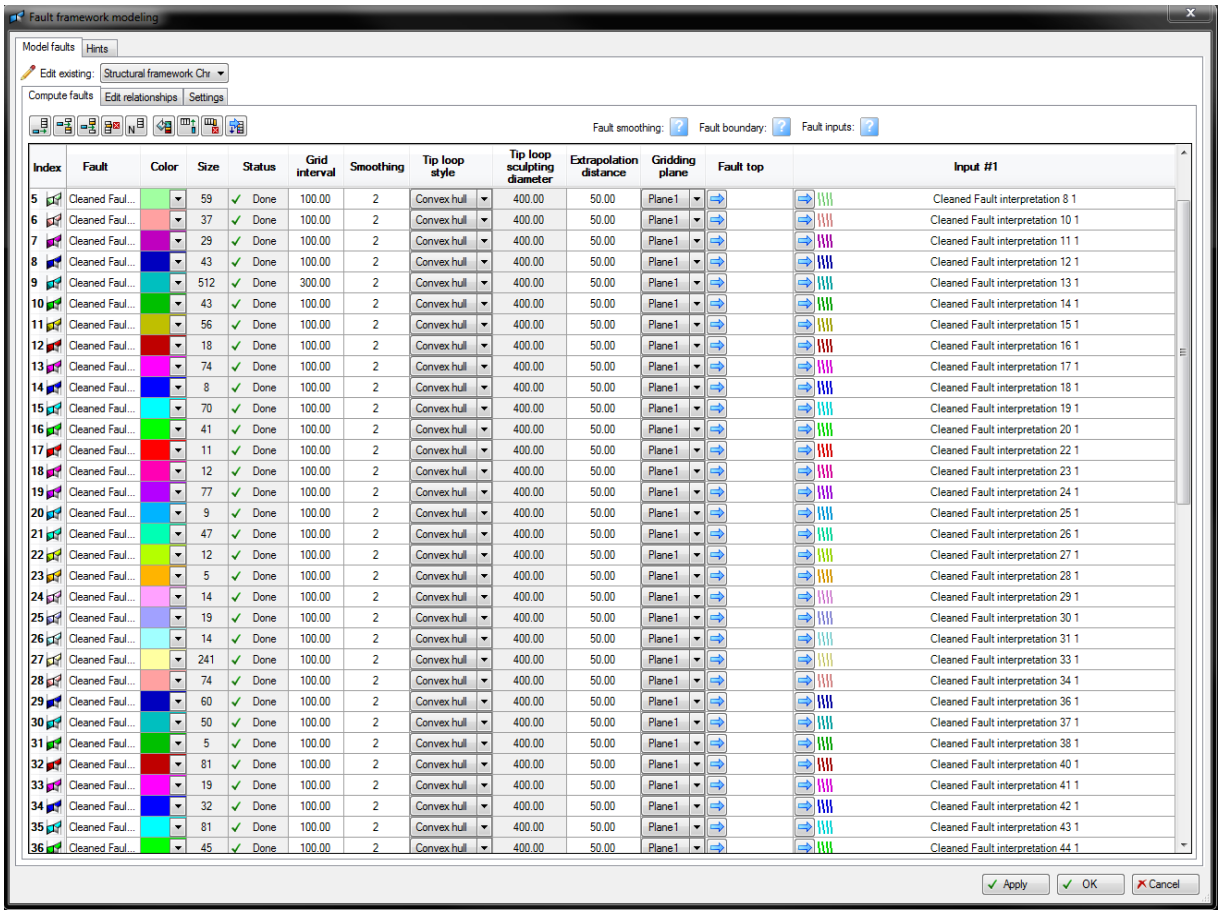

Figure 3.12: Showing Structural Framework Construction Process.

This was followed by horizon modeling using the fault centre grid dislocation and subsequently, definition of zones between two formations that overlies each other other unconformably. The horizons were loaded in the interface following the conventional chronostratigraphic order, as seen in Figure 3.13. Subsequently the dip and azimuth of faults and horizons were estimated using the Petrel Calculator.

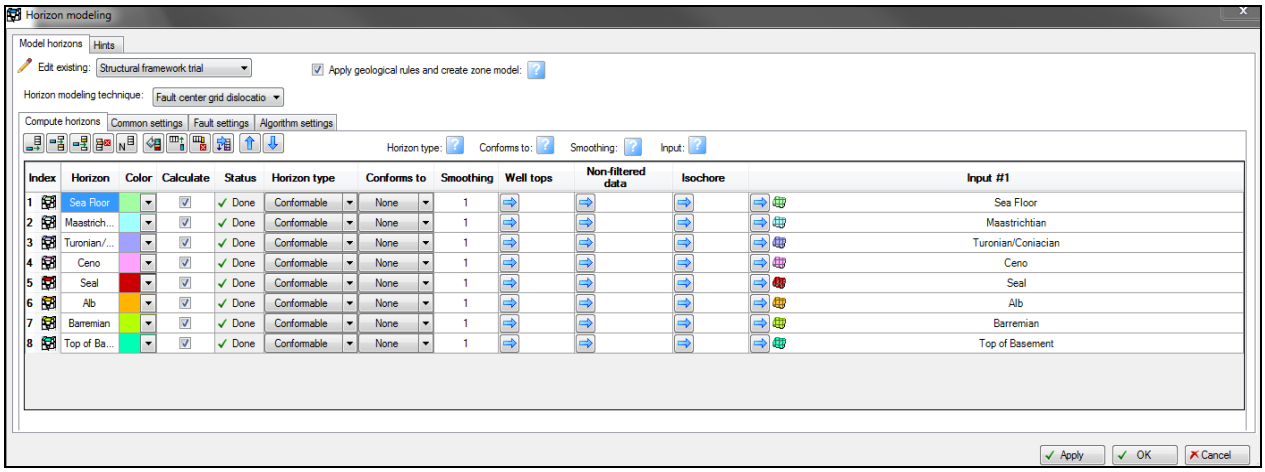

Figure 3.13. Showing Horizon Modelling Techniques.

3.2.11 Seismic Impedance Inversion and Frequency Attributes

In this study, pre-stack seismic data was not available; also, there is a lack of near-, mid- and far-offset post-stack data, and by implication, Amplitude Versus Offsets (AVO) analysis could not be performed. This makes the application of seismic impedance inversion to characterize possible hydrocarbon bearing sediments a task that should be completed. Variance edge detection, seismic impedance inversion, instantaneous frequency and iso-frequency attributes were performed on the 3D seismic volume to characterize faults, stratigraphic features and 'sweet spots'. In applying Seismic Impedance to characterize hydrocarbon saturated zones, porosity inversion was used to calibrate because of the inverse relationship that exists between the two, in that while impedance is expected to increase with depth, porosity is expected to decrease with depth. Normal conventional seismic data contains 60-80 Hz frequency bandwidth, and the presence of hydrocarbon in rocks attenuates this frequency. This theoretical understanding made the application of Iso-frequency analysis a tool in the prediction of hydrocarbon presence in reservoir sections. Iso - Frequency analysis is a patented seismic decomposition method used in generating a user defined frequency attribute.

In this study, the application of Iso- Frequency analysis was performed to decompose seismic signals into different frequency components of 45, 24 and 10 Hz. The decomposition at different frequency bandwidths (Figure 3.13.) allowed its

juxtaposition with observations made from seismic impedance inversion and enables inferences to be drawn as to the possible areas of hydrocarbon presence.

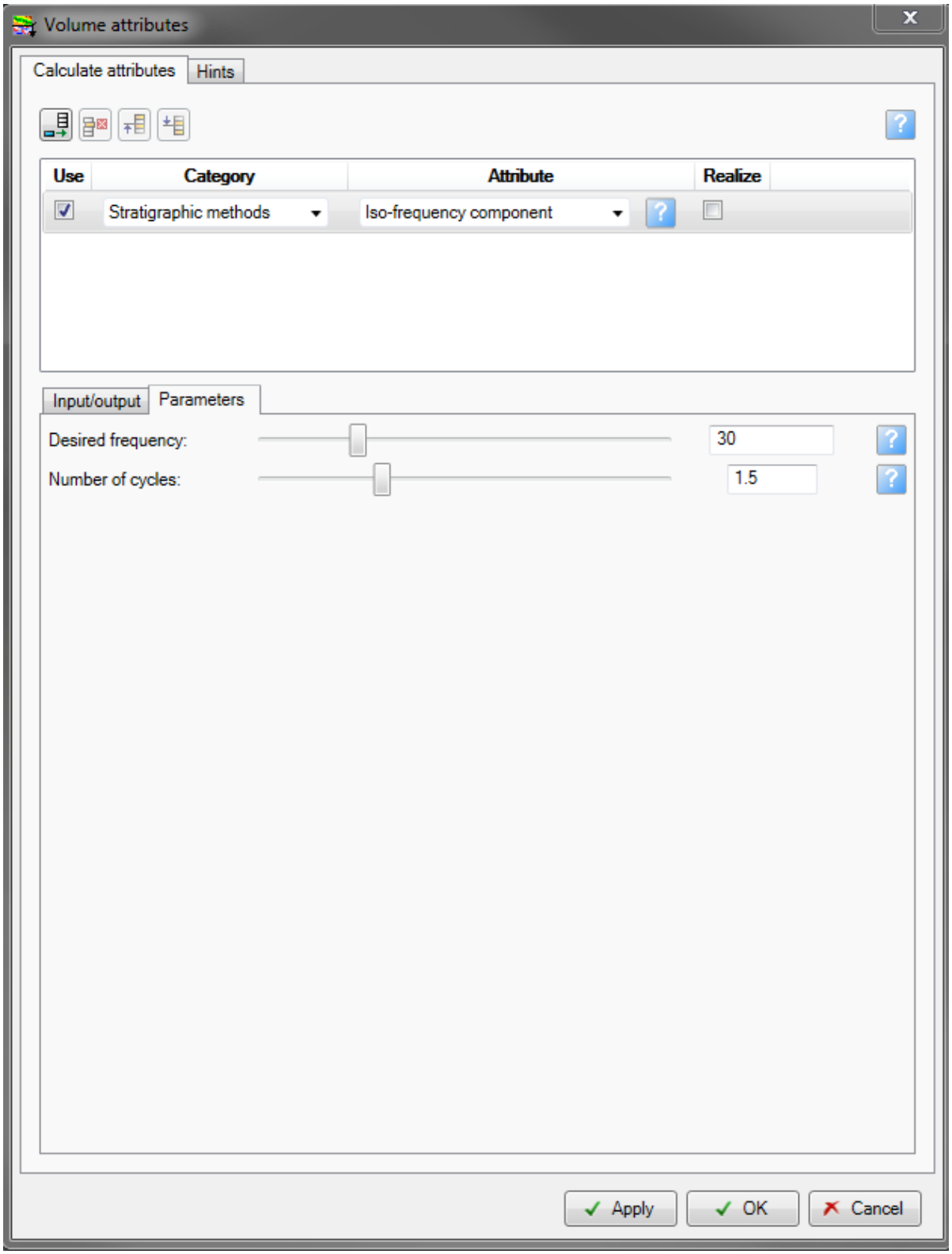

Figure 3.14: Showing the interface of Frequency Decomposition Process.

The interactive parameters control in Figure 3.13 show the desired frequency for the attributes and the number of cycles used.

3.2.12 Seismic Stratigraphy interpretation Methods

Seismic stratigraphy offers a different dimension to interpretation of seismic datasets because the technique is based on the combination of methodologies at two different scales of observation. The scales of observation of using seismic data on basinal scale with well-control makes the inferences drawn from the application of this technique more reliable. This method allows the lateral prediction of lithofacies from the well bore to a basin extent. With the general geology and tectonic style of the Basin in mind, especially with references made by previous studies on the Orange Basin, angular truncations, major lap-outs like onlap, toplap and downlap were mapped. Onlap and angular truncation terminations are a candidate for sequence boundary while downlaps could be candidates of Maximum Flooding Surfaces (MFS) (Snedden and Sarg, 2008).

The seismic facies mapping code of Ramsayer, (1979), Badley, 1985 (Table 1) and Bally (1982) (description in Figure 3.15) was used to identify the external geometry of reflection terminations and associated characters, continuity, and amplitude of seismic reflections that were mapped. Because of the passive margin setting of the Orange Basin, a stable shelf that will preserve sediment deposition history is expected and indeed a parallel/divergent seismic facies was identified in the Basin. Parallel facies suggests sediments deposited in a uniformly subsiding environment while divergent seismic facies suggests variation in the rate of deposition (Mitchum et al., 1977). Observations made were later integrated with litho-facies interpretations from well-logs.

Table 8: A-B-C seismic facies technique of Ramsayer (1979).

Descriptor	Position	Code	Explanation	Comments
Top	A	C	Concordant	often assoc'd with parallel internal reflections
		Top	Toplap	non-erosional, c.f. truncation
		Dwn	Downlap	double downlaps oc. assoc'd with mounding
		Di	Divergent	
		Tr	Truncation	associated with erosional unconformities
Base	B	C	Concordant	
		Top	Toplap	
		Dwn	Downlap	
		Di	Divergent	
		Tr	Truncation	
Internal	C	P	Parallel	
		Ob	Oblique	
		Si	Sigmoidal	assoc'd w/ dinoforms
		Mo	Mounded	shallow (deltas), deepwater
		Subp	Subparallel	rare, c.f. oblique

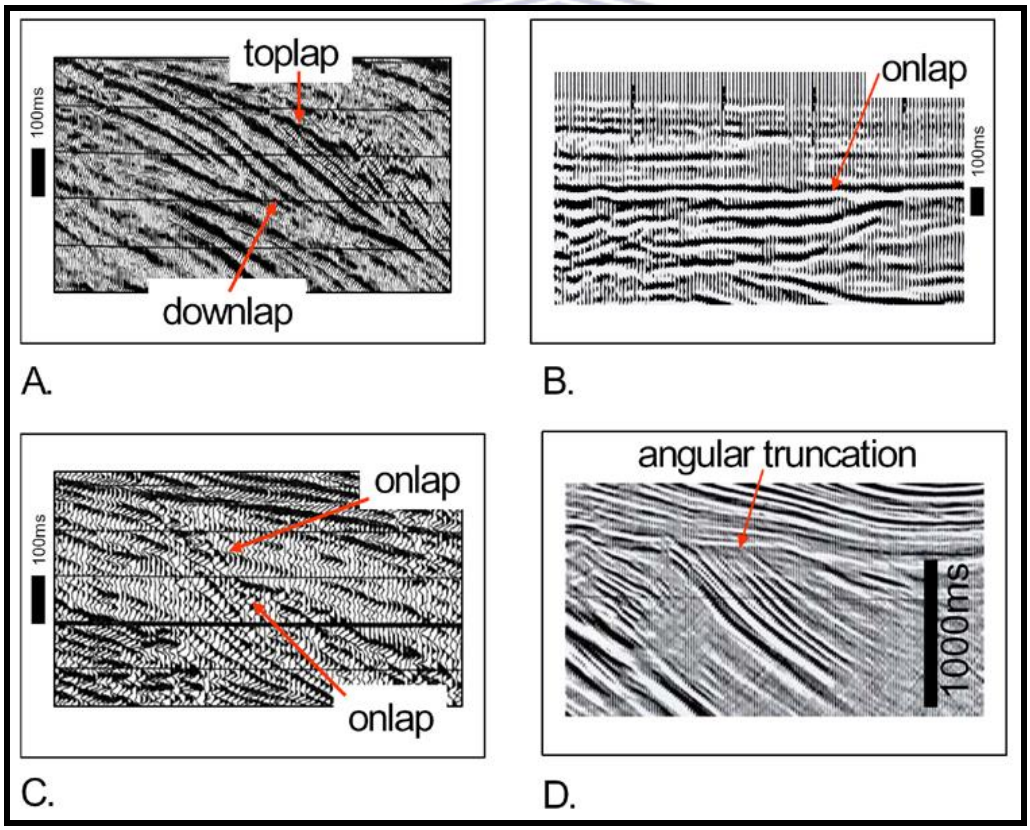

Figure 3.15: Lapout Surfaces from Bally, 1982.

3.2.13 Construction of Hydrocarbon Migration Modeling

The simulation of hydrocarbon migration pathways in sedimentary basins is critical to understanding the interactions of faults and stratigraphy on the hydrocarbon flow vectors. The lithology, ravinement surfaces, permeability (lithology dependent), faults, temperature, heat flow, erosion, paleo-bathymetry, Sediment Water interface, Temperature and pressure are some of the properties that should be mimicked to have a broader understanding of hydrocarbon migration patterns in the sub-surface. In addition, Total organic carbon content, kinetics (HI and OI), thermal (T-max) and maturation (Vitrinite reflectance) data are some of the input parameters needed to simulate generation and expulsion of hydrocarbons. In constructing a hydrocarbon migration model for this work, the workflows discussed below were completed in a sequential order, and simulation performed using the Hybrid method (Darcy and flowpath) on the Petromod 2014© workstation. The advantage of the Hybrid method as the most preferred option is explained under the 3D forward simulation explanations.

3.2.14 Data Used for the Construction of a Hydrocarbon Migration model.

The data used in this study are summarized in an excel spread sheet below. The lithology that represents each formation was derived from three sources; the generalized chrono-stratigraphic framework of the Orange Basin, the core description reports and from using the Petrel 2013© calculator to write a discriminant python script equation for different lithologies (Shale, Sand and Silt) using the Gamma ray log. The script written was; Facies=If (GR_Merged_new<60, 0,

If (GR_Merged_new>60 And GR_Merged_new<100,1 ,2)).

GR_Merged new represents gamma ray value in API while the coding 0 represent Sand, 1 represent Silt and 2 represent Shale.

The lithology from this source was compared with facies description reports of the wells used in this study and mixed according to their relative abundance to have a reliable representation of facies present within each sequence. Subsequently,

Petroleum system elements were assigned to different lithologies. Other data that were used are listed in Table 9.

Table 9: Table showing some of the data used in performing 3D forward simulation modelling.

PetroMod 1D A-F1 WELL																
BREDASDORP Model																
Layer	Top (m)	Base (m)	Thickness (m)	Eroded	Deposition from (Ma)	Deposition to (Ma)	Lithology	PSE	TOC / HI	Kinetics	Depth (m)	Pressure (Mpa)??	Depth	Porosity	Depth	Permeability
											1345.00	7.24				
								Seal			2733.00	15.86				
								Res								
								Seal								
Cenozoic	0				65	10	Sand									
Maastrcitian/Cenozoic	500		-500		67	65	Shale (typical)									
Turonian/Coniacian	867		-867		90	85	Siltstone									
Cenomanian/Turonian	1186		-1186		93	90	Shale (typical)	P/SR	3 / 285							
Late Albian/Cenomanian	1600		-1600		100	93	Shale (typical)	Seal								
Late Albian	2140		-2140		103	100	Sand	Res								
Albian	2509		-2509		112	103	Sand	Res								
Barremian/Aptian	3385		-3385		115	112	Shale (typical)	SR	0.6 / 290							
Barremian	3999.4		-3999.4		117.5	115	Sand (typical)									
Basement	4424		-4424		126.5	117.5	Basalt (normal)									
													0			

Depth (m)	VRo (%)	Tmax	Temperature		Well Data									
			Depth (m)	Temperature (°C)										
			700	60										
			900	72	Well Data									
			1300	81	Vertical Well (UTM Coordinates well report)								Seal	
1200	0.39	425	2000	92	Name	X (m)	Y (m)	TVD (m)	KB (m)					
1500	0.5	430	3000	105	A-F1	616587.92	6766561	4001	25					
1600	0.42	428												
1700	0.5	430			SWIT									
1780	0.8	450			Southern Africa ???									
1900	0.59	455			Lat									
3000	1.3	465												
3100	0.9	458												
3400	1	460												

	HF event		PWD			HF		
	Peak time (Ma)	Peak HF (mW/m2)	Age	Value (m)		Age		Value (mW/m2)
Rift event 1	130	52				0		65
Rift event 2						210		65
Margin uplift at		80ma						

3.2.15 Importing of Depth Maps and Fault Model into Petromod 2014© Workstation.

Chronological time maps that were converted to depth maps using the velocity model constructed in Petrel 2013© were loaded into the Petromod 2014© workstation using the Irap Classic grid lines (ASCII/binary) format. In addition to this, fault sticks that were mapped previously in the Petrel 2013© workstation were exported in the same format as the depth maps, and were gridded.

3.2.16 Boundary Conditions

Boundary conditions are geological factors on which the prediction of hydrocarbon generation and -migration are based. In any form of forward modeling process, boundary conditions for the study area must be accurate before simulation could be carried out and could also be altered during data calibration processes. The influence of Paleo-water depth, Sediment Water Interface Temperature, and Heat flow history on hydrocarbon generation and migration are discussed below.

3.2.16.1 Sediment Water Interface Temperature (SWIT)

The latitude of a sedimentary Basin influences the temperature variations during source rock deposition. In the southern Africa, there are latitude variations across all sedimentary Basins. In the eastern Coast of South Africa, latitude could have been the reason for the warmer nature of waters encountered in the basins along the eastern Coast (Zululand and Durban Basins), when compared to the less -warm waters in the basins along the western coast (Orange Basin). In this case, 'the present is the key to the past', the present day SWIT could be known and could be used to estimate the SWIT at the onset of source rock deposition. Using the Wygrala (1989) model of summarized surface temperature of time-latitude diagram, the SWIT data used in this study was estimated based on latitude of 33S for the Orange Basin (Figure 3.16).

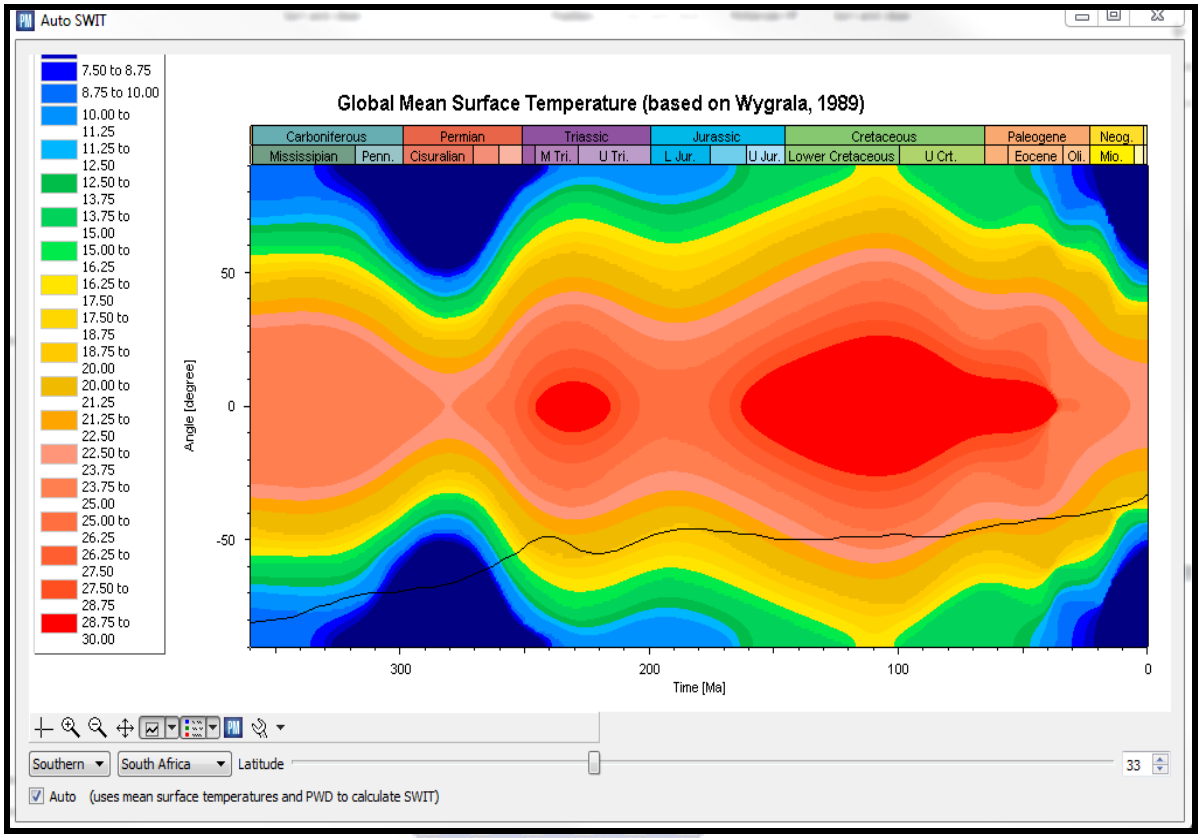

Figure 3.16: Figure showing a plot of latitude and Global Mean Surface Temperature, after Wygrala (1989).

3.2.16.2Paleo-Water Depth

The evolution of the sedimentary sequence of the Orange Basin, like other sedimentary basins of the world, is affected by the paleo-water depth. However, there is a direct relationship between SWIT and Paleo-water depth, as fluctuations of average surface temperatures impact directly on the average water depth. Also, benthic foraminifera have been used in the oil industry to provide information about paleo-water depth at the sea floor. In this study, the estimation of paleo-water depth from SWIT was used as it has been proven accurate for similar studies in other sedimentary basins globally. Figure 3.17 shows the variation of water depth over geologic history.

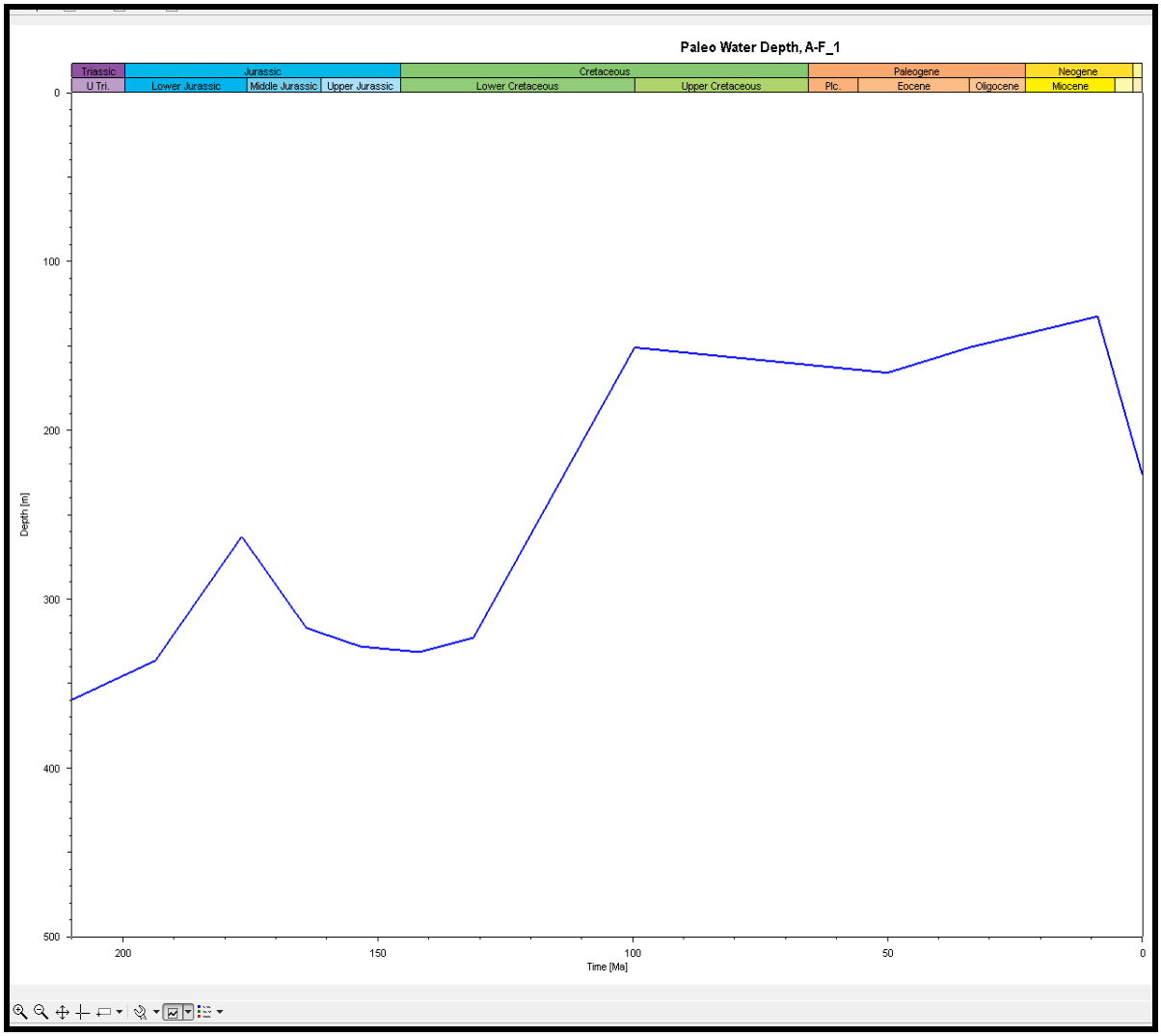

Figure 3.17: Showing variation of Paleo-water depth over geological ages used in this study.

3.2.16.3 Heat-Flow History

Different heat models are applied for various tectonic regimes of sedimentary basins. A rift basin is expected to have a considerable magnitude β factor of lithospheric stretching when compared to the level of stretching in other tectonic regimes. In modeling the subsidience and thermal history of extensional basins, McKenzie's (1978) model for rift basins is commonly applied. The Mckenzie's model is used to explain that lithospheric extension occurs as a pure shear; an example of elongation of a body in a particular direction and an accompanied shortening in a perpendicular direction. The Mckenzie's model is applicable in this study because the Orange Basin is a classic passive margin on which the Mckenzie's model was based on. Heat flow from rifting disappears with time and could cease after rifting (Pollack and Chapman,

1977), therefore, due factoring was given to tectonic events that could impact on heat flow in this Basin. Events like uplifting and erosion were factored into the generation of the heat model and the values of heat flow were increased especially during the late Cretaceous and Miocene. Late Cretaceous and Neogene uplift affected the African continent and southern Africa respectively (Partridge, 1997; Emery and Uchupi, 1984) and was taken into consideration for the study. Figure 3.18 shows the heat flow plot used for the study.

Figure 3.18: Showing the Heat flow model used in this study (After Mckenzie, 1978).

3.2.17 Age Assignment for Surfaces and Faults

Ages were assigned to the maps and faults used in the Petromod 2014© interface. Age assignment was done for all depth maps (unconformity surfaces) and fault sticks based the regional chronostratigraphic framework of the Orange Basin (Brown et al., 1996) ,while the age assignment of faults were done based on the geometry and the layers intersected. For instance, a fault which emanated from the Albian and truncates at Maastrichtian is assigned an age range of these periods. Prior to age assignment of

faults, a fault model was constructed to enable gridding of the faults. Subsequently, as seen in Figure 3.19 and Figure 3.20, faults' characteristics were defined as; syn-rift faults are deemed closed faults while post-rift faults are open faults.

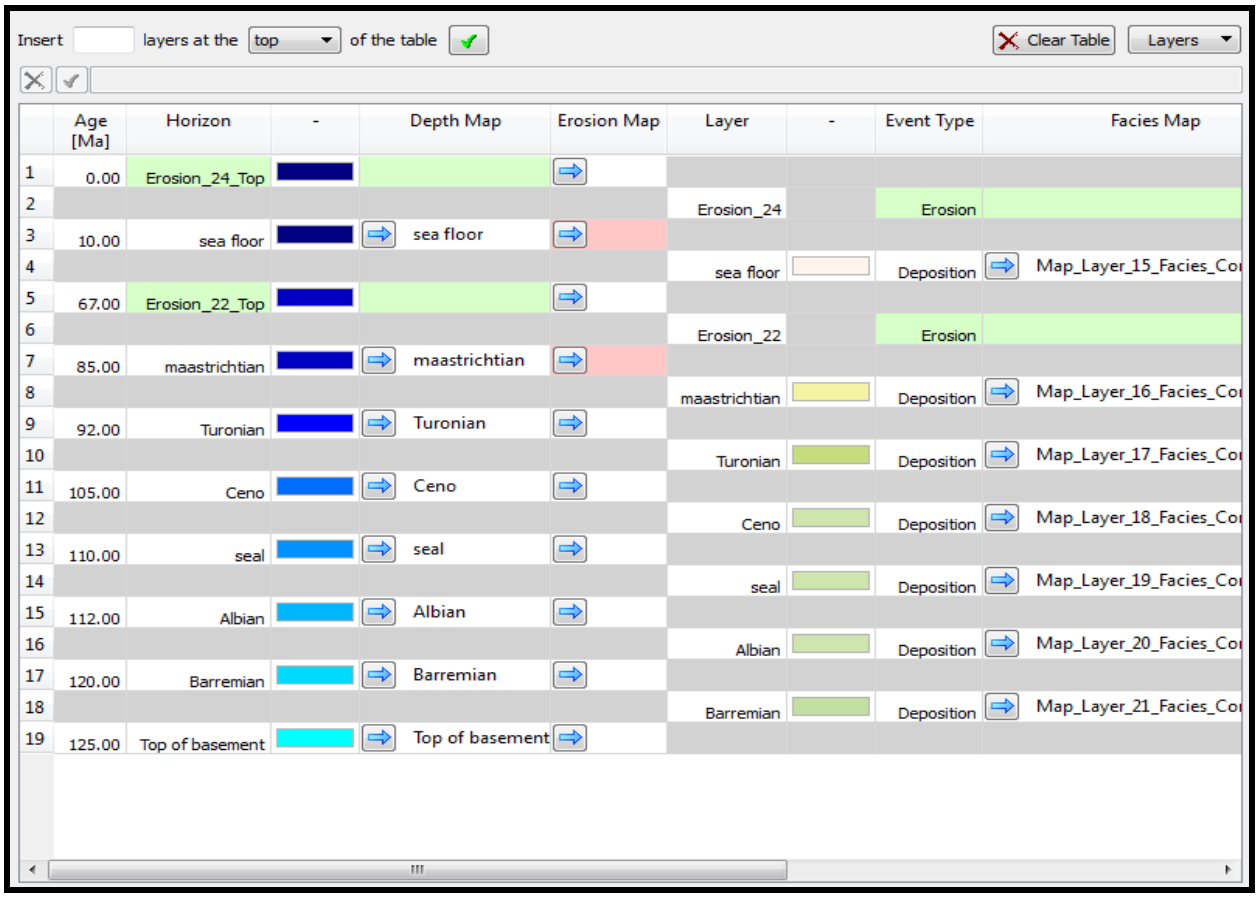

	Age [Ma]	Horizon	-	Depth Map	Erosion Map	Layer	-	Event Type	Facies Map
1	0.00	Erosion_24_Top							
2						Erosion_24		Erosion	
3	10.00	sea floor		sea floor					
4						sea floor		Deposition	Map_Layer_15_Facies_Co
5	67.00	Erosion_22_Top							
6						Erosion_22		Erosion	
7	85.00	maastrichtian		maastrichtian					
8						maastrichtian		Deposition	Map_Layer_16_Facies_Co
9	92.00	Turonian		Turonian					
10						Turonian		Deposition	Map_Layer_17_Facies_Co
11	105.00	Ceno		Ceno					
12						Ceno		Deposition	Map_Layer_18_Facies_Co
13	110.00	seal		seal					
14						seal		Deposition	Map_Layer_19_Facies_Co
15	112.00	Albian		Albian					
16						Albian		Deposition	Map_Layer_20_Facies_Co
17	120.00	Barremian		Barremian					
18						Barremian		Deposition	Map_Layer_21_Facies_Co
19	125.00	Top of basement		Top of basement					

Figure 3.19: Showing Age Assignment process for Depth Surfaces and corresponding facies used in the study.

.

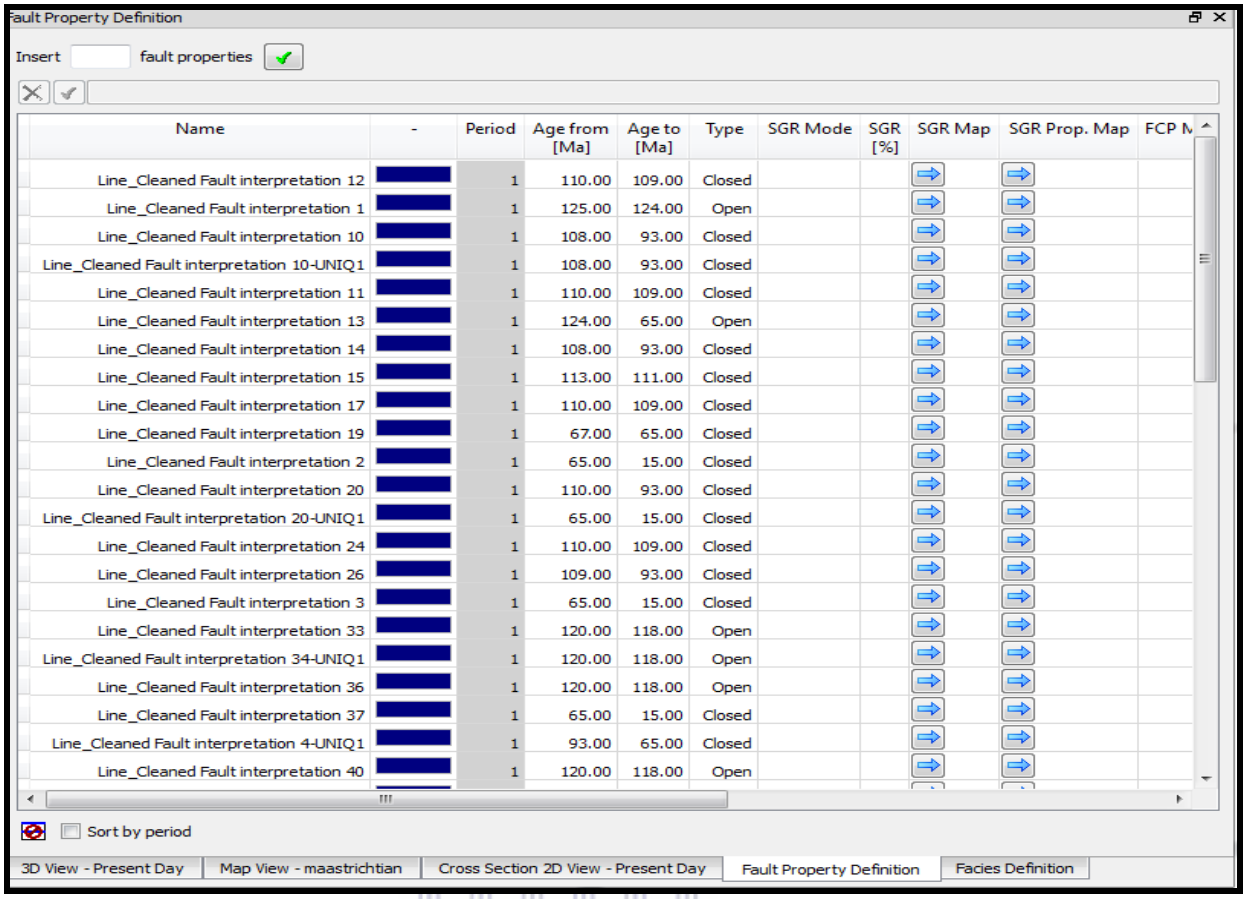

Figure 3.20: Showing Faults used in the study and their Assigned Ages.

3.2.18 Facies Assignment.

Facies classification in this study was done based on the python script equation as earlier discussed in this chapter. Three lithology were identified; Shale, Silt and Sand. A regional lithology correlation was performed across the three wells drilled in the study area and facies were assigned to each sedimentary sequence by ascribing relative approximate values of sand, silt or shale in the lithology editor interface; a process called lithology mixing. Below is the facies assignment table done for this study, Sh-Shale, Si-Siltstone and S-Sandstones while the values written infront of these codes are the relative abundance estimates which totals 100% for each sequence. Facies maps were generated from the facies assignment and were used in the 3D simulation of hydrocarbon generation and migration.

Name	Color	Lithology Value	TOC Mode	TOC Value [%]	TOC Map
sea floor_Facies_1		Sh25Ss70Si5			
maastrichtian_Facies_1		Sh25Ss70Si5			
Turonian_Facies_1		Sh70Ss25Si5	Value	3.00	
Ceno_Facies_1		Si70Ss25Sh5			
seal_Facies_1		Sh70Ss25Si5			
Albian_Facies_1		Sh50Ss50			
Barremian_Facies_1		Sh70Ss25Si5	Value	0.60	

Figure 3.21: Figure showing Facies Assignments for this study.

3.2.19 Petroleum System Elements and Kinetics

Source, reservoir and seal were ascribed to individual facies maps based on the general delineation of the Petroleum system elements of the Orange Basin. The Barremian-Aptian source rock (13AT1), mid-Albian reservoirs (14AT1), late Albian seal (14JT1) and Turonian source rock (16 AT1) were all assigned as the elements of the Petroleum System. Pepper and Corvi (1995) type II and III kinetics were assigned to the Turonian and Barremian-Aptian source rocks respectively. The Barremian/Aptian gas-prone source rock was deposited during the rift-drift process of the late Jurassic/Early Cretaceous and is mappable throughout the basin. The Turonian source rock was deposited during the global anoxic event in the Turonian period. However, the Turonian source rock is believed to be oil prone westward of the Orange Basin (Aldrich et al., 2003; Barton et al., 1993).

3.2.20 3D Simulation of Hydrocarbon Generation and Migration.

The simulation of hydrocarbon generation was done based on the boundary conditions and input parameters; all discussed earlier in this chapter. The simulation was optimized by increasing the run control steps to 400 m size. This is important especially if the study area to be simulated is wide. Temperature, pressure and thermogenenic cracking of source rocks were analyzed for the generation (primary migration) process (Figure 3.22). Faults, petroleum and water vectors were analyzed for the 3D migration simulation using the Hybrid migration method. Hybrid migration method combines Darcy and flow path migration methods (Hantschel et al., 2000). The Hybrid Flow Path Method is advantageous, when compared to other methods of migration simulation because it factors 30% for porosity and 100 millidarcy for

permeability during the evolution of sedimentary layers (Gusterhuber et al., 2013). It also factors full Darcy's calculations for all layers with less permeable lithologies. Faults models constructed in the Petromod 2014© interface were incorporated to evaluate fault interaction with hydrocarbon migration.

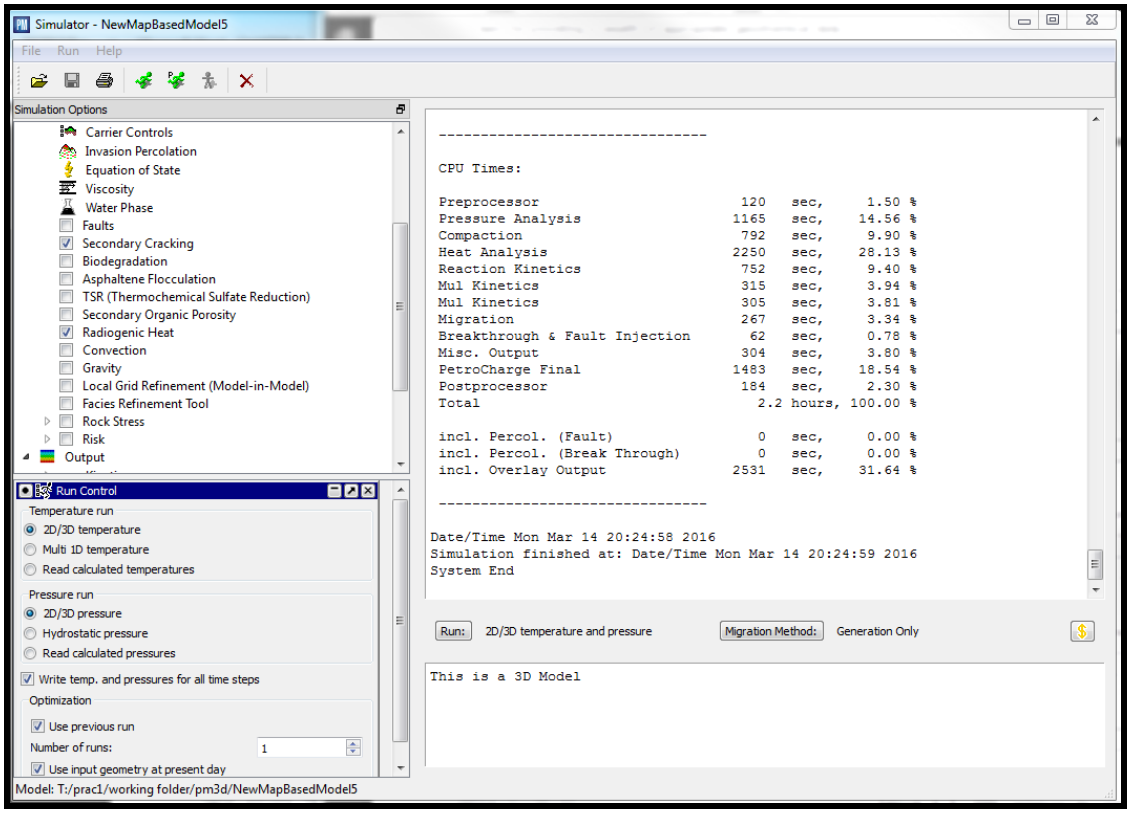

Figure 3.22: Figure showing hydrocarbon generation Simulation Report.

3.2.21 3D Forward Model Calibration

To test the accuracy of the boundary conditions (Paleo-heat flow, SWIT and Paleo-water depth) used in this study, maturity, temperature and pressure data analyzed and measured from the source rock intervals in the three wells were used to calibrate the model. Formation temperature data was used to calibrate the heat flow model and thus becomes an iterative process by adjusting the heat flow model and re- simulating the model to ensure that the predicted temperature from the model matched the actual formation temperature. Similarly, an iterative process was done for the model by using Vitrinite reflectance (%R_0) data for the three wells. In certain cases, where the predicted R_0 does not match the measured R_0, the period of erosion caused by uplift of the continental margin was considered and inserted into the simulation process. Erosion could impact on thermal maturity by transporting sediments from the shelf to

deeper part of the basin, thereby increasing the overburden subsurface temperature and pressure. Also, erosion after uplift of the margin could reduce thickness of sediments and reduce the thermal maturity (Welte et al., 2007). Table 10 below shows the Vitrinite and Temperature and Pressure data used for model calibration.

Table 10: Showing data used for model Calibration excluding porosity data.

	AE-1					
Depth (m)	VRo (%)	Tmax	Temperature		**Depth (m)**	**Pressure (Mpa)??**
1900	0.68	438	Depth (m)	Temperature (°C)	1903.00	6.89
2200	0.8	446	2000	72	3905.00	6.89
2400	0.74	444	2500	90		
2600	0.75	445	3000	108		
2800	0.82	452	3500	126		
3000	0.9	454	4000	144		
3200	1	464				
3400	1.35	470				
3600	1.4	475				
3800	1.5	485				
4000						
	AF-1					
Depth (m)	VRo (%)	Tmax	Temperature		**Depth (m)**	**Pressure (Mpa)??**
			Depth (m)	Temperature (°C)	1345.00	7.24
1200	0.39	425	700	60	2733.00	15.86
1500	0.5	430	900	72		
1600	0.42	428	1300	81		
1700	0.5	430	2000	92		
1780	0.8	450	3000	105		
1900	0.59	455				
3000	1.3	465				
3100	0.9	458				
3400	1	460				
	AO-1					
Depth (m)	VRo (%)	Tmax	Temperature		**Depth (m)**	**Pressure (Mpa)??**

1050	0.3	438	Depth (m)	Temperature (°C)	1806.00	18.14
1100	0.32	446	2000	54.6	3360.00	18.63
1200	0.39	444	2500	67.6		
1250	0.38	445	3000	81.9		
1300	0.56	452	3500	95.2		
1400	0.5	454	4000	108		
1590	0.59	464				
1900	0.56	470				
2000	0.57	475				
2050	0.63	485				
4000						

Chapter Four

MAPPING AND INTERPRETATION OF DEPOSITIONAL SUPER- SEQUENCES USING WELL LOGS SIGNATURES AND LITHO-FACIES MODELING OF SEDIMENTS IN BLOCK1, NORTHERN ORANGE BASIN, SOUTH AFRICA.

Keywords: Orange Basin- Well Logs- Depositional Sequences-Litho-Facies

4.1 Abstract

The comprehensive interpretation of well-logs' signatures to determine litho-facies and depositional sequences' environment are performed in wells (AO-1, AF-1 and AE-1) drilled in block1, Orange Basin. The sequences are mapped and interpreted from the older Barremian / Aptian to the younger Cenozoic sequence, trending from the southern to the northern portion of the block. In the Barremian-Aptian sequence, a massive deposit of shale with intermittent siltstone in the southern part (AE-1) of the basin is marked by a corresponding deposition of siltstone and shale on top of each other in the northern part; such a deposit is a common feature of a pro-delta environment. The Albian marine flooding in this basin affected the northern section more, and led to the deposition of massive shale units and a diachronous deposition of an intercalated shale and siltstone unit in the southern part, which later grades into fluvio- marine sandstone at shallower depths. The Cenomanian-Turonian facies is dominantly siltstone especially in the northern part, with occassional sandstone intervals. However, there is correlative deposition of a fluvial distributary channel sandstone deposit southward in wells AE-1 and AF-1. Coarsening upward Deltafront marine deposits and fining-upward fluvial sandstones are potential reservoir targets and possible carrier beds for secondary migration process. A 3D Stochastic Facies Modeling process was applied to understand the spatial distribution of facies across the study area. The model reveals dominance of sandstones and siltstones in all depositional sequences and localized shale deposits prominent in the

Barremian/Aptian and Albian sequences only. The depositional environments within these sequences range from fluvio-deltaic in the north to a marine pro-deltaic environment in the South.

4.2 Introduction

The relevance of this chapter to the objectives of this study is to highlight the presence of stratigraphic depositional features (stratigraphic control) that could impact on the hydrocarbon migration by interpreting a suite of geophysical wireline logs and creation of a facies geo-cellular model. A geo-cellular model enables the population with various values representing facies distribution that would be used for the interpretation of lithology mixing during numerical simulation of hydrocarbon generation and migration pathways later in chapter seven of this study.

Stratigraphic and depositional features such as clastic and carbonate rocks are essentially carrier beds of subsurface fluids in many sedimentary basins worldwide. This chapter provides a detailed interpretation of litho-facies and depositional environments derived from well-log signatures and results from a 3D Stochastic litho-facies modeling using the Sequential Indicator Simulator in Petrel 2013©, to gain an insight into the distribution of these facies across the study area.

The litho- facies and chrono-stratigraphic sequence are interpreted from the South of the study area (well AE-1) where the Olifants River deposits a lot of sediments, and to the AF-1 well drilled in the middle of the study area, and in the northern part, where well AO-1 was drilled close to the mouth of the Orange River (Figure 4.1). A previous study documents the deposition of a prominent marine source-rock in the Orange Basin during the Barremian / Aptian period (116Ma); this is evident because of the deposition of the marine-prone Barremian / Aptian source rock interval at this time (Jungslager, 1999). During this period, there was an influence of Olifants River deltaic systems (Barton et al., 1993), more prominent in the South while Orange River deposits are prominent in the northern part of Orange Basin (Jungslager,1993). Potential reservoir targets are found within the Barremian / Aptian, Albian and Cenomanian sequences consisting of sub-aqueous channel deposits, upper paralic intercalated sands and shale deposits (Adekola, 2010).

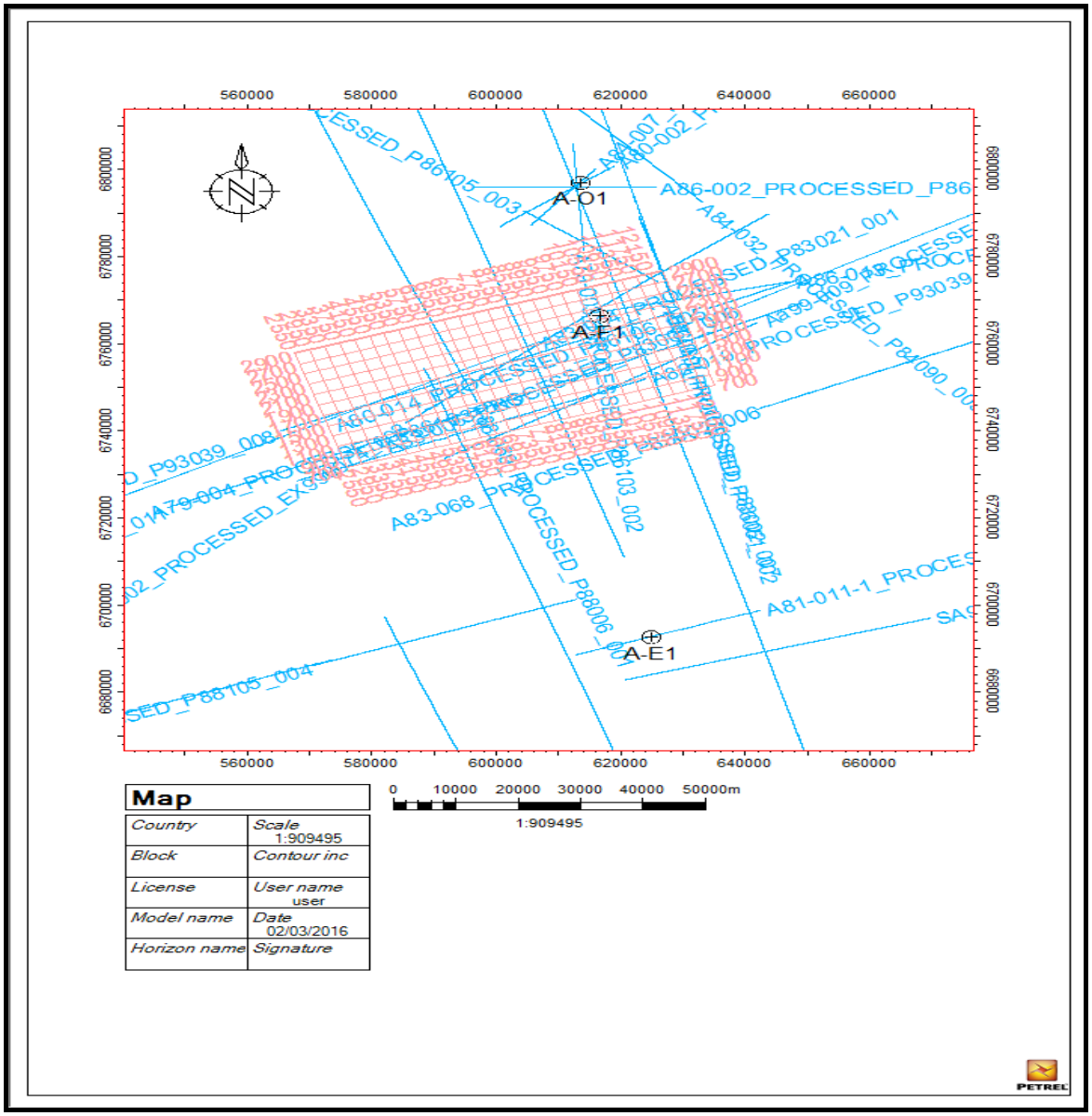

Figure 4.1: Locality Map of the study area and spatial distribution of the three wells drilled in Block 1, Orange Basin. The 3D seismic volume acquired in the centre covers well AF-1, while selected 2D lines within this study area cover the two other wells.

4.3 Methodology

Depositional super-sequences in this study are referred to as major unconformities which represent a diachronous end and a start of a new geological age. Therefore, to understand the sequential depositional events within different ages, sequences are divided based on formation tops and interpreted within a chronological framework. The litho-facies discriminant was based on the Python script; (Gamma Ray (GR)_Merged_new<60,0, If (GR_Merged_new>60 GR_Merged_new<100,1 ,2)).

where 0 represents sandstone, 1 represent siltstone and 2 represents shale. GR values less than 60 API are classified 0, GR values between 60-100 API are classified as Siltstone while GR values greater 100 are classified as Shale. Facies modeling was done by using a sequential indicator simulator to simulate a discrete property (facies) using Kriging indicator, which is determined by taking an average frequency and variation of the discrete spatial continuity. This method is advantageous over other methods for facies modeling because of its ability to simulate complex facies heterogeneity (Yu and Li, 2012).

The litho-facies interpretation of each super-sequence was done from the southern part of the study area (well AE-1), the middle section (well AF-1) and the northern part (well AO-1).

4.4 Results

4.4.1 Interpretation of Depositional Sequence from well logs Signature.

4.4.1.1 Barremian-Aptian Sequence (13AT-1) AE-1 well.

In well AE-1, the facies (Track2., Figure 4.2A) indicates a sub-aqueous depositional system as the continental drift sequence moved from restricted marine to open marine conditions, allowing the deposition of fine grained materials in the form of thick shale beds with intermittent siltstone laminae at depth intervals 4388-4460m. In this case, deposition of shale and siltstone on top of each other reflects on the GR log as a slightly irregular trend, indicating little variation in grain sizes. This observation is supported by the irregular GR –trend observed here which suggests variations in grain sizes. At 4543 m, there is an anomalous increase in impedance contrast at the silt interval, possibly occasioned by a high compaction rate due to overlying sediments (Figure 4.2). The intermittent deposition of fine-grained materials on each other is a common feature of a marginal marine environment in the distal part of a pro-delta environment and could be a sub marine canyon fill (Rider, 1986). This period represents a drift period, and sediments deposited during this time contain mainly siliciclastic clays, intercalated with siltstones and with occasional sand deposit (Dingle et al., 1983).

At a depth of 4537m, the high impedance contrast is associated with a corresponding reversal of polarity of the Reflection Coefficient (RC) and extremely low porosity (Red circle in Figure 4.2.A). Another explanation of high impedance contrast could be due to an unconformity (Miller et al., 2013), and this is likely associated with lateral changes in RC polarity (Veeken, 2013). However, as an expectation, an increase in impedance should be associated with a corresponding increase in the density log values but at this depth (4537m), the density log values do not increase. Therefore, the high impedance contrast may not have been due to the high compaction rate as earlier suggested but rather due to an unconformity which is a candidate for a sequence boundary.

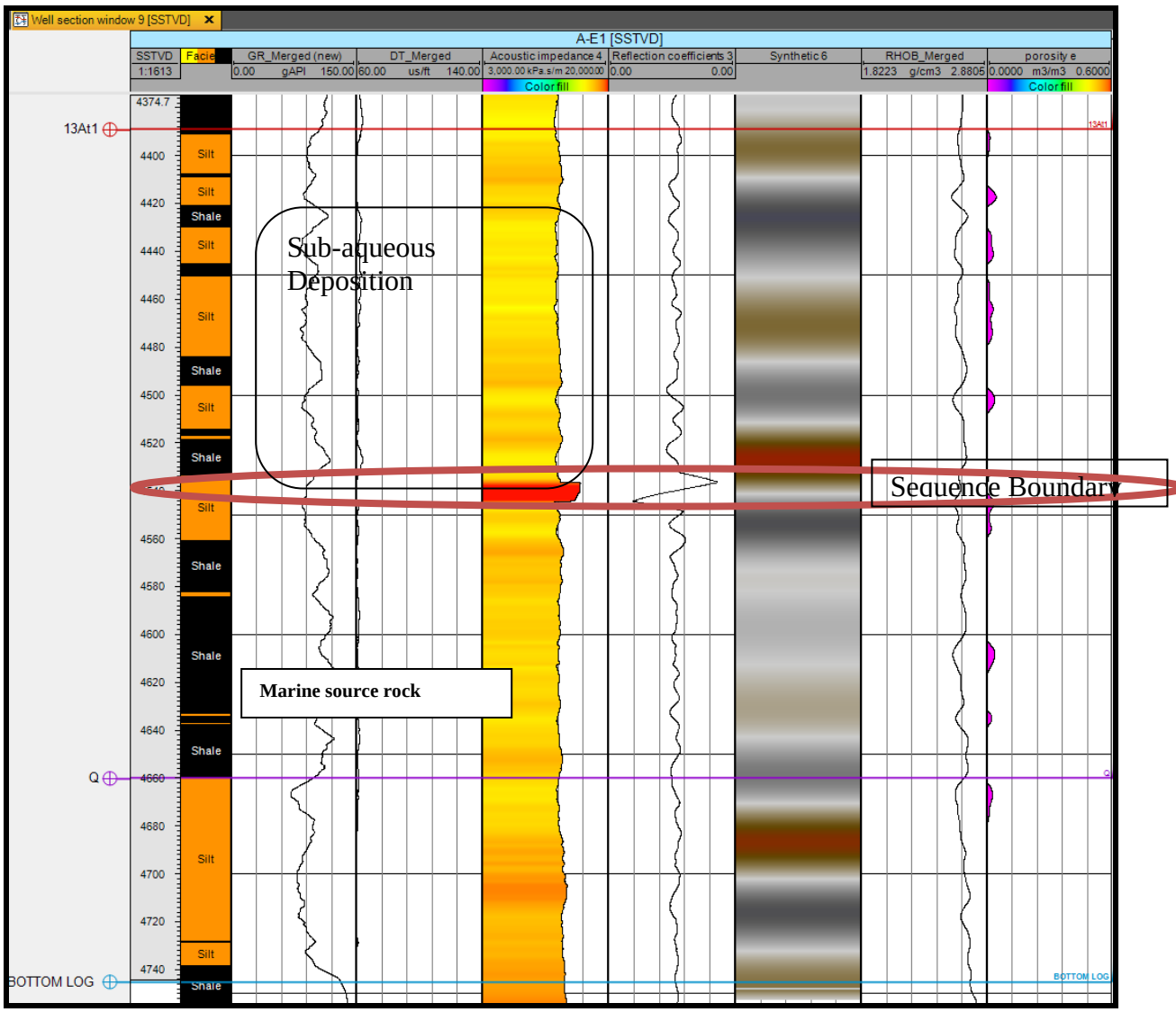

Figure 4.2A: Geophysical logs interpreted for the Barremian-Aptian Sequence. Facies, Gamma ray, Sonic, Acoustic impedance, Reflection Coefficients, Synthetic, Density and Porosity are in track 2, 3, 4, 5, 6,7,8,9 respectively in well AE-1.

4.4.1.2 Barremian / Aptian Sequence (13AT-1) Well AF-1.

Observing the facies change from the southern part of the study area where well AE-1 was drilled, towards the middle section of the study area where AF-1 well was drilled, the Barremian / Aptian sequence appeared to develop regionally but with major facies change as seen in well AF-1(Figure 4.2B). The marine prone source rock was poorly developed in well AF-1(Figure 4.2B) and could suggest a restricted marine influence, particularly because of the development of fining-upward sandstone beds which suggest a fluvial influence. Fluvial influence during this period is significant as the Olifants River contributed a lot of sand-rich sediment, especially near Lamberts Bay around 117.5 Ma, whilst the Orange River contributes a lot of sediments post 112Ma in the northern section (Barton et al., 1993). Because of the poor development of shale beds in well AF-1 (Figure 4.2B), it is envisaged that the sandstones encountered within this sequence could be Fluvio-deltaic front distributary-channel sandstones as a result of restricted marine conditions and good influence of the Olifants River system during this period. The chronostratigraphic sequence here indicates a change in sandstone sequence overlaid by occasional deposition of silt and shale laminae at shallower depth. This is suggestive of a fluvial point bar, channel fill, or it could be a delta-front environment (Bush et al., 1972). Typical distributary channel sandstones are common in delta fronts which could cut sometimes into a fluvial meandering channel landward and grade into finer pro-delta sediments seaward (Bush et al., 1972). Well AF- 1 sandstones show high porosity typified as a fluvial channel fill judging by the fining upward sequence from deeper depth into an aggradational sequence upward. The sandstone beds grade into massive siltstone beds and occasional fluvial sands upward. It is envisaged that shelf progradation as a result of falling sea level could have caused more fluvial influence of the Olifants River system that led to incision of the shelf and subsequent deposition of distributary delta-front channel sandstones.

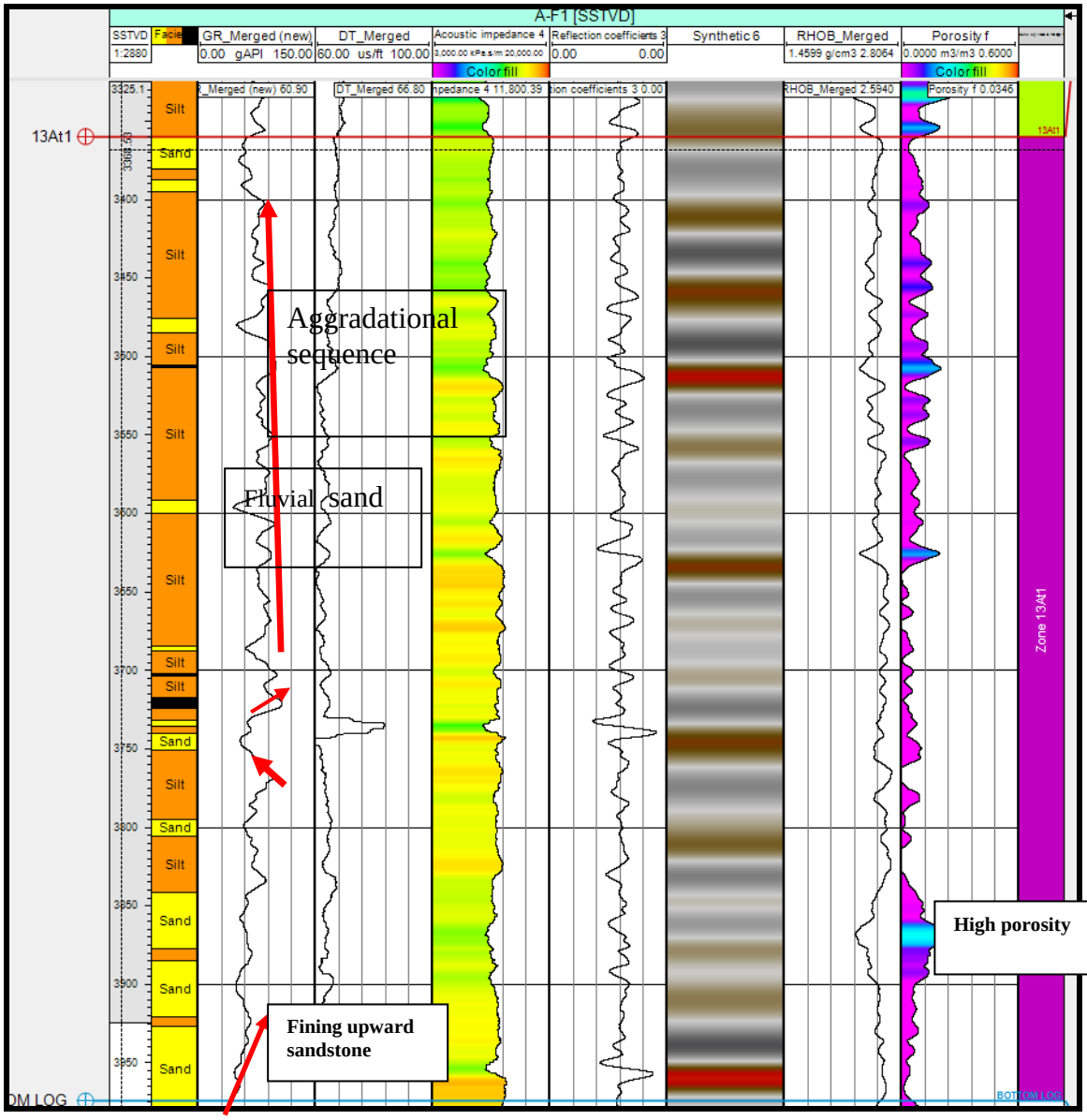

Figure 4.2B: Geophysical logs interpreted for the Barremian-Aptian Sequence. Facies, Gamma ray, Sonic, Acoustic impedance, Reflection Coefficients, Synthetic, Density and Porosity are in track 2, 3, 4, 5, 6,7,8,9 respectively in well AF-1.

4.4.1.3 Barremian-Aptian Sequence (13AT-1) AO-1 Well.

In well AO-1; the northernmost well drilled within the South Africa section of the Orange Basin (Figure 4.2C). The Barremian –Aptian sequence shows significant facies change leading to the deposition of massive shale beds with intermittent siltstone. The sequence shows a typical aggradation sequence around 3200m coupled with less rapid sedimentation rates probably caused by the inactivity of the Orange river systems in the northern part (Brown et al., 1996). There occurs a change in the sequence deposition caused by marine transgression and a fining upward shale sequence suggesting increased organic content from 3050 m, the transgression

steadily reaches maximum level at 3030m, this is marked as an MFS and followed by steady decrease in sea level which marks the onset of progradation and led to coarsening of shale into siltstone around 2940m (figure 4.2C). Maximum Condensed sections exist within sequences 13AT-1, 15AT-1 and 16 AT-1(Brown et al., 1993). Interestingly, at the beginning of steady progradation, there is an increase in the acoustic impedance, reduction in density complimented with high porosity at around 3030m (Figure 4.2C, black circle). Acoustic impedance contrast is commonly affected by lithology, porosity and fluid content. At this depth, which is suggested to be an MFS, the shale interval here is highly rich in thermally matured organic matter which possibly explains the lower density kick at the (Martel, 2013). Marine prone shales with high porosity imply the retention of some generative organic matter (Martel, 2013). Also, kerogen maturation could change shale texture by generating cracks and microstructures, thereby increasing the porosity (Prasad et al., 2009). The latter reason is tenable judging from the anomalous increase in acoustic impedance, polarity reversal on RC, low density and high porosity observed here. The hydrocarbon generative capacity of this shale interval is obvious at this depth and consequently, the organic matter could be attaining thermal maturity here.

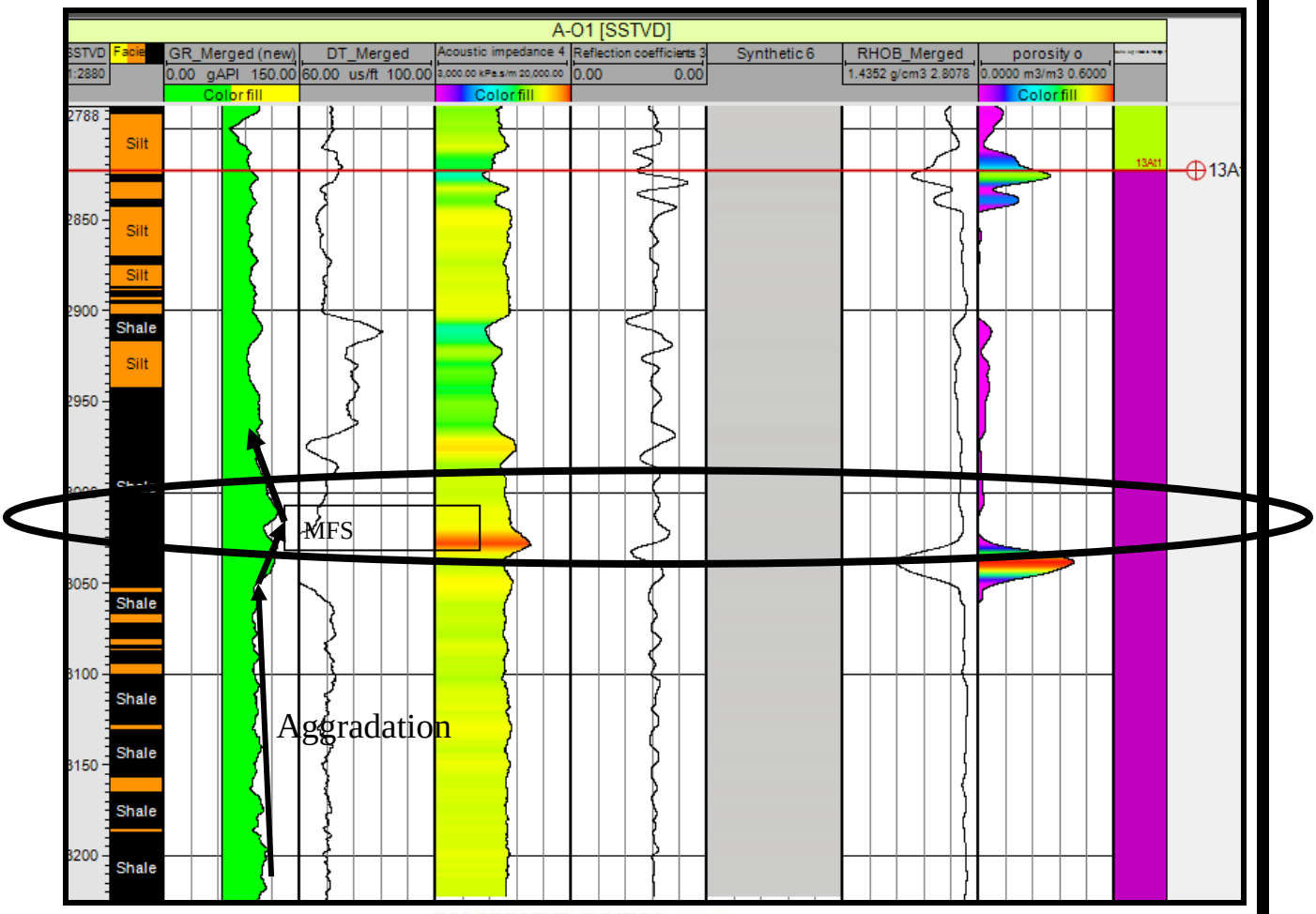

Figure 4.2C: Showing the geophysical logs interpreted for the Barremian-Aptian Sequence. Facies, Gamma ray, Sonic, Acoustic impedance, Reflection Coefficients, Synthetic, Density and Porosity are in 2, 3, 4, 5, 6,7,8,9 respectively in well AO-1.

4.4.1.4 Summary of Barremian/ Aptian13AT-1 Sequence.

In well AE-1 there is an occurrence of massive planar shale facies at deeper depth with low porosity. The facies changed to a massive siltstone unit at a shallower depth and could be attributed to deposition in a pro-deltaic environment. The intermittent deposition of siltstone and shale on top of each other is a common feature of the pro-delta environment. The combination of low porosity, low sonic and high impedance as observed here is suggestive of an unconformity which could be a candidate for sequence boundary (Snedden and Sarg, 2008). In well AF-1, shelf progradation led to the deposition of fluvial-deltaic sandstone units, suggestive of delta-front distributary channel sands, which later shallows into siltstone at the onset of transgression. The sandstone unit shows high porosity at 3855m (figure 4.2B), yet a lower density log reading, suggesting the likely presence of gas in the pore spaces. Litho-facies analyses

of well AO-1 indicate that the drift succession was fully opened to marine conditions within the northernmost sequence (AO-1) as evidenced by the deposition of marine organic-rich shale marked as MFS (figure 4.2C). Acoustic and porosity logs interpretation suggests the likely maturation of organic matter which could have changed the shale bed texture and create micro-structures that led to the high porosity and high acoustic impedance seen in well AO-1 (Figure 4.2C).

4.4.1.5 Early Aptian-Mid Aptian 13CT1 Sequence.

Generally, the drift sequence contains mainly siliciclastic clays, siltstones and occasional sandstone layers (Gerrard and Smith, 1982). The deposition of marine shales and siltstones here suggests that marine flooding was sustained for a long time span and gradually waned in the mid- Aptian leading to the deposition of fluvio-deltaic sandstones, specifically at depth 3850m (Figure 4.3). This is evident from the Gamma-Ray log changing from a coarsening upward sequence of sandstones (Prograding), to a fining upward sequence of the sandstone interval (Retrograding). The sandstone log signature here suggests a regressive-transgressive shore-face deltaic deposit (Rider, 1986). Meanwhile, the marine flooding which led to the deposition of the 13CT1 sequence is only restricted to the southern part of the study area (AE-1) and does not affect the central and northern part judging by the absence of this sequence in wells AF-1 and AO-1, hence a correlative unconformity ceases to exist going northwards. This observation aligns with Kuhlmann et al., 2010 suggesting that the first major marine transgression did not affect the northeastern part of the Orange Basin. This restricted the deposition of sequences 13CT1, 13DT1, 13FT1 and 13GT1 to the southern part of the basin.

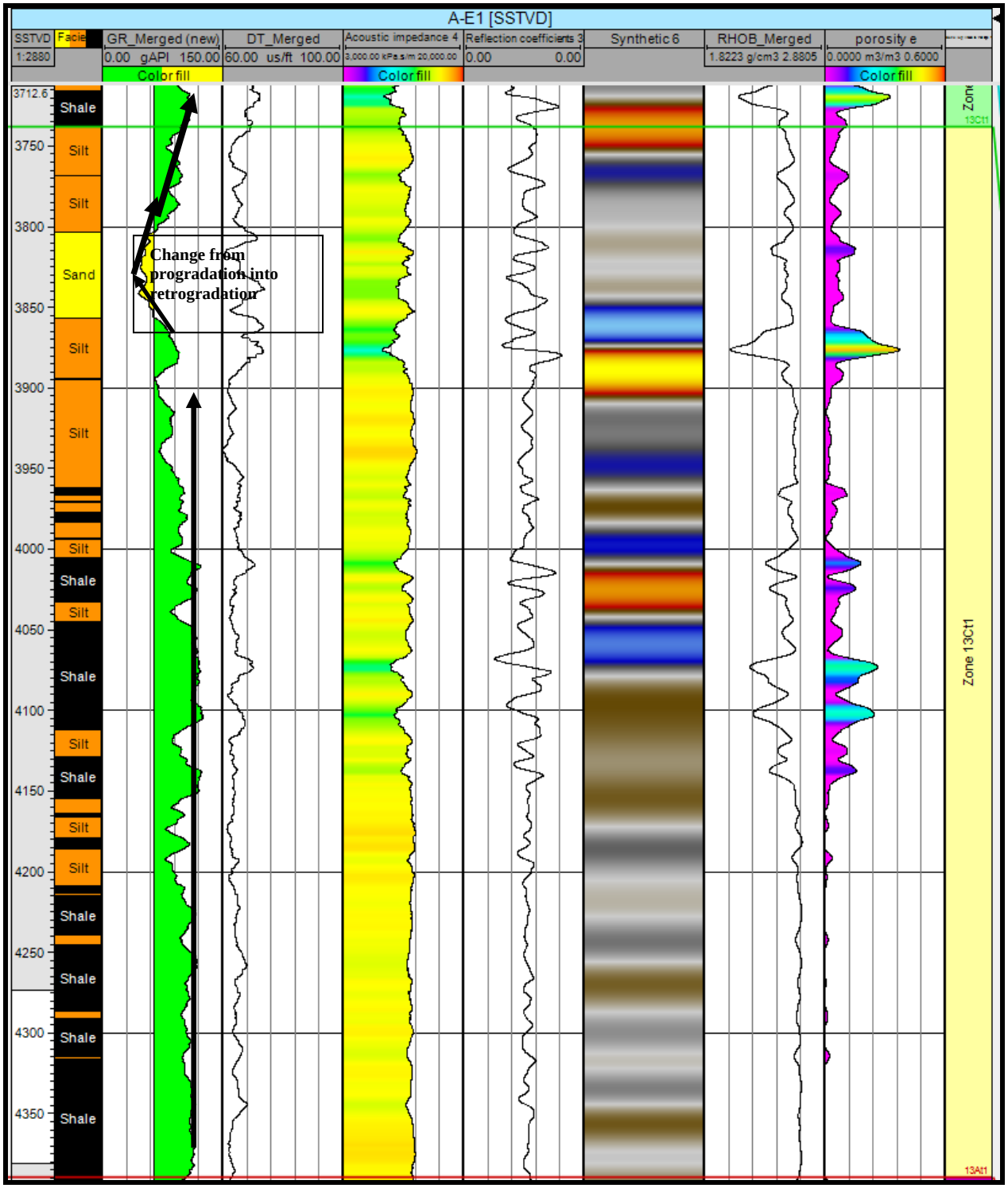

Figure 4.3: Geophysical logs interpreted for the Early-Aptian-Mid Aptian Sequence. Facies, Gamma ray, Sonic, Acoustic impedance, Reflection Coefficients, Synthetic, Density and Porosity are in 2, 3, 4, 5, 6,7,8,9 respectively in well AE-1.

4.4.1.6 Early -Mid Albian 14 AT-1 Sequence AE-1 Well.

Marine pro- deltaic environment system seems dominant and was sustained for a longer period because of the deposition of fine grained materials in the form of shale and siltstone. This appears to be followed by regression accompanied by the incision of Orange river into the shelf area, depositing sandstones observed at depth 3252m. The fluvial incision during this period could likely be accompanied by the deposition of Basin floor fans in the deeper part of the basin. Basin floor fans deposition are prominent and common within the sequences 14B, 14C, 14D and 15B (Brown et al., 1996). A gradual increase in sea level triggered by more accommodation space was probably matched with high sediment fluvial influx which culminated into deposition of shallow marine sandstone at the onset of regression (Progradational sequence) as seen at depth 3210m (Figure 4.4A).

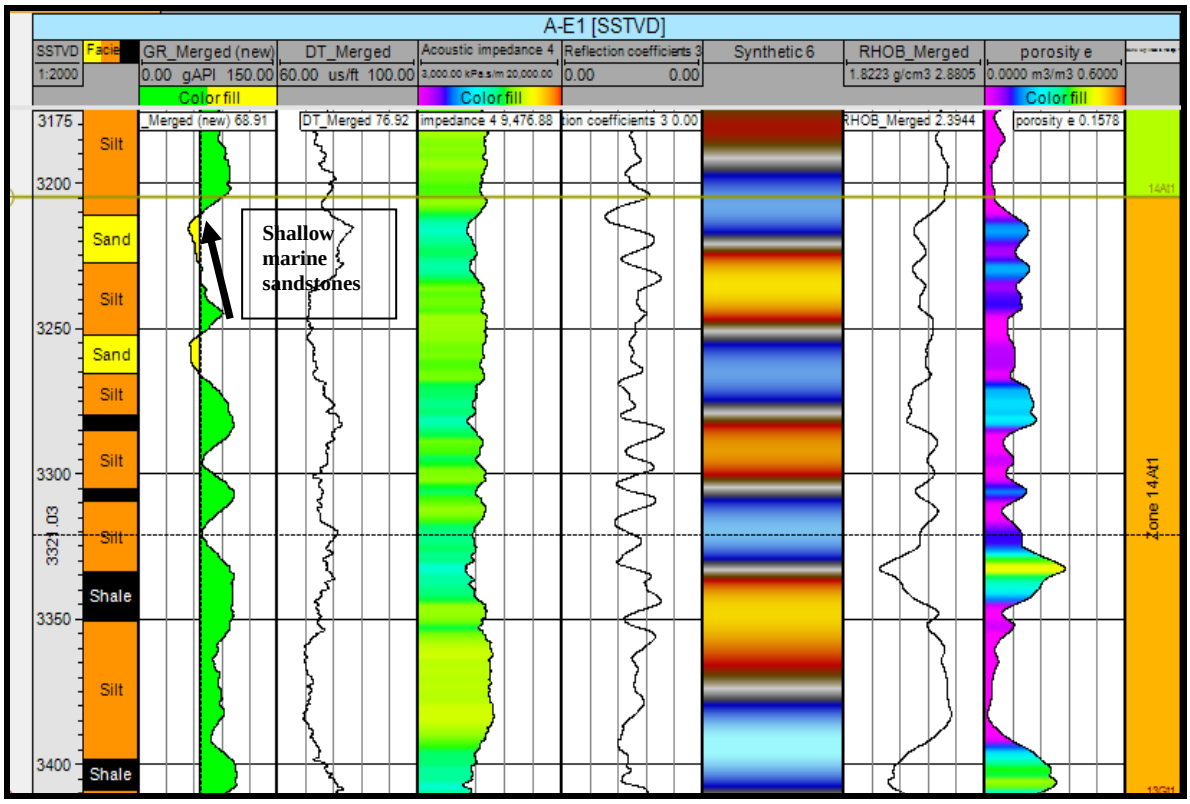

Figure 4.4A: Showing the geophysical logs interpreted for the Early-Mid Albian Sequence. Facies, Gamma ray, Sonic, Acoustic impedance, Reflection Coefficients, Synthetic, Density and Porosity are in 2, 3, 4, 5, 6,7,8,9 respectively in well AE-1.

4.4.1.7 Early -Mid Albian 14 AT-1 Sequence AF-1 Well

In well AF-1 (Figure 4.4B), the 14AT-1 sequence shows similar log signatures as in well AE-1 but, with the exception of the deposition of a massive siltstone unit. The deposition of massive siltstone units was probably due to high rate of sedimentation coupled with a switch to a dominant Orange River system accompanied by a change of depocentre to further north in the basin. This observation is supported by Brown et al.,1993 which explained that a high rate of deposition coupled with thermal subsidence, exerted a major control on the stacking pattern of the 14AT-1 sequence, especially northward of the Orange Basin. However, there is evidence of frequent interchange between progradation and retrogradation throughout the entire sequence judging from the Gamma Ray log signature.

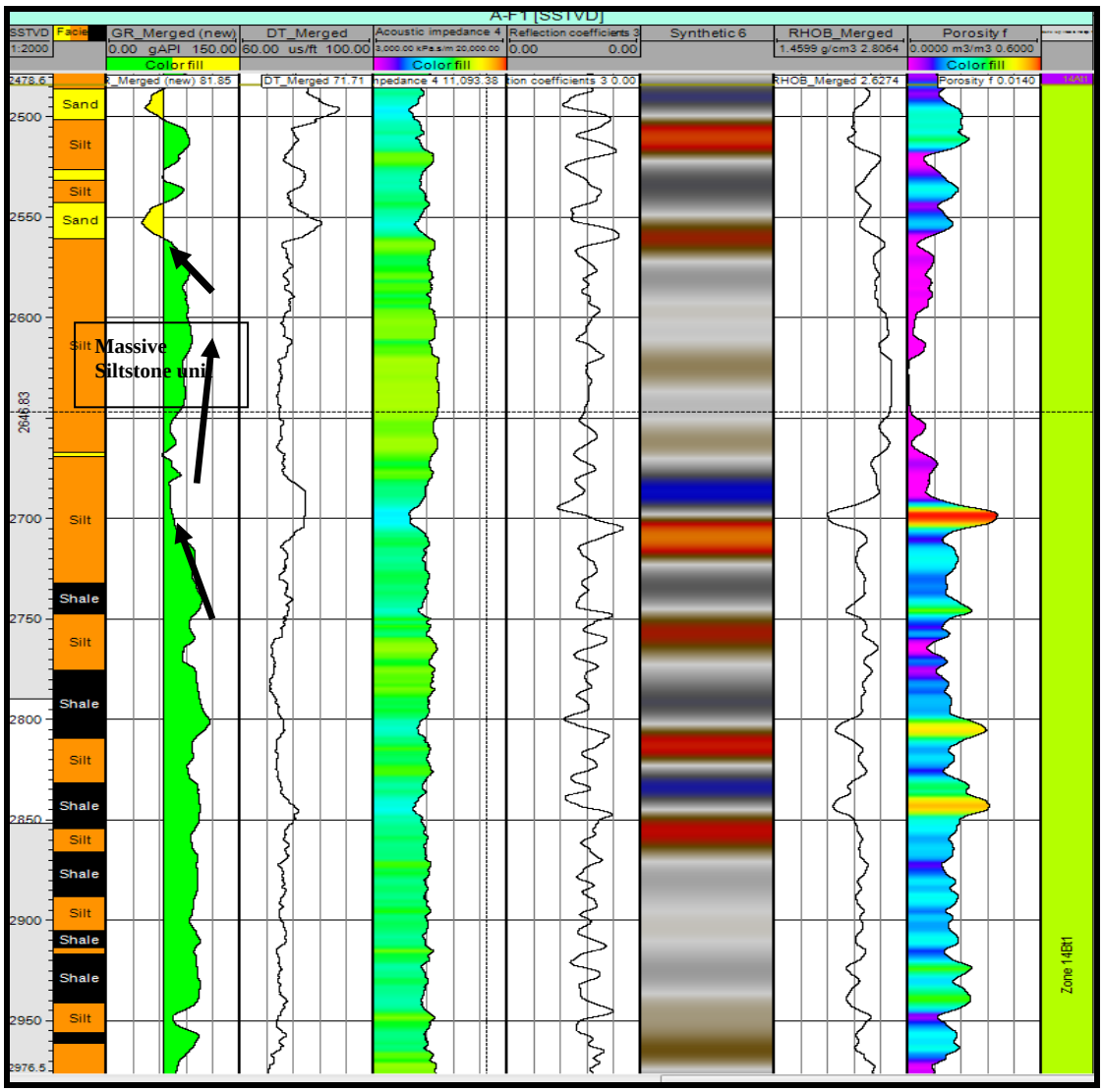

Figure 4.4B: The geophysical logs interpreted for the Early-Mid Albian Sequence. Facies, Gamma ray, Sonic, Acoustic impedance, Reflection Coefficients, Synthetic, Density and Porosity are in 2, 3, 4, 5, 6,7,8,9 respectively in well AF-1.

4.4.1.8 Early -Mid Albian 14 AT-1 Sequence AO-1 Well.

Furthermore, in well AO-1(Figure 4.4C), high rate of sedimentation continues deep into the northern section which led to the deposition of massive shale in well AO-1 (Figure 4.4C). The massive siltstone with shale interbeds facies observed in the central part (AF-1) (Figure 4.4B) changed to dominant shale in the most northern area (AO-1). The deposition of this massive shale unit is likely due to a rise in sea level matched with a corresponding high rate of sedimentation and extreme river energy level that forced an aggradational/progradational shift in sediment deposition into the pro-delta environment. Generally, the 14AT-1 sequence is part of the drift succession in which limited but gradual regression caused the progradation and aggradation (sigmoidal) of this sequence in the northern Orange Basin (Brown et al., 1996).

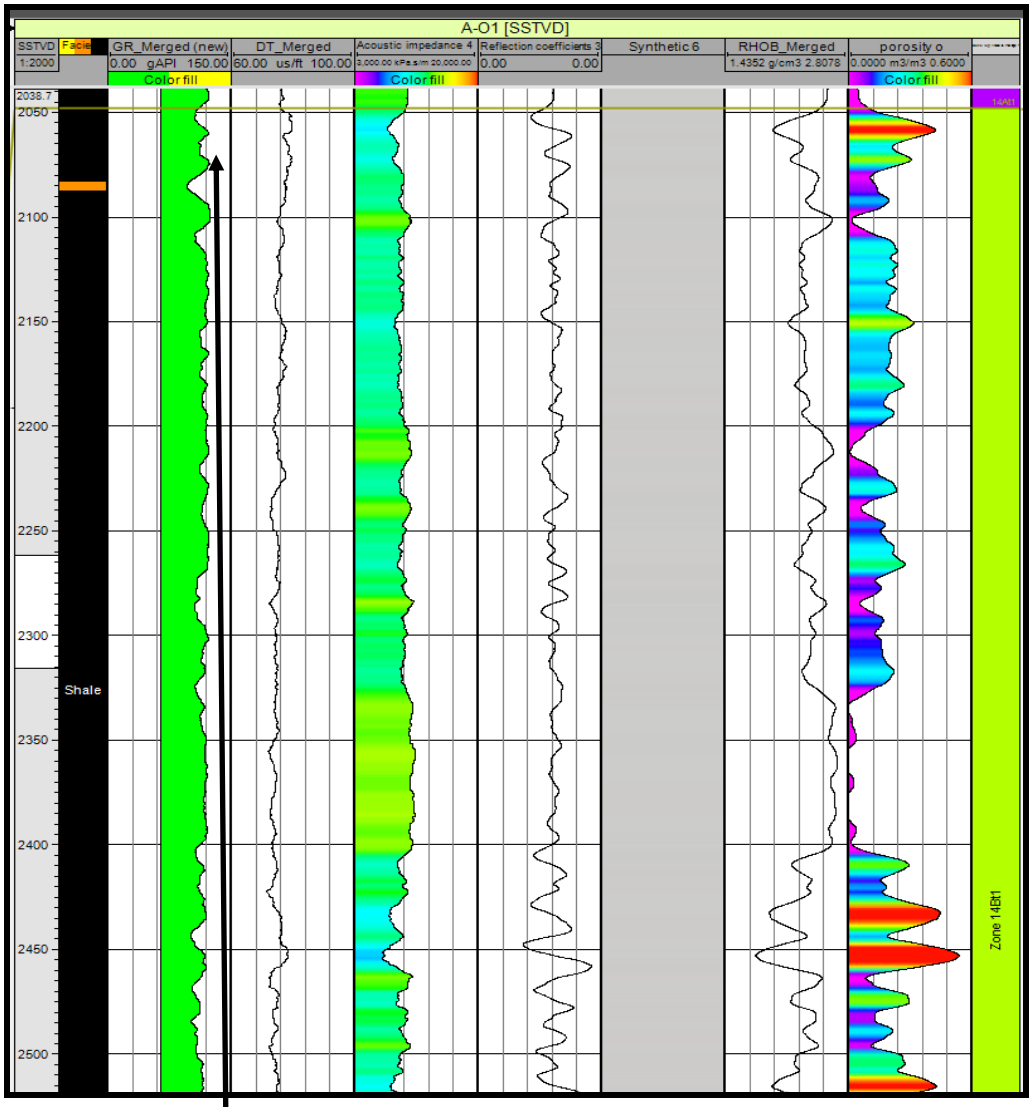

Figure 4.4C: The geophysical logs interpreted for the Early-Mid Albian Sequence. Facies, Gamma ray, Sonic, Acoustic impedance, Reflection Coefficients, Synthetic, Density and Porosity are in 2, 3, 4, 5, 6,7,8,9 respectively in well AO-1.

4.4.1.9 Summary of 14AT-1 Sequence.

The marine flooding that characterized this period led to the deposition of massive shale and siltstone units which later grade in to fluvio- marine sandstones at shallower depth occasioned by fluvial incision into the shelf area (AE-1 and AF-1) at the onset of regression but not evident in the northernmost part of the basin. The presence of massive shale units in the northernmost area (AO-1) and the absence of fluvio-marine sandstones could be due to the activity of the Orange River system, coupled with concurrent rise in sea level which forced an aggradational/ progradational sequence in

the pro-delta area that led to the deposition of thick massive shale but lesser siltstone units.

4.4.1.10 Mid-Late Albian Sequence (14Bt-1, 14Ct-1, 14Et-1 and 14Gt-1 Unconformities) AE-1 Well (Southern part).

These sequences were encountered in the southern part of the study area only because there was either no deposition or likely erosion in the northern part; these units are dominated by an alternating transgression and regression regime (Figure 4.5) and characterised by serrated GR log curves. Commonly serration is due to interbeds caused by domination of an aggradation sequence coupled with a storm dominated shelf environment (Rider, 1986). The depositional system of these sequences judging by the serrated GR log curve could thus be associated with storm dominated shelf environment. In this case, there is deposition of more siltstone units with more shale interbeds and occassional sandstone interbeds. This is likely due to a high sedimentation rate coupled with the creation of less accommodation space in the basin. There was massive deposition of sediments from Orange River systems during this period (Brown et al., 1996), and as such, this compliments the observation made about high rate of sedimentation during the Mid-Albian sequences.

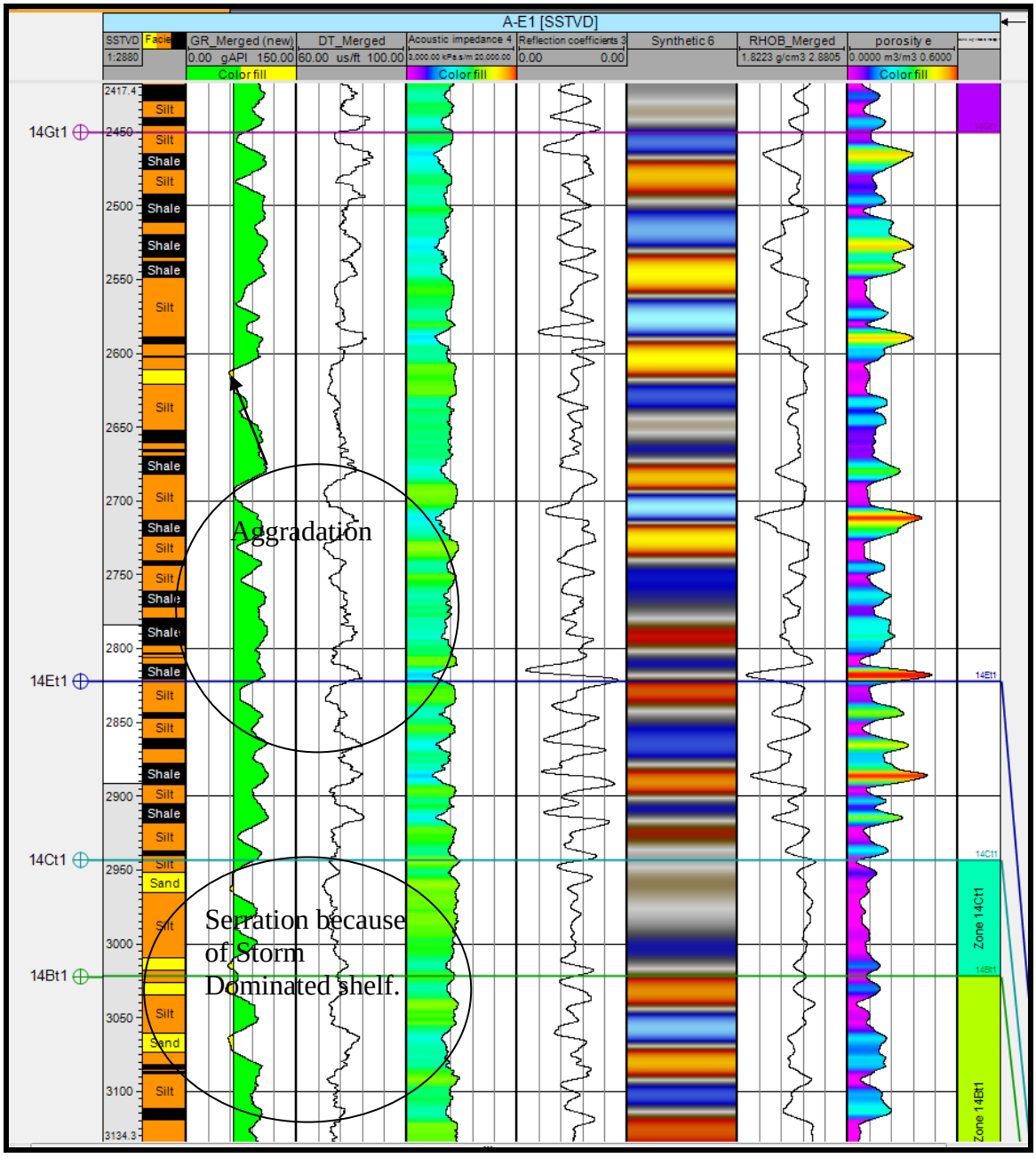

Figure 4.5: The geophysical logs interpreted for the Mid-Late Albian Sequence. Facies, Gamma ray, Sonic, Acoustic impedance, Reflection Coefficients, Synthetic, Density and Porosity are in 2, 3, 4, 5, 6,7,8,9 respectively in well AE-1.

4.4.1.11 Late Albian/Cenomanian Sequence (14HT1 and 14JT1) AE-1 Well (Southern section).

With marine conditions dominance during this period as margin evolution entered the upper Cretaceous, the Gamma Ray log in AE-1 shows an aggradational/ progradational sequence judging from the Gamma Ray log signature. The Gamma Ray log curve shows an initial aggradation sequence, followed by likely reduction in

sea level which caused progradation that led to the deposition of sandstone intervals observed here (Figure 4.6A). Subsequently, an aggradation regime dominates throughout the entire Cenomanian sequence.

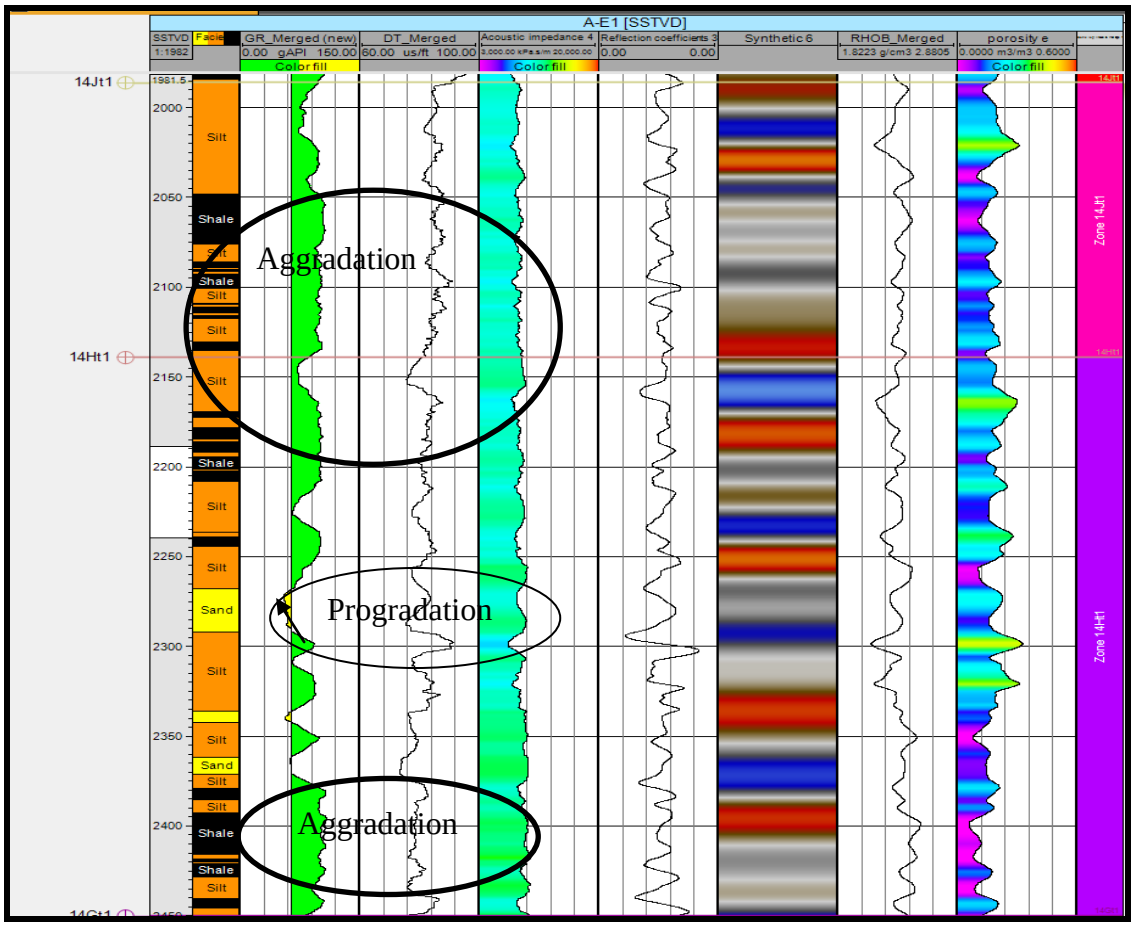

Figure 4.6A: The geophysical logs interpreted for the Late Albian-Cenomanian Sequence. Facies, Gamma ray, Sonic, Acoustic impedance, Reflection Coefficients, Synthetic, Density and Porosity are in 2, 3, 4, 5, 6,7,8,9 respectively in well AE-1.

4.4.1.12 Late Albian/Cenomanian Sequence (14HT1 and 14JT1) AF-1 Well (Central section).

In well AF-1(middle section), these sequences started with deposition of a massive siltstone unit at depth 2480m which gradually turns into a thin laminated sand at around 2170m (figure 4.6B). The log signature looks serrated possibly because of storms associated with the deposition. In addition, the log signature shows a cylindrical GR signature at a depth of 2300m, indicative of braided distributary channel-fill sandstones unit (Onyekuru et al., 2012). Following the deposition of these Albian-aged distributary channel sandstones, the depositional system changed to a

progradational/aggradational system allowing the intercalation of siltstone and sandstones as evident from Figure 4.6B.This continues till the end of the sequence.

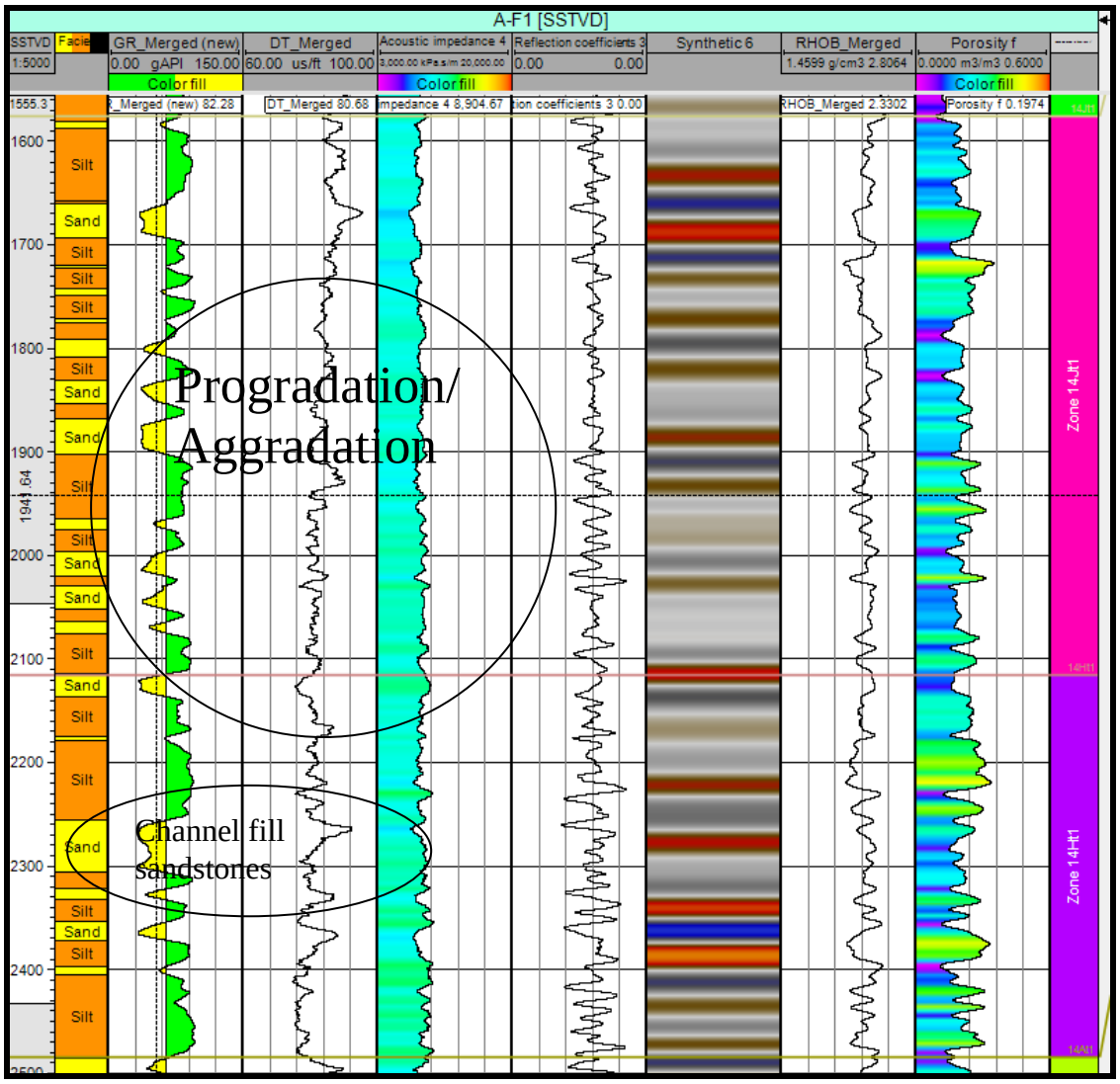

Figure 4.6B: Geophysical logs interpreted for the Late Albian-Cenomanian Sequence. Facies, Gamma ray, Sonic, Acoustic impedance, Reflection Coefficients, Synthetic, Density and Porosity are in 2, 3, 4, 5, 6,7,8,9 respectively in well AF-1.

4.4.1.13 Late Albian/Cenomanian Sequence (14HT1 and 14JT1) AO-1 Well (northern section).

In well AO-1 (northward), these sequences show a clearly defined coarsening upward sequence in which facies changed abruptly from shale in the 14HT1 sequence to siltstone in 14JT-1 sequence suggesting steady onset of regression and a change of facies from a massive marine shale to massive siltstones at a depth of 1650m(Figure 4.6C). This marks the transition from Late Albian to Cenomanian. The marine shales and siltstones are massive, thereby suggesting a gradual regression matched by high

sedimentation rate. High porosity and lower density values observed in the shale interval 1700m-1900m may be indicative of brittleness, which may be as a result of high organic content shale that has been subjected to high temperature conditions leading to textural cracking and consequently an increase in the porosity.

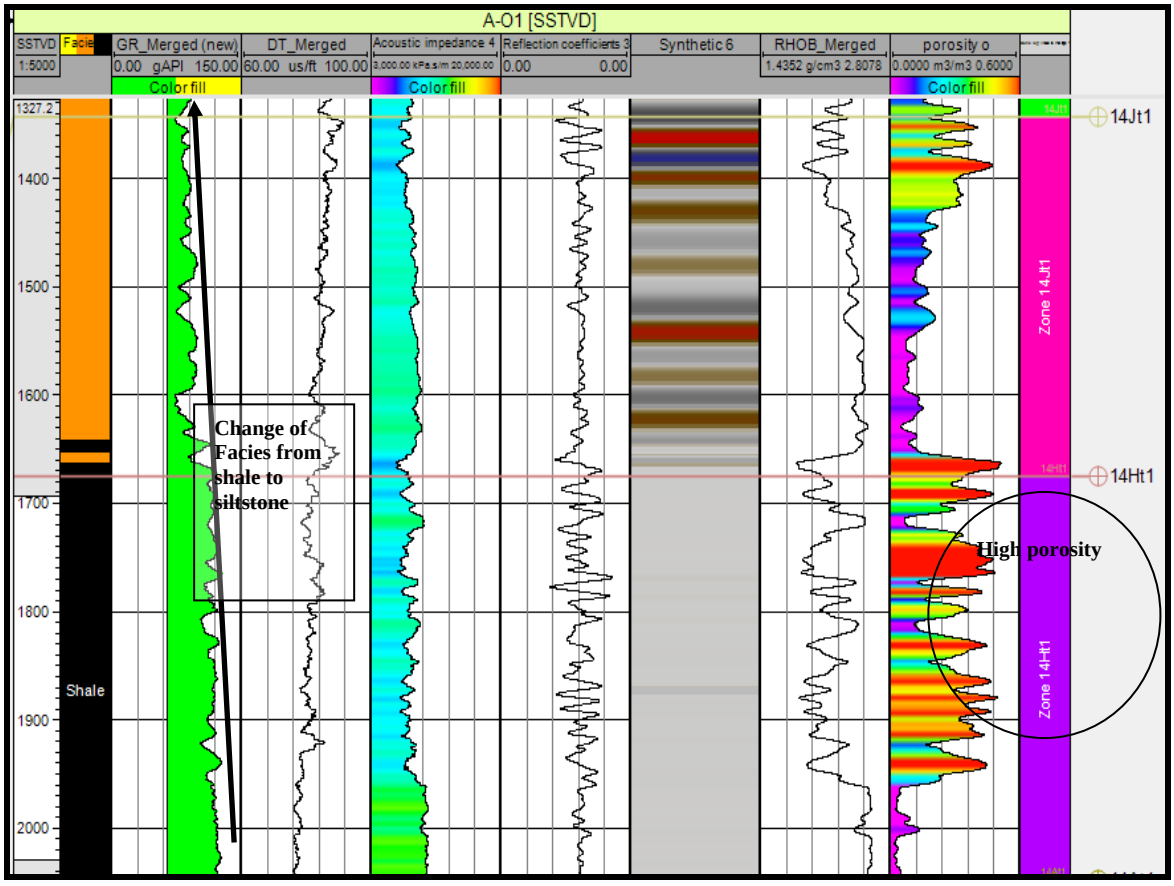

Figure 4.6C: Geophysical logs interpreted for the Late Albian-Cenomanian Sequence. Facies, Gamma ray, Sonic, Acoustic impedance, Reflection Coefficients, Synthetic, Density and Porosity are in 2, 3, 4, 5, 6,7,8,9 respectively in well AO-1.

4.4.1.14 Summary of Sequences Late Albian/Cenomanian (14GT1, 14HT1 and 14JT1).

The gradual change of facies from massive shale beds into siltstone at shallower interval in the northernmost part (AO-1) of the study area laterally becomes an intercalation of siltstone and sandstone southwards (AF-1), and later a dominant shale and siltstone unit (AE-1). These massive shale and siltstone units' deposition within these sequences is suggestive of it being interpreted as the distal portion of the study

area because finer grained materials are often transported far into the distal portion of the basin.

4.4.1.15 Cenomanian-Turonian Sequences (14KT1, 15AT1 and 15BT1) AE-1 Well (southern section).

This sequence is the youngest sequence recorded by the wireline logs data acquired for AE-1 well and is dominated by sandstone units. However, there is no presence of the expected Turonian source rock within this sequence (Figure 4.7A). The global anoxic event which led to the deposition of the Turonian source rock localized its distribution within the Orange Basin and is not present throughout the entire basin (Jungslager, 1999). The Gamma Ray log within the lower part of the sequence shows a well-defined coarsening upward sequence characteristic of delta front sandstone within the 14KT-1 sequence, which later changed into siltstone within the overlaying 15AT1 sequence. The Gamma Ray log signature of the sandstones within the 15AT-1 sequence shows a cylindrical pattern, typical of an aggradational sequence which later shallows into a retrogradational fluvial sandstone in the uppermost section (Figure 4.7A).

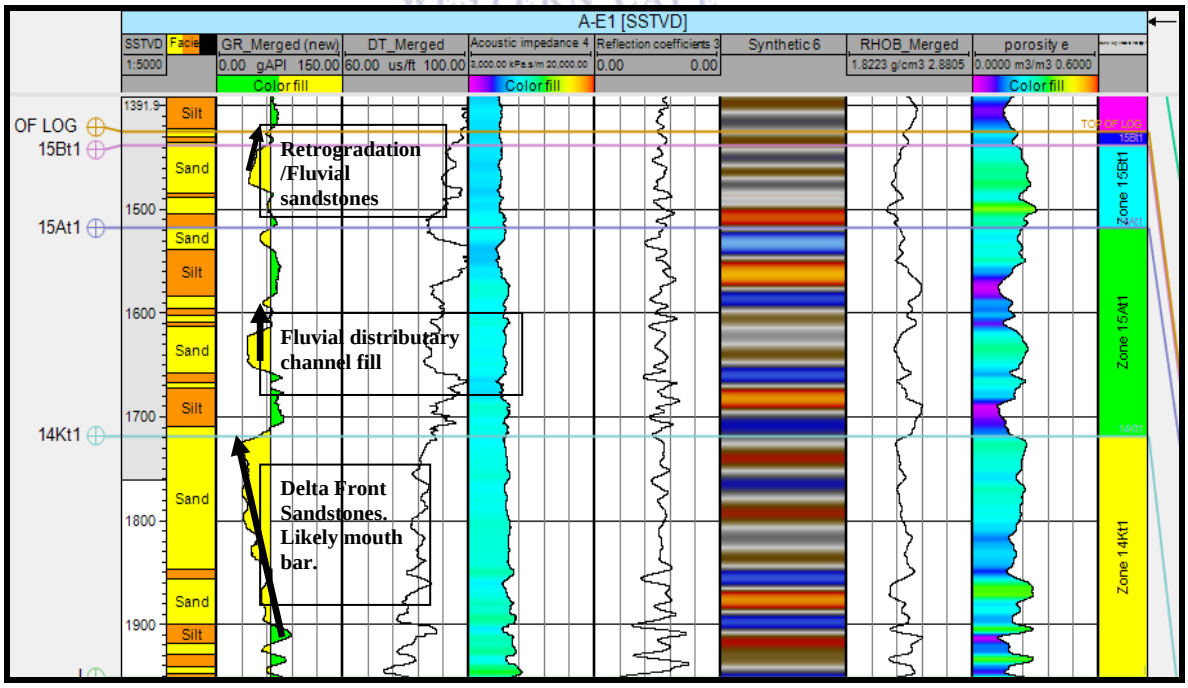

Figure 4.7A: Showing the geophysical logs interpreted for the Cenomanian- Turonian sequence in well AE-1. Facies, Gamma ray, Sonic, Acoustic impedance, Reflection Coefficients, Synthetic, Density and Porosity are in 2, 3, 4, 5, 6,7,8,9 respectively in wel AE-1

4.4.1.16 Cenomanian-Turonian Sequence (15AT-1) AF-1 Well (Central section).

Mapping the sequences further, towards the central section of the study area specifically in well AF-1 (Figure 4.7B), only sequence 15AT1 was deposited while sequences 15BT1 and 14KT1 seen in AE-1 well (Figure 4.7A) may have been eroded or not deposited. There is deposition of progradational massive siltstone at a deeper depth within this sequence which changed into distributary channel sandstone at 1350m (Figure 4.7B). The sandstone unit here correlates well with the 15AT-1 sandstone unit previously seen in AE-1 well, suggesting a distributary channel fill (Figure 4.7B).

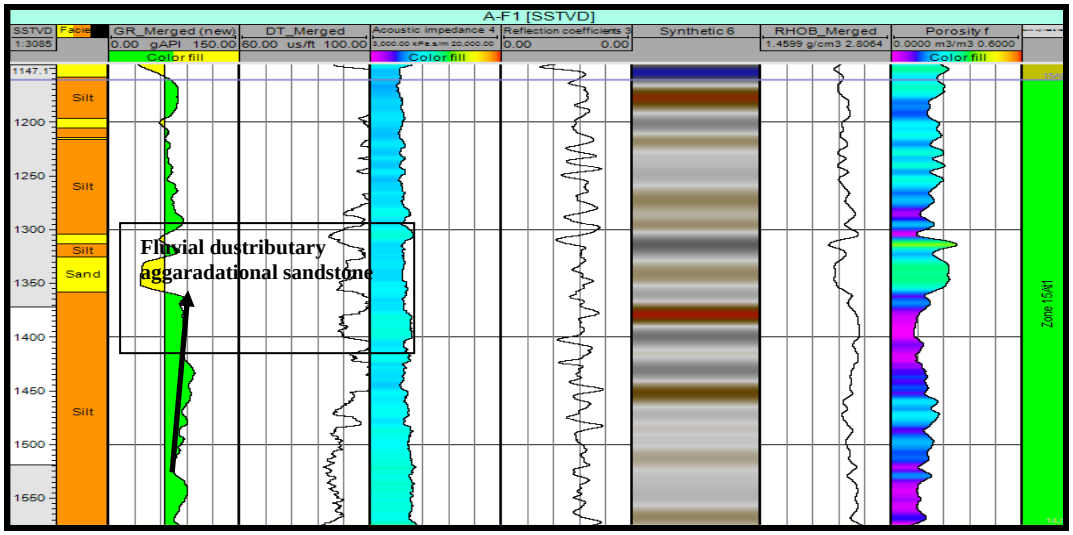

Figure 4.7B: Geophysical logs interpreted for the Cenomanian–Turonian Sequence. Facies, Gamma ray, Sonic, Acoustic impedance, Reflection Coefficients, Synthetic, Density and Porosity are in 2, 3, 4, 5, 6,7,8,9 respectively in well AF-1.

4. 4.1.17 Summary of Cenomanian- Turonian Sequences.

Sequences 14KT1 and 15BT1 were only encountered in well AE-1 while 15AT 1 sequence was deposited across the three wells. The facies is dominantly siltstone especially in well AO-1 with rare sandstone intervals. However, there is correlative deposition of a fluvial distributary channel aggradational sandstone deposit in wells AE-1 and AF-1.

4.4.1.18 Turonian-Coniacian-Maastrichtian Sequences.

These sequences represent the late Cretaceous sequence and the youngest sequences completely logged by the geophysical logs. Because of the uplift in the late Cretaceous, part of these sequences may have been eroded and may not be regionally present, particularly the Coniacian-Campanian sequence. However, the Maastrichtian appears to be regionally correlative across the study area. Consequently, to avoid complexity in interpreting individual sequences, the Turonian-Maastrichtian sequences are interpreted together. A fractional part of the Cenozoic sequence was also geophysically logged for AF-1 and AO-1 wells but not for AE-1 well. The Cenozoic sequence will be discussed under the seismic facies analysis section in chapter five. These late Cretaceous sediments are characterized by fining upward sandstone intervals probably deposited during changing subsidence and eustatic rates which caused marine transgression and consequent retrogradational sequences (Figure 4.8). The steady sea level rise matched by high fluvial sedimentation rates which characterizes this period (Brown et al.,1996), could have caused delta progradation which led to the deposition of the fluvio-deltaic sandstones and subsequent siltstone deposit as evident from fining upward Gamma Ray log signature (Figure 4.8). As seen from Figure 4.8, the acoustic impedance is low but with a corresponding high porosity as a result of lesser compaction caused by a relatively thin Cenozoic overburden succession. This figure is a representation of similar observations made from the other wells AO-1 and AE-1, hence observations made in AF-1 are a replica of AE-1 and AO-1 wells. This suggests lesser or no variations in the depositional systems and tectonics across the study area during this period.

The total Cenozoic strata in the Orange Basin are thin with thickness variation of 50-250m in the southern part (McMillan, 2003). The highlight of the event that characterized this period is intensity of erosion caused by a previous uplift on the deposited sand rich sediments of the Low system tract, and an associated gravity induced faulting (de Vera et al., 2010; Brown et al., 1996).

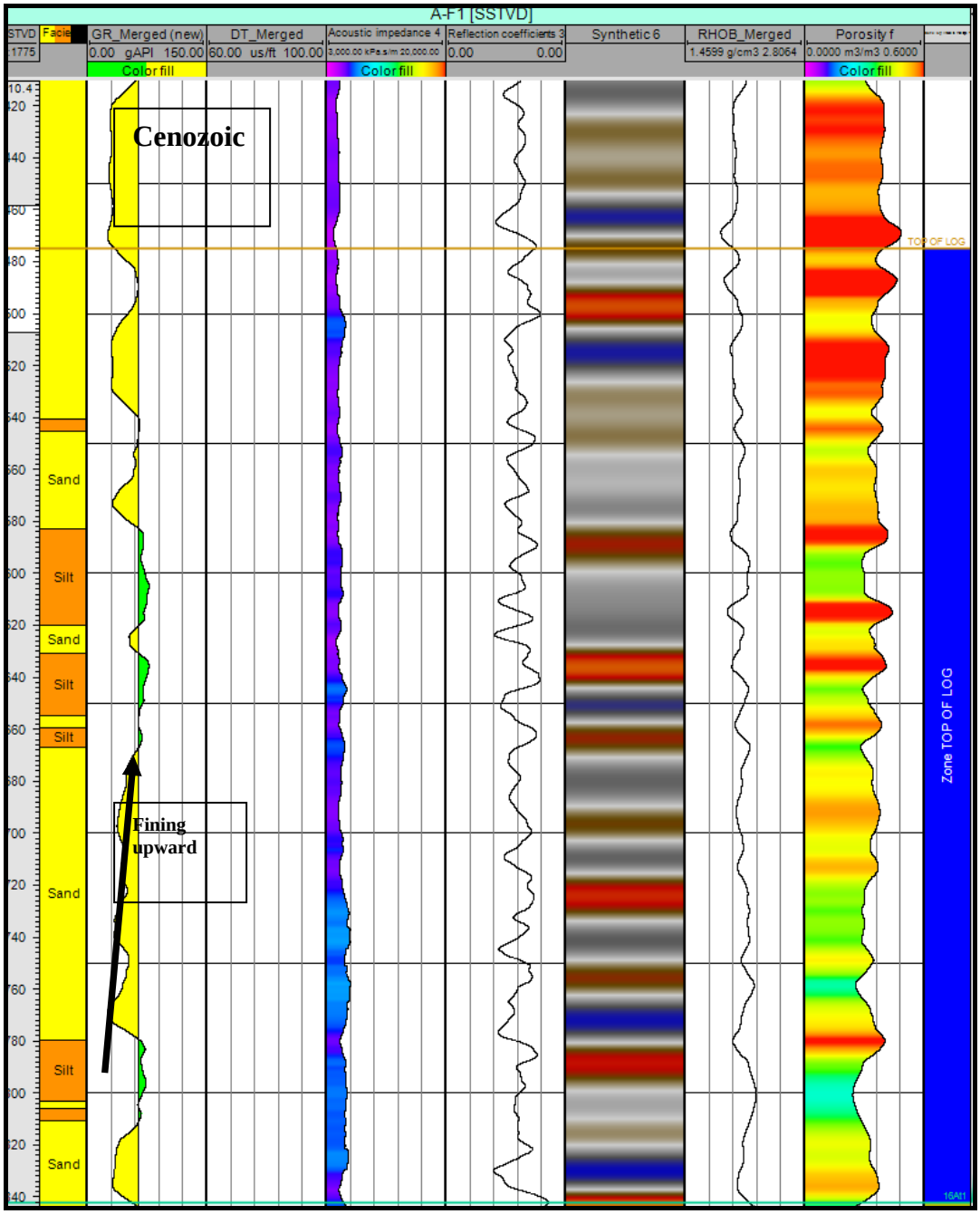

Figure 4.8: Showing the geophysical logs interpreted for the Turonian- Coniacian-Maastrichtian sequence in well AF-1. Facies, Gamma ray, Sonic, Acoustic impedance, Reflection Coefficients, Synthetic, Density and Porosity are in 2, 3, 4, 5, 6,7,8,9 respectively.

4.4.2 Litho-Facies Modelling.

3D Facies modelling can provide quantitative information on lithology distribution, internal geometry and spatial correlation of these lithologies. While internal geometry of facies can reveal fluvial depositional environment deposit because of distinctive shape they exhibit, (distributary channels and levees), it is more complex to determine the internal geometry of sediments from non-fluvial environment because they exhibit non-distinctive patterns.

The facies modelling process for each unit of super sequence was performed to understand the spatial deposition of different litho-facies (Silt, Sand and Shale) across the study area and create a good framework for numerical simulation. Simulation of reservoir parameters is outside the scope of this study, however, a statistical variogram; Sequential indication simulator was used to simulate the distribution of facies as a discrete property across the study area. Prior to this, upscaling of facies log for each of the three wells used for this study was done. The modelling input parameters include the upscaling of facies log created by using the python script as mentioned under the methodology section of this chapter and the population of it on a gridded geo-cellular model using the averaging weighing factor of cells in performing the population of cells with the upscaled facies log.

The litho-facies modelling results for each super sequence are discussed below; starting from the youngest sediments (Cenozoic) to the oldest Barremian-Aptian aged sediments. The results explained below are a representative of the upper view of each super sequence.

4.4.2.1 Cenozoic and Maastrichtian Sequences

The Cenozoic and Maastrichtian sequences (Figure 4.9 A and B, respectively) are dominated by siltstone and sandstones deposit with the former prominent in the western portion of the study area. The sandstones appear to be randomly distributed within these sequences except for a definitive internal structure observed within the Maastrichtian sequence suggesting a mouth bar deposit in the north-eastern section of the study area (Figure 4.9B)

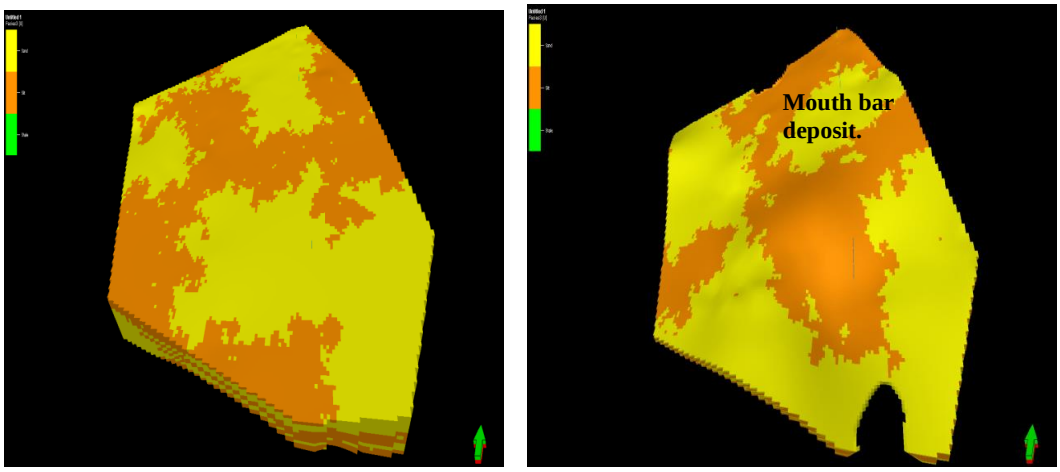

(A) **(B)**

Figures (4.9 A and B): Top view of Cenozoic (A) and Maastrichtian (B) sequences litho-facies model showing the distribution of Sandstones (Yellow) and Siltstones (Brown) across the study area. The geometry of sandstone deposit within the Maastrichtian suggests the presence of a mouth bar deposit.

4.4.2.2 Turonian and Cenomanian Sequences

The Sandstone deposit geometry of the Turonian sequence occupies the central portion of the study area and suggest it as possible floodplain deposits with siltsones as overbank deposits (Figure 4.9C). The Cenomanian sequence consist dominantly of siltstones with occassional shale deposit occuring as possible laminae, while sandstones deposit is prominent in the northeastern section of the study area.

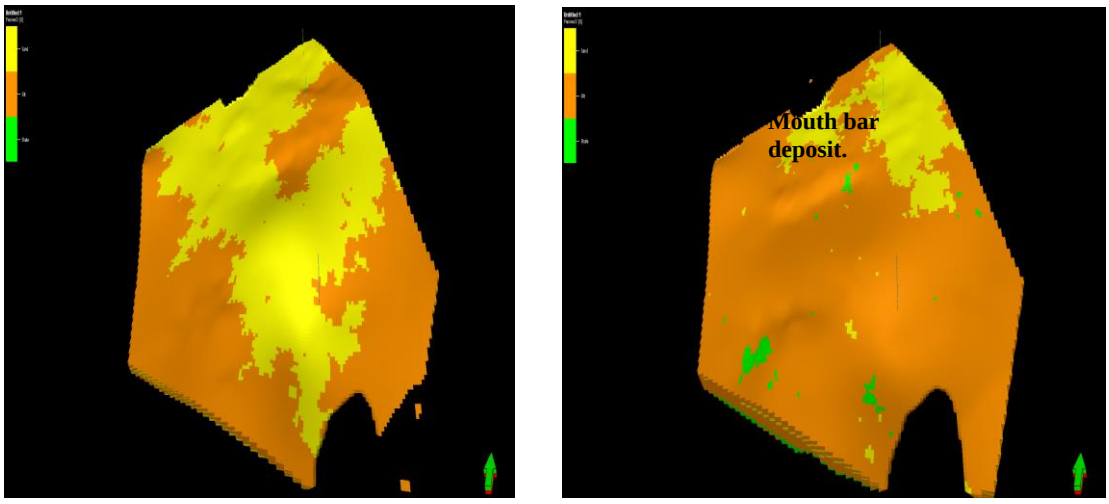

(C) **(D)**

Figures (4.9C and D): Top view of Turonian (C) and Cenomanian (D) sequences litho-facies model showing the distribution of Sandstones (Yellow), Shale (Green) and Siltstones (Brown) across the study area. The geometry of sandstone deposits occurs as possible mouth bar deposit in the Cenomanian sequence.

4.4.2.3 Late Albian and Albian Sequences

Late Albian sequence consists dominant siltstones, rare sandstones in the southern part and rare random shale deposit occuring as bars within the late Albian sequence (Figure 4.9E). The Albian sequence consists of dominant shale deposits, rare sandstones and siltstone deposit in the northern part of the study area (Figure 4.9F). The sandstone geometry suggest point bar deposit and and an adjoining channel-filled silstone deposit in the northern part of the area.

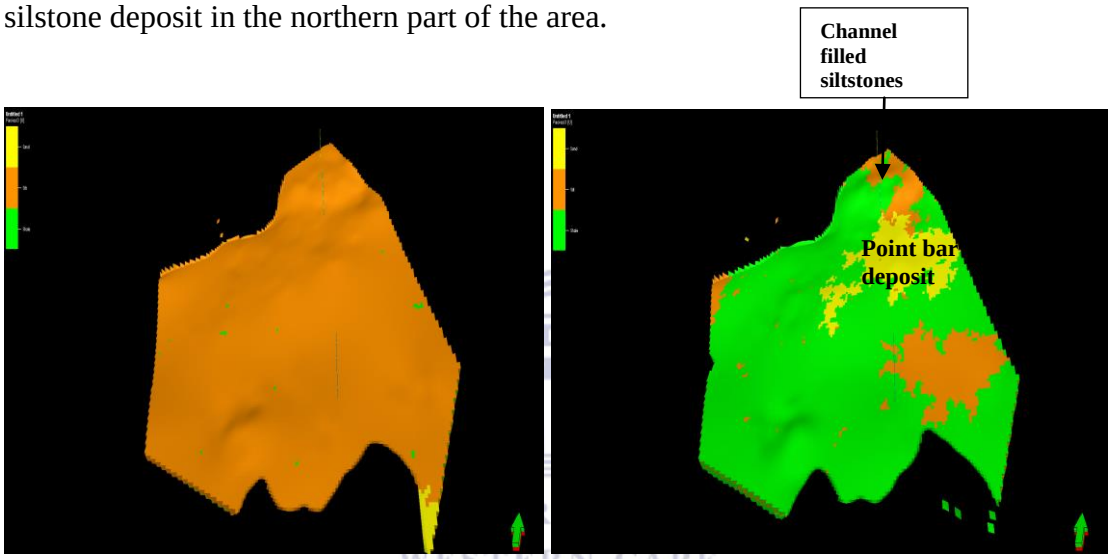

(E) **(F)**

Figures (4.9E and F): Top view Late Albian (E) and Albian (F) sequences litho-facies model showing the distribution of Sandstones (Yellow), Shale (Green) and Siltstones (Brown) across the study area. The geometry of sandstone deposit within the Albian sequence.

4.4.2.4 Barremian-Aptian Sequence

The oldest Barammian-Aptian sequence consist dominant silstones and rare shale deposit in the northern section of the study area. The shale deposit encountered at the top of the sequence is an indication of the presence of organic rich marine shale deposit prominent within the Barremian-Aptian sequence in the Orange Basin, South Africa (Figure 4.9 G). The shale deposit is widespread and the view here shows just the top of the Barremian/Aptian sequence. This shale deposit is later utilized as the source rock unit simulated in chapter seven of this study.

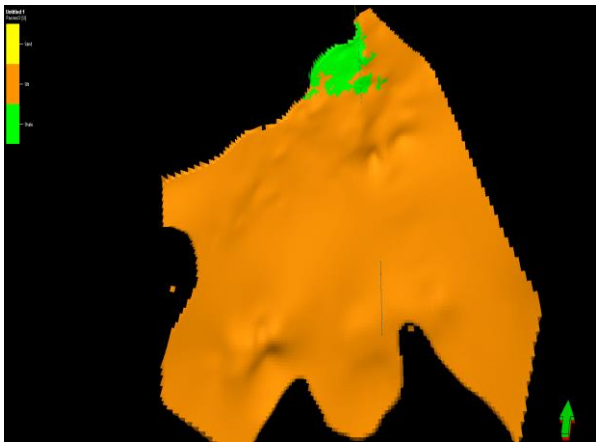

(G)

Figure (4.9 G): Top view of Barremian-Aptian sequence litho-facies model showing the distribution of Siltstones (Brown) and Shale (Green) across the study area. The shale deposit here is the expression of the marine organic-rich shale deposit within this sequence.

4.5 Conclusions

Litho-facies interpretations from the three wells (AE-1, AF-1 and AO-1) utilizing relevant geophysical logs indicates occurrence of delta-front sandstones unit and fluvial channels as possible stratigraphic depositional features that could serve as carrier beds for hydrocarbon migration. Consequently, depositional environment ranges from fluvial to fluvio-deltaic shallow marine sandstones.

Anomalous high porosity values encountered within shale units of AO-1 well suggest possible micro structures, likely aided by thermally matured kerogen content within the shale unit. This could have caused the unexpected high porosity observed here. Litho-facies modeling of sediments encountered within all sequences reveal abundance of massive siltstone and shale deposit within the Barremian-Aptian and Albian sequence respectively. In addition, modelling results show definitive non-marine deposition of point bars within the Albian and mouth bar deposit within the Cenomanian sequences, both of which could be a good target as hydrocarbon reservoirs.

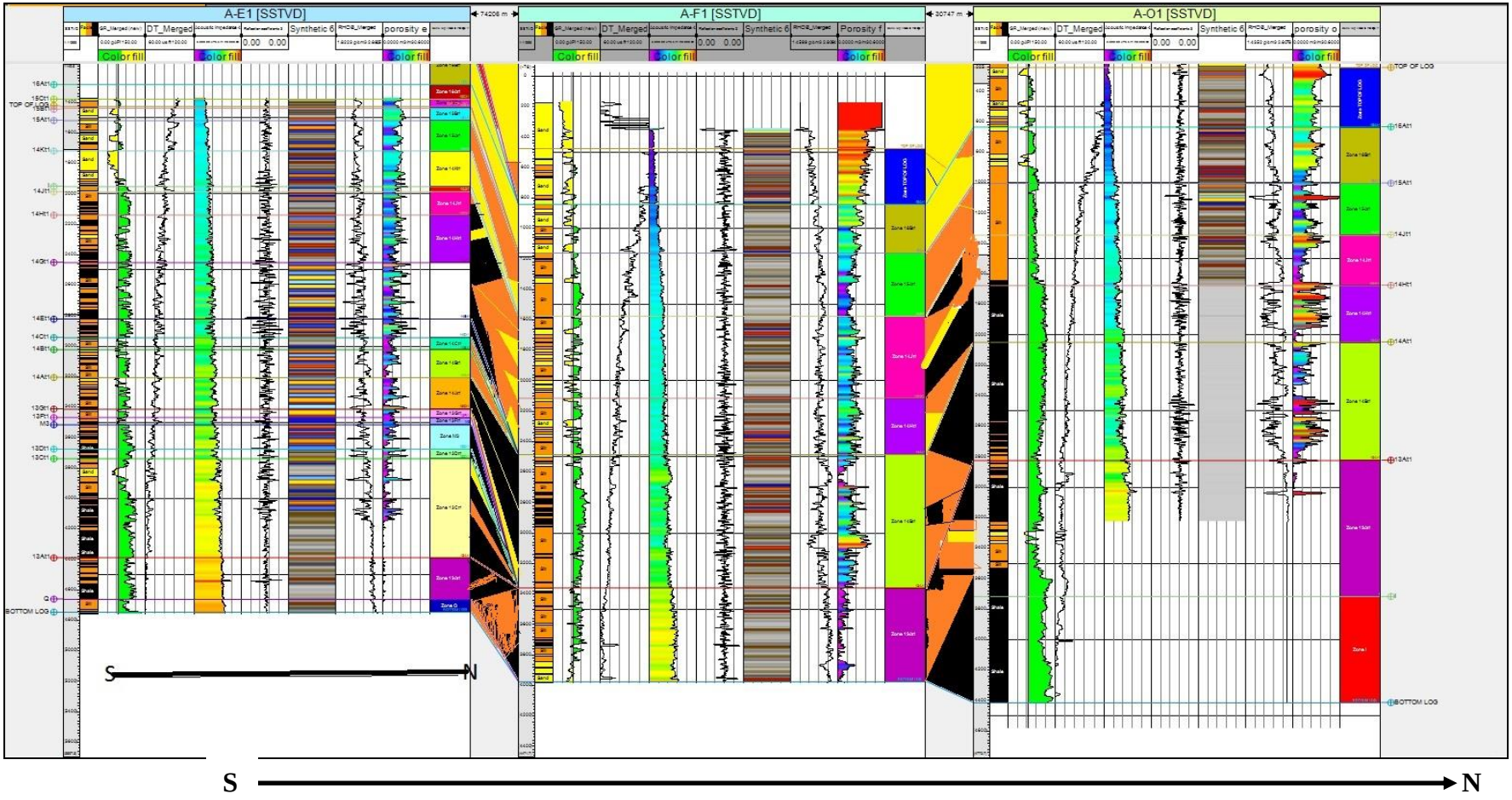

Figure 4.10: Litho-chronostratigraphic correlation of Sedimentary Sequences mapped across the three wells in the study Area (northern Orange Basin), West Coast, South Africa.

An integrated approach to understanding the geological controls on gas escape and migration pathways in offshore northern Orange Basin, South Africa.

Chapter Five

Seismic-stratigraphy, structural interpretations, mapping of Hydrocarbon escape features and their relationship to stratigraphic and structural features.

Keywords: Seismic Sequence analysis-Seismic Facies- Gas escape features-Faults-Paleo-stress

5.1 Abstract

Seismic-stratigraphy analyses of selected seismic lines in the study area are done based on the principles established in the literature, which are seismic sequence analysis, seismic facies analysis and its calibration with litho-facies analysis. The aim of seismic-sequence analysis is to understand reflection terminations of sequences and their concordant relationship with one another, therefore enabling the identification of erosional features and lap-out terminations. In addition, seismic facies analysis is done to understand amplitude, continuity and internal reflection geometry of strata, which, when calibrated with litho-facies analysis, ascertain reliability of using this concept in identifying lithology and depositional environments. Also, as part of this chapter, the relationships between gas escape features, faults and stratigraphy are established, vis-à-vis how they control gas escape. In addition, paleo-stress review of the Southern Africa continental margin is done to understand the evolution of faulting systems and to categorise the faults according to their different episodes of evolution.

In the northern section of the study area, specifically close to well AO-1, seismic sequence analysis of line A84-007 shows an apparent onlapping of the Barremian/Aptian sequence against the surface of down dipping basement. Also, a low-stand prograding wedge was observed within the Mid-Albian (14AT1) sequence on seismic line A86-002. In the central portion of the study area, a downlapping sequence was observed within the Cenozoic on seismic line A99-009.

Seismic facies analysis reveals channel fill deposits in the northern section because of a chaotic reflection pattern observed in the late Cenozoic sequence. Also, there is a change in reflection amplitude from low in the Maastrichtian to high in the Cenozoic. Three seismic facies of parallel, chaotic and divergent signatures were seen within the

Maastrichtian and Cenozoic sequence suggesting fluvial to fluvio-deltaic and shallow marine distributary point bars. Isopach maps show huge depositions of Cenozoic sediments up to 1500m thick towards deeper part of the basin (westward) while the Maastrichtian sequence shows an undulating depositional pattern where areas of high sediment accumulation are at close proximity to areas of low sediment accumulation.

Within the Cenomanian and Turonian sequences, the seismic facies reveals the deposition of sedimentary sequences which exhibit hummocky, wavy and parallel internal configurations. This architecture has been identified as deltaic deposits. The Turonian sequence reduced from about 500m thick in the centre of the study area to almost 0m in the southern part, suggesting an erosional unconformity.

Barremian/Aptian sequences indicate moderate amplitude, sub-parallel, sheet-wedge clinoforms while the Albian has low amplitude, sub parallel to wavy, discontinuous clinoforms suggesting shallow marine shelf-edge prograding deposits in this part of the basin. The Albian sequence thickness ranges from 450m in the south to 900m in the north. In addition, the Barremian/Aptian sequence reaches up to 1800m in thickness in the centre of the basin which has positive implications on the thermal maturity of organic matter of the source unit.

Listric normal fault detaching from the basement and antithetic faults are observed in the central portion of the study area. A paleo stress review of the South Atlantic continental margin by means of fault dipping orientations, suggests three different clusters of faulting systems dip direction orientation, which are NNW-SSE, NNE-SSW, ENE-WSW. Structural framework modelling indicates that compressional events and uplift are evident in the late Cretaceous, coupled with evidence of erosional terminations.

Gas escape features like gas chimneys and pockmarks which are directly linked to some of these faults are observed, while stratigraphically controlled chimneys are observed as well. A ’bright spot’ anomaly is noticed on both sides of a listric normal fault suggesting possible leakage of gas across the fault.

5.2 Introduction

The application of seismic stratigraphy techniques in basin analysis entails the mapping and correlation of sedimentary rocks, the recognition of sequences, the identification of major lap outs and the geological interpretation of geophysical well logs. The seismic stratigraphy concept is invaluable in frontier exploration to characterize stratigraphy and depositional systems when cores, which represent ground truth, are not available. In this study, seismic stratigraphy has been adopted to characterize erosional surfaces and identify lithologies and depositional systems. The application of the seismic stratigraphy concept as detailed in chapter two of this study, involves three steps as outlined by Vail (1987):

Seismic sequence analysis,
seismic facies analysis and
interpretation of depositional environments and litho-facies analysis.

However, the refinement of this technique over the years has ensured its integration with litho-stratigraphic interpretation from well logs to improve accuracy of observations.

In interpreting and mapping seismic sequences, consideration is given to successions that are genetically related and can be separated based on bounding unconformities, as erosional surfaces (onlap, truncation, downlap, top lap) can be mapped. This is followed by seismic facies analysis which involves interpreting the seismic character of depositional sequences based on Sangree and Widmier's (1979) reflection features criteria (amplitude and strata continuity and character), followed by verifying it with litho-stratigraphic interpretations. In this study, seismic facies analysis and litho-facies distribution are integrated and interpreted together.

Therefore, while mapping out the reflection terminations, continuity and its geometry on seismic data to determine depositional sequences (facies), it is important to verify such observations with litho-stratigraphic interpretations.

In addition, regional tectonic faults are essential features that could impact hydrocarbon migration pathways, hence understanding faults and their interactions with the stratigraphy is crucial to achieving one of the objectives of this study . The timing of formation of these faults can be related to different paleo-stress regimes and episodes of regional tectonism in the South Africa continental margin. Mapping of faults to establish their relationship with gas escape features seen on seismic sections, and to understand how they enhance hydrocarbon migration processes is an essential component of this study. In this study, six reflector packages from the Barremian syn-rift package- to the youngest Post-rift Cenozoic sequence were mapped.

5.3 Methodology

5.3.1 Seismic Stratigraphy

The methods applied in the interpretation of seismic stratigraphy results were based on the interpretative methods of Vail et al., (1977) and Badley, (1985). After the seismic well-tie had been performed as explained in chapter three of this study, seismic sequence analysis was performed by mapping erosional surfaces which are recognized as follows:.

Onlap: Termination of a parallel, continuous seismic reflector against a down-dip reflector.

Toplap: Termination of an up-dip reflector against a parallel overlying reflector.

Downlap: Termination of a down-dip reflector against an underlying continuous parallel reflector.

Erosional truncation: Termination of strata reflector against an unconformity surface.

The second step which is seismic facies analysis, was performed by analyzing amplitude and continuity of reflectors coupled with identifying reflector configurations and patterns, which include parallel, divergent, hummocky, chaotic and sub-parallel patterns as these sets of configurations point to various litho-facies and depositional environments. To ascertain the reliability of these observations, they were verified with the litho-facies logs interpreted earlier in chapter four.

5.3.2 Structural Interpretations and Structural Framework Modelling.

Faults were mapped on the seismic sections, both as a plane of discontinuity and as a plane of displacement. In addition, a structural framework was constructed using the faults mapped and unconformity surface maps created in the Petrel 2013© environment to understand faults and stratigraphic architecture. This gives insight into the depositional sequences patterns in the study area.

5.4.1 Results of Seismic Stratigraphy Analysis.

5.4.1.1 Seismic Sequence Analysis around Well AO-1 (Northern Section).

Selected seismic lines (A84-007, A80-002, A86-002) are interpreted around well AO-1(northernmost well drilled) to identify subtle stratigraphic features within the stratigraphic sequence. Apparent or erosional truncations as observed from line A84-007, trending SSW-NNE, shows the termination or onlapping of the Barremian/Aptian sequence against the surface of a down dipping basement represent an unconformity (Figure 5.1B). This commonly represents a sequence boundary (Snedden and Sarg, 2008).

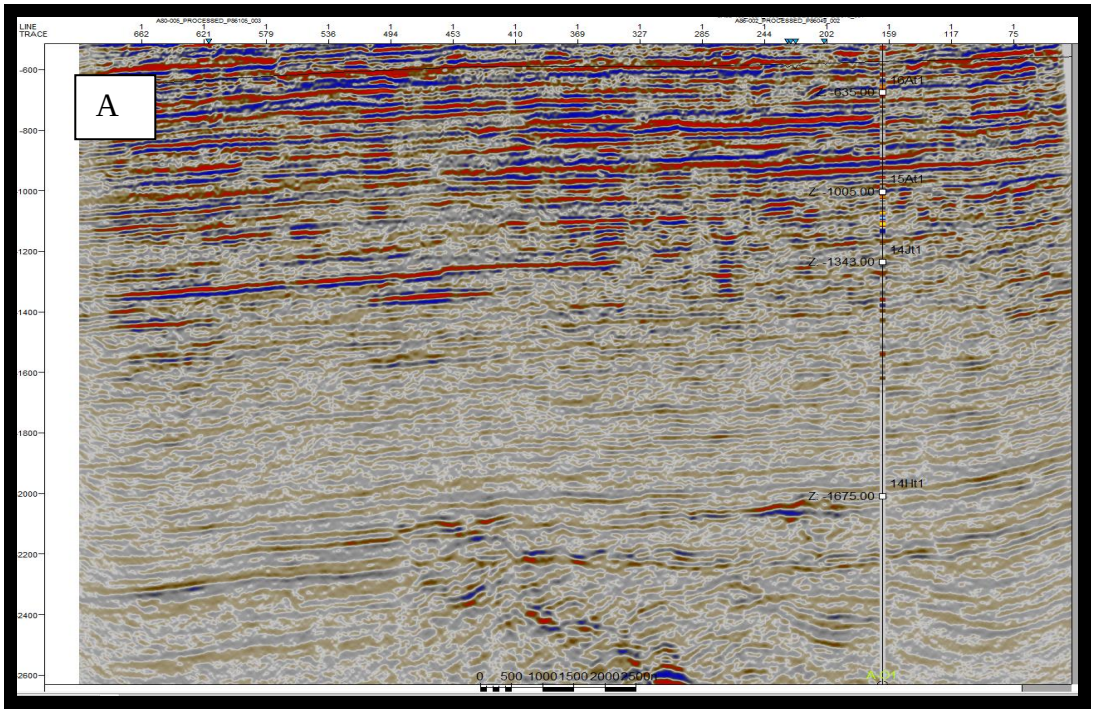

An integrated approach to understanding the geological controls on gas escape and migration pathways in offshore northern Orange Basin, South Africa.

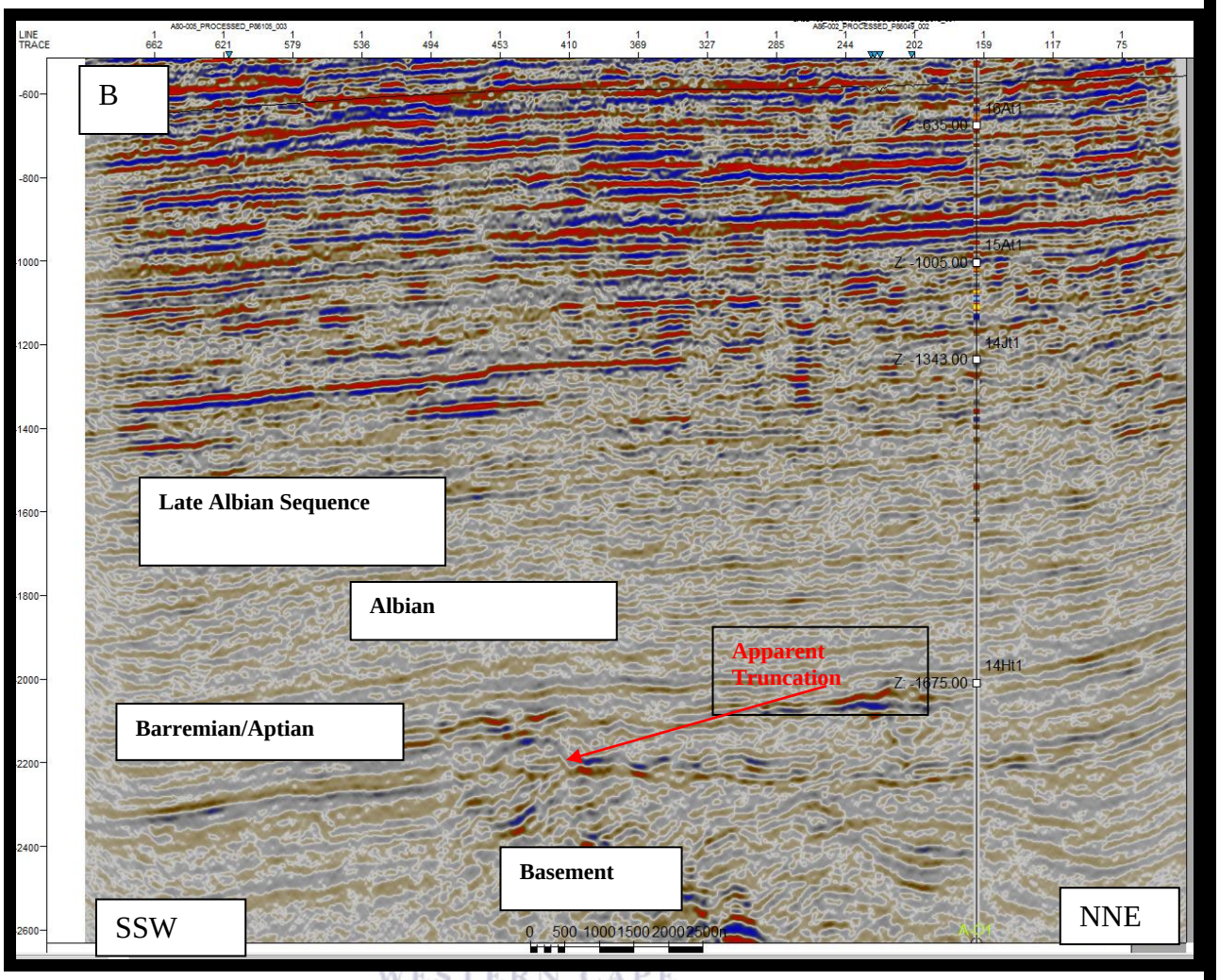

Figure 5.1Aand B: Un-interpreted Seismic Line A84-007 and interpreted Seismic Line A84-007 showing apparent truncation caused by termination of Barremian-Aptian Sequences on down dipping basement.

On line A80-002 (Figure 5.2), trending SSW-NNE within the inner tertiary sequence, there is a termination of a clinoform against parallel or low angle overlying reflection strata. This apparently represents a pinchout and is commonly caused by fluvial by pass of sediments across a deltaic or coastal plain.

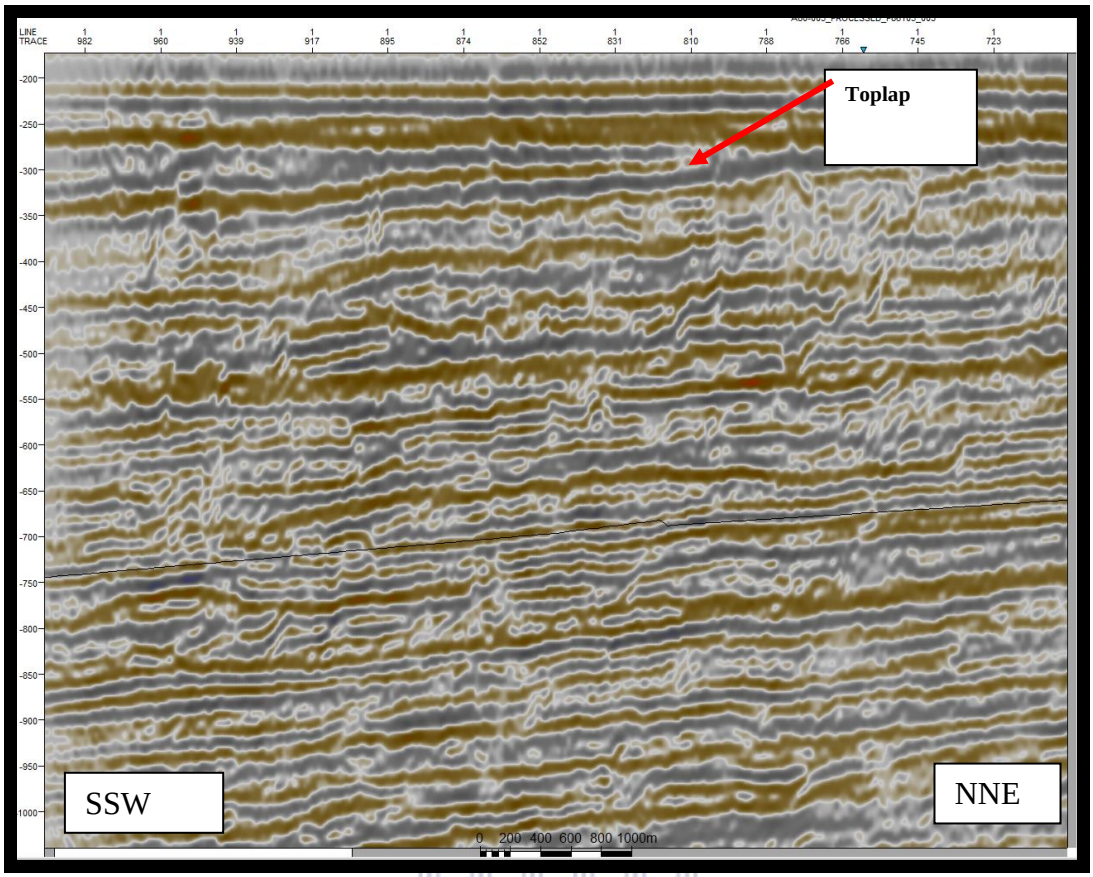

Figure 5.2: Interpreted Seismic Line A80-002 showing termination of a reflector against an overlying reflector (Toplap) in the Tertiary.

On line A86-002, trending E-W, a low-stand prograding wedge was observed within the Mid-Albian (14AT1) sequence (Figure 5.3B). This is not unexpected as the Orange River deposits huge amounts of sediment during the Albian thereby forcing a progradation sequence as sedimentation exceeds space created by tectonism; this led to the formation of many low-stand wedges during this era (Brown et al., 1996).

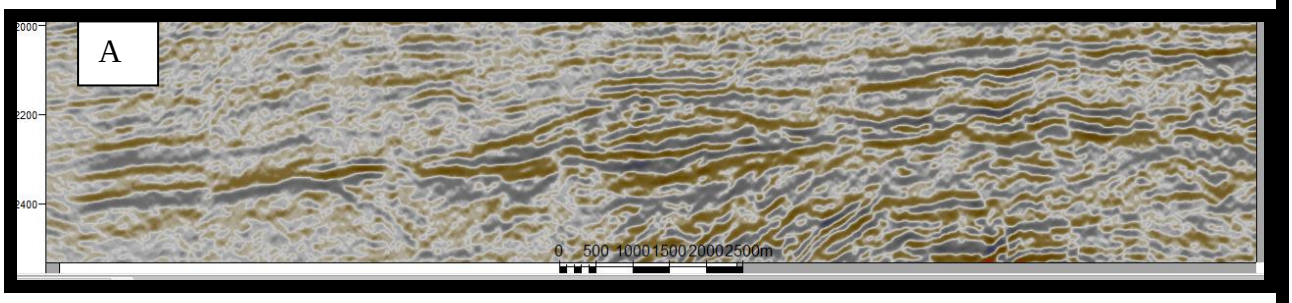

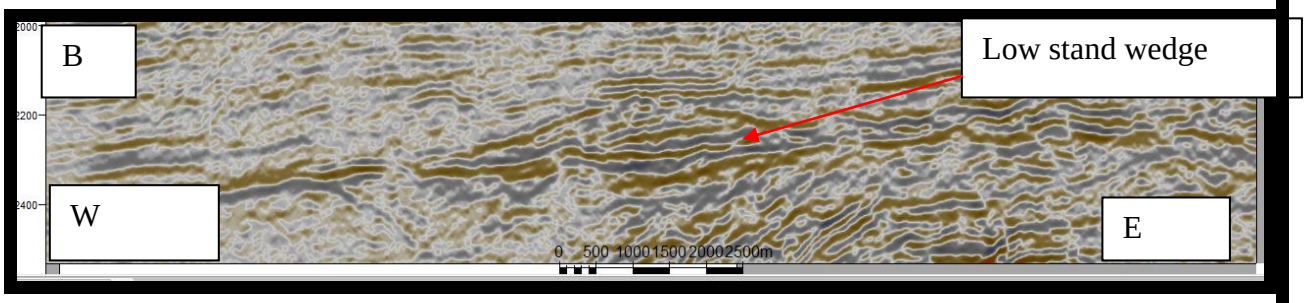

Figure 5.3 A and B: Seismic line A86-002 showing a lowstand wedge of Mid- Albian age.

5.4.1.2 Seismic Sequence Analysis around Well AF-1 (Central Section).

The seismic inline 2310, trending SWW-NEE as displayed below was taken from the 3D volume and enhanced by a "bump mapping technique" to enhance subtle stratigraphic features. However, due to the poor resolution of the 3D volume, many subtle stratigraphic features could not be mapped. Although, the application of different seismic attributes in chapter six could delimit this difficulty. There is an occurrence of a half-graben (circled in red) in Figure 5.4. Series of graben and half-graben parallel to the present day coastline characterized the margin evolution of the Orange Basin (Barton et al., 1993).

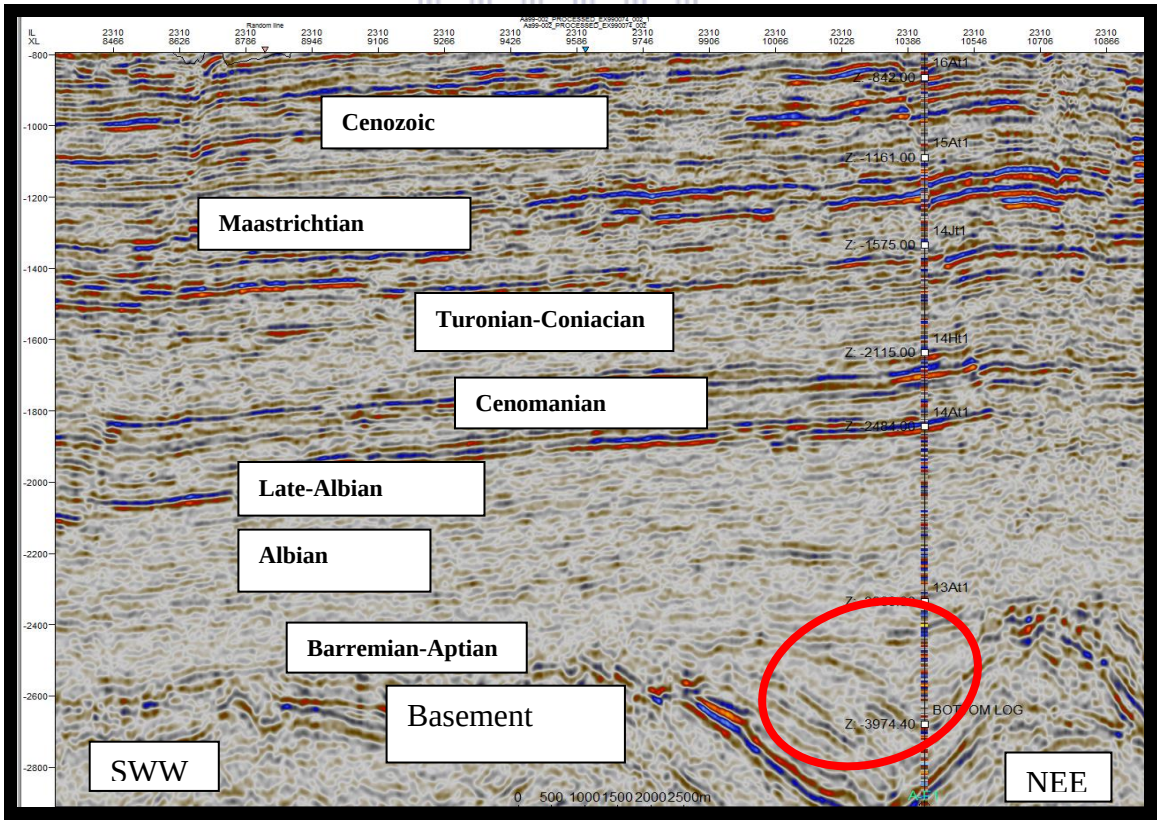

Figure 5.4: Seismic section showing the seismic Sedimentary Sequence of the study area and an occurrence of a half –graben (red circle) at Inline 2310.

5.4.1.3 Seismic Sequence Analysis around Well AE-1 (Southern Section).

There is downlapping of a Tertiary sequence which represents the base of prograding clinoforms in the Cenozoic on line SA 92-131. Trending SSW-NEE.

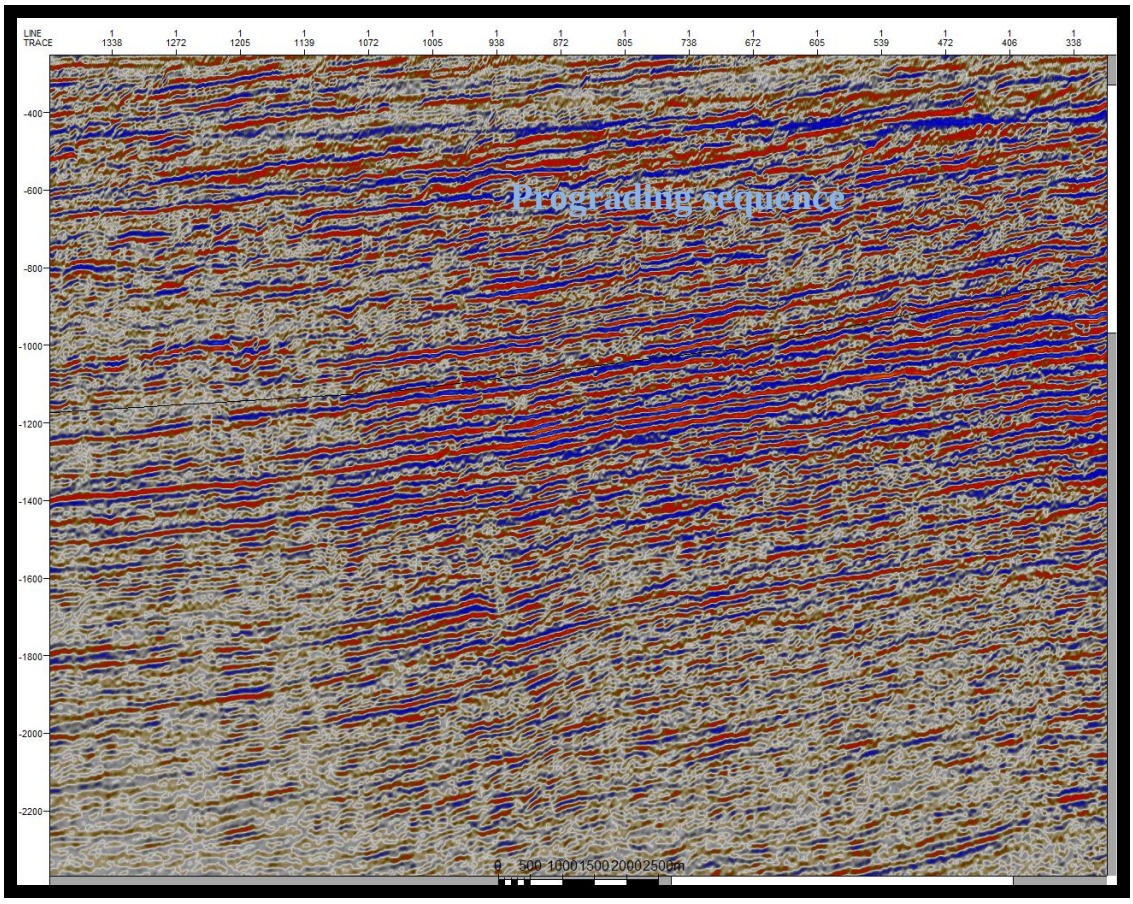

Figure 5.5: Seismic section showing prograding sedimentary sequence in the Cenozoic around AE-1 well at Line SA 92-131in the southern section.

5.4.1.4 Seismic facies and Litho-facies Analysis of Maastrichtian –Cenozoic Sequence of well AO-1 (Northern section).

The reflection shows wavy, disrupted geometry and high amplitude in the Maastrichtian and Cenozoic sequences. The chaotic seismic reflection pattern in a black circle (Figure 5.6 A) on the seismic section suggests a channel fill deposit (River delta mouth bar or sub-marine fan) in the Cenozoic. The channel fill deposit (black circle in Figure 5.6 A) which indicates a bit of chaotic disruption relative to other patterns in this sequence, is likely associated with either a delta front mouth bar deposit or a sub –marine channel fill. In addition, the well-completion report explains a close proximity between well AO-1 and the mouth of the Orange River, thereby

pointing to the likely presence of a delta front mouth bar rather than a sub-marine channel fill. This deduction is also corroborated by the gamma ray log signature which shows a funnel shape coarsening upward prograding sequence from the Maastrichtian into the Cenozoic, suggesting a basin ward shift in deposition (Figure 5.6B). Progradation mostly paves the way for fluvial system encroachment of an older, already eroded sub-aerial surface especially when sedimentation rate is high as this could cause a fluvial-delta deposition on existing older channels.

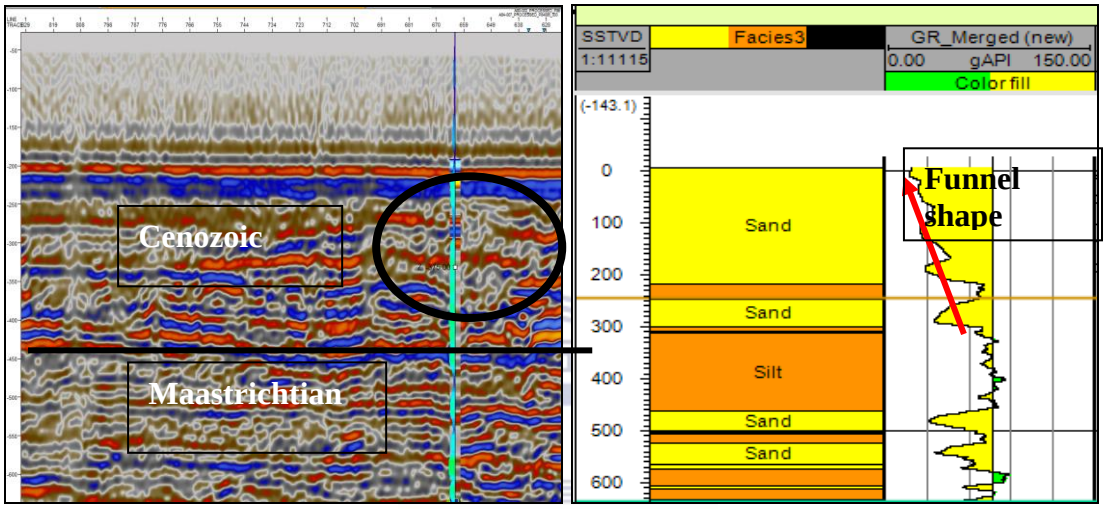

A B

Figure 5.6 A and B : Showing Seismic (Line A84-007) and Litho-facies Analysis of Cenozoic and Maastrichtian around well AO-1 respectively. The Gamma ray log shows a cleaning upward trend (black arrow).

5.4.1.5 Seismic facies and Litho-facies Analysis of Maastrichtian –Cenozoic Sequence of well AF-1 (Central section).

The lower part of the seismic section which represents the very late Cretaceous period (Maastrichtian) indicates a sheet becoming a wedge, with disrupted and low-moderate amplitude reflection configurations (Figure 5.7A). This grades into high amplitude, continuous, and sub-parallel reflection configurations in the upper part (Cenozoic) (Figure 5.7A). These configurations diagnose a fluvial facies in the Maastrichtian which might be channel fill sandstone or an alluvial or a marine reworked delta that changed to shallow marine delta front sandstone in the Cenozoic (Vail et al., 1977). These observations agree with the gamma ray log signature which shows a rapid changing from a fining upward retrogradational sequence probably caused by

landward shift in deposition site in the Maastrichtian, to an aggradational sequence, and finally to a progradational sequence in the Cenozoic (5.7B).

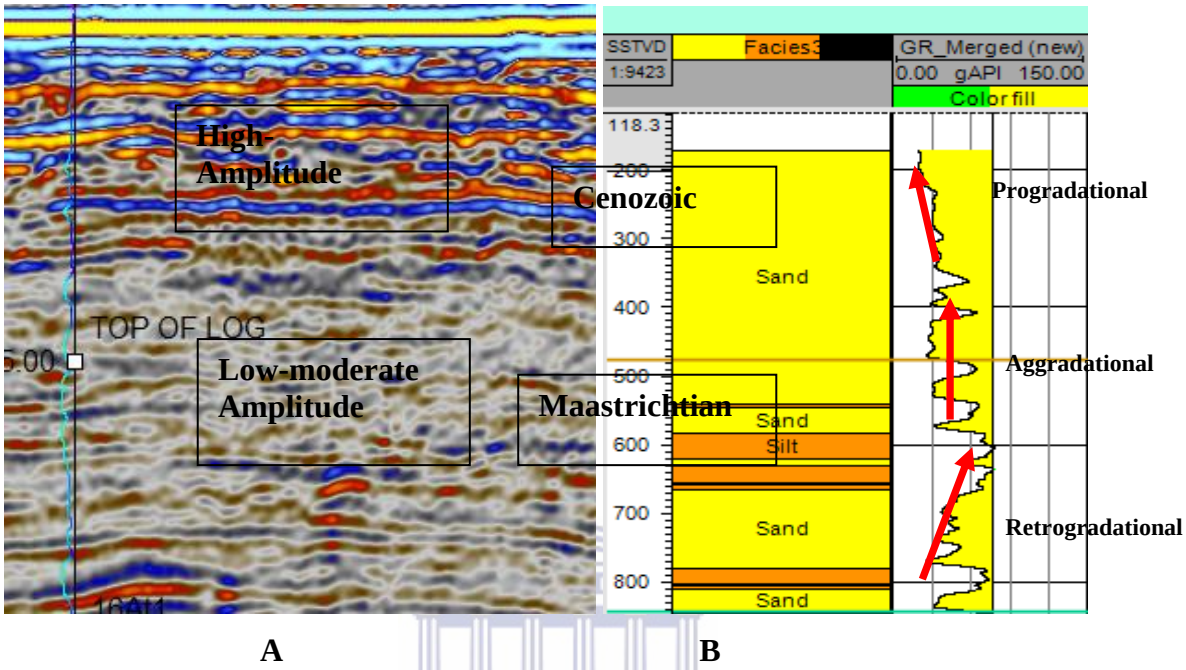

Figure 5.7A and B: Showing Seismic (Inline 2370) and Litho-facies Analysis of Cenozoic and Maastrichtian around well AF-1 respectively.

5.4.1.6 Seismic facies and Litho-facies Analysis of Maastrichtian –Cenozoic Sequence of well AE-1 (Southern section).

The Cenozoic sequence in the southern part of the study area where well AE-1 was drilled, was not logged with geophysical tools, hence lithofacies cannot be interpreted. The seismic facies however indicates a moderate to high amplitude, with disrupted and sub parallel clinoforms in the Maastrichtian to a slightly divergent pattern in the Cenozoic (Figure 5.8).This is a common feature of an aggrading sequence (Mahieux et al., 1998). These observations are a diagnostic of the possible deposition of a shallow marine sequence in the Maastrichtian which may grade into delta-plain shale landward in the Cenozoic. The divergence pattern often suggests variations in sediment deposition rates.

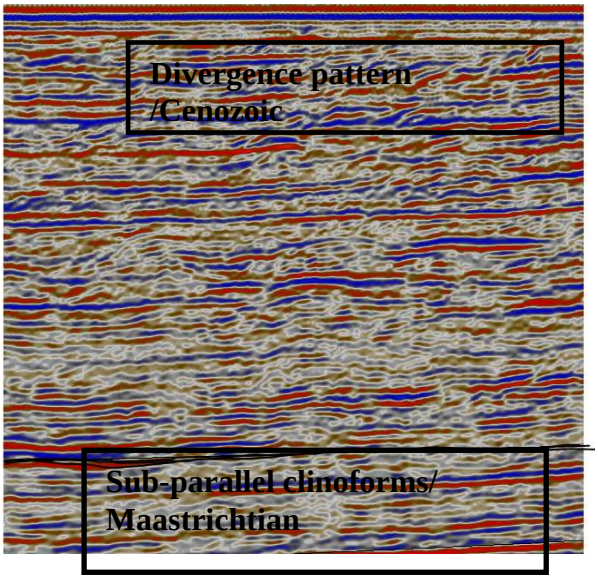

Figure 5.8: Showing Seismic (Line SA-92-131) and Litho-facies Analysis of Maaschritian-Cenozoic sequence around well AE-1.

5.4.1.7 Isopach variation (Thickness map) and Summary of seismic facies for Maastrichtian and Cenozoic sequences.

Three seismic facies with internal configurations of parallel, chaotic and divergent patterns were recognized in both sequences and their depositional environment ranges from fluvial to fluvio-deltaic and shallow marine distributary point bars. The Cenozoic sequence thickens from the northern part of the study area towards the South with thickness variation of around 200m to 900m respectively (Figure 5.9A). However, basinward and westward of the study area, huge quantities of sediments accumulated with thickness up to 1500m (Figure 5.9A). This can be explained by the regressional phase that happened after the late Cretaceous that caused slumping and progradation of sediments further into the basin (Dingle et al., 1983). As explained by Dingle (1993), the regression caused a shift in the depocentre offshore and westward of the basin which led to the deposition of about 1.5km of strata. The observation of Dingle at al., (1983) agrees with the present observation because of the progressive thickening of Cenozoic strata from the shallower part into the deeper part (Westward) of the basin (Figure 5.9 A).

In contrast, in the Maastrichtian, thickness variation has no particular trend (Figure 5.9B). There are pockets of high accumulation of sediments and shallow accumulations. The different pockets of higher and lesser sediment accumulation could best be explained by the possible uplift and subsequent erosion that has been

documented during the late Cretaceous, notably during the Campanian-Maastrichtian (Broad et al., 2007). The areas of lesser sediment accumulation appear to be at a close range to areas of higher sediment accumulation. This could mean that areas affected by the uplifts were subjected to intense erosion which removes a certain volume of sediments which was later deposited in areas with high accommodation space as crustal subsidence occurred after uplift, thereby causing thick sediments accumulation variation in the Maastrichtian.

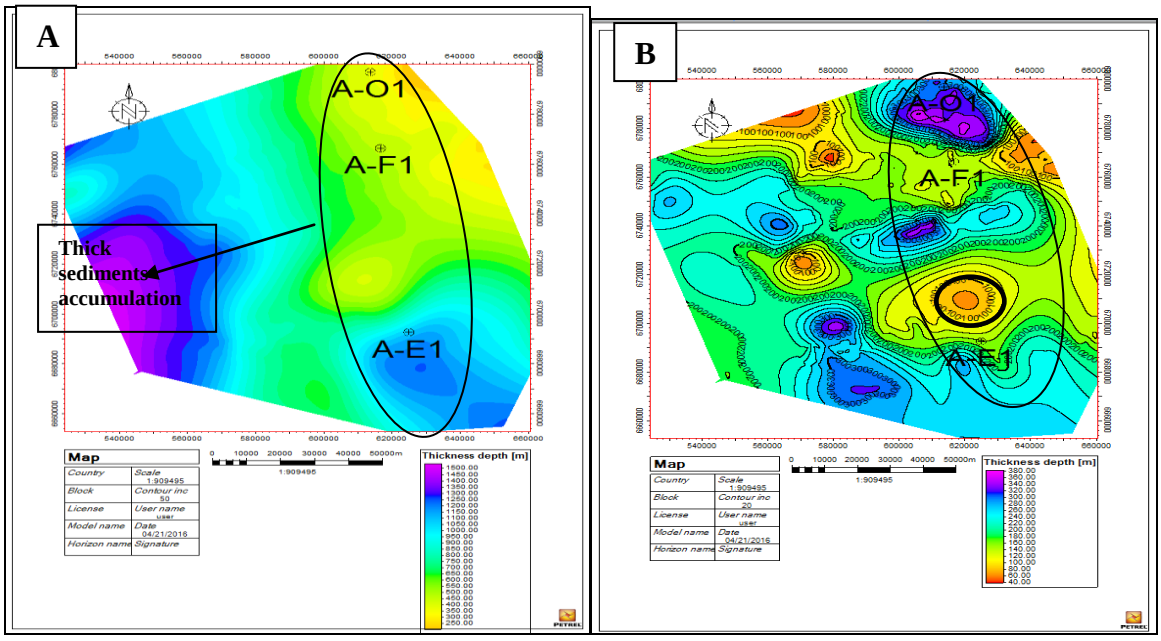

Figure 5.9 A and B: Figures showing the thickness variation maps for Cenozoic (A) and Maastrichtian (B) Sequences. There is thick sediment accumulation westward of Cenozoic sequence.

5.4.1.8 Seismic and Litho-facies Analysis of Cenomanian and Turonian Sequence (AO-1) (Northern Section).

These sequences have moderate amplitude, sub parallel to hummocky, disrupted and oblique reflection configurations in the Cenomanian sequence of the seismic section. These configurations changed into high amplitude, parallel, continuous clinoforms in the Turonian upper part of the section (Figure 5.10A). The hummocky clinoform is commonly associated with pro-delta siltstone and sandstones (Badley, 1985), while the parallel clinoforms at the upper section suggest an aggradational sequence (Mahieux et al., 1998). High amplitude, continuous and parallel clinoforms are a common feature of shelf or delta platform (Badley, 1985). Calibration of these observations with gamma ray log signature indicates the deposition of a well-

laminated pro-delta siltstone. The log signature evidently suggests a high rate of sedimentation matched with sea level rise at the middle part of the sequence as the gamma ray log signature values increases there. However, the gradual sea level drop might have allowed the gradual basinward deposition of delta front sandstones (Figure 5.10B) in the Turonian sequence, evident with low gamma ray log signature. This suggests a continuously high sedimentation rate as the sea level drops gradually.

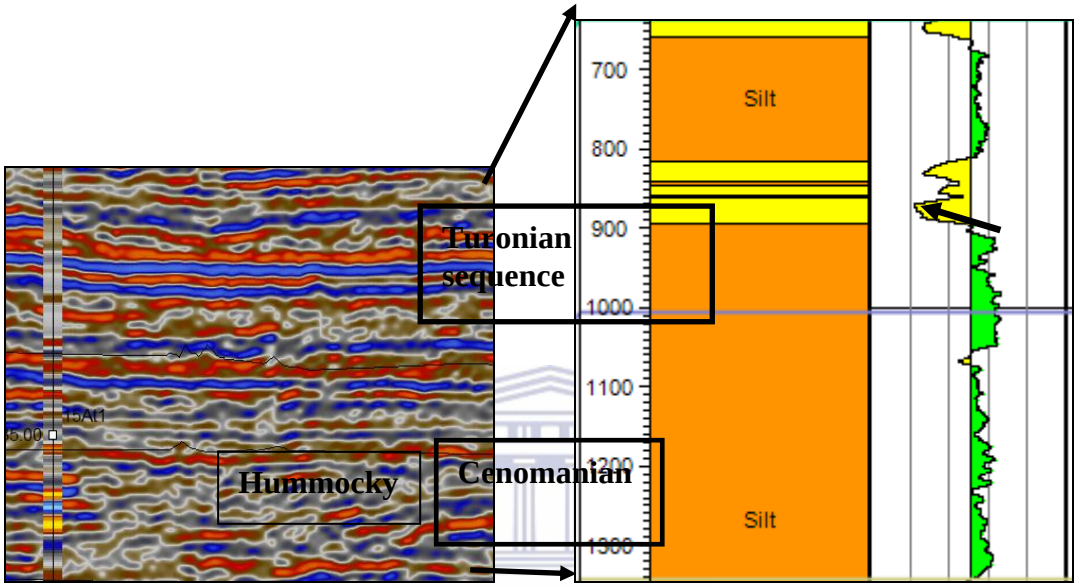

Figure 5.10: Showing Seismic facies (Line A79-003) (A) and Litho-facies Analysis (B) around well AO-1(northern section) respectively.

5.4.1.9 Seismic facies and Litho-facies Analysis of Cenomanian and Turonian Sequence (AF-1) (Central Section).

These sequences' reflection patterns show evidence of moderate amplitude, with semi- continuous to disrupted reflection configurations (Figure 5.11A). These characteristics are a pointer to pro-delta or a delta front depositional environment (Badley, 1985). The gamma ray log within these sequences shows a varying energy regime in which a high rate of sedimentation is matched with alternating but gradual sea level changes. The varying energy regime could be as a result of a storm - dominated shelf that accompanied alternation of sea level changes. This variation led to the intercalation of sandstones and siltstones and leaves a vertical aggrading stacking pattern in the Turonian, as seen from the gamma ray log signature.

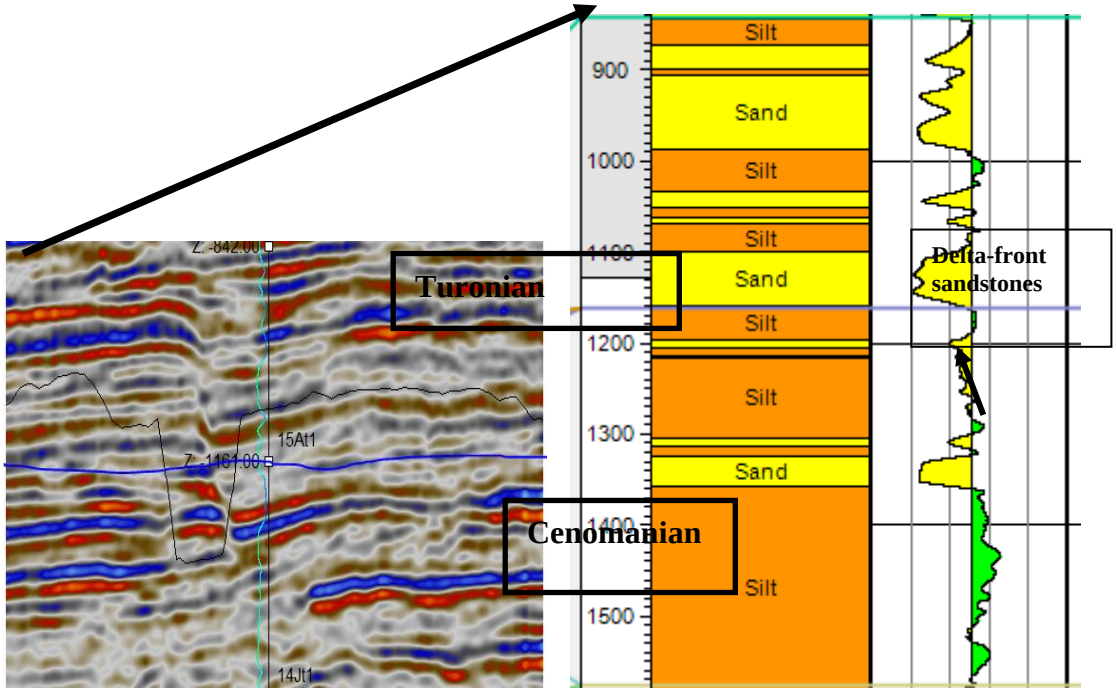

A B

Figure 5.11 A and B: Showing Seismic facies (Inline 2370) for Turonian (A) and Litho-facies (B) Analysis around well AF-1(Central Section).

5.4.1.10 Seismic facies and Litho-facies Analysis of Cenomanian andTuronian Sequence (AE-1) (Southern Section).

These sequences are characterized by low amplitude, hummocky clinoforms in the lower section which are changing to wavy and discontinuous clinoforms in the upper section. The hummocky clinoforms as observed could be as a result of switching delta lobes (Mitchum et al., 1977). This observation, when calibrated with the gamma ray log signature could suggest a switch from a prograding delta as evident from the coarsening upward sequence, into an aggradational deltaic sequence.

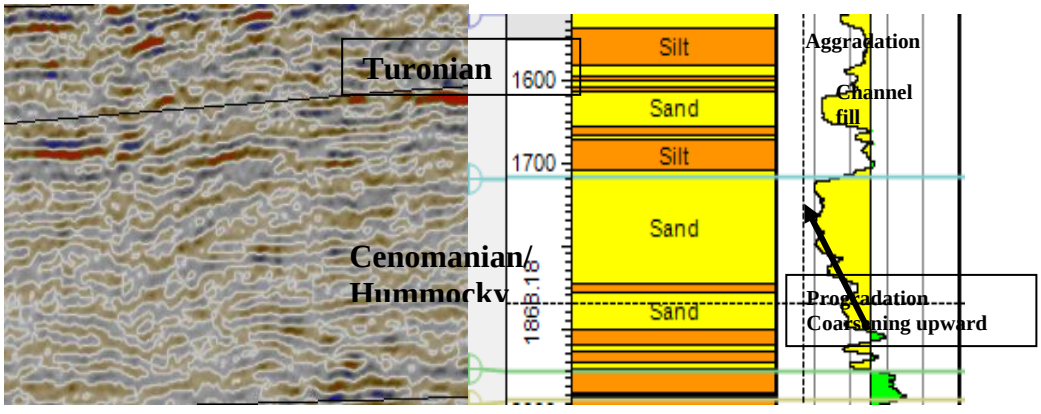

A B

Figure 5.12 A and B: Showing Seismic facies (SA-192-131) (A) and Litho-facies Analysis (B) around well AE-1(Southern part).

5.4.1.11 Isopach variation (Thickness Maps) and Summary of Seismic and Litho-Facies Analysis for Cenomanian and Turonian Sequences

The seismic facies reveals the deposition of sedimentary sequences which exhibit moderate to low amplitude (southern section only), hummocky, wavy and parallel internal configurations. This architecture has been identified as representing deltaic deposits (Badley, 1985). In addition, the Isopach thickness map for these sequences revealed deposition of Turonian sediment of up to 500m thick within the centre of the study area and could be referred to as the depocentre for the study area. Further north, around the AO-1 well, the sequence appears to be thinning out to an average of 90m thick. Also, in the southern part of the study area, the thickness of the Turonian sequence reduces and terminates to zero (Figure 5.13A). This suggests an erosional unconformity towards the southern part. In contrast to the Turonian sequence, the Cenomanian period witnessed rapid deposition of large volumes of sediments which points to progradation (Figure 5.13B). This is evident as the sediment thickness increases towards the deeper section of the study area (Figure 5.13A). In the southern part, about 200m thick sediments were deposited, while the northern part witnessed lesser deposition with a thickness of 150m (Figure 5.13B). The sediments thickness in the Cenomanian is estimated at approximately half (540m) of the thickness of Turonian (1000m), in the middle section of the study area.

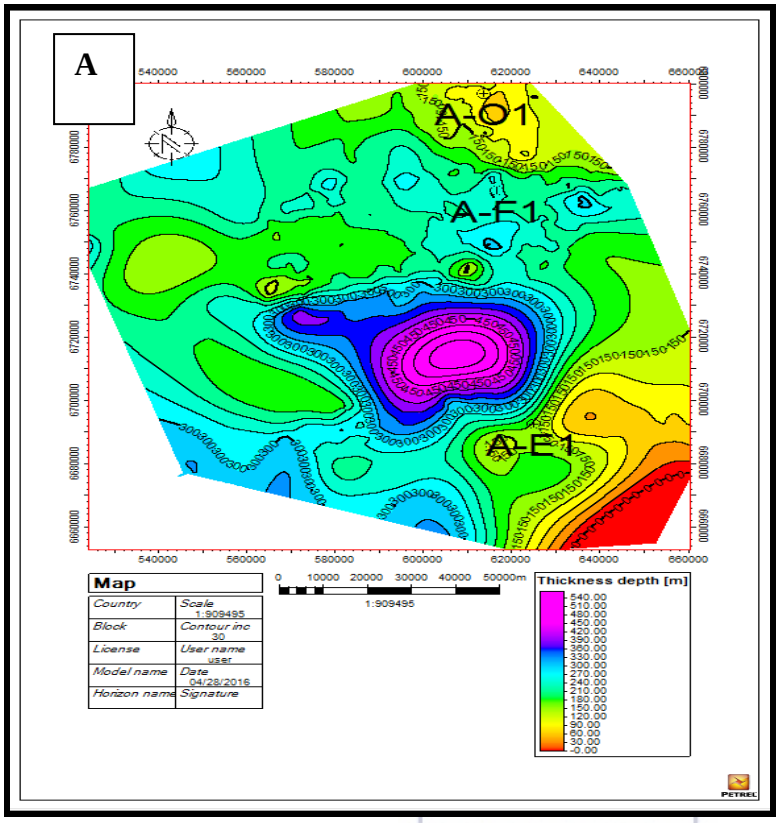

Turonian

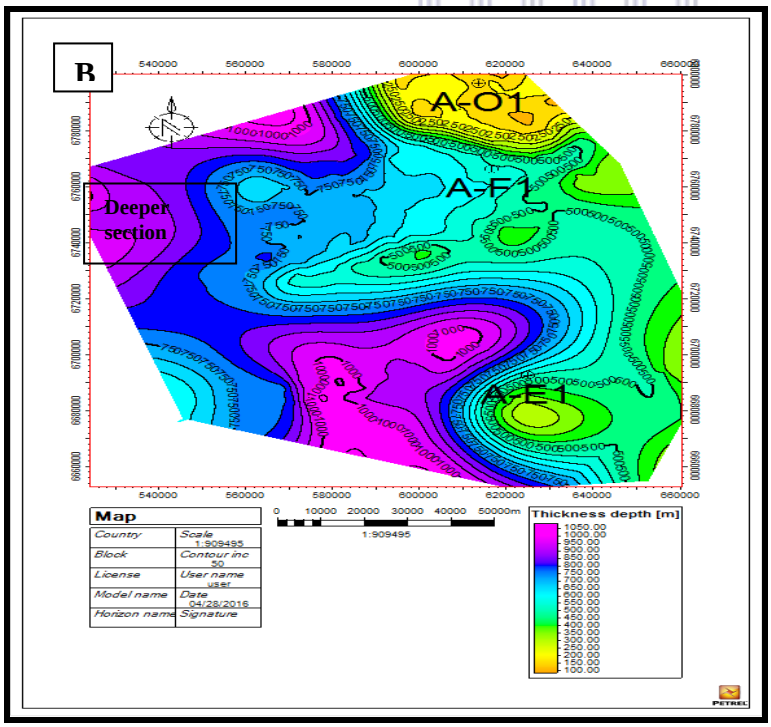

Cenomanian

Figures 5.13 A and B: Figures showing the thickness variation maps for Turonian (A) and Cenomanian (B) Sequences. Thick sediment accumulation Westward suggest progradation.

5.4.1.12 Seismic facies and Litho-facies Analysis of Barremian/Aptian-Albian Sequence (AO-1) (Northern Section).

The basal portion of these sequences (Barremian-Aptian) indicates moderate amplitude, sub-parallel and sheet to wedge clinoforms while the upper part (Albian) has low amplitude, sub parallel-wavy, discontinuous clinoforms (Figure 5.14A). The characteristics of these sequences indicate shallow marine / shelf edge prograding deposits or pro-deltaic deposits. The calibration of these observations with Gamma ray logs shows a dominant coarsening upward (delta progradation) sequence in the Barremian/Aptian (Figure 5.14A) sequence interpreted as the deposition of delta front/shallow marine sandstones, followed by a period of progradation/aggradation depositing shale and siltstone intercalations in the Albian (Figure 5.14B). This, later was followed by a period of initiation of marine influence which switched into full regression depositing a massive shale unit in the Albian as can be seen on the facies log within the Albian sequence in the northern part (Figure 5.14B).

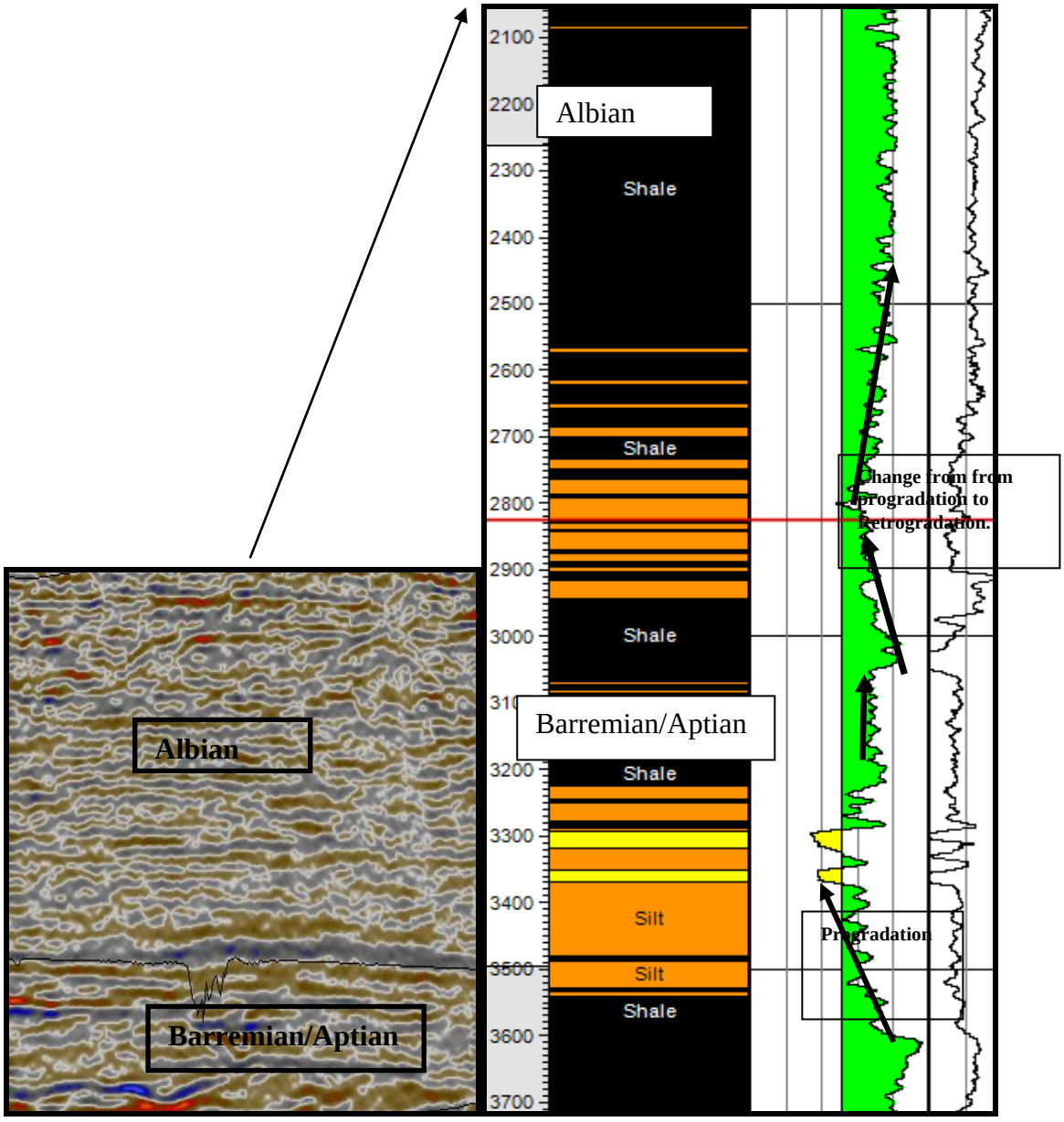

Figure 5.14A and B: Showing Seismic facies (Line A79-003) (A) and Litho-facies Analysis (B) around well AO-1(Northern Section).

5.4.1.13 Seismic facies and Litho-facies Analysis of Barremian/Aptian-Albian Sequence in well AF-1 (Central Section).

In the central part of the study area, the basal portion of these sequences (Barremian/Aptian) shows moderate amplitude, sub-parallel, discontinuous, and sheet- to wedge-clinoforms (Figure 5.15 A). In addition, the upper section (Albian) shows low amplitude, wavy-, and discontinuous-clinoforms which are a characteristic of shelfal deposits. The gamma ray log indicates deposition of fluvial sequence

sandstones with minor siltstone intercalations which change into planar siltstones with minor sandstone intercalations, suggesting a switch from a retrogradational fluvial/tidal deposit to an aggrading sequence in the Barremian/Aptian (5.15B). The Albian sequence indicates an aggradational sequence which was matched by lesser sedimentation rates that led to the deposition of thin laminated sandstone. Subsequently, a storm influenced, shelfal aggradational sequence dominated, leading to a GR log serrated curve and intercalation of shale with **B** nes in the Albian.

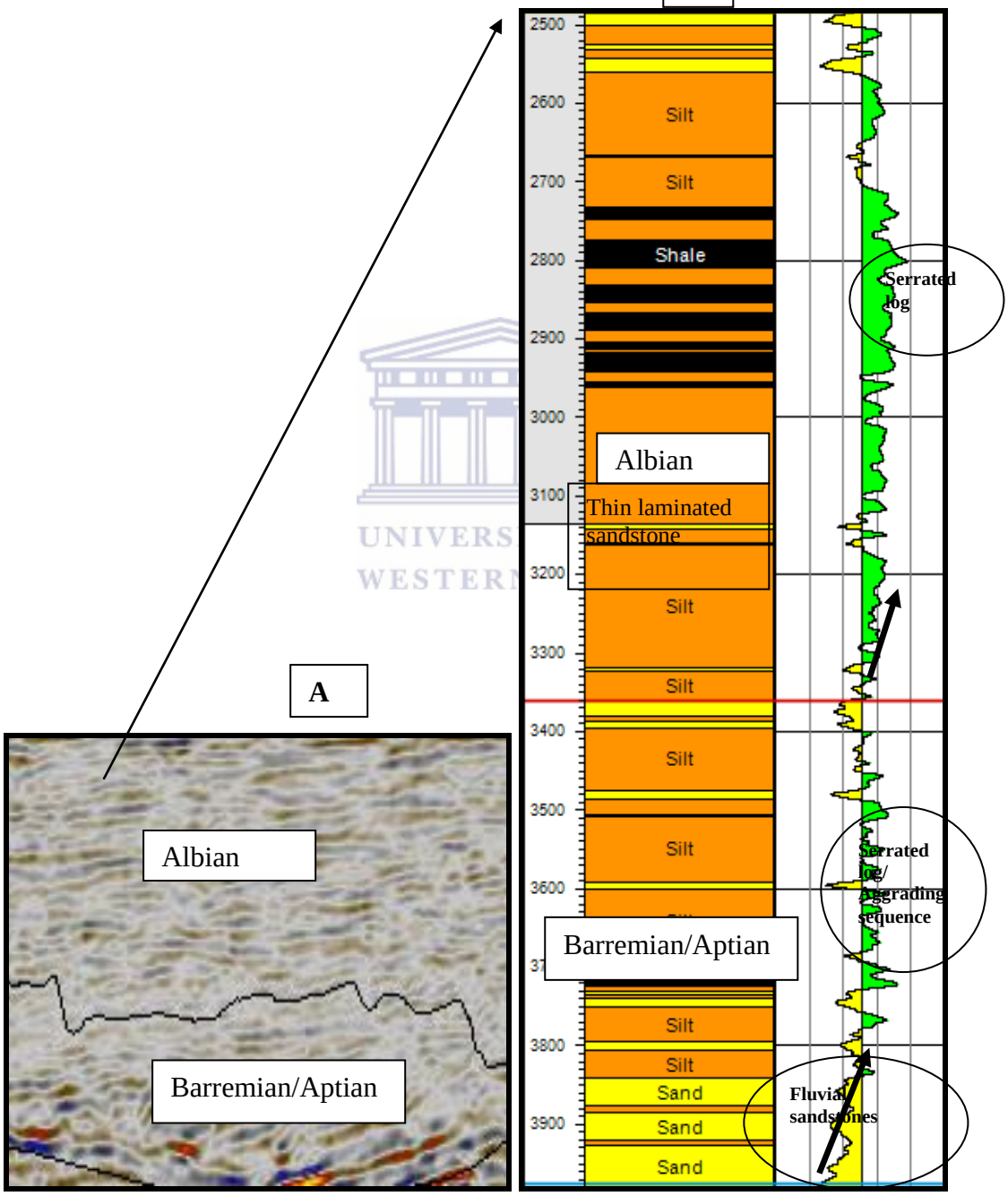

Figure 5.15 A and B: Seismic facies (Inline 2370) and Litho-facies Analysis around well AF-1. Serrated logs at both Barremian/Aptian and Albian sequences suggest as storm dominated Shelf environment.

5.4.1.14 Seismic facies and Litho-facies Analysis of Barremian/Aptian-Albian Sequence (AE-1) well (Southern Section).

The Barremian/Aptian sequence in the southern part of the study area where well AE-1 was drilled shows low amplitude, wavy to parallel, continuous clinoforms (Figure 5.16A). The upper section (Albian) shows low amplitude, hummocky, discontinuous clinoforms. Depositional systems of these sequences suggest upper pro-delta or shallow slope facies or submerged shelfal deposits. These observations as matched with gamma ray log signature reveal aggradational process dominance and serration of gamma ray log signature to be prominent in the Barremian-Aptian sequence. At the start of Albian sequence is an aggradational sequence which shallows into a progradational sequence depositing shallow marine sandstones within this sequence as evident from the log signature, thereby suggesting shelfal deposits (Figure 5.16B).

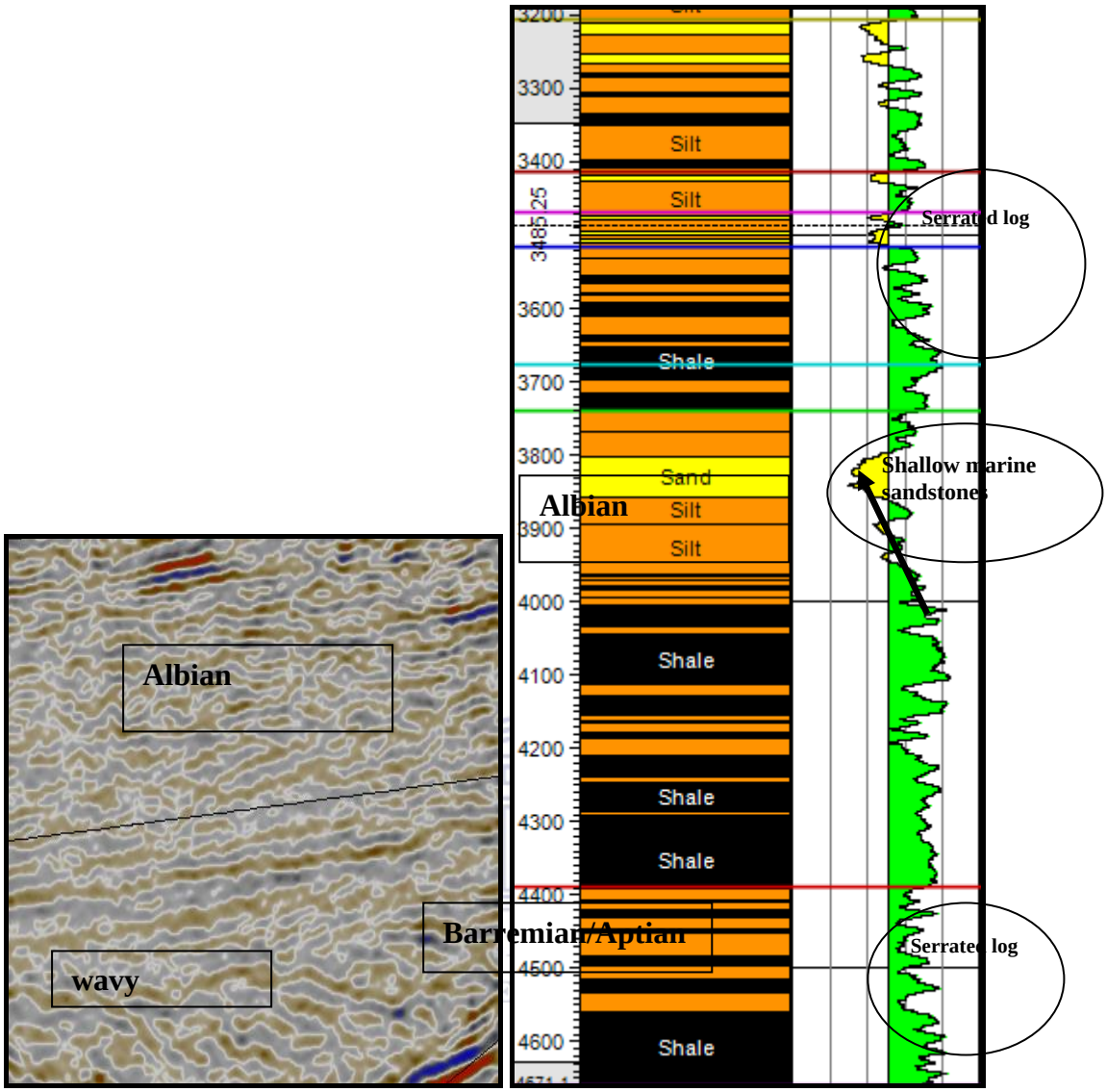

A B

Figure 5.16 A and B: Showing Seismic facies (Line A79-003) and Litho-facies Analysis around well AE-1(southern section).

5.4.1.15 Isopach variation and Summary of Seismic and Litho-facies Analysis for Barremian-Aptian/Albian Sequences.

The litho- facies suggests the deposition of planar siltstones, massive shale deposits prominent in the northern part and minor sandstones deposits. The hummocky clinoforms facie observed in the southern part on the seismic profile suggest shelf deposits probably associated with storm influence within the aggradational sequences. As seen from Figure 5.17 A below, the Albian sequence thickness ranges from around 450m in the south to about 900m in the northern part; the increased sediment supply during this period could be attributed to either an increased energy regime of the

Orange fluvial systems or an aggressive regression. The northern part of the study area has close proximity with the present day Orange River systems which might account for more sediments observed in the northern part and with further evidence from Brown et al. (1996), that the Albian period marked the switch from the dominance of the Olifants river system to the Orange River systems. This could explain the thicker sedimentary sequence in the northern part. Furthermore, the Barremian/Aptian sequence has huge quantities of sediment deposited within the depocentre, which coincidentally is the central section of the study area. The thick sedimentary sequence within the depocentre could have implications for the thermal and organic maturity of the source rock unit deposited during this period. The sequence is about 500 m thick around wells AO-1 and AE-1 but reaches up to 1800 m in the depocentre (Figure 5.17 B). In addition, the southernmost and the northernmost section of the study area evidently shows no deposition of the Barremian/ Aptian sequence, as it was terminated on the up- dip flanks of the basement in both northernmost and southernmost parts of the study area, hence clarifying the probable erosion or non-deposition of this sequence in that area.

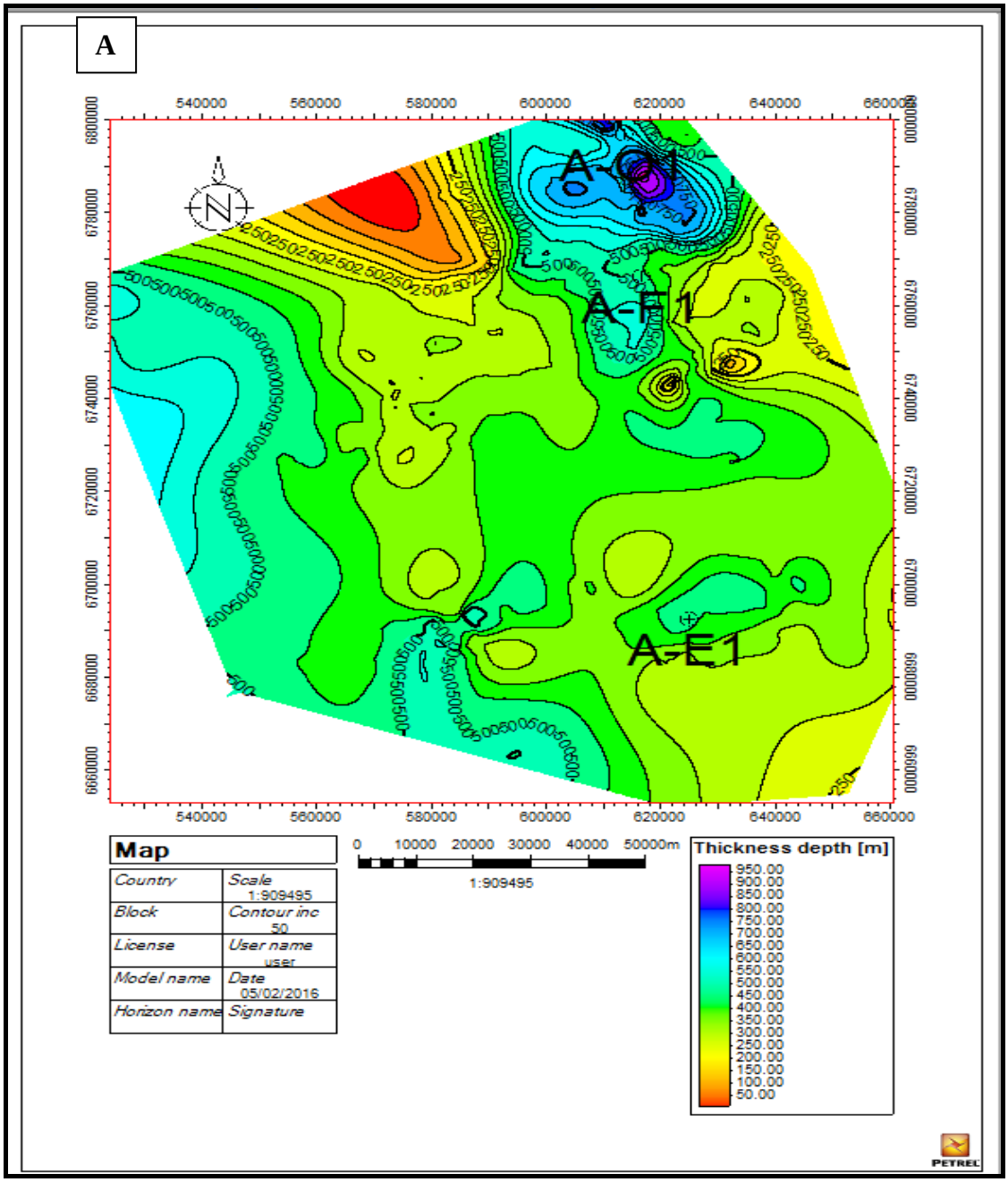

Albian

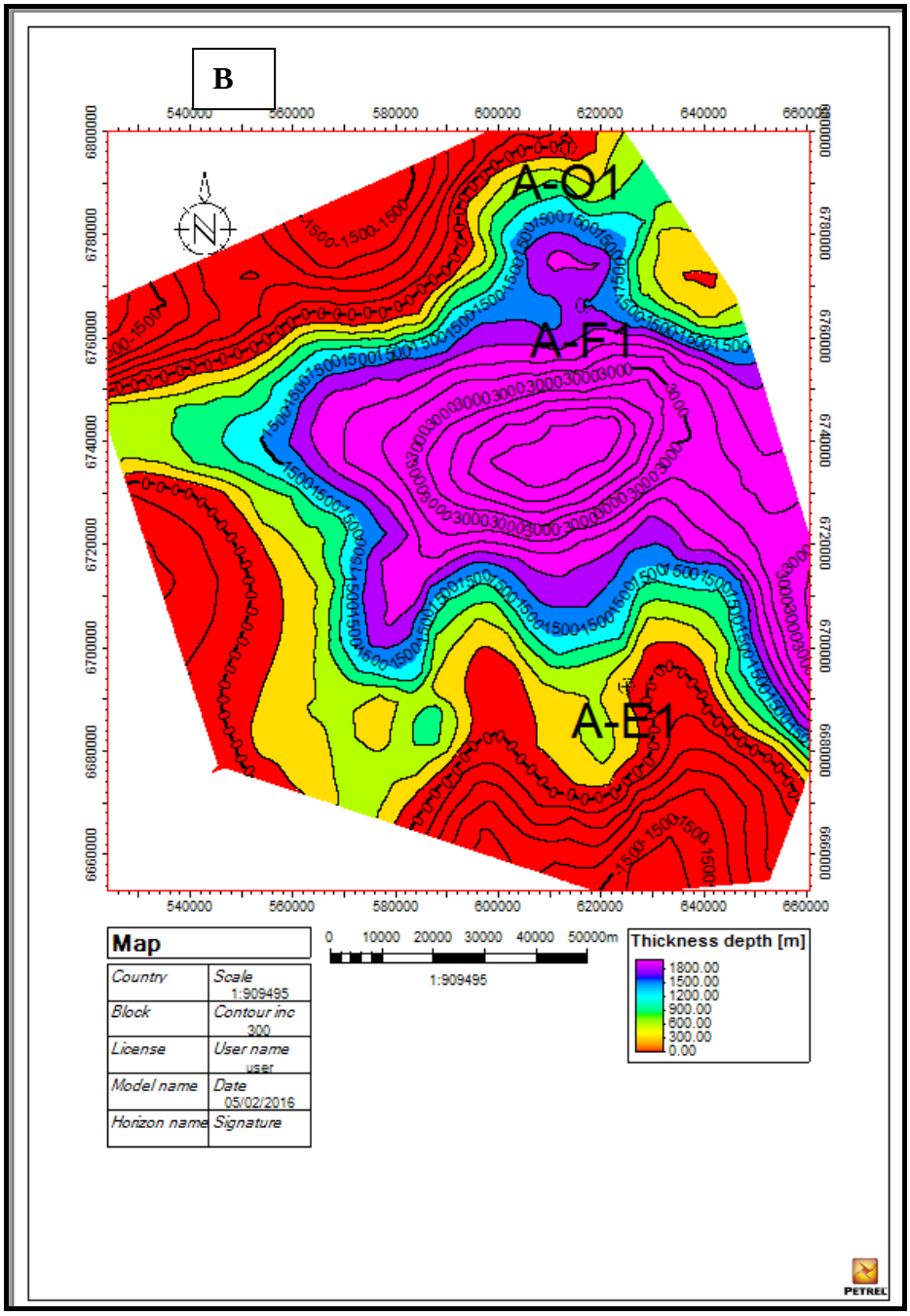

Barremian/Aptian

Figure 5.17A and B: Thickness variation maps for Albian (A) and Barremian/Aptian (B) Sequences. Erosion of this sequence occurs in the northernmost and southernmost part of the study area.

5.4.2 Results of Structural Interpretations, Paleo stress Analysis and Structural Modelling.

The structural evolution of the Orange Basin as documented by Hirsch et al. (2007); de Vera et al.(2010), Nurnberg and Muller (1991), Clemson et al. (1997) and Barton et al. (1993), described it as a divergent passive margin setting and by implication a tectonically-quiescent basin. The structural styles usually associated with this type of basin include listric growth- or normal faults and series of antithetic and synthetic faults. In addition, most continental passive margins are renowned to be driven by gravity systems caused by a region of up-dip extension and down- dip contraction (Rowan et al., 2004). In this study, a number of seismic lines are interpreted to examine the major structural styles, establish the relationship between faults systems and paleo-stress for adequate understanding of the timing of their formation and ultimately construct a 3D structural framework for the study area to provide an additional insight on the tectonic and stratigraphic evolution of the basin.

5.4.2.1 Structural Interpretations (Inline 756) (Fault Mapping)

There is a listric normal fault detaching from the basement and extending up to the late Cretaceous. The listric fault was probably formed from crustal extension during the breakup of the Gondwanaland and separation of the South American and African plates, which caused its detachment from the basement. Uplifts and tectonic event could have also played a role in the up-dip extension of the fault into the Cenomanian. Uplift events are suggested as the likely cause of the fault geometry extension as opposed to sediment loading because the latter would have increased curvature of the fault down dip as the fault geometry extends. In addition, there is an occurrence of a bright spot anomaly on both sides of the fault which could suggest fault saturation with hydrocarbon. The occurrence of bright spots (black circle in Figure 5.18B) on both sides of the fault implies that the fault could be serving as a control on the gas migration by serving as a leak as opposed to a seal.

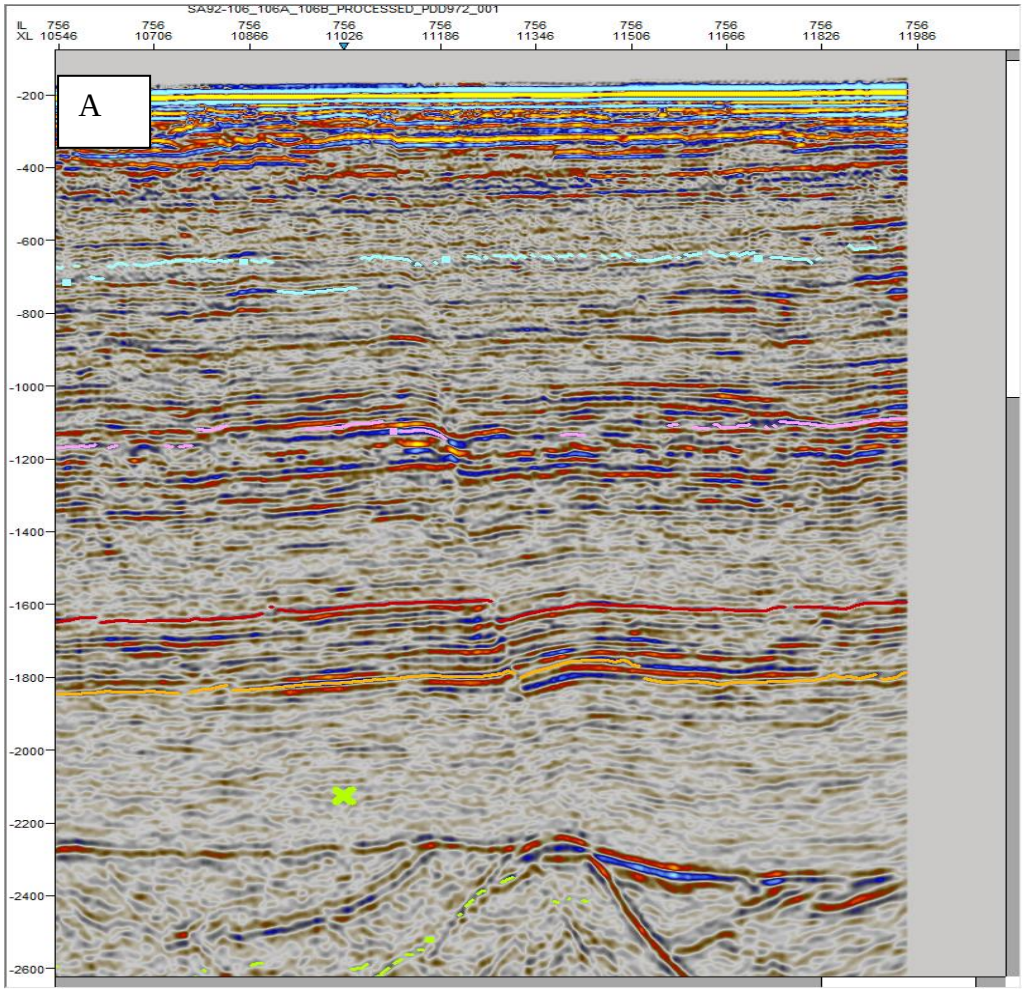

An integrated approach to understanding the geological controls on gas escape and migration pathways in offshore northern Orange Basin, South Africa.

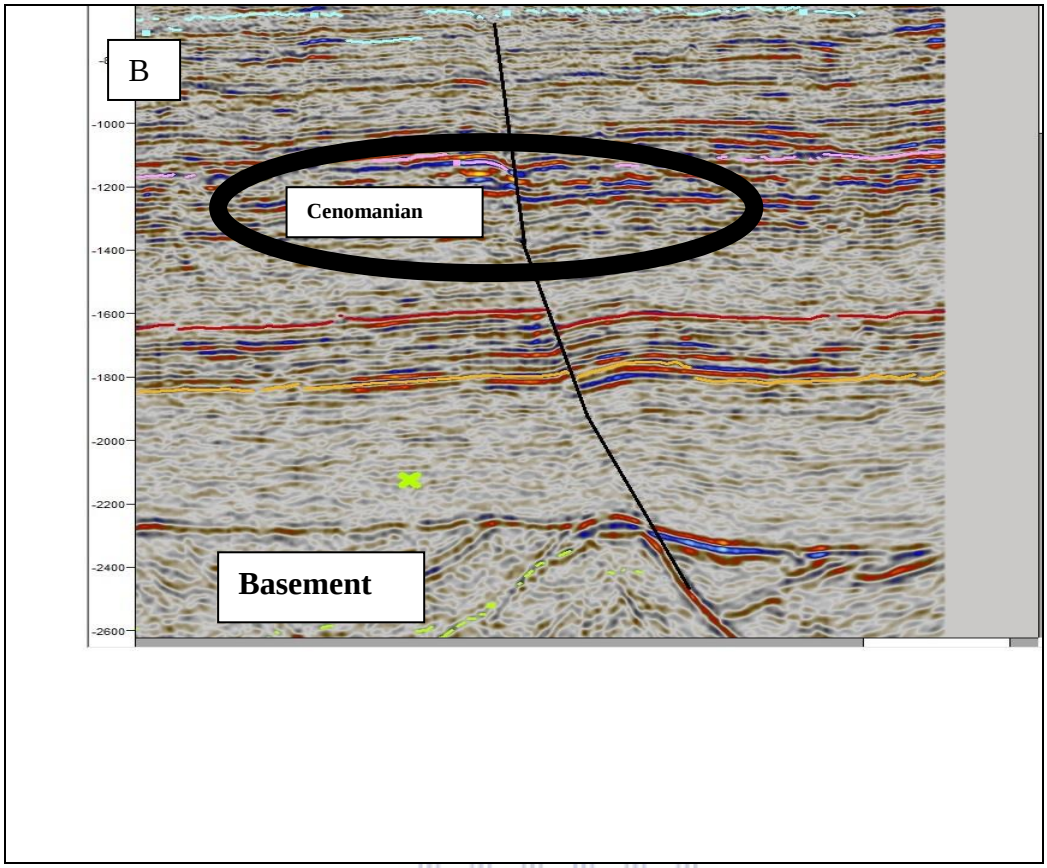

Figure 5.18 A and B: Figures showing un-interpreted and interpreted seismic section of Listric normal fault terminating at the Cenomanian Sequence respectively (Inline 756). Bright spot anomaly is noticed around the fault.

5.4.2.2 Structural Interpretations for Inline 1256.

At this inline a SW bounding early Cretaceous major fault which extends to the Tertiary occurs. The geometry of the fault is regional and spans accross different periods which suggest it could have been reactivated either by sediment loading or other tectonic events (Figure 5.19A and B).

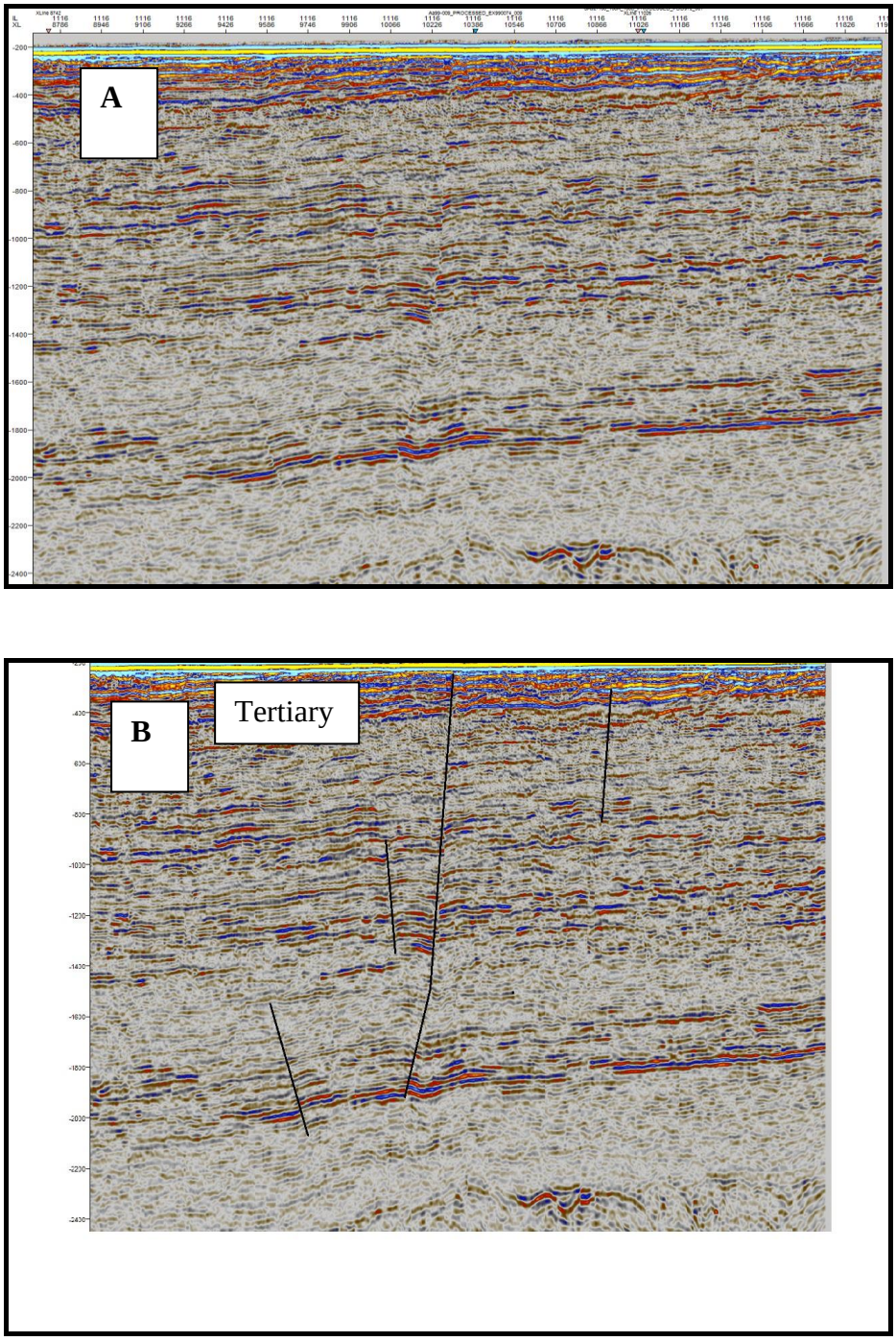

Figure 5.19 A and B: Un-interpreted (A) and interpreted (B) seismic sections of normal fault spanning from Cretaceous and stops just before the Tertiary Sequence respectively (Inline 1256).

5.4.2.3 Structural Interpretations for Inline 1326.

The seismic line reveals the presence of secondary faults branching off the main normal faults in opposite orientation. These minor faults referred to as antithetic faults. The causes of antithetic faults are commonly due to change of stress orientation which constrains shear sense of movement to the opposite direction of the main faults. These antithetic faults are of late Cretaceous age (Figure 5.20A and B).

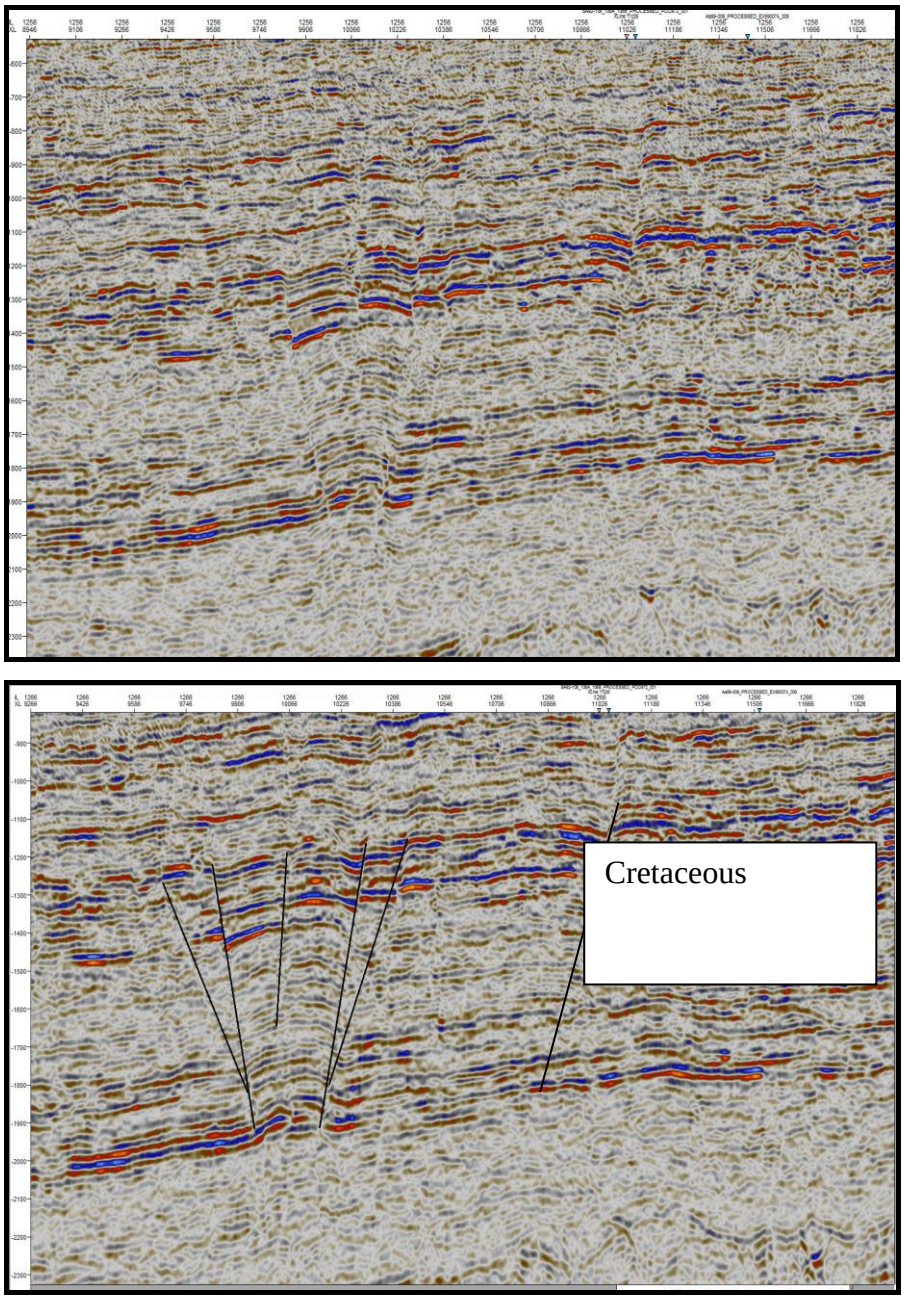

Figure 5.20A and B: Un-interpreted (A) and interpreted (B) seismic sections of Antithetic normal faults of Cretaceous age for Inline 1326.

5.4.2.4 Structural Interpretations for (Inline 1426).

The set of normal faults mapped in this line were formed in the early cretaceous and extend into the late Cretaceous. As explained in the description of other inlines above, the minor fault branching of the main fault here is an antithetic fault suggesting a space shortage which has to be accommodated by a pop-structure because of external sense of shearing and resulted into the formation of antithetic faults seen here.

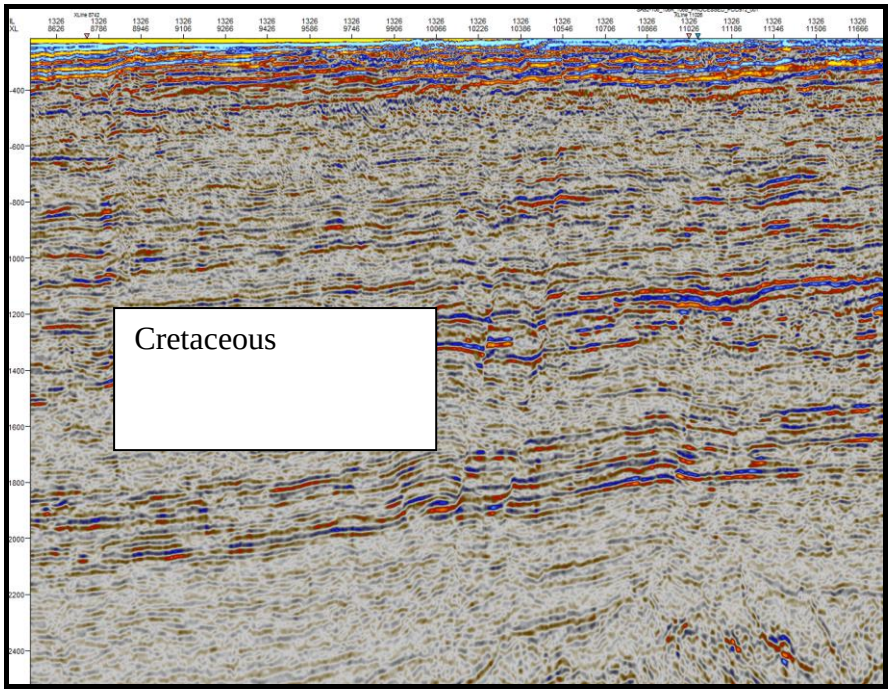

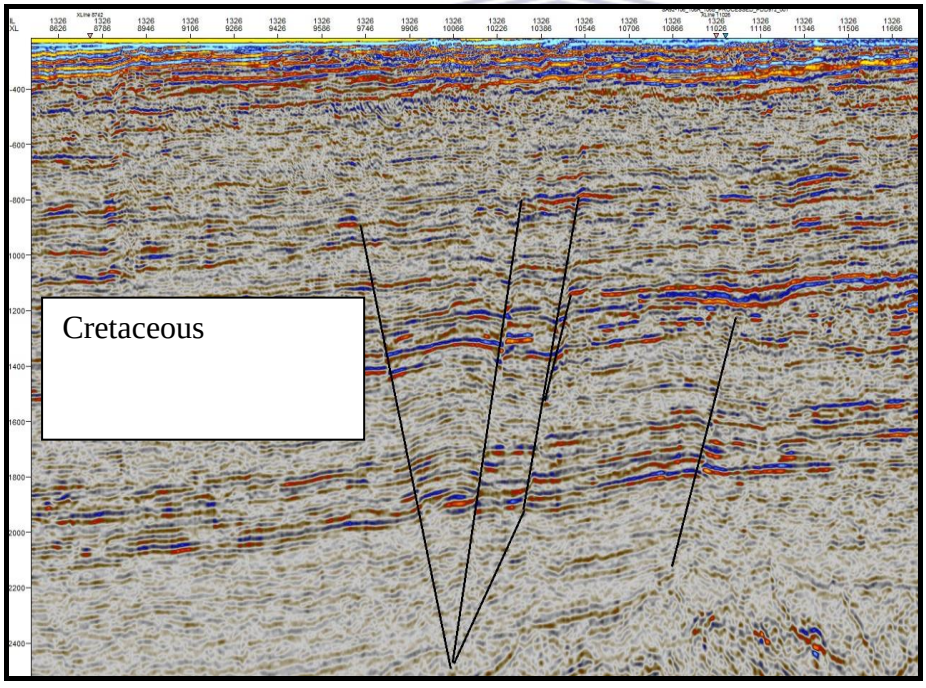

Figures 5.21A and B: Un-interpreted (A) and interpreted (B) seismic sections of Antithetic normal faults of Cretaceous age respectively for Inline 1426.

5.4.2.5 Structural Interpretations for (Inline 1586).

The occurrence of antithetic faults is confined to the late Cretaceous and branched off early Cretaceous normal faults as observed in other inlines (Figure 5.22 A and B).

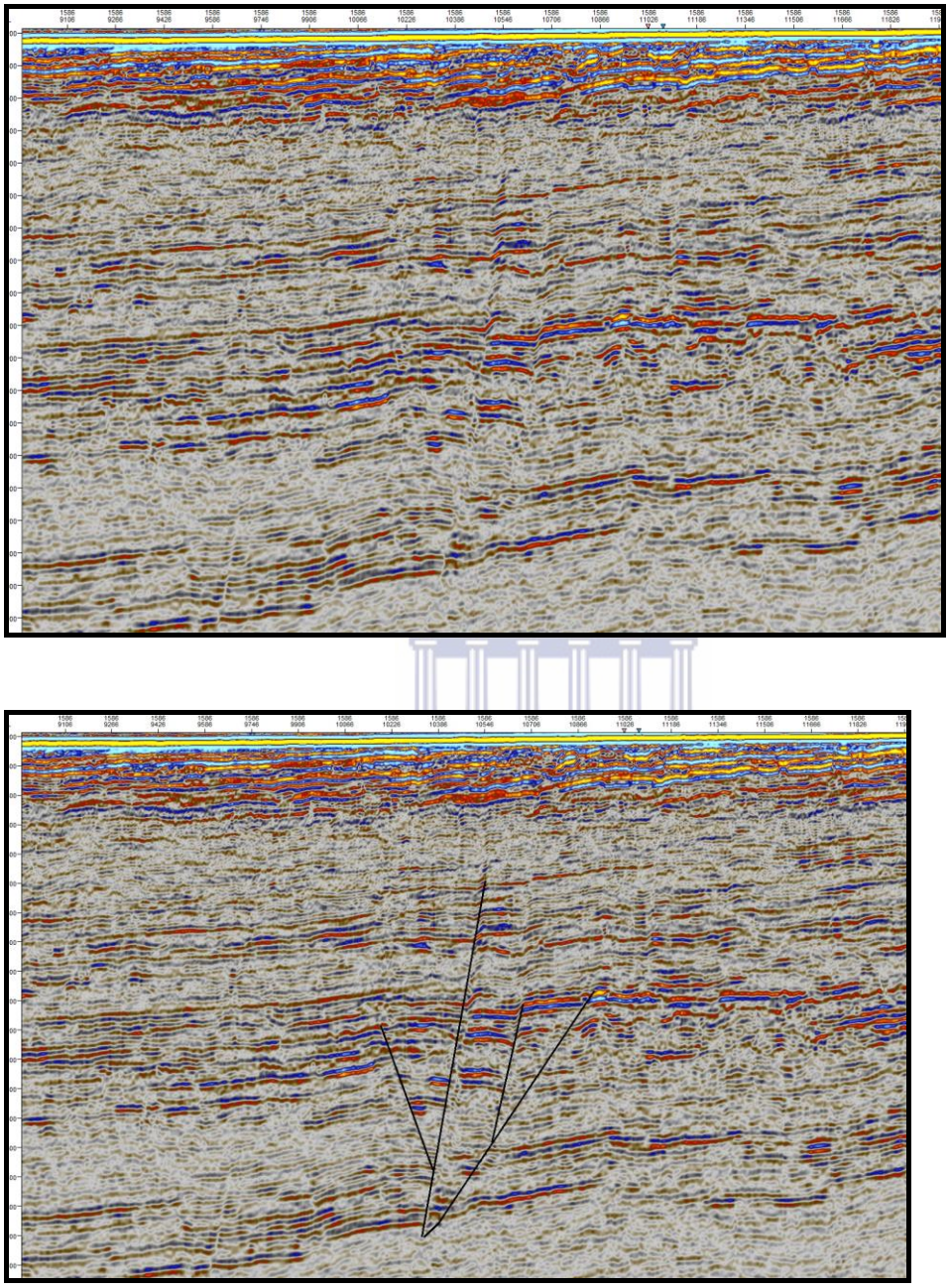

Figures 5.22 A and B: Un-interpreted (A) and interpreted (B) seismic sections of Antithetic faults of Cretaceous age.

5.4.2.6 Paleo stress Analysis Review and Results.

Stress leaves evidence or imprints on rocks as strains in form of joints, thrust belt or -faults. Stress and stress orientations emanate from continental plates rifting and drifting, pore fluids, margin uplifts which are all parts of crustal deformation. In an extensional regime, like in this study, tectonic stresses determine the principal axis of the fault planes and as such the dip and dip azimuth. Using Andersonian theory of faulting (Anderson, E.M., 1951), it is generally acceptable that $^{\delta}1$ and $^{\delta}3$ lies in the P and T-axes (Seismologist code) and correspond to maximum and minimum compressive stress respectively. The essence of a paleo- stress study is to investigate the empirical relationship between the stress history of the SACM (South Atlantic Continental Margin) and faulting systems observed in the offshore Orange Basin. The basic understanding of this is that faulting occurs as a result of a response to homogenous stress per period. The understanding of this, in relation to faulting system will enable adequate understanding of the timing of the formation of the faults, and subsequently, in relation to timing of the generation of hydrocarbons in Orange Basin in Chapter Seven of this study.

Andreoli et al.(2009), Viola et al.(2012) and Salomon et al.,(2014) documented the regional stress field of the South Atlantic Margin. Andreoli et al.,(2009) specifically itemized the paleo stress history and selected events in the Namaqualand based on studies from other authors. These previous works on stress history documented in Namaqualand by different authors were used to interpret observations made in this study. Studies done in Namaqualand are best used to calibrate structural styles of the offshore Orange Basin as structurally, Namaqualand is the onshore equivalence of offshore Orange Basin. Therefore, they are likely to have similar structural styles.

Since uplift does affect the whole continental margin, faults that were formed from same episode of uplift or stress should have similar dip orientation. While the faulting systems in this basin have been attributed to extensional faulting as a result of gravitational margin failure induced by margin uplift (deVera et al., 2010) , it is also believed that there were regional stress variations which might be caused by sediment loading offshore and the continuous uplift of the African super plume (deVera et al.,2010) .

The question now arises, could formation of faults in Orange Basin be linked to different episodes of stress that have affected the SACM?

In this study, there are over 300 faults that were mapped and plotted on the stereonet diagram (Figure 5.23), and with the understanding that these faults were constrained to a particular orientation based on the tectonic stress that produced them. Clusters of faults around the stereonet revealed three trends (Figure 5.23); NNW-SSE, NNE-SSW and WNW-ESE based on dip and dip azimuth of the faults.

The NNW-SSE faulting system as observed in this study (Figure 5.23) could have occurred in the late Cenozoic based on the Shmax (Maximum Circumferential Stress) calibration of Andreoli et al., (2009). The late Cenozoic faulting (neotectonics) observed in Namaqualand has been linked by Viola et al.(2012) to the existence of offshore mud volcanoes in the Orange Basin and by implication neotectonism affected the offshore Orange Basin. This suggests that the NNW - SSE faulting system observed here could be a product of neotectonism as mentioned by Andreoli et al.(2009).

Furthermore, the NNE-SSW faulting system observed in this study (Figure 5.23) might have occurred in the late Cretaceous due to bi-deformational events (extension and compression) that occurred in Namaqualand (Andreoli et al., 2009). The extensional phase postulated here affected the whole African continent in the Campanian-Maastrichtian (Guiraud and Bosworth, 1997) and may have been due to the uplift of the African superplume and the resulting “bulge” could be responsible for the extensional faulting and gravitational failure-induced faulting in the Orange Basin (de Vera 2010; Butler and Paton, 2010). The margin tilting as a result of the uplift coupled with a sea level drop was responsible for the slumping events and development of progradational sequences in the late Cretaceous respectively (Tinker et al., 2008; Seranne and Anka, 2005). Faults mapped within the Cretaceous post-rift sequence were plotted on a stereo plot; the trend reveals dominance of NNE-SSW faulting system with negative dip angles, which is commonly associated with footwall rotation (Spencer 1984; Buck, 1988).

The third trend is the ENE-WSW faulting system (Figure 5.23). This trend as observed here may be part of the synrift-drift succession that accompanied the separation of the South America and Africa plates which manifested dominantly as ENE-WSW as seen in figure 5.23. This postulation agrees with the observation made from Namaqualand by Andreoli et al., 2009 that around 120 mya, faulting is constrained to the NE-SW orientation. This also agrees with a previous study of Granado et al., 2009 which suggests that the synrift and drift sedimentary succession of the Orange Basin were deposited via a NE-extensional faulting system.

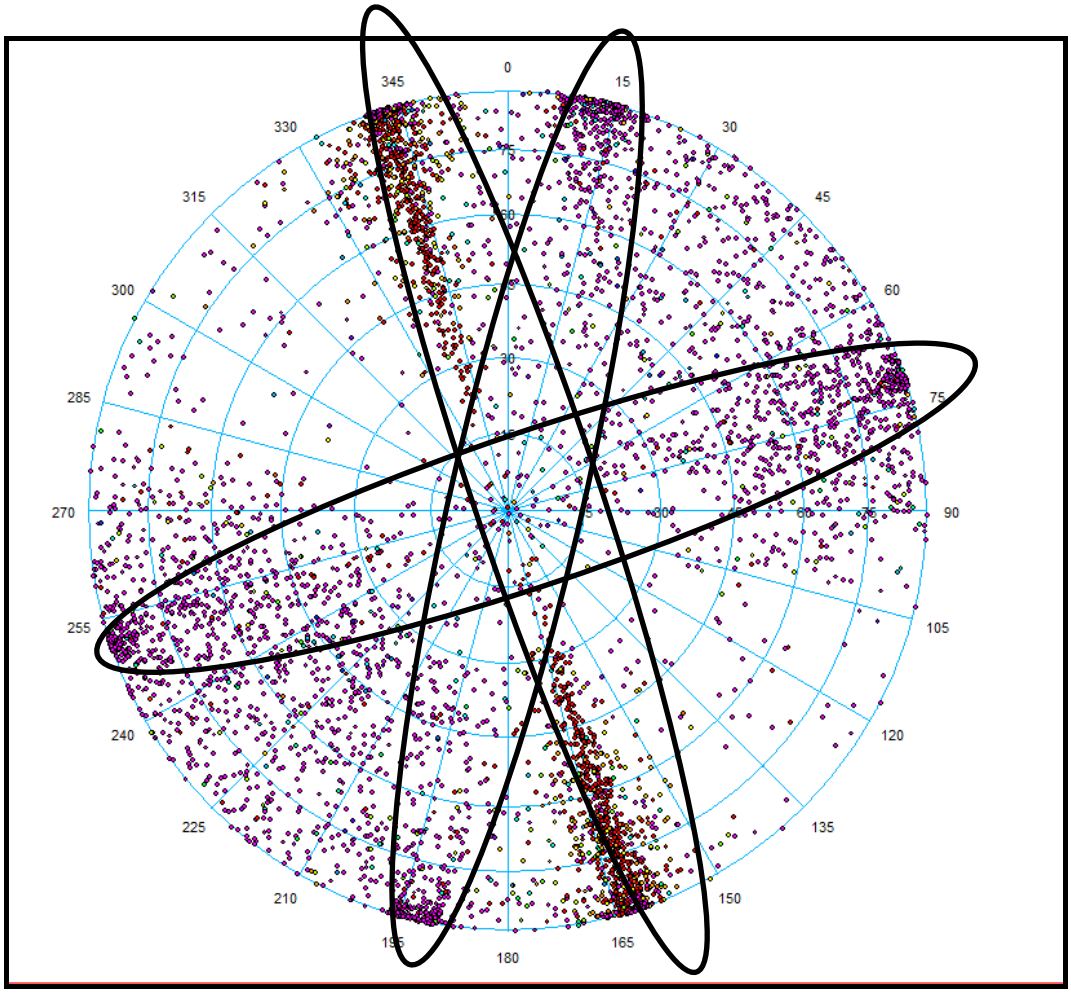

Figure 5.23: Stereoplot of faults mapped in the study area. Plot shows three Bi-directional trends of deformation from the Fault Extraction Process using Petrel 2013.

Furthermore, In Figure 5.24, selected faults plotted on the stereonet to determine the dominant stress regime, using the Andersonian method reveal that the T-Pole(the minimum compressive stress is horizontal and lies within the main principal plane of the faults suggesting an extensional regime. Also, the L-pole (β) falls within the main principal plane of the faults along with the T-pole. The T-pole along the fault plane is

perpendicular to the P-pole, which is the maximum compressive stress (Mean Principal Pole) affirming the dominance of extensional stress regime.

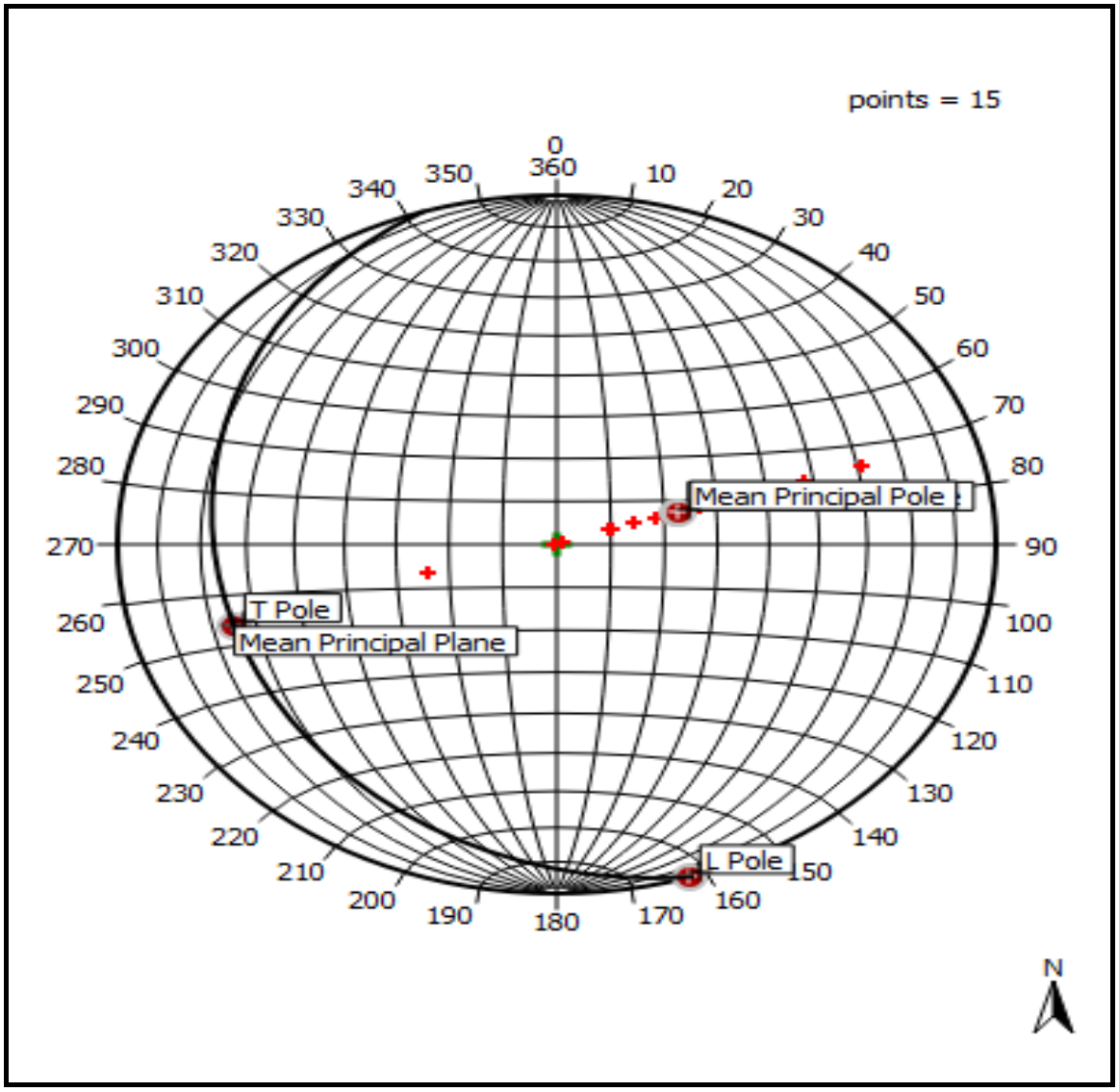

Figure 5.24: Principal stress Orientation suggesting dominance of extensional Regime as the T-Pole (extension) lies within the mean principal plane.

5.4.2.7 Structural Inversion or Drag Fold

There is a likely evidence of a change in stress regime as shown in Figure 5.25. While normal faults as seen here terminate in the late Cretaceous, they are accompanied by mild contraction at the top horizon bounding these set of faults. This is suggestive of either a mild basin inversion or a drag fold associated with normal faulting. The latter is highly suspected.

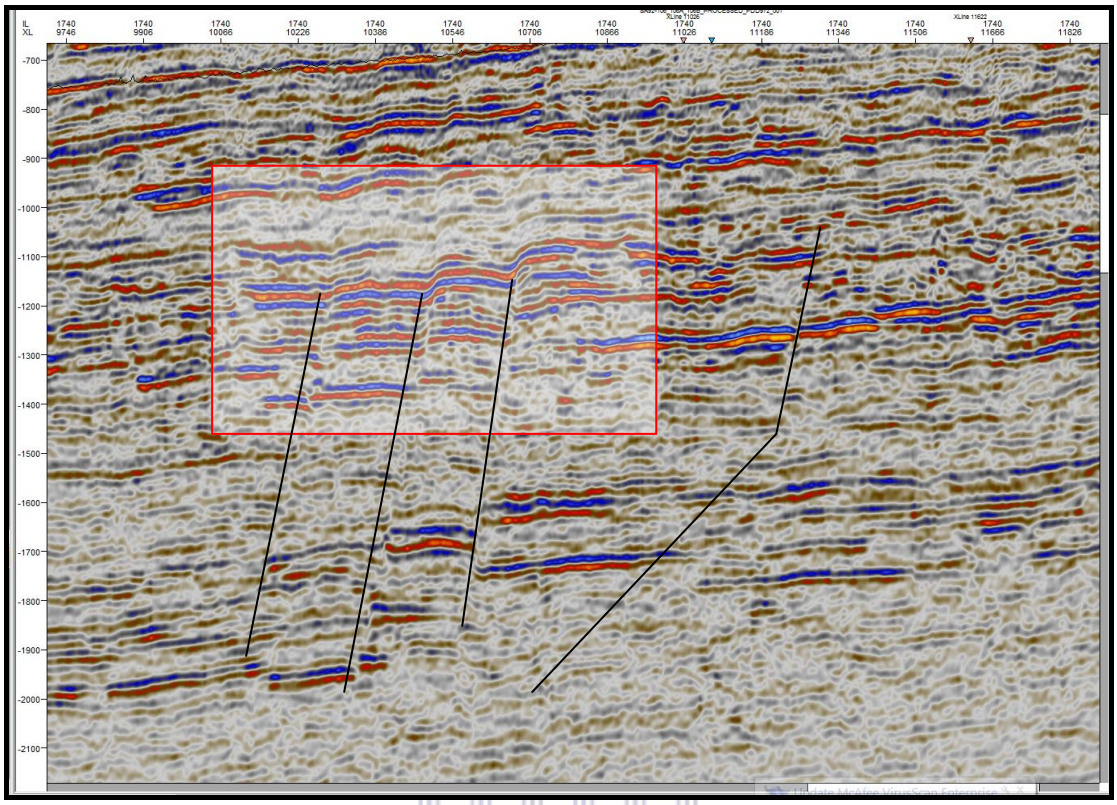

Figure 5.25: A seismic section showing normal fault drag and fold due to Extensional regime.

5.4.2.8 Structural Model/ Framework

A structural model was constructed for the study area to examine the stratigraphic evolution and structural deformation relationship. The northern view shows the Barremian –Aptian sedimentary sequence deposited as graben fill which thins out and partly eroded towards the western part of the study area. Also, part of the Turonian sequence has been eroded which makes that the sequence terminates on the underlying Cenomanian sequence (Figure 5.26A). The Maastrichtian and Turonian sequences show possible compression which is evident only in the northern and western part of the study area (Figure 5.26B). There is clear evidence of an erosional unconformity as part of the Maastrichtian and Turonian sequence down lapped on the Cenomanian (Figure 5.26A). In the eastern and southern section of the study area, the basement slope up-dip in the southern and eastern portion of the study location and coupled with evidences of extensional faulting. The up-dip inclination of the basement in the eastern and southern section of the area explains why the northern and western area of the study is the depocentre of the study area and consequently has

more sediment deposited. Compressional event is observed only in the late Cretaceous (Figure 5.26B).

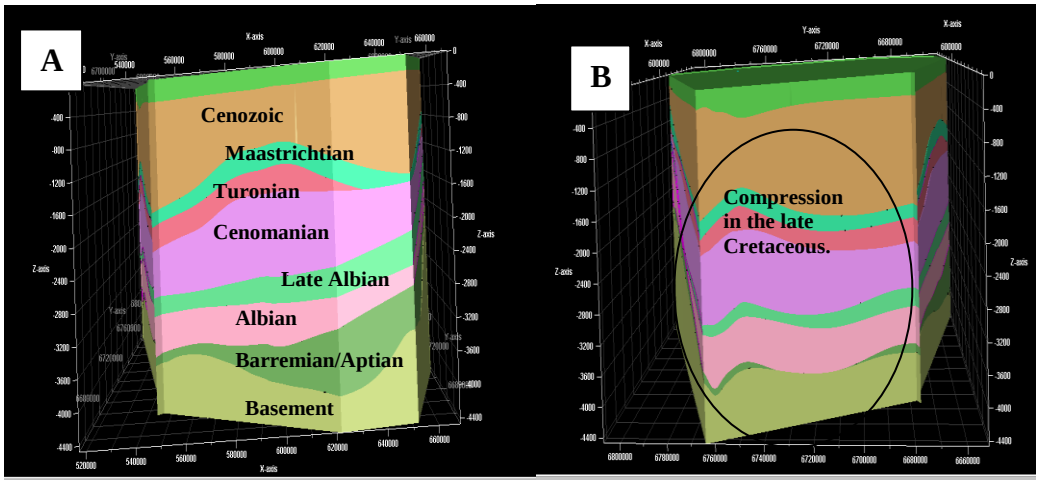

The Northern Section **Western Section**

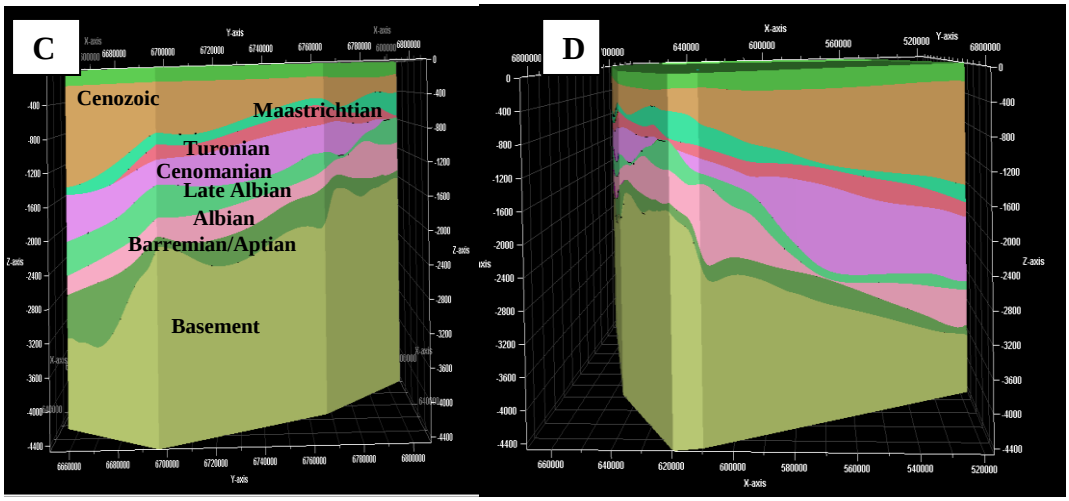

Eastern Section **Southern Section**

Figure 5.26 (A-D): Figures showing the structural framework of the study area across the four quadrants. There is an evidence of compressional event in the late Cretaceous. Model size is 140kmby 130km.

5.4.3 Results of Gas escape features mapping and their relationship with faults and stratigraphy.

Controls on gas escape features in the Orange Basin have been classified as either structurally controlled or stratigraphically controlled (Boyd et al .2011). Therefore, mapping of gas escape features provide the understanding of possible migration pathways of hydrocarbon in a sedimentary basin. A selected number of seismic lines were selected and interpreted below to map gas escape features and their likely controls.

5.4.3.1 Pock mark (Inline 800)

Pockmarks are one of the prominent sea floor expressions of gas escape in extensional basins. At inline 800, there exists a pockmark which is about 150m wide (Figure 5.27). The genesis of this pockmark could not be ascertained but often, pockmarks are an expression of gas migration through fine-grained sediments.

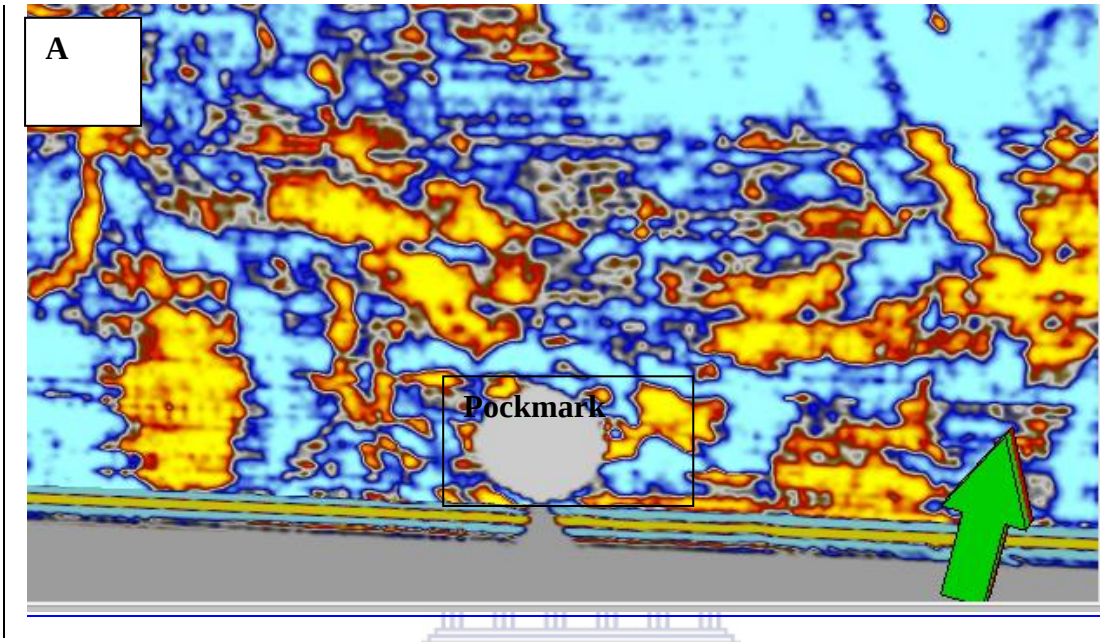

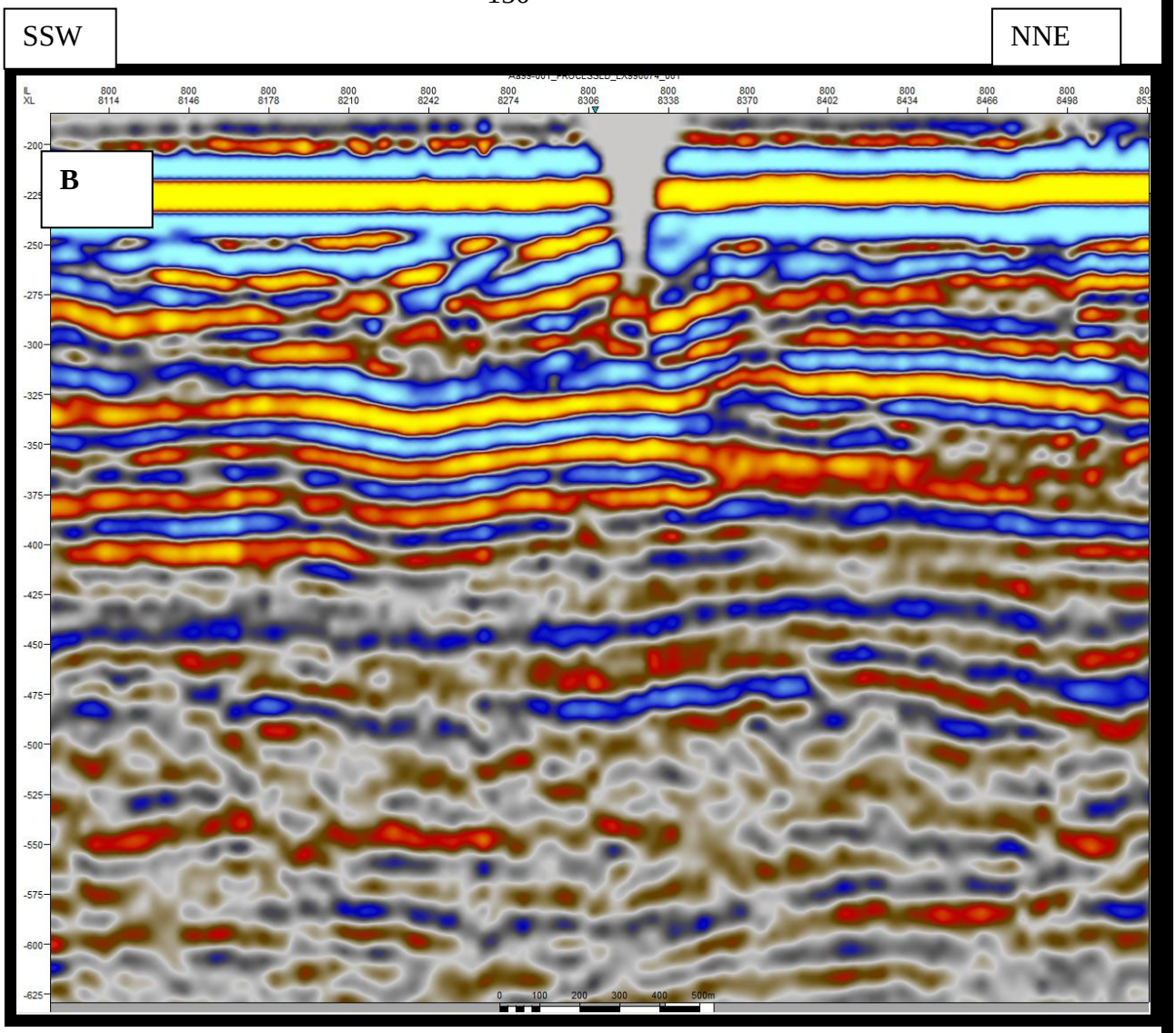

Figure 5.27: Pock mark observed on the sea floor at Time slice 250ms (A) and inline 800ms(B).

5.4.3.2 Fault controlled Gas Chimney at Inline 2240

The seismic chimney observed at inline 2240 indicates a columnar disturbance within the sedimentary sequence and is associated with a Cretaceous fault which is believed to have triggered the migration of gas. The disturbance occurs along both sides of the fault from the Cenomanian to the Cenozoic suggesting migration of gas along the fault plane. Considering the fact that the fault extends from upper Cretaceous (Cenomanian) sequence upwards in to the Cenozoic points to a possible reactivation of an older fault which makes the fault not just a conduit, also a trigger of gas escape. The fault plane shows dilation at the inner Cenozoic. The gas however, does not escape to the sea floor but appears to be confined to the Tertiary sediment in this case (Figure 5.28).

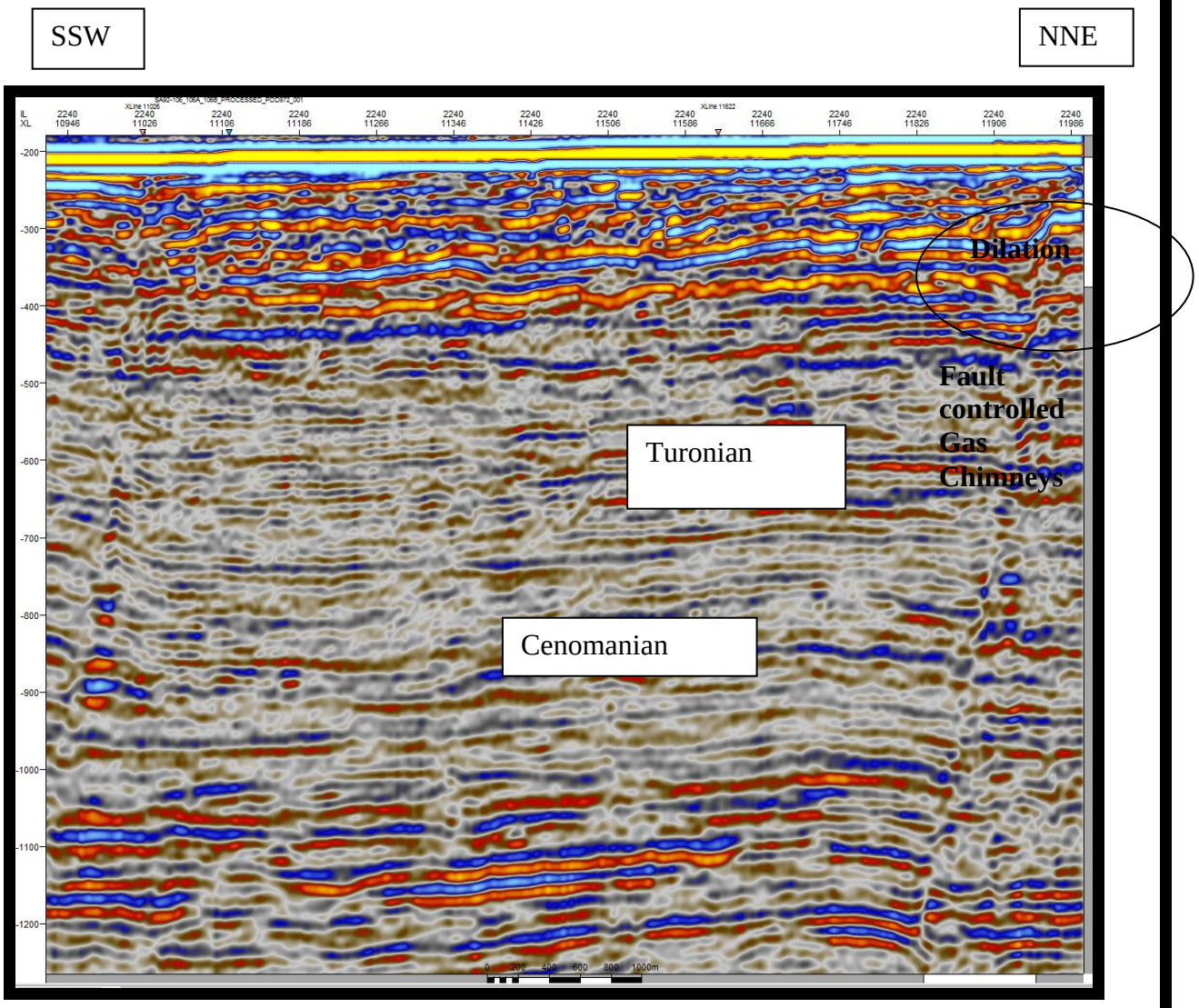

Figure 5.28: Fault Controlled Gas Chimney observed at inline 2240.

5.4.3.3 Fault Controlled Gas Chimney at Inline 2400

At Inline 2400 there occurs a normal fault confined within the Cretaceous sequence which serves as a trigger of a gas chimney. The gas chimney occurs directly on top of the normal fault. In this case, this fault serves as a trigger of gas escape only because the chimney occurs just at the top of the fault (Figure 5.29).

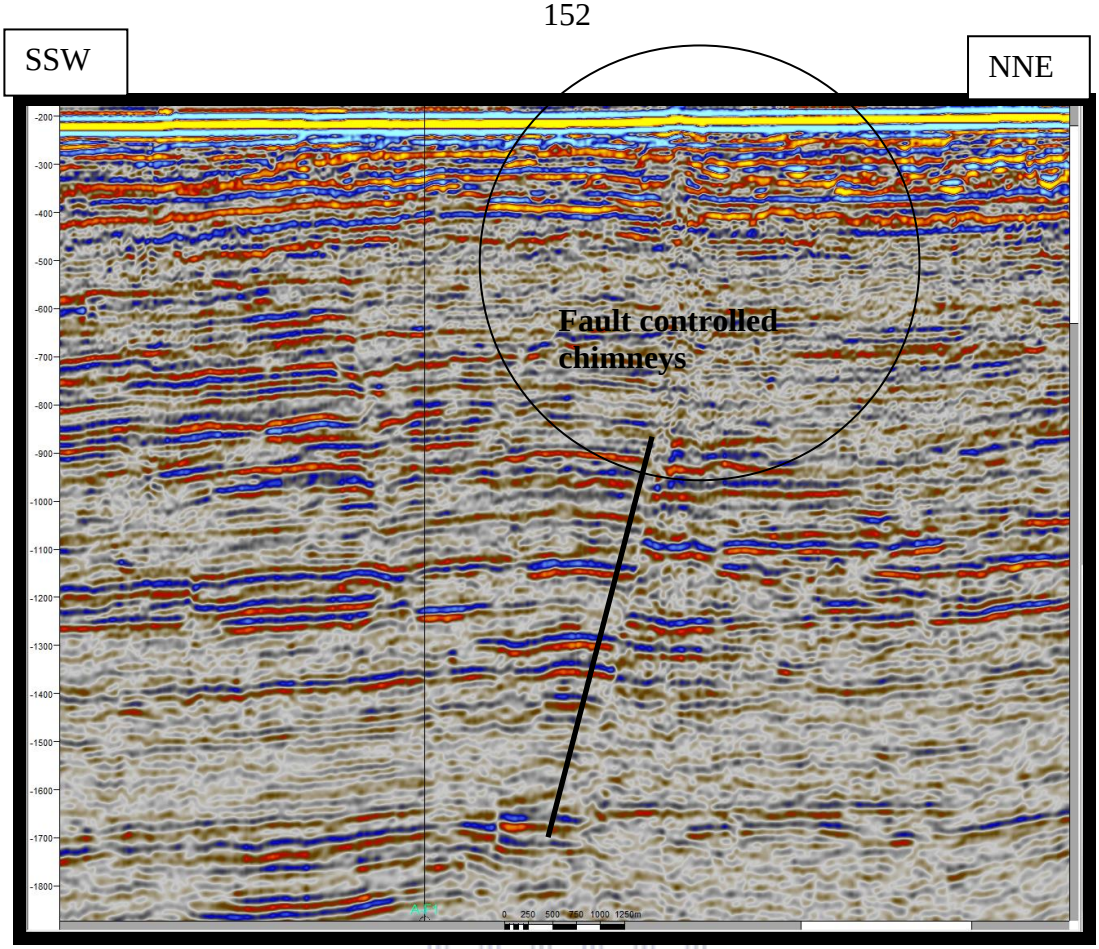

Figure 5.29: Fault Controlled Gas Chimney observed at inline 2400 terminating within the Tertiary.

5.4.3.4 Acoustic Wipeout at Seismic Line 79-004 and 82-010.

On seismic lines 79-004 and 82-010 an acoustic wipeout has been observed. An acoustic wipeout is generally associated with loss of seismic reflection data as seen here and is often associated with gas-charged sediments which is expressed on the sea floor. It is common in near surface sediment as it represents rapid flux of gas or fluids in near surface sediments (Roberts et al., 1999).

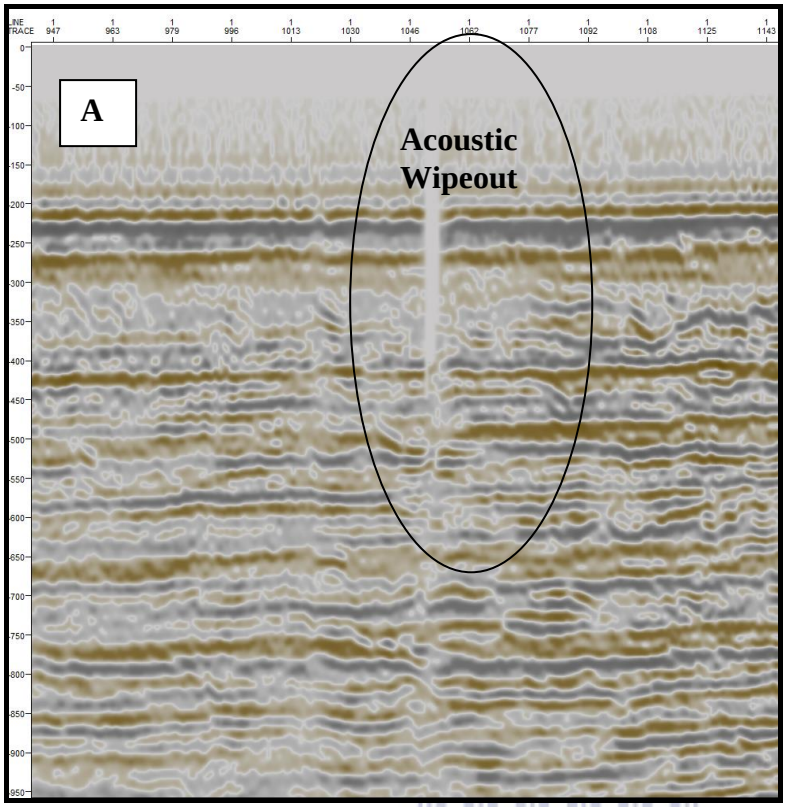

Line A79-004

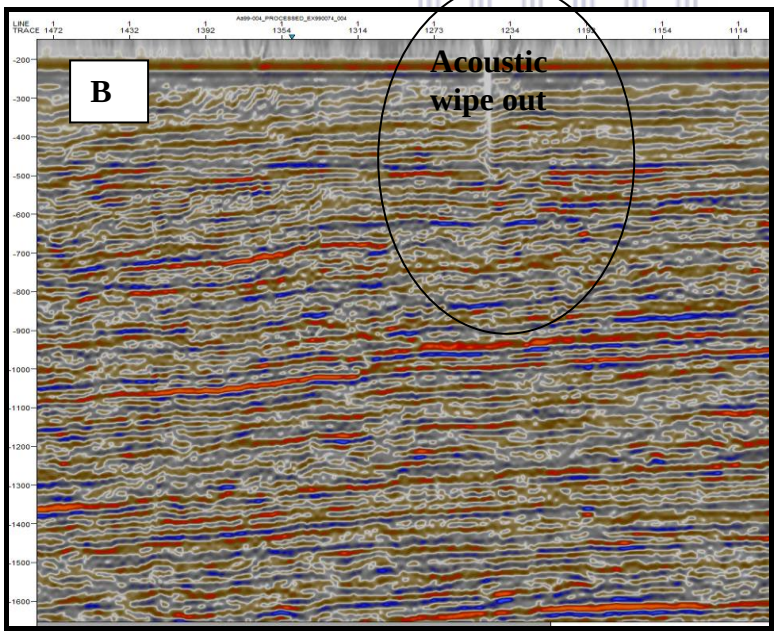

Line A82-010

Figure 5.30 A and B: Stratigraphically controlled Acoustic Wipeout at Lines 79-004(A) and A82-010(B).

5.4.3.5 Stratigraphically Controlled Chimney at Seismic Line K80-014.

The vertical columnar disturbance of the seismic reflection exists here and represents a chimney. In this case, the chimney is not associated with any faults but likely originates from a deep seated gas charged-depositional unit and moves through the stratigraphic sequence and terminates at the near surface Tertiary sequence (Figure 5.31).

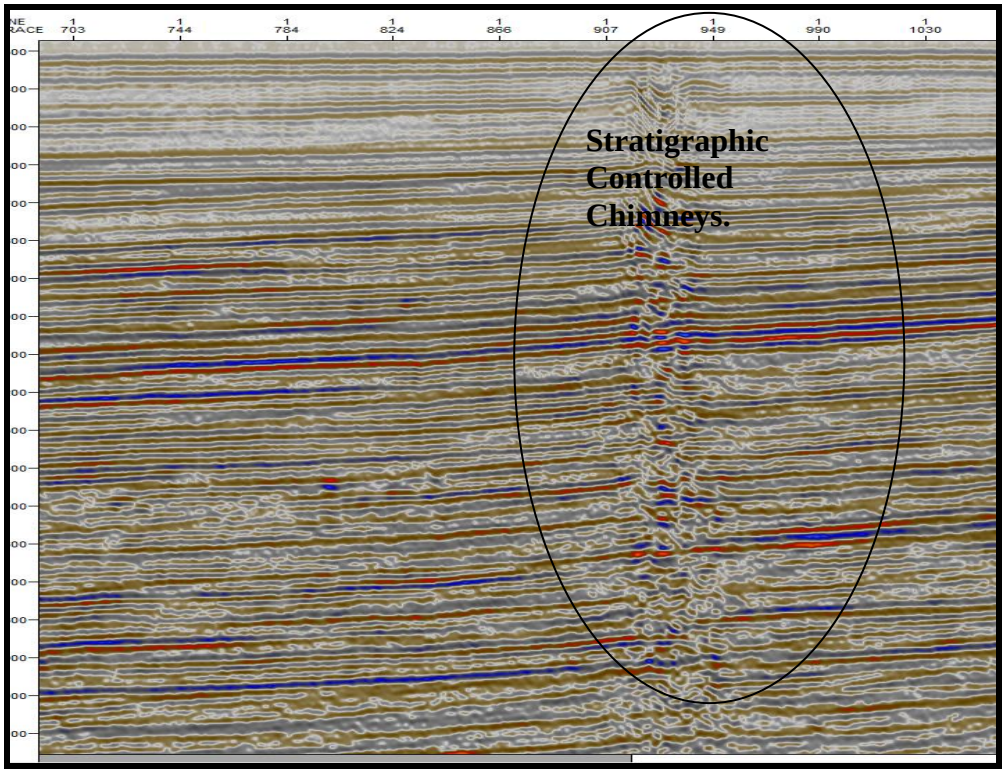

Figure 5.31: Stratigraphically controlled Gas Chimney at line K80-014

5.4.3.6 Bright Spot at Inline 756

There is an occurrence of a bright spot anomaly on both sides of a listric normal fault that detached from the basement. This occurrence on both sides of the fault could mean the fault is opened which caused gas to migrate freely across it (Figure 5.32).

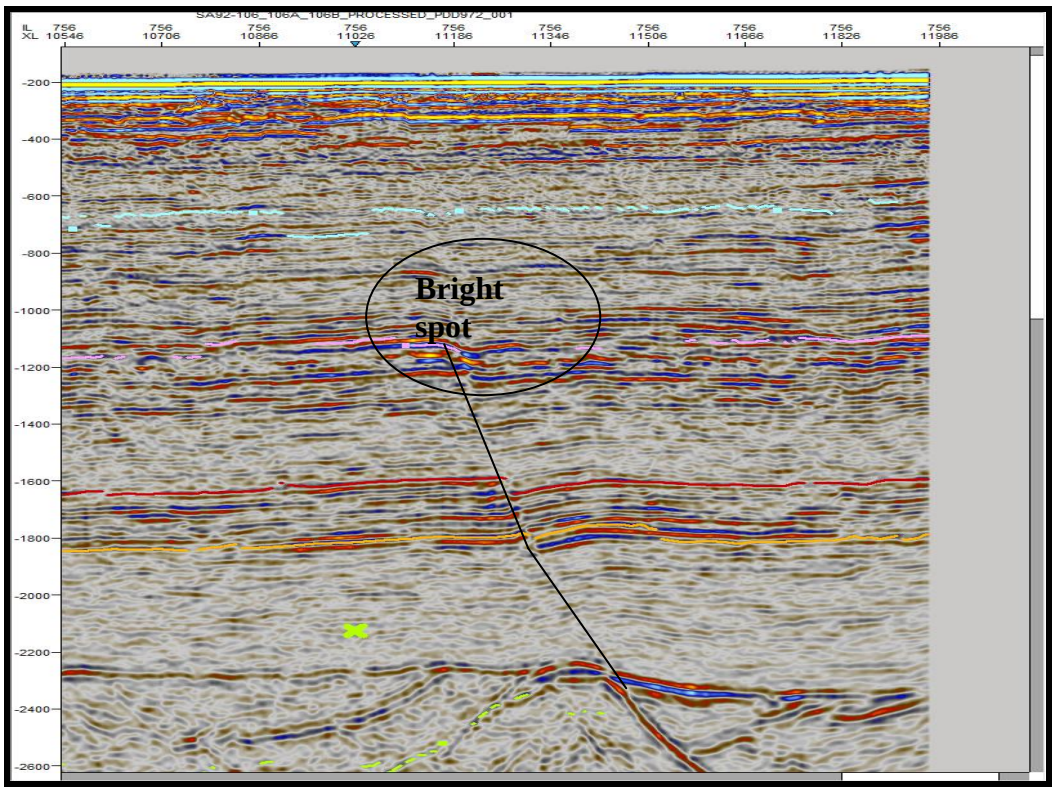

Figure 5.32: Bright spot anomaly occurrence on both sides of a listric normal fault at inline 756.

5.4.3.7 Mud Volcano at Inline 800.

At inline 800, exists a 615m wide, 20m long mud volcano or a carbonate mound. While mud volcano is common in convergent margins, it is rarely seen in divergent margins. In addition, tectonism is not the only cause of mud volcanism, it could be caused by pressure build up caused by a mixture of fluid and gas in argillaceous sediments which makes it buoyant to evolve on the sea floor. Therefore, gas presence as opposed to tectonism could have caused the occurrence of this mud volcano (Figure 5.33).

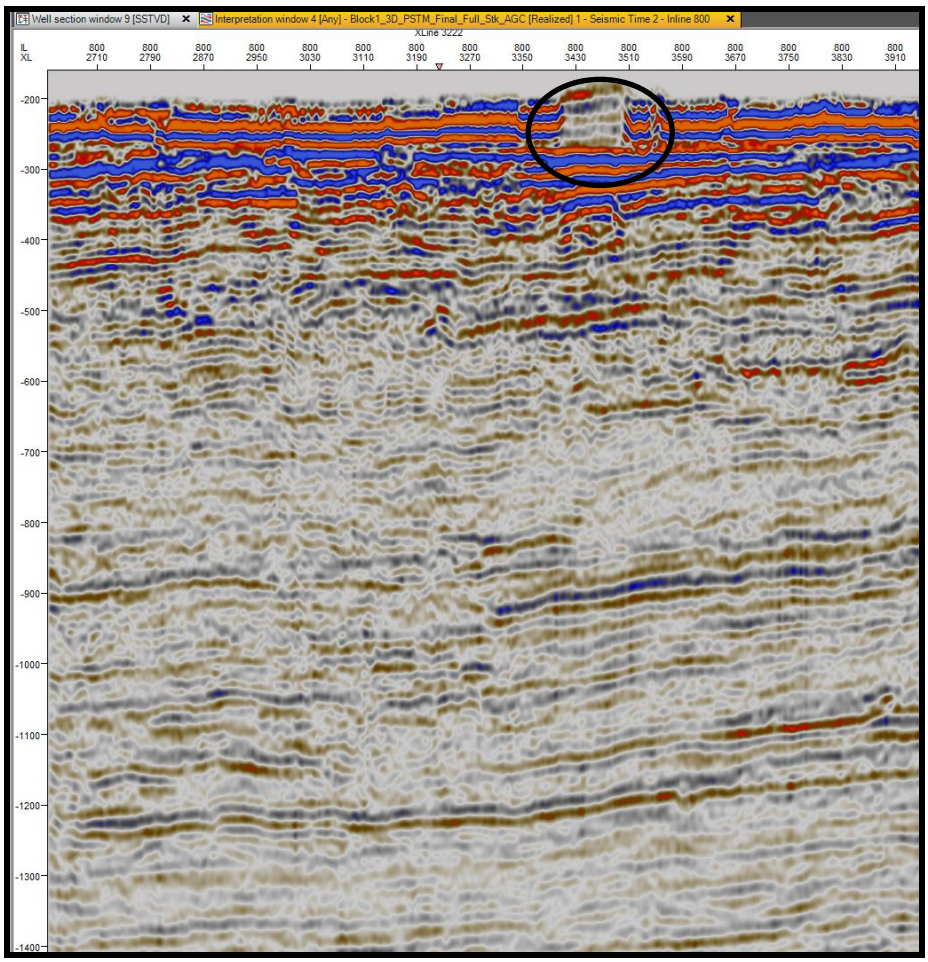

Figure 5.33: Mud volcano occurrence on the sea floor at inline 800ms.

5.5 Conclusions

Seismic sequence analysis shows evidences of erosional features like truncation, top lap and a stratigraphic feature; a low-stand prograding wedge in the northern part of the study area. In addition, observations made from seismic facies analysis with focus on strata reflection configurations, internal characters of reflectors and amplitude shows a good match with observations made from litho-facies analysis, especially in interpreting depositional environment and identifying stratigraphic features such as fluvial channels and point bars. Consequently, inferences made from calibration of seismic facies and litho-facies analysis here can thus be considered to be reliable. These stratigraphic features, suggestively, are essential carrier beds for hydrocarbon migration processes. Thickness maps reveal progressive thickening of up to 1.5km of Cenozoic sediments westward of the study area. There is evidence of an erosional unconformity during the Turonian as the sediment thins to almost zero m towards the southern part of the study area. Evidence of Barremian/Aptian sequence erosion is also seen, based on the thinning out of this sequence, notably in the southern part.

Structural model/framework suggests possible mild inversion in the late Cretaceous, while review of paleo-stress analysis suggests three different trends of faulting systems which could be linked to the different episodes of stress evolution of the South Atlantic continental margin. Listric normal fault associated with bright spots amplitude, and antithetic faults are the major faults observed in the study area. Finally, there are evidences of fault- and stratigraphy-controlled gas escape features, specifically chimneys and sea floor expression of it; such as pockmarks.

Chapter Six

Application of Seismic Attributes Analysis for mapping of Faults and gas escape features, Identification of stratigraphic features and delineating hydrocarbon-charged sediments.

Keywords: Acoustic Impedance, Frequency

6.1 Abstract

A combination of genetic inversion (Seismic Impedance and Porosity), variance and seismic attributes (Instantaneous Frequency and Iso-Frequency) are used to characterise clastic reservoir targets and faults in offshore, northern Orange Basin. The area of interest (AOI) was limited to 3D seismic volume within the central portion of the study area because of the inadequacy of using 2D lines to perform seismic attributes analysis.

Frequency filtering was performed as a form of post stack seismic processing technique to remove passive noise and enhance geological features. Variance attributes reveal the presence of faults (Listric and antithetic) and mud volcanoes at the sea floor. Seismic acoustic impedance inversion calibrated with porosity inversion reveals the presence of meandering fluvial channels and associated point bars deposit within the Cenomanian and Albian sequence. The identified channels expectedly show high porosity along its geometry compared to its surrounding lithology. Iso – Frequency (Frequency decomposition) using the Cosine Correlative Transform (CCT) was applied to identify the sweet spots. Iso- frequency of 45 Hz, 12 Hz and 8Hz windows were captured to isolate hydrocarbon charged reservoirs within the Albian and Cenomanian sequence. The CCT method shows that 8Hz window resolved stratigraphic feature present within the seismic volume and able to resolve the presence of likely hydrocarbon charged sediments judging by the frequency attenuation seen around a listric fault.

However, the application of Instantaneous Frequency (IF) attribute reveals the presence of hydrocarbon charged Cenomanian reservoirs in close proximity to a fault judging by the attenuation of frequency observed. This was achieved by using Thirty –three seismic traces as an input in the Hilbert transform window, subsequently, trace envelope and instantaneous phase were transformed into instantaneous frequency. This study demonstrates the effectiveness of integrating different seismic attributes as a non-invasive approach in characterising faults, stratigraphic features and hydrocarbon-charged sediments.

6.2 Introduction

Seismic attributes in this study are applied for qualitative measurement of seismic data to detect structural and stratigraphic features of interest. Generally, the varieties of seismic attributes that exist are applied in exploration studies to decipher structural or depositional environment features in sedimentary basins. Different seismic attributes are tested for different geological features. While some are adequate for detecting specific geological features, some could be inappropriate. However, previous authors have demonstrated the successful application of seismic attributes in detecting stratigraphic and structural features and in detecting hydrocarbon presence (Chopra and Marfurt, 2006; Hardage et al., 1996). In this study, attributes like variance, seismic impedance, instantaneous frequency, Iso- frequency attributes and porosity inversion are applied as imaging tools for stratigraphic features (erosional features, channels and wedges) and structural features (faults) associated with gas presence and gas escape features. Prior to this, structural smoothing and frequency filtering were performed for optimization of faults mapping and stratigraphic features imaging as a form of post –stack quality check processes.

6.3 Methodology

The seismic cube was subjected to frequency filtering to remove incoherent noises from the data and enhance geological features.

In carrying out the seismic impedance genetic inversion, a Time- depth relationship and seismic- well tie were performed between the well and the 3D seismic volume

using formation tops and checkshots data. Subsequently, the Fourier transform process was completed by first generating a velocity log from a sonic log using the formula; Velocity= 1/Sonic. Thereafter, the velocity log was used to generate an acoustic impedance log by multiplying the values with formation density values. In addition, a reflection coefficients log was generated together with a synthetic seismogram to calibrate with seismic data at the well position. The acoustic impedance log generated from the Fourier transform process was genetically inverted and observations made were calibrated with the genetic porosity log inversion results because of the relationship between these two rock properties. Iso-frequency attributes applied here image the potential reservoirs using the Correlation Cosine Transform (CCT), which is a mathematical equation for the Discrete Fourier Transform (DFT) model. Each bin in the DFT output is an equivalence of a particular frequency, where the Frequency of a K^{th} bin =k× (sampling rate/N), and N is the number of samples or cycles. In this study, N is 1.5. On the other hand, "instantaneous frequency attributes" is one of the many complex seismic attributes, which also include phase and amplitude. A default value of 33 was used as an input in the Hilbert filter window on Petrel 2013©. This value represents the amount of seismic trace of which the amplitude (trace envelope) and instantaneous phase are transformed into instantaneous frequency.

Faults which are a structural attribute were imaged by applying Variance technique. This is an enhanced edge detection method which uses Gaussian spatial smoothing in isolating fault systems. Prior to this, frequency filtering was performed on the seismic datasets to enable coherency of seismic datasets before this Variance technique was performed. Frequency coherence filtering increases the precision of identifying these features because it removes passive noise and enhance geological structures. Fault imaging by variance method could be limited by variations in a fault's density along its plane; the greater the fault's density, the better the illumination.

6.4 Results

The results of the application of Seismic attributes to resolve stratigraphic and structural features are presented below. In addition, seismic attribute is used to image sea floor for anomalies of gas escape expressions and identification of discontinuities.

Horizontal time slices were cut through the seismic volume at different inlines for a detailed interpretation of features observed.

6.4.1 Application of Variance Attributes for Structural features and Sea Floor Imaging.

6.4.1.1 Inline756 and Time Slice 1140ms

At time slice, 1440 and inline 756 (Figure 6.1 A and B), faults were identified because of the discontinuous geometry, notably, listric fault was observed with decreasing curvature (Figure 6.1B). High variance as can be seen from the legend indicates area of high structural dip and discontinuity, while grey suggests area of low structural dip and consistency. The 3D image shows the presence of listric fault which terminates just around the late Cretaceous. Variance attribute resolve the presence of this listric normal fault by showing medium variance (black) in comparison to areas of continuous geometry(grey) (Figure 6.1A and B)

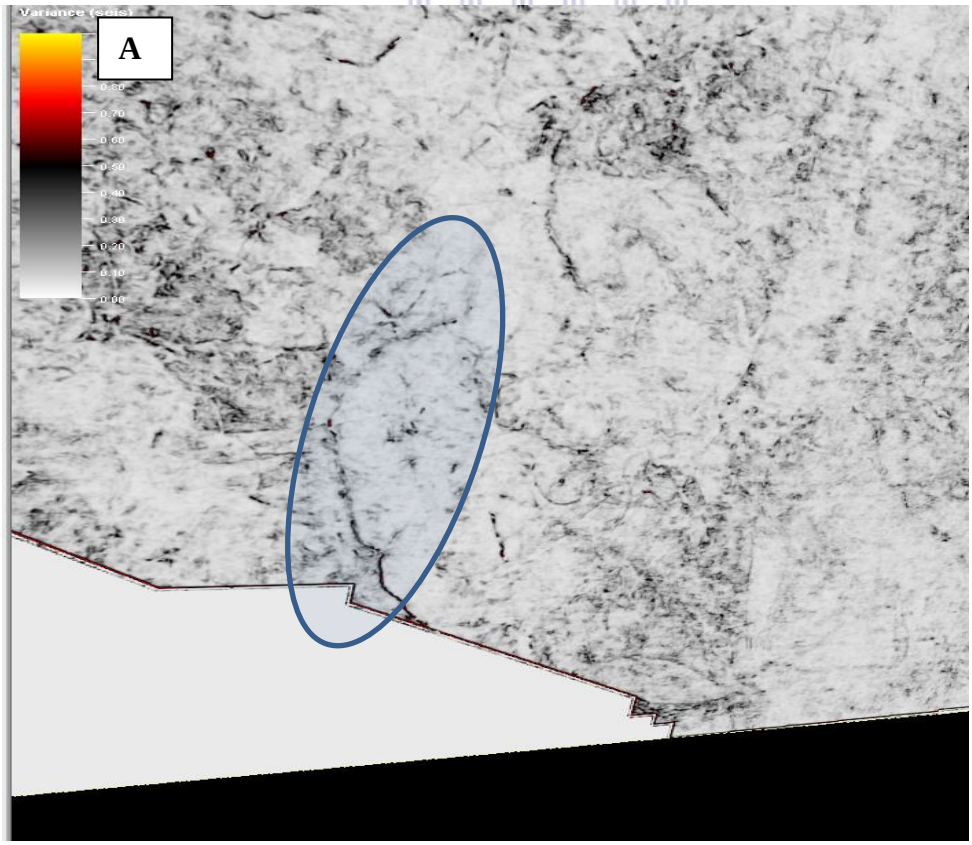

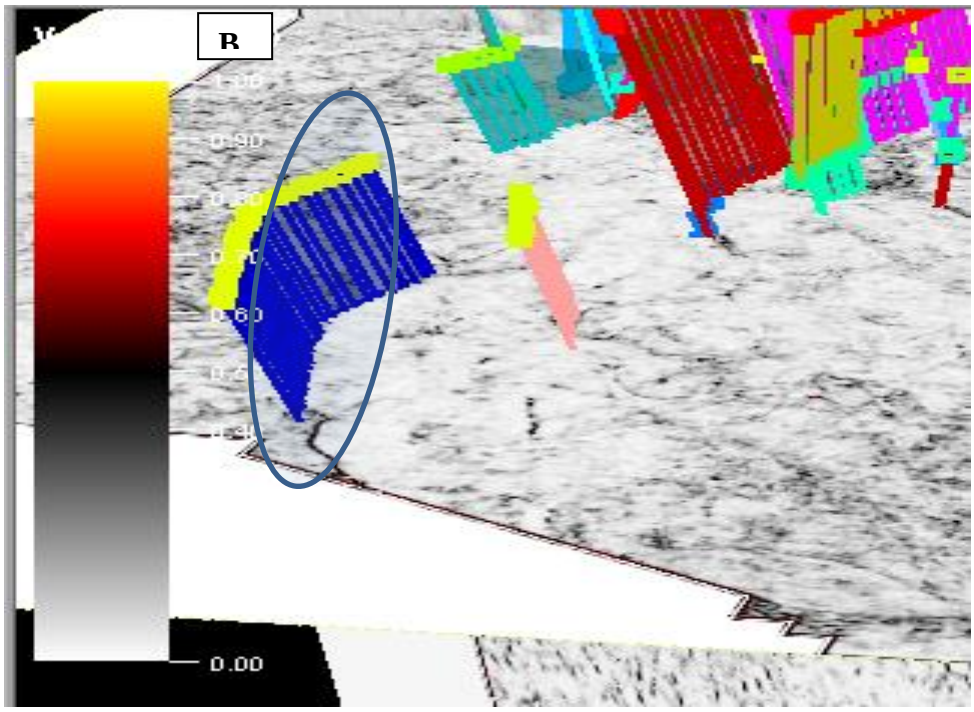

Figure 6.1 A and B: Figures showing a listric normal fault(blue circle in figure 6.1A and blue sticks in 6.1B) on Variance Time Slice intersection for an un-interpreted section (A) and interpreted Section(B) at Time Slice 1140 and Inline 756.

6.4.1.2 Inline 2400 and Time Slice 1644ms

At time slice 1644 and inline 2400, there occurs a series of antithetic faults (Figure 6.2 A and B) as earlier interpreted in chapter five of this study. Change of faults orientation by upthrusting do accounts in an extensional regime, for an occurrence of antithetic faults (Lowell, 1970).

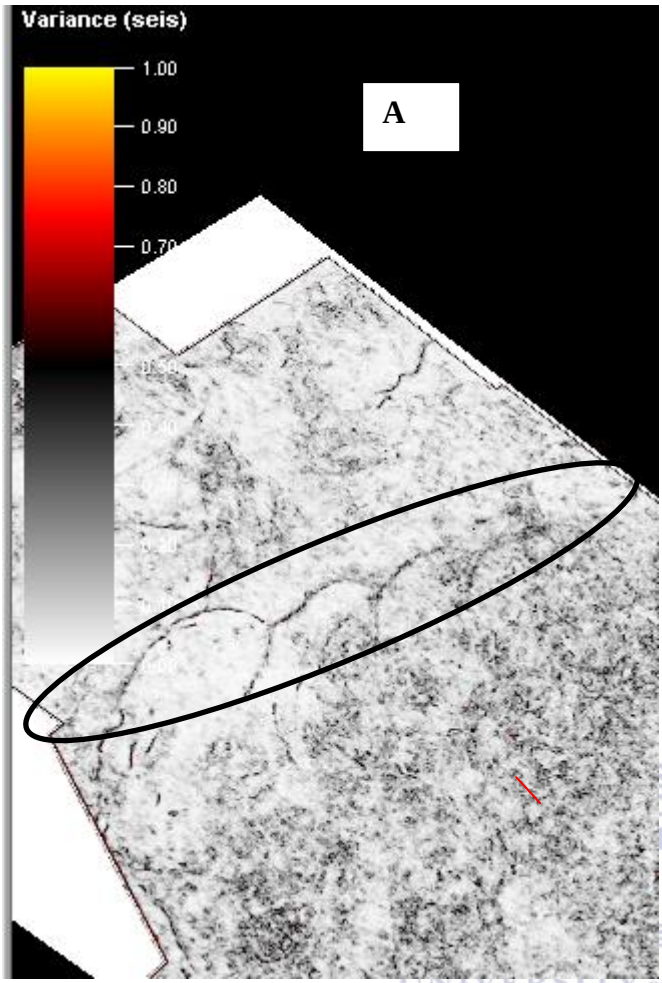

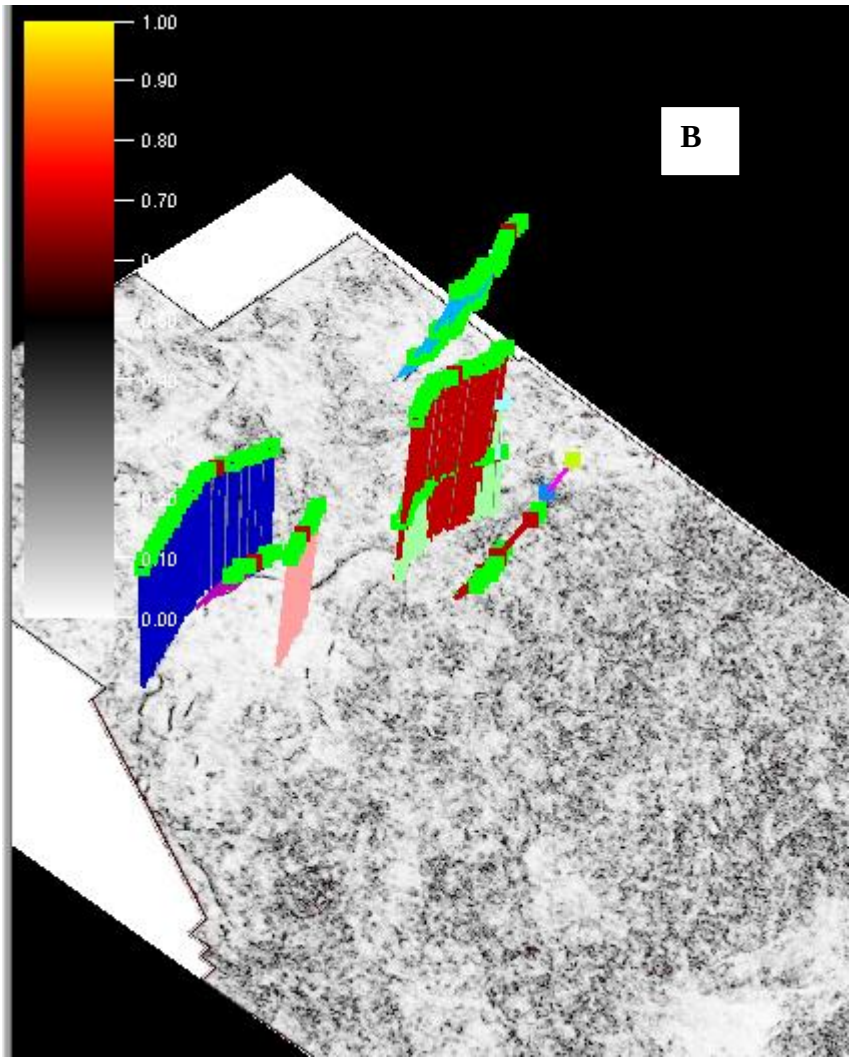

Figure 6.2 A and B: Horizontal Variance Time Slice intersection for an un-interpreted section (A) and interpreted (B) Section of Antithetic faults at Time Slice 1644ms and Inline 2400.

6.4.1.3 Inline 800 and Time Slice 180ms

In order to verify the gas escape features observed on the sea floor in the form of mud volcano and pockmarks as discussed in chapter five, variance attribute is applied and time slices cut through the sea floor are used to image the features. At Inline 800 and Time Slice 180ms, the variance shows a high structural dip for the mud volcano judging from the chaotic red colouration observed at the sea floor (Figure 6.3A). The mud Volcano is estimated to be 1066m width. However, there is no direct relationship between faults mapped and the mud volcano observed here. In addition, pockmarks were observed as shown in Figure 6.3B, they are known to have a circular expressions on the sea floor as it is seen below (Figure 6.3B).

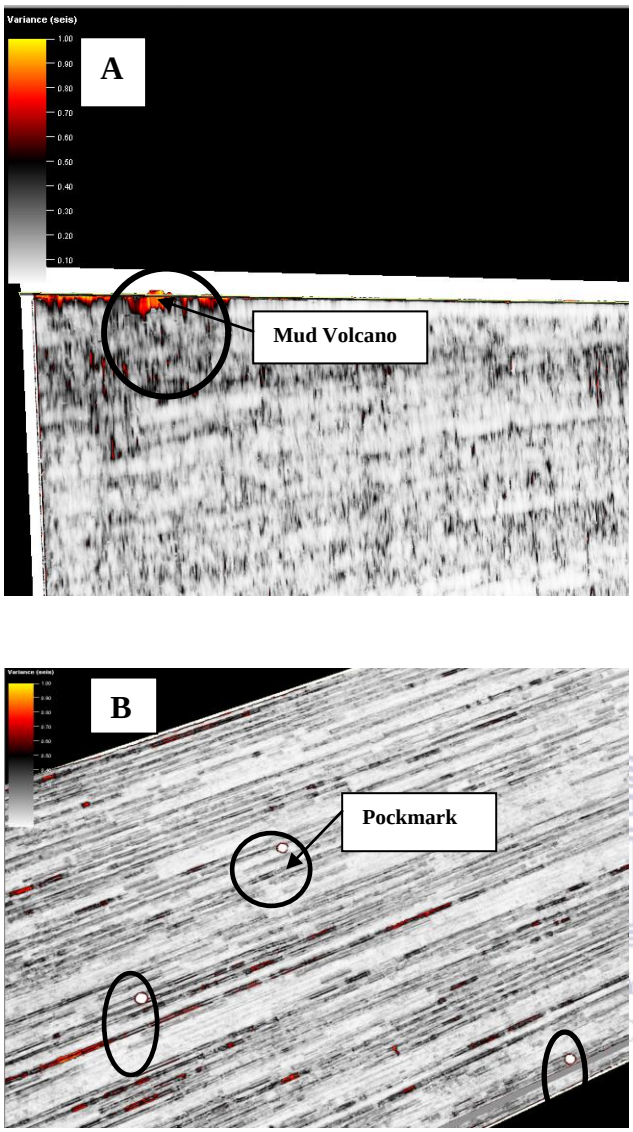

Figure 6.3 A and B: Figures showing Variance Time Slice intersection for an un-interpreted section and interpreted Section of mud volcano at Inline 800(A), and Pockmarks at Time Slice 180ms(B) at the Sea floor.

6.4.2 Application of Seismic Impedance and Frequency for Stratigraphic Attributes

Clinoforms, fluvial channels and meandering river systems are stratigraphic features that could be isolated by seismic impedance inversion; to ascertain the presence of these stratigraphic features, observations made from seismic impedance could be calibrated with porosity inversion. In addition, instantaneous frequency and seismic frequency decomposition could be used to confirm observations made from seismic impedance. These attributes have proven to be effective by many authors, in detecting river channels and sweet spots i.e; hydrocarbon charged sediments.

6.4.2.1 Time Slice 1160 for Seismic Impedance and Porosity Inversion

Seismic Impedance contrast for time slice 1160ms shows occurrences of two fluvial channels within the Turonian sequence (Figure 6.4A). These channels occur parallel to each other and with lower impedance contrast. When this observation is calibrated with porosity inversion (Figure 6.4B), expectedly, these fluvial channels show high porosity (red) compared to the surrounding sediments, thereby confirming the presence of fluvial channels. Both channels are about 378 and 254 metres in width respectively.

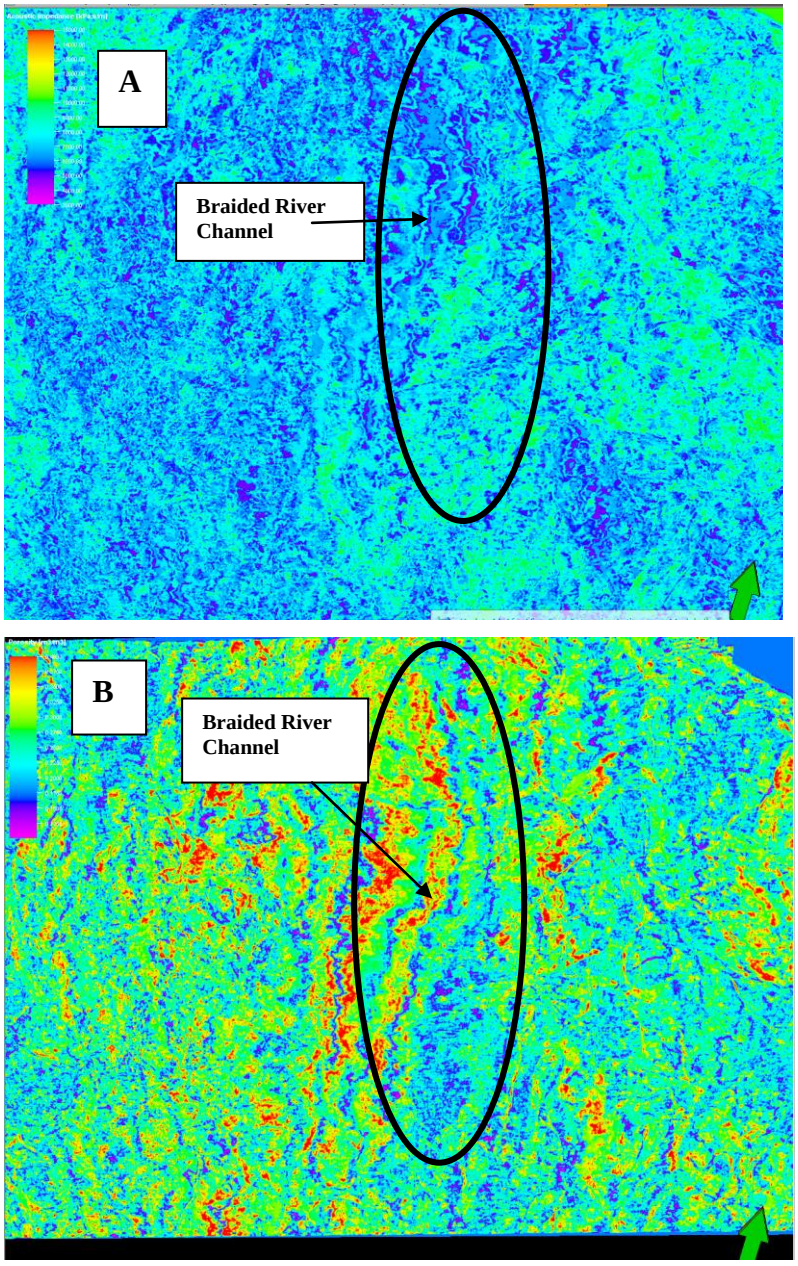

Figure 6.4 A and B: Figures showing Impedance Time Slice intersection and Porosity slice of braided fluvial channels at Time Slice 1160ms respectively. The porosity is high along the channels.

6.4.2.2 Time Slice 968(Late Cretaceous) for Instantaneous Frequency Inversion.

Instantaneous frequency attribute was performed to identify gas-charged sediment (secondary migration). This attribute is based on the theoretical understanding of the characteristic of gas- charged sediments to attenuate frequency because of its compressible nature (Castagna et al., 2003). Having observed bright spots associated with a listric normal faults earlier in chapter five, an instantaneous frequency inversion was performed and surface sliced chosen just at the top of this fault to observe possible frequency attenuation around this fault. Observation shows frequency attenuation on both sides of the fault (red dots in Figure 6.5A), which indicates gas migration across the fault that subsequently charged highly porous sediments which are interpreted to likely be mouth bars. When the observation from the frequency attribute is calibrated with porosity inversion, the fault plane shows high porosity as expected (black circle in Figure 6.5B), suggesting that the fault rock is porous.

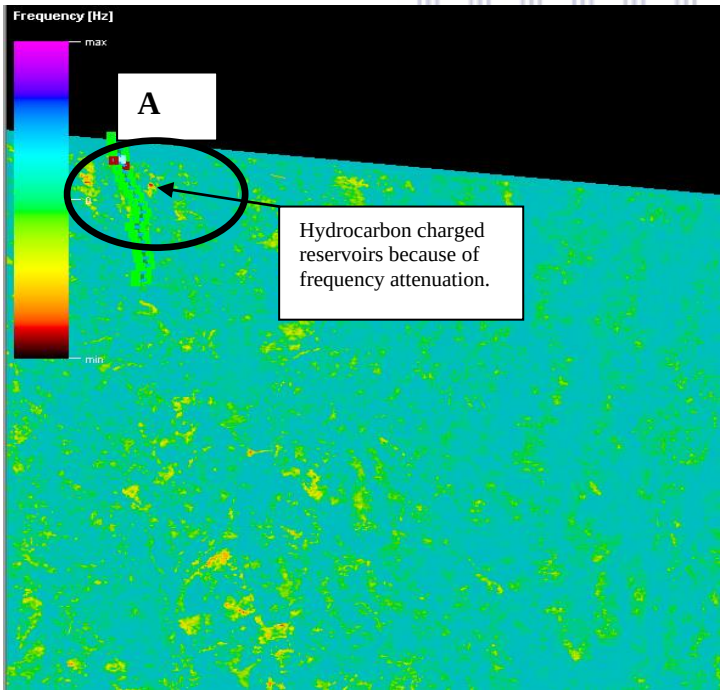

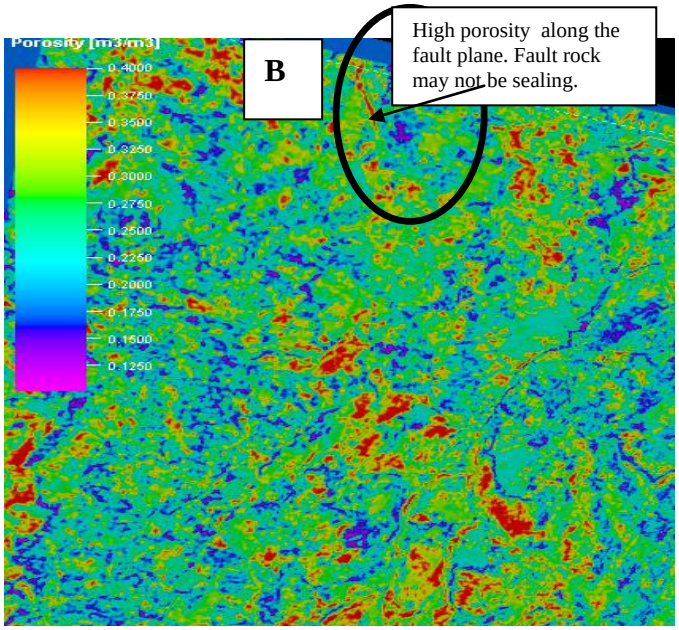

Figure 6.5A and B: Instantaneous Frequency Time Slice intersection (A) and Porosity inversion (B) of fault controlled gas-charged sediments at Time Slice 968ms. Frequency attenuation is observed on both side of the fault plane.

6.4.2.3 Time Slice 968ms for Iso-Frequency Attribute (Frequency Decomposition)

Frequency decomposition was applied as a stratigraphic attribute in this study as a method to calibrate observations and inferences drawn from other attributes interpreted above. Seismic bandwidth was decomposed at frequencies of 45 and 8 Hertz respectively, to identify gas charged sediments just above the listric normal fault. Frequency has an inverse relationship with cycle, expressed with the formula F=1/T. At 45Hz and 1.5s period, there was no clear trend of frequency attenuation to suggest hydrocarbon presence in the sediments (Figure 6.6A). Consequently, the seismic was decomposed at 8Hz and a higher cycle of 3.0s. It became evident that the seismic bandwidth is more coherent to observe geological features at lower frequency. Also, there is evidence of more frequency attenuation on both sides of the fault (black circle in Figure 6.6B). These observations correspond with similar observations made on instantaneous frequency in figure 6.5A. Geological formations have varying frequency behaviours due to rock and fluid properties (Chen et al., 2008), and this

explains why the frequency of 8Hz appears more suitable to reveal attenuation related to hydrocarbon presence than 45Hz frequency.

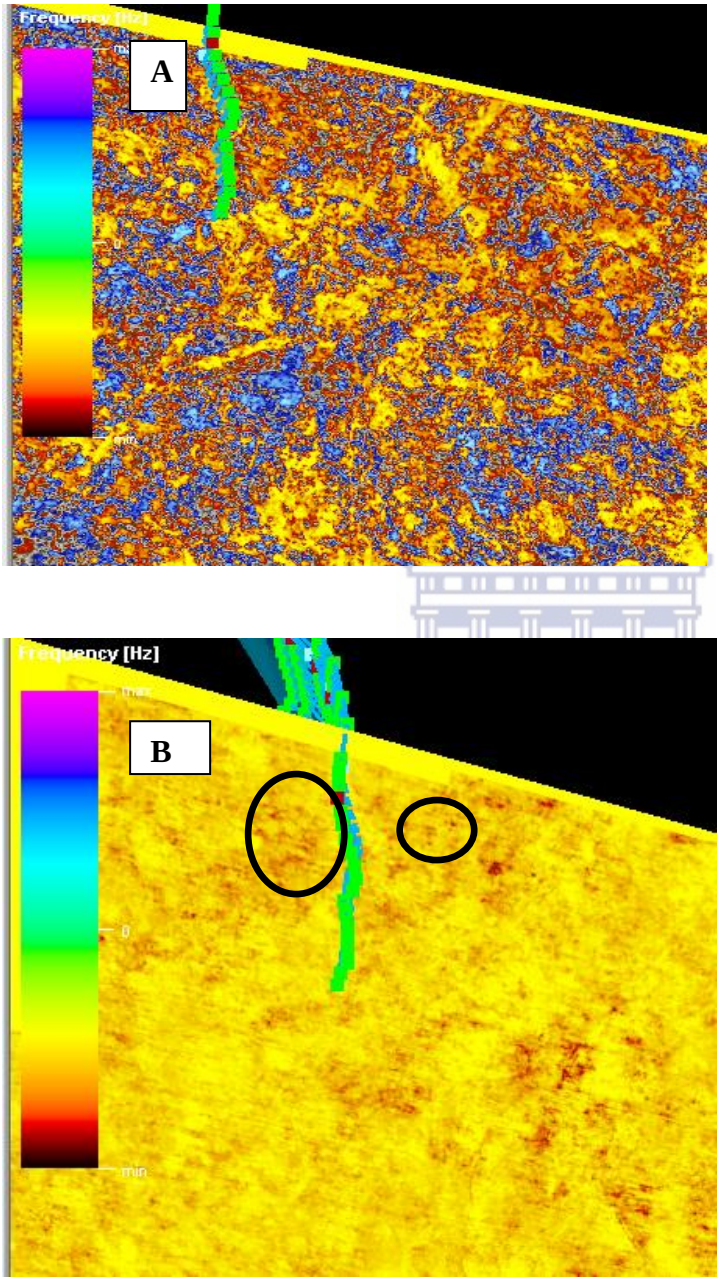

Figure 6.6A and B: Showing Time Slice intersection 968ms for Frequency Decomposition at 45Hz (A) and 8Hz (B) of fault controlled, gas-charged sediments. Low frequency attribute is suitable for the delineation of features for the seismic data.

6.5 Conclusions.

The variance edge method has been proven to be efficient in fault- and seafloor imaging. The observations here have not suggested otherwise. However, there is no direct relationship between the mud volcanoes mapped here and the faults to suggest the former is being controlled by faulting. However, a recent neotectonic event as suggested by Andreoli (2005), is believed to trigger mud volcanoes in the offshore Orange Basin, yet there is no faulting associated with mud volcanoes to suggest this mechanism in this study. Although, there is a possiblity that neotectonism could have made gas saturated argilaceous sediment unstable which led to its venting at the sea floor as a form of volcano.

Seismic impedance inversion technique calibrated with porosity inversion reveals a subtle stratigraphic feature (Braided River channels) buried in the subsurface as can be observed in Figure 6.4A. This method could not resolve hydrocarbon presence around the listric normal fault. However, when a combination of frequency attributes (Instantaneous and Frequency decomposition) was applied to resolve hydrocarbon presence around the fault, hydrocarbon presence on both sides of the fault plane was revealed because of the frequency attenuation observed, which suggests possibility of hydrocarbon-charged sediments at close proximity to the fault and migration of hydrocarbon, certainly gas, across the fault.

Chapter Seven

3D Numerical Modeling of Hydrocarbon-generation and Faults control on Migration pathways.

Keywords: Source rock- generation- migration-reservoirs

7.1 Abstract

3D Numerical modelling of hydrocarbon-generation and migration are performed on the Barremian/Aptian source rock intervals encountered within block 1 of the Orange Basin. The simulation of hydrocarbon-generation was done based on boundary conditions such as Heat flow (HF), Sediment Water Interface Temperature (SWIT), and Paleo-Water Depth (PWD) to know the timing of hydrocarbon-generation from the source interval. In addition, hydrocarbon migration was simulated to understand interaction between hydrocarbon and faults and to juxtapose the timing of formation of regional faults and the timing of hydrocarbon expulsion.

Model results for thermal and organic maturity (Vitrinite Reflectance) evolution of this source rock indicate that it reached a sufficiently mature stage just before 108 Ma, with VR values ranging from 0.64 to 0.72 from the northeastern to southwestern section of the study area. The Model reveals transformation of organic matter began from the centre of the study area and increases towards the fringes of the study area. Hydrocarbon-generation reached its peak during the late Cretaceous. As at present day (0.0Ma), 100% transformation of organic matter has generated hydrocarbon only at the centre of the study area while the extreme northeastern section is yet to be transformed into hydrocarbon. Consequently good potential for future source rock transformation into hydrocarbon in the Northern part of the area may be expected.

Source rock bulk generation and expulsion statistics as at present day show that 430701.94Mtons of gas and 38399.53Mtons of oil had been generated by primary and secondary cracking processes, representing 91.81% and 8.19% of organic matter transformed into gas and oil respectively. The source rock has an expulsion efficiency of 0.77 which suggests good efficiency. 1D Calibration of this model is done with organic matter and temperature data obtained for wells AO-1, AE-1 and AF-1. The

modelled temperature agrees well with calibrated temperature data from the three wells, while there are slight variations in modelled vitrinite data and calibrated vitrinite data in the three wells, especially during the Cenomanian-Turonian period. These variations suggest the influence of additional localized heat flow during the Cenomanian-Turonian for the three wells. Calibration data for well AO-1(northern part) also show that the source rock is not yet thermally matured as predicted by the model. This confirms the precision of this model.

The hydrocarbon Migration model suggest that gas expulsion from the source rock unit started from the central part and southeastern part of the study area as early as 108Ma. There are evidences of vertical migration of gas into the Albian and Cenomanian reservoirs at this time, however at the present day, Albian-aged reservoir remains only gas –prone while Cenomanian reservoir unit is also gas prone but with proneness to oil westward (deep waters) of the study area

A fault model constructed was used to test possible fault controls on migration pathways. The results show a syn-rift listric fault to be 100% gas saturated as at 93 Ma and lost its saturation by 65Ma, suggesting a breakthrough path through the listric fault which caused it to lose its saturation. The breakthrough part is linked to fault reactivation which enables further migration of gas.

In conclusion, the model reveals evidence of gas escape at the sea floor and there is no evidence of hydrocarbon accumulation within the study area.

7.2 Introduction

Hydrocarbon-generation (Primary migration) and -expulsion (secondary migration) are part of the workflow of Basin and Petroleum system modeling (BPSM). The essence of modeling hydrocarbon-generation and -migration in this study is to investigate the timing of hydrocarbon-generation, -expulsion in relation to faults and stratigraphy. The first approach in this study is a detailed explanation of depth maps of major super sequences obtained by velocity modelling of time maps generated from different seismic vintages.

Depth maps are extracted based on the major unconformities encountered in this area. The term "super sequences" was used because within these super sequences are parasequences which are not regionally correlative in the study area and in order to construct a 3D hydrocarbon migration model, regionally correlative unconformities (super sequences) should be mapped. Within the different super sequences are rock types which have characteristics of elements of a Petroleum system. These are defined under the methodology section of this chapter.

In this study, numerical simulation of hydrocarbon-generation is performed to know the timing of hydrocarbon-generation, timing of peak expulsion and to determine the type and volume of hydrocarbon expelled. In addition, it is used to ascertain the maturity of the source rock unit across the study area. Consequent upon this, faults model constructed was used as an input for the 3D construction of the hydrocarbon migration model using the Hybrid Flow Path model. With this, perspectives will be drawn on how faults do serve as control on migration pathways.

7.3 Methodology

The methods and materials used to achieve the objectives of this chapter are highlighted below. Prior to discussing the results from 3D modelling of hydrocarbon-generation and -migration, 1D numerical simulation modeling was performed at the well positions to calibrate observations made from the 3D results.

7.3.1Model Input

The depth maps of all sequences interpreted which represent different events that characterized the evolution of this basin, were imported into the Petromod 2014© workstation. Layers of conformable super sequences are created and facies assignment was performed on each of the layers. This was done using information from petrographic reports and facies modeling done in chapter four of this study. Total organic carbon, Hydrogen Index and Tmax of the Barremian/Aptian source rock unit obtained from the geochemical completion reports of the three wells used in this study were averaged and used as input. The properties of each facies were assigned based on the existing models in Petromod 2014. The Sekiguchi model (1977) was used for thermal conductivity, radiogenic heat calculated based on lithology using the the Waples model (2004), and Athy's law (1930) was used for porosity prediction. In addition, the model described by Schneider et al., (1996) for prediction of chemical compaction of rocks was used, while multipoint model for permeability, bilinear equation to determine sealing properties and bulk modulus for rocks elasticity were used. Furthermore, Pepper and Corvi (1995) was used for kerogen type and the different lithologies that represent each layer were mixed in the lithology editor interface on Petromod 2014©.

The timing of faults formation and its properties was assigned (syn-rift faults are kept opened and post rifts faults are closed), lithology mixing for each super sequence was based on the relative abundance of each rock unit present within the sequence. All modeling input parameters and boundary conditions as detailed in chapter three of the study will be used to simulate hydrocarbon-generation and migration.

Finally, 1D calibration data using vitrinite reflectance data, porosity and temperature data are applied to test the accuracy of the model at well positions.

7.3.2 Boundary Conditions

Adjusted boundary conditions as discussed in the methodology (chapter three) were used for this study. The boundary conditions were adjusted based on the knowledge of the geology of the study area. Average Paleo-water depth (PWD) values derived from the well completion report were averaged and used as the present day value, while PWD values were estimated from it as a trend. Also, adjustment was made on the Mckenzie heat flow model used. Higher heat flow values were considered during the early Cretaceous which represent break-up and separation of continents, late Cretaceous, which represent the uplift that affected the whole African continent and the Miocene uplift documented for South Africa Continental Margin

7.3.3 Hydrocarbon Migration Modelling

As earlier discussed in chapter three, hydrocarbon migration pathways simulation using hybrid model as applied here, is based on flowpath tracing method using lithology with more than 30% porosity as carrier beds and in the absence of such lithology switches to bed surface geometry as the flowpath tracing method.

7.4 Results

7.4.1 1D Numerical modelling of Hydrocarbon-generation and Burial history.

Prior to the construction of a 3D numerical modelling of hydrocarbon-generation in the study area, 1 D simulation was performed at the well position in order to predict the accuracy of the 3D model to be constructed. Thermal and organic maturation data from three wells (AE-1, AF-1 and AO-1) are used to calibrate the predictive hydrocarbon-generation model. Data such as vitrinite reflectance and temperature are used to calibrate this model. The results of these 1D modelling and calibration results are explained below.

7.4.1.1 1D modelling of Barremian/Aptian source unit and calibration with thermal and organic maturation data for well AE-1 (southern section).

7.4.1.1.1 Vitrinite Reflectance

In well AE-1, the predicted Sweeney and Burnham (1990) VR predicted (straight line) and measured calibrated data (asterisks points) are used to demonstrate the accuracy of the 3D model to be constructed. The predicted vitrinite reflectance estimates match the calibrated VR estimates for the late Albian during which the seal rock unit was deposited; however, there are calibrated data outliers in the Albian and Cenomanian. These calibrated outliers suggest that there is an additional heat flow source which led to high VR values in the Albian and Cenomanian. This is commonly due to tectonics (uplift, subsidence or intrusion) inversion in the basin which could have greater impact on the thermal maturity of organic matter of rock units during these periods. In this case, outliers indicate higher measured VR values than the predicted VR estimates (Figure 7.1A), implying a localized increased thermal effect which increases the maturity of organic matter during this period and consequently could have greater impact on the transformation of the organic matter into hydrocarbon.

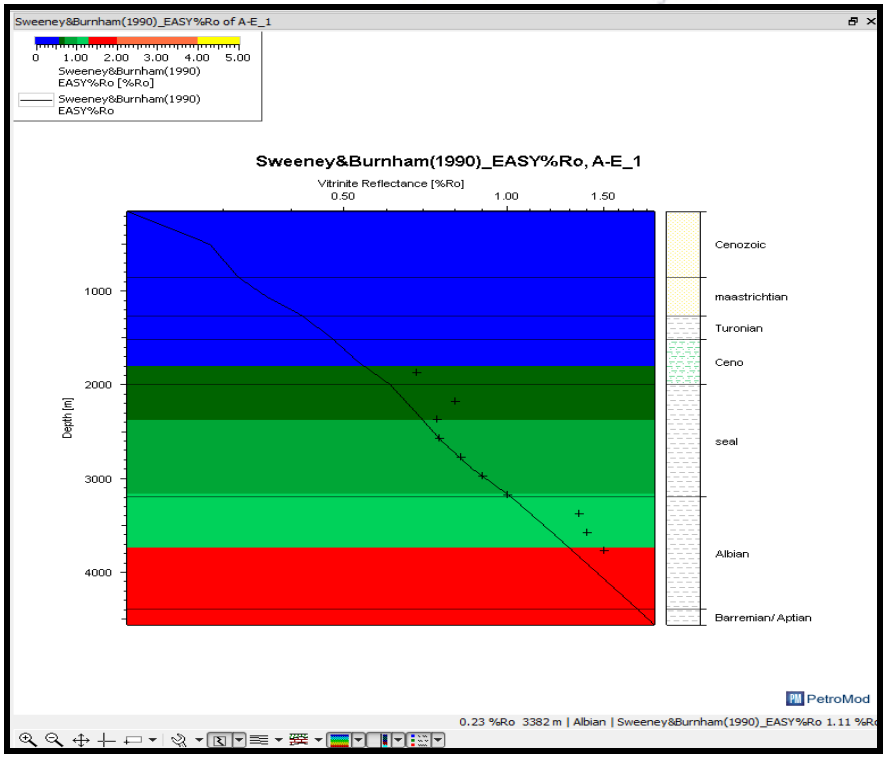

Figure 7.1 A: Graph of calibrated measured Vitrinite data values (*) with the modelled Vitrinite values (straight line) for well AE-1, southern section of the study area.

7.4.1.1.2 Temperature

In addition, the modelled formation temperature calibrated with bottom-hole temperature for well AE-1 matches almost accurately as seen in figure 7.1B below. This confirms the accuracy of the heatflow model used for this study.

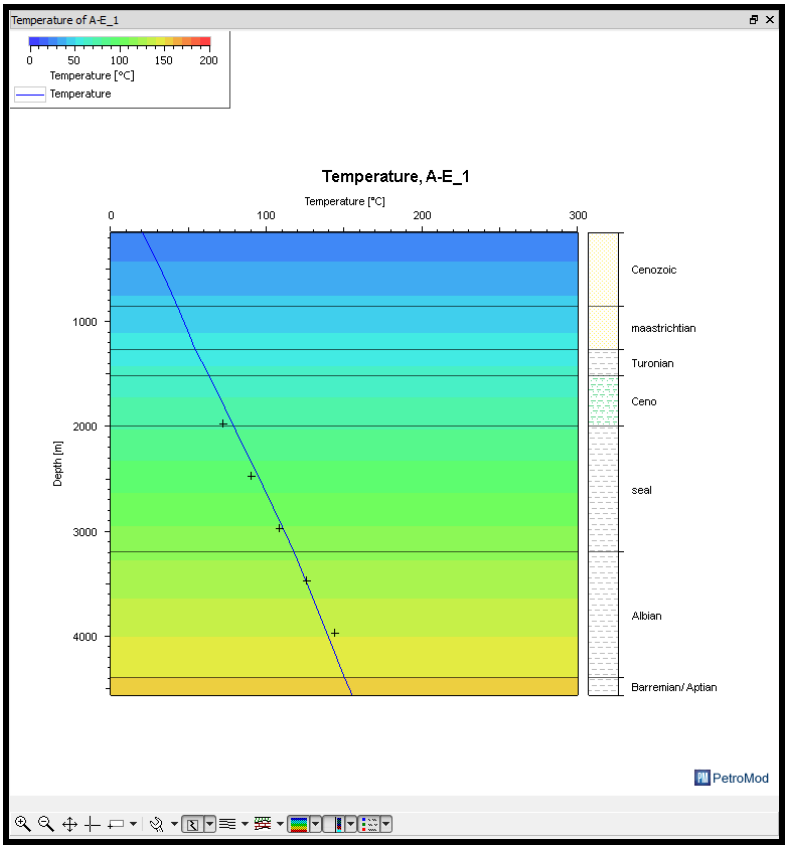

Figure 7.1B: Graph of the calibrated Temperature data values (cross points+) with the modeled Temperature values (straight line) for AE-1 well (southern section). Figure shows a good match between the modelled temperature and calibrated temperature data.

7.4.1.1.3 Burial History and Transformation Ratio.

Burial history reveals that about 80% (as seen from the TR key in figure 7.1C) of organic matter had been transformed into hydrocarbon from the upper Cretaceous to the present day. The Miocene uplift that affected Southern Africa was factored into the modelling process by increasing the heatflow during this period, this uplift has no effect on the transformation ratio of organic matter into hydrocarbon. Overall, there is just about 20% of organic matter that is yet to be transformed into hydrocarbon in this area.

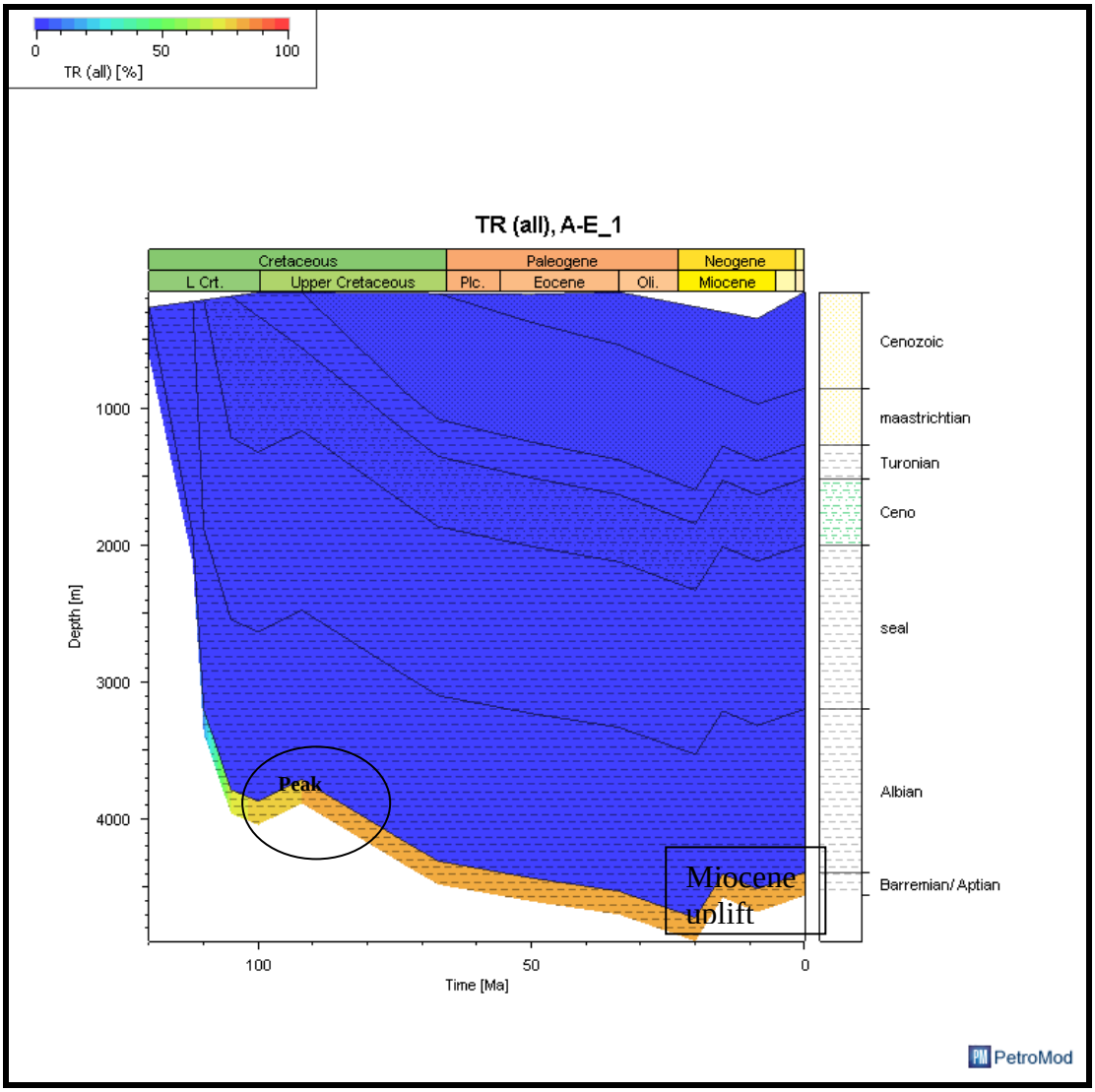

Figure 7.1C: Well AE-1 burial plot showing the Transformation Ratio for the Barremian-Aptian Source rock Unit in this well. Figure shows transformation reached a peak in the upper Cretaceous.

7.4.1.2 1D modelling of Barremian/Aptian source unit and calibration with thermal and organic maturation data for well AF-1 (Central section).

7.4.1.2.1 Vitrinite Reflectance

The predicted Sweeney and Burnham vitrinite model and calibrated vitrinite measurements for well AF-1 (central part of the study area) as seen below (figure 7.2A) indicates that two of the measured vitrinite reflectance estimates calibrate properly with the modelled VR estimates. This implies that the organic matter was subjected to a higher heat flow than predicted for the Maastrichtian and Turonian-

Coniacian period. As a result, the source rock is more thermally matured than anticipated. The high thermal event deduced from the VR values is likely due to the late Cretaceous thermal uplift which affects the whole African continent and leaves an impact on the central section of the study area. These were periods when intense erosion was expected because of the regional uplift that characterized these periods.

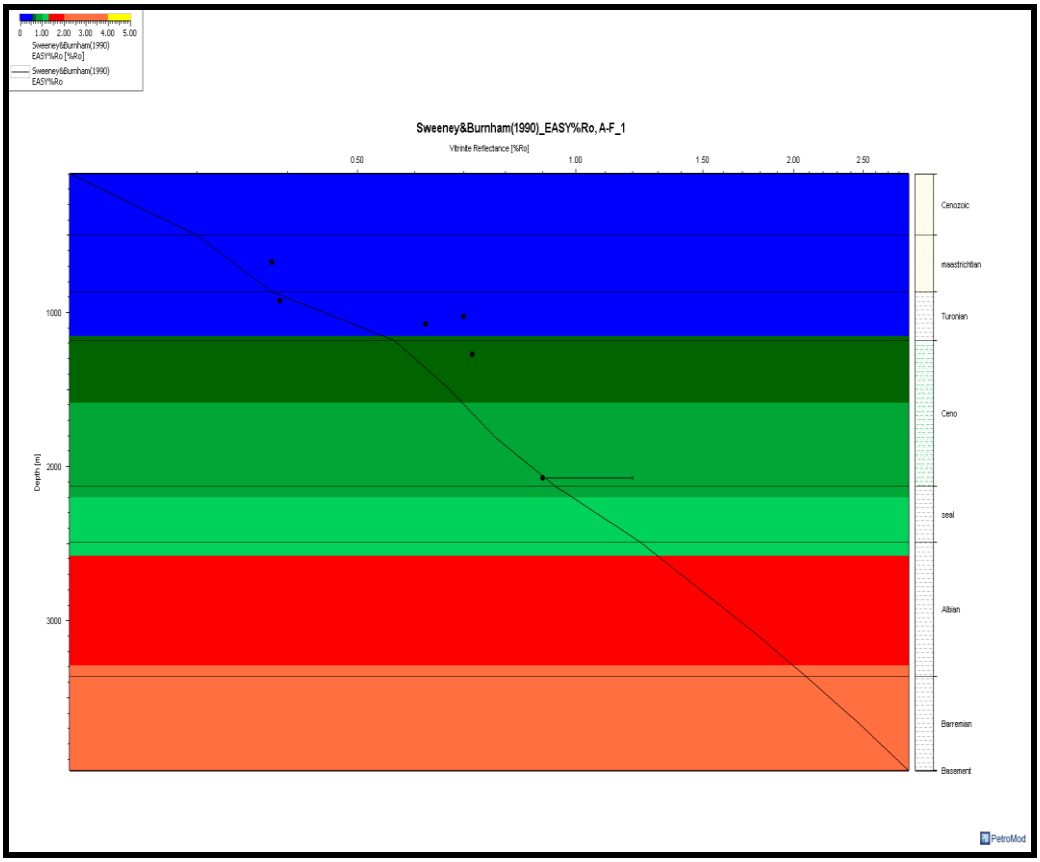

Figure 7.2A: Well AF-1 shows the calibrated (asterisks) and predicted Vitrinite Reflectance values (straight line). There are high calibrated VR values in the Maastrichtian suggesting the possibility of basin inversion and more prominent in the central section.

7.4.1.2.2 Temperature

Modelled temperature values are fractionally lesser than the calibrated temperature data for well AF-1 except in the Maastrichtian and Cenozoic. This suggests that the rock unit encountered more subsurface temperature due to increased heatflow prior to the Maastrichtian-Cenozoic. A reason for this may be due to the presence of thick rock unit, possibly rich in feldspars which increases thermal conductivity and could have caused the high temperature values observed here (Figure 7.2B).

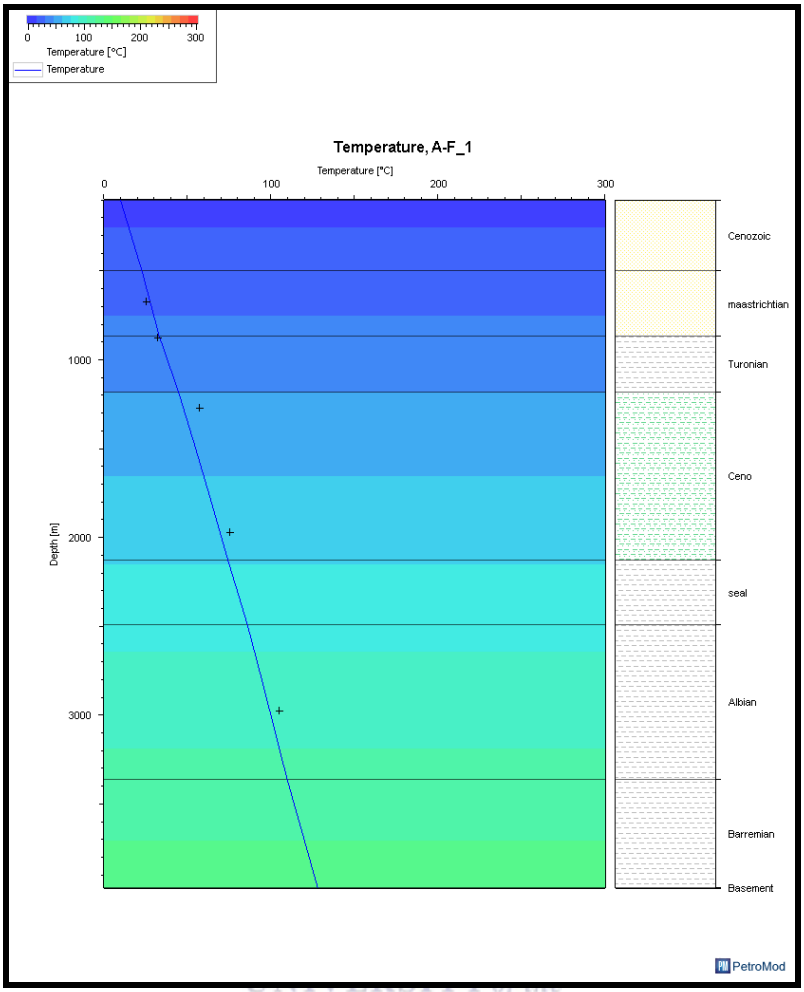

Figure 7.2B: Well AF-1 showing the calibrated (cross points+) and predicted Temperature (straight line) values for the central section. Figure shows slight variation in predicted and temperature values in the Albian and Cenomanian periods and a perfect fit in the Maastcrihtian

7.4.1.2.3 Burial History and Transformation Ratio.

Hydrocarbon generation became more significant (peak) around 85My in the early-upper Cretaceous in well AF-1, with an approximate transformation ratio of over 90% attained by the source rock unit (Figure 7.2C). The source rock unit here is thicker than the unit in well AE-1 (south of study area). AF-1 was drilled within the graben-fill sequence and this could explain why the source rock unit is thicker here than in well AE-1 (southern part).

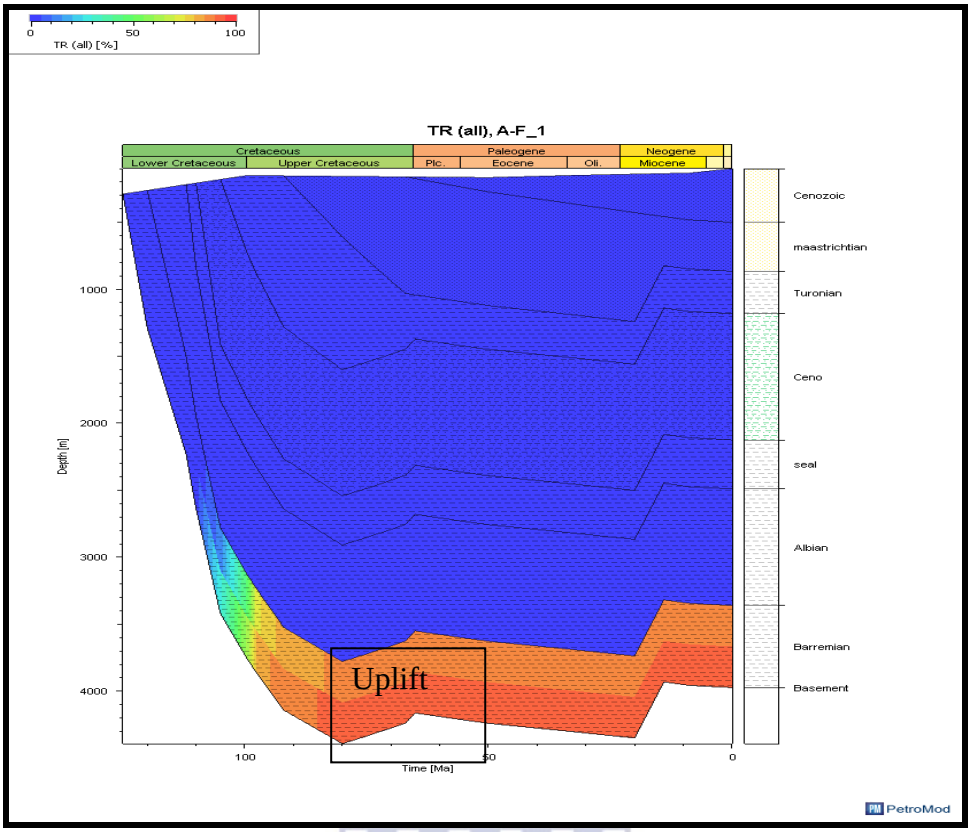

Figure 7.2C: Well AF-1 showing the Transformation Ratio of the Barremian-Aptian Source rock unit. 90% of the source rock unit has been transformed into hydrocarbon within the central part.

7.4.1.3 1D Modelling of Barremian/Aptian source unit and calibration with thermal and organic maturation data for well AO-1 (Northern section).

7.4.1.3.1 Vitrinite Reflectance

.The predicted Vitrinite model for this well indicates a good fit between the modelled VR and calibrated VR data, but only in the Albian and Cenomanian. The calibrated VR values in the Turonian are lower than the modelled VR values for this period, hence the outliers observed (Figure 7.3A). The lower calibrated VR values during this period suggests erosion could have impacted on the VR, reduced the thickness of the rock unit, thereby reducing the thermal conductivity and heat flow, causing lesser thermal maturity.

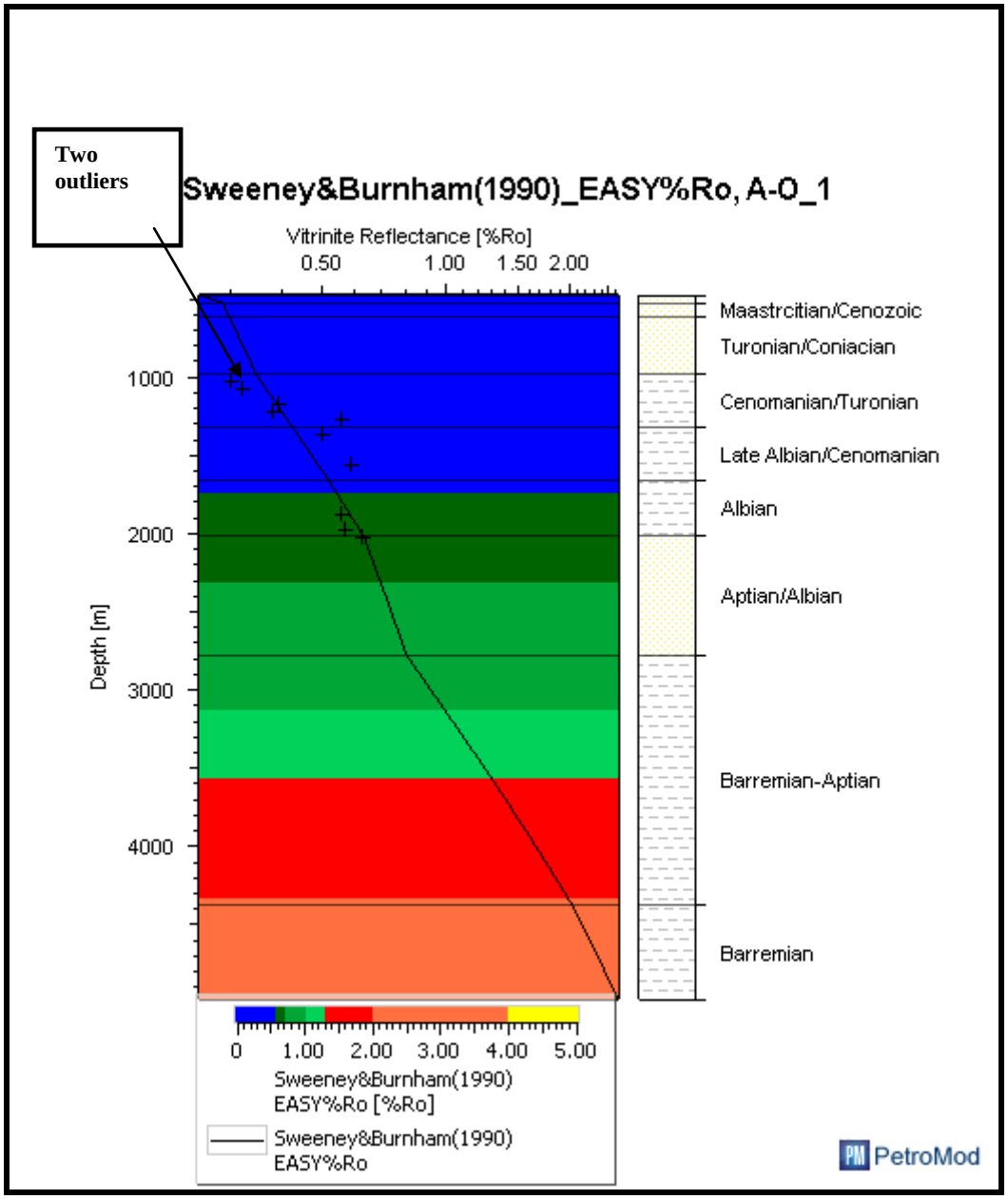

Figure 7.3A: Well AO-1 showing the calibrated Vitrinite Reflectance data (cross points+) and Modelled (straight line) of the Barremian-Aptian Source rock unit.

.

7.4.1.3.2 Temperature

The Temperature model below (Figure 7.3B) indicates a good match between the predicted temprature and the calibrated temperaure values. This confirms the accuracy of heatflow modelused for this study.

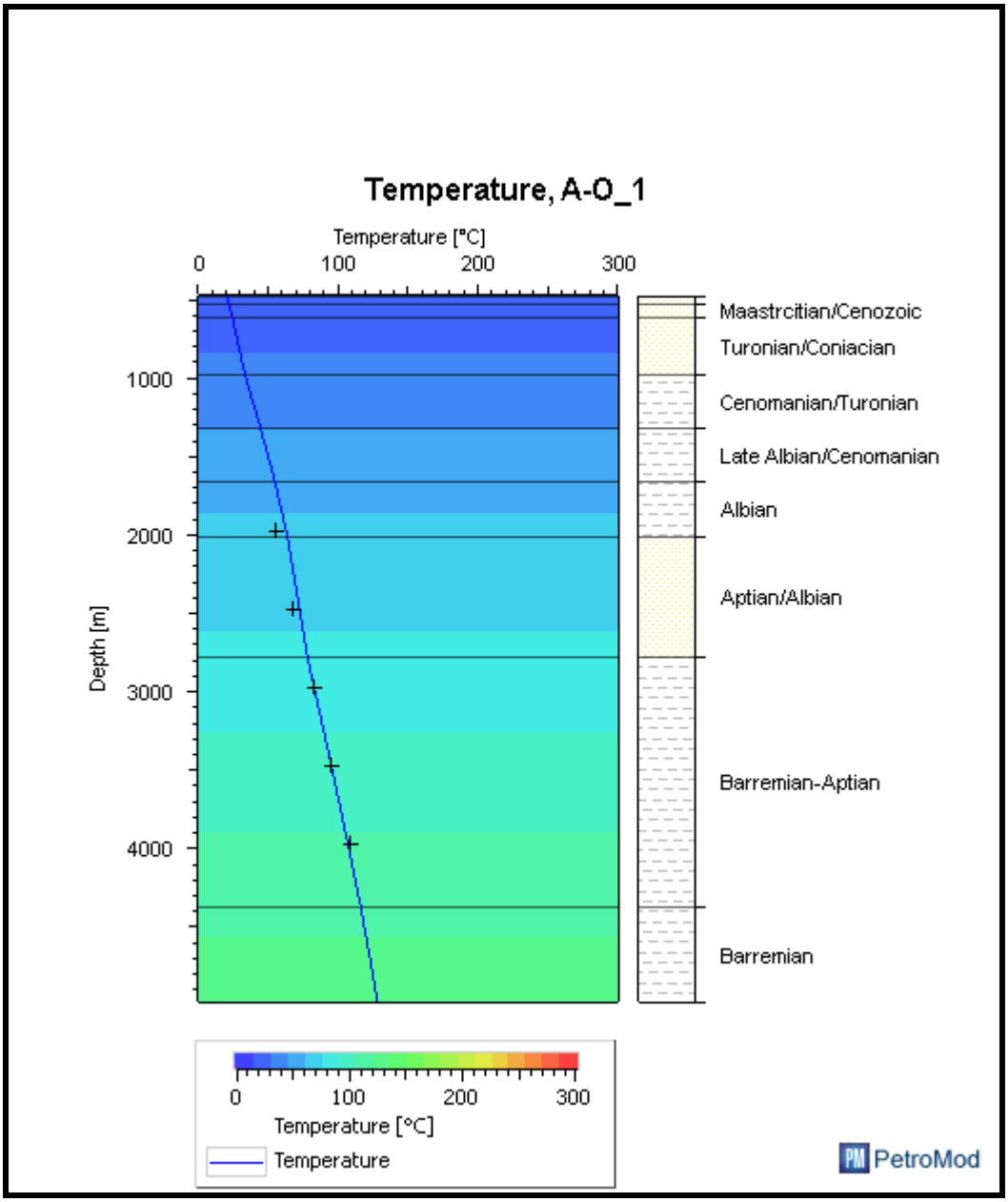

Figure 7.3B: Well AO-1 showing the calibrated measured Temperature (cross points+) and Modelled temperature (straight line) values.

7.4.1.3.3 Burial History and Transformation Ratio.

The transformation ratio map (7.3C) shows THAT no transformation of kerogen into hydrocarbon had occurred in the most northern section of the study area, where AO-1 was drilled. Apparently, the Barremian-Aptian source rock in this area has not reached an adequate thermal maturity stage for transformation into hydrocarbon.

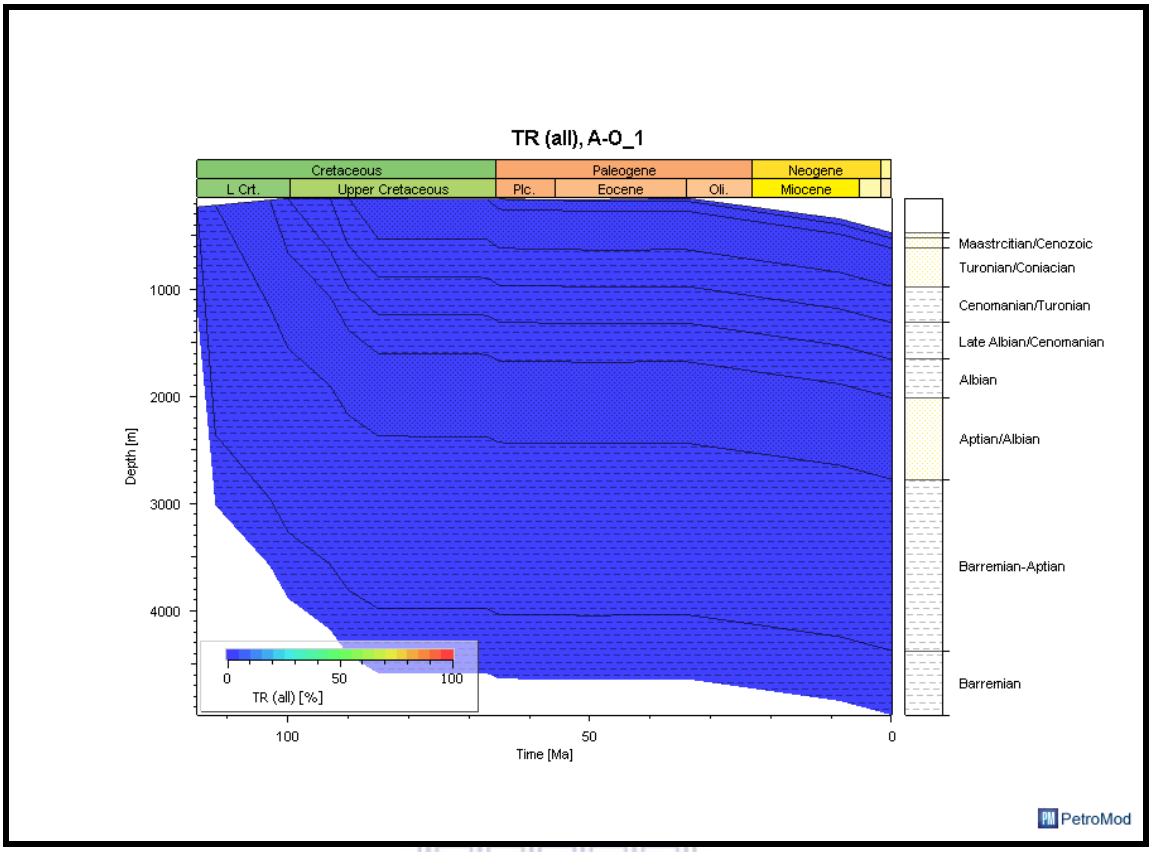

Figure 7.3 C: Well AO-1 showing the Transformation ratio of the Barremian-Aptian Source rock unit. The transformation ratio shows the source rock is immature and none of the organic matter has been transformed into hydrocarbon in the northern part.

7.4.2 Depth Maps of major super sequences.

Depth maps of these super sequences are interpreted below, from the Top of Basement to the sea floor.

7.4.2.1 Top of the Basement

The depth map indicates basement inclination in the north and south, and a wide graben in the centre of the study area. The depth at which basement is encountered ranges from 4000m in the north and south, and 5500m in the centre of the area (Figure 7.4A).

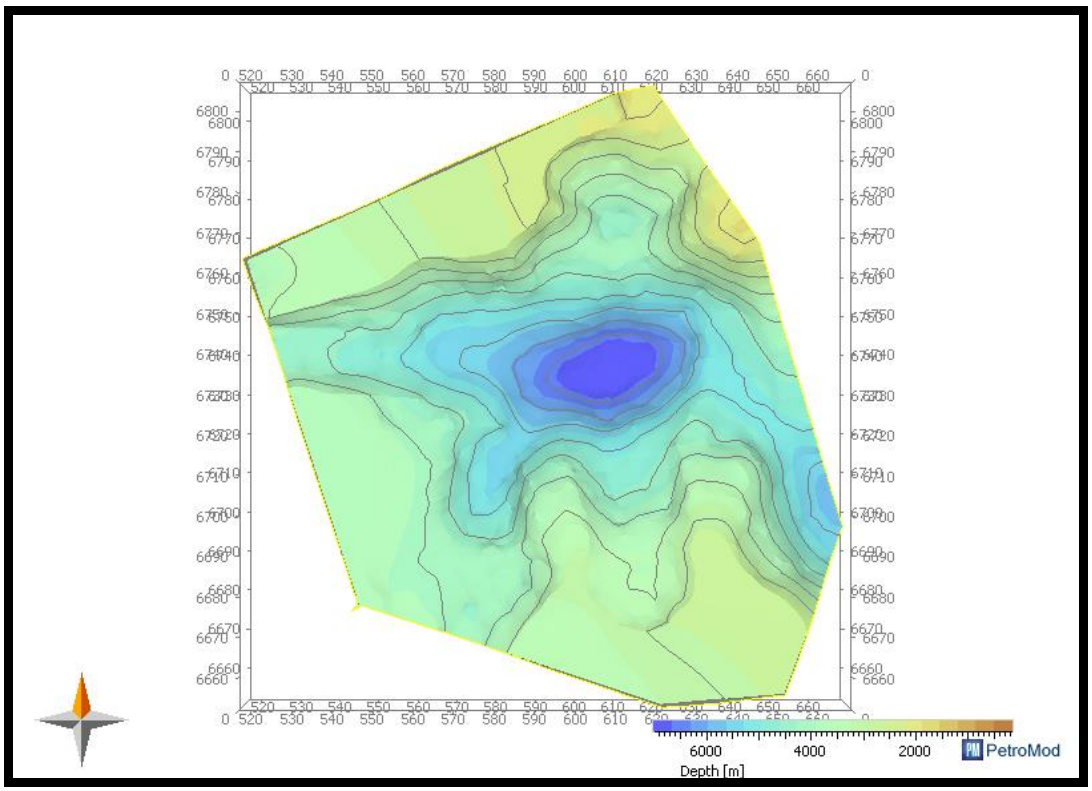

Figure 7.4A: Depth map of the top of the Basaltic Basement in the Study Area.

7.4.2.2 Barremian/Aptian (Source Rock)

The Barremian-Aptian surface here represents the Barremian-Aptian aged sedimentary sequence. Coincidentally, the regional potential source rock was deposited within this sequence. The depths at which this surface is encountered ranges between 1500m in the north to 4200m in the south (Figure 7.4B).

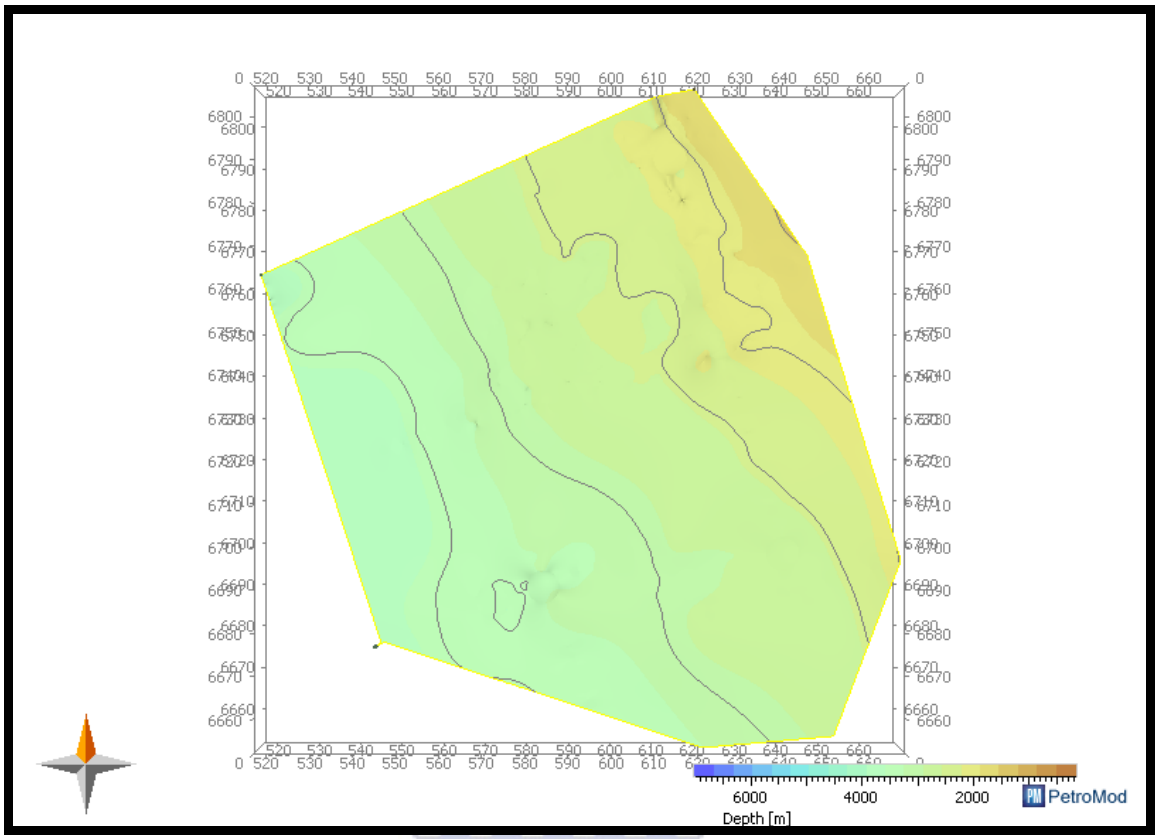

Figure 7.4B: Depth Map of the top of Barremian/Aptian sequence in the study Area.

7.4.2.3 Mid-Albian (Reservoir Rock)

This is encountered at 1100m in the north to around 3200 m in the South (Figure 7.4C). This sequence represent the major reservoir target in this basin. The Albian siliciclastic sandstones have been identified as potential reservoir targets in the Orange Basin basin (Adekola, 2010). Specifically, Albian –aged sandstone deposits are target reservoirs in the discovered Ibubhesi gas field in the southern part of Orange basin.

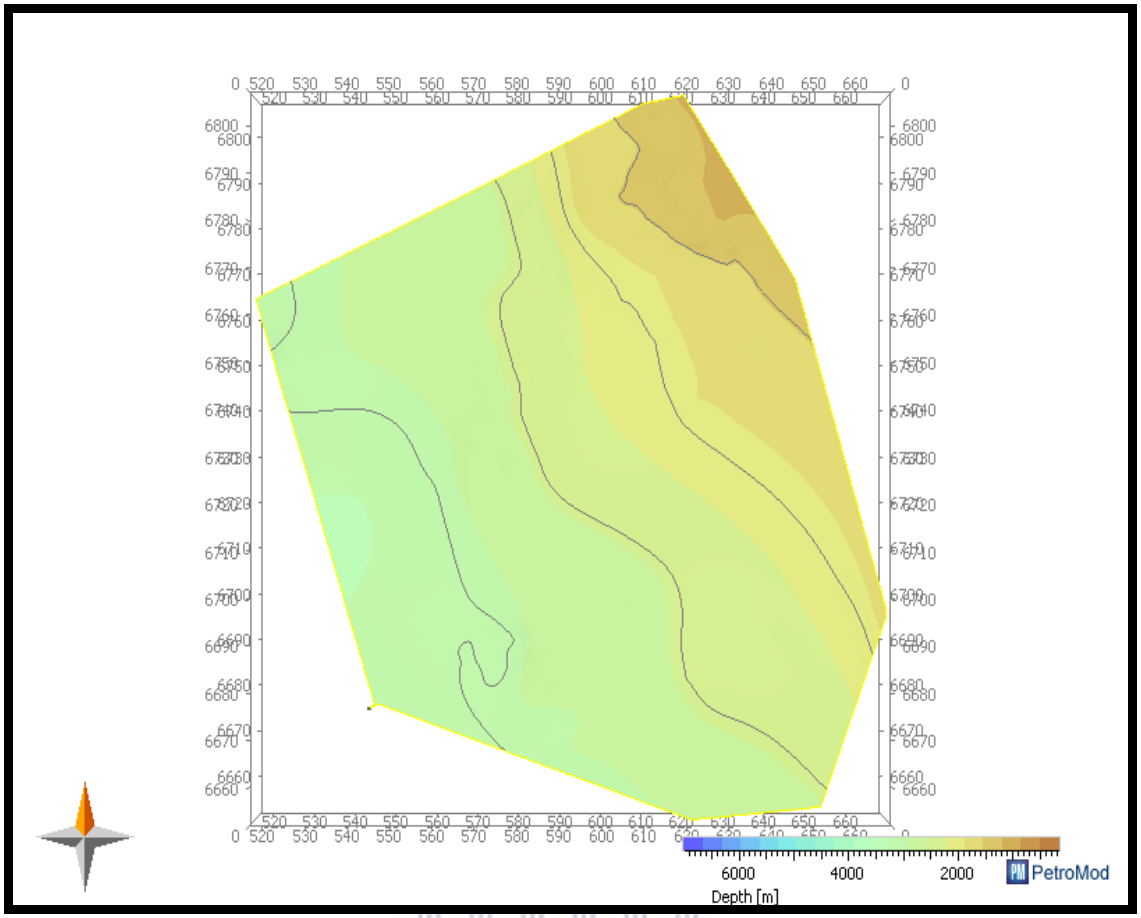

Figure 7.4C: Depth Map of Mid-Albian sequence in the study area.

7.4.2.4 Late-Albian (Seal)

Prior to the deposition of this particular supersequence, there were parasequences that were deposited. These parasequences are not able to act as a major regional seal for this study area. The late Albian super sequence itself on the other hand consists of thick shale and siltstone, which makes it a potential seal. Comparatively, shale has a better sealing capacity than siltstone but there are instances where the later, specifically, calcareous siltstone and argillaceous siltstone could act as a very good seal. The sequence was encountered at a depth of 800m in the north to around 3000m in the south (Figure 7.4D).

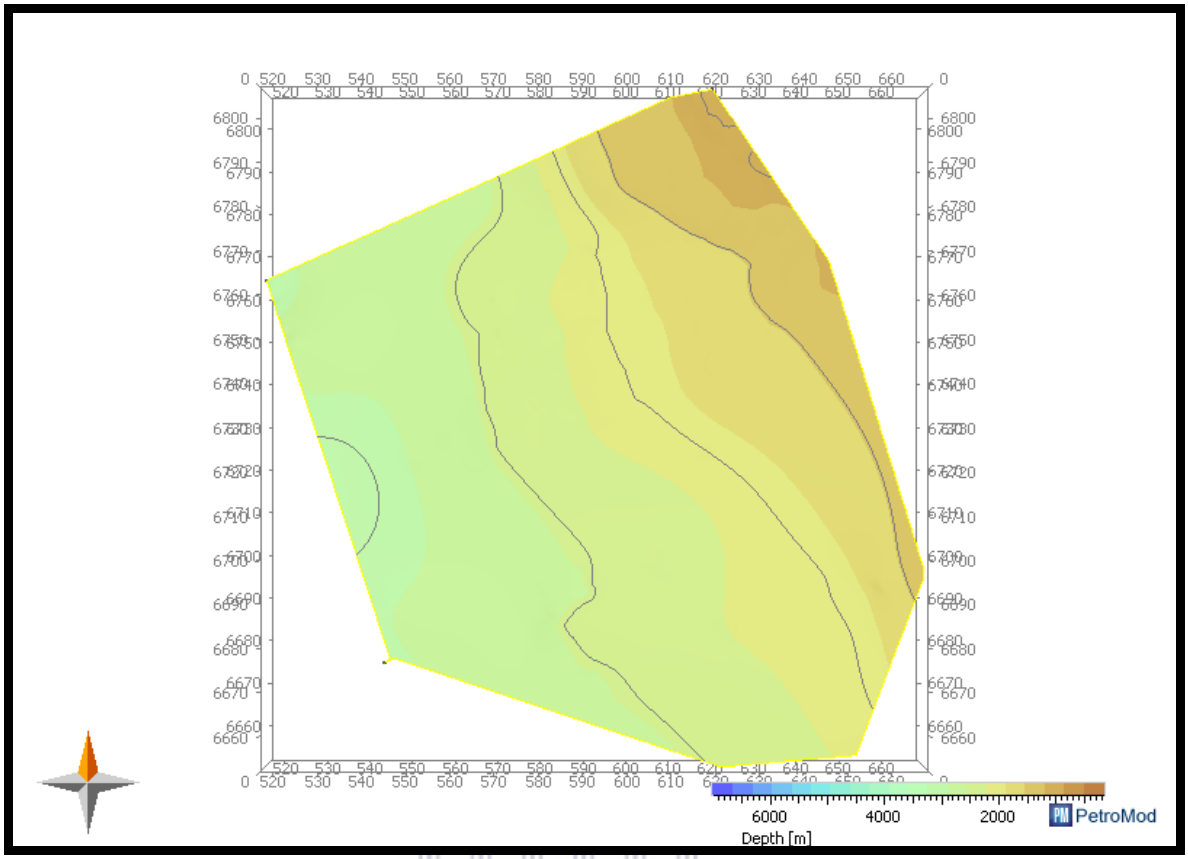

Figure 7.4D: Depth Map of Late-Albian sequence in the study area.

7.4.2.5 Cenomanian (Reservoir Rock)

The depth at which this sequence is encountered ranges from around 900m in the North to 2300m in the South (Figure 7.4E). The Cenomanian age marks the onset of the deposition of upper Cretaceous sediments. There is deposition of potential clastic reservoir sandstone which makes this sequence an element of a petroleum system.

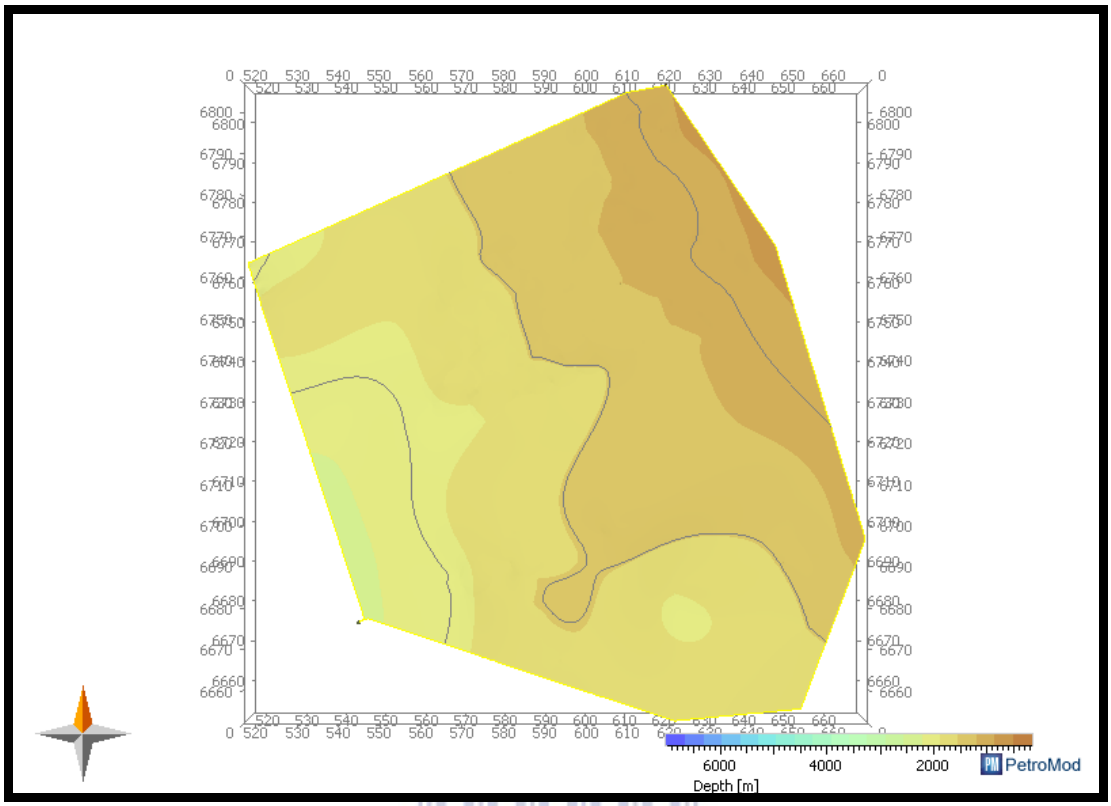

Figure 7.4E: Depth Map of Cenomanian sequence in the study area.

7.4.2.6 Turonian Sequence

The Turonian super sequence in the Orange Basin is believed to have a deposit of organic-rich shale which is believed to be localized to certain parts of the Orange Basin, and an element of a petroleum system. However, in this study, facies interpretations in chapter four of this study explained the absence of a developed potential shale source rock within this interval as no potential source rock is encountered within this sequence. Depth ranges from 750m in the north to 1500m in the south (Figure 7.4F).

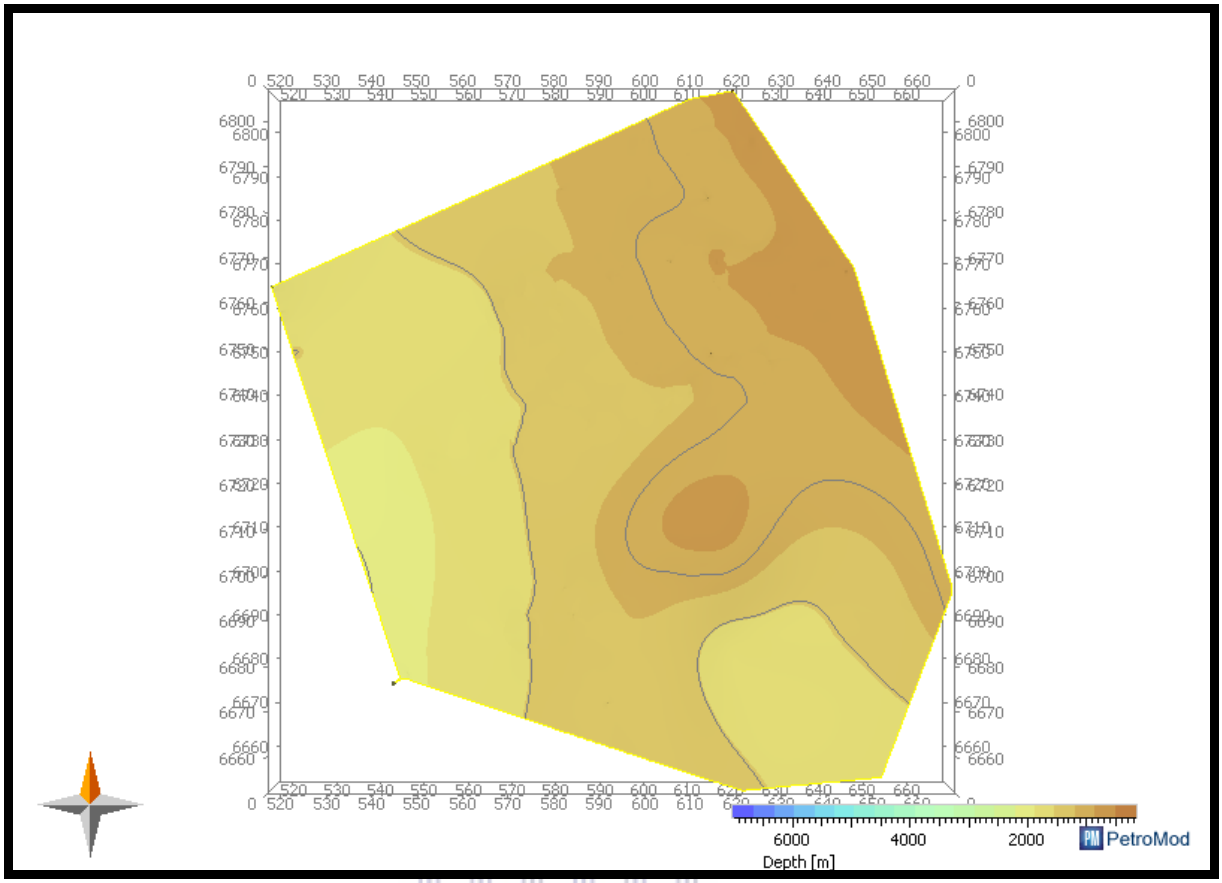

Figure 7.4F: Depth Map of Turonian sequence in the study area.

7.4.2.7 Maastrichtian Sequence

The depth map equivalent which marks the sequence is from 500m in the North to 1400m in the South. This sequence marks the end of Cretaceous sediments deposition (Figure 7.4G).

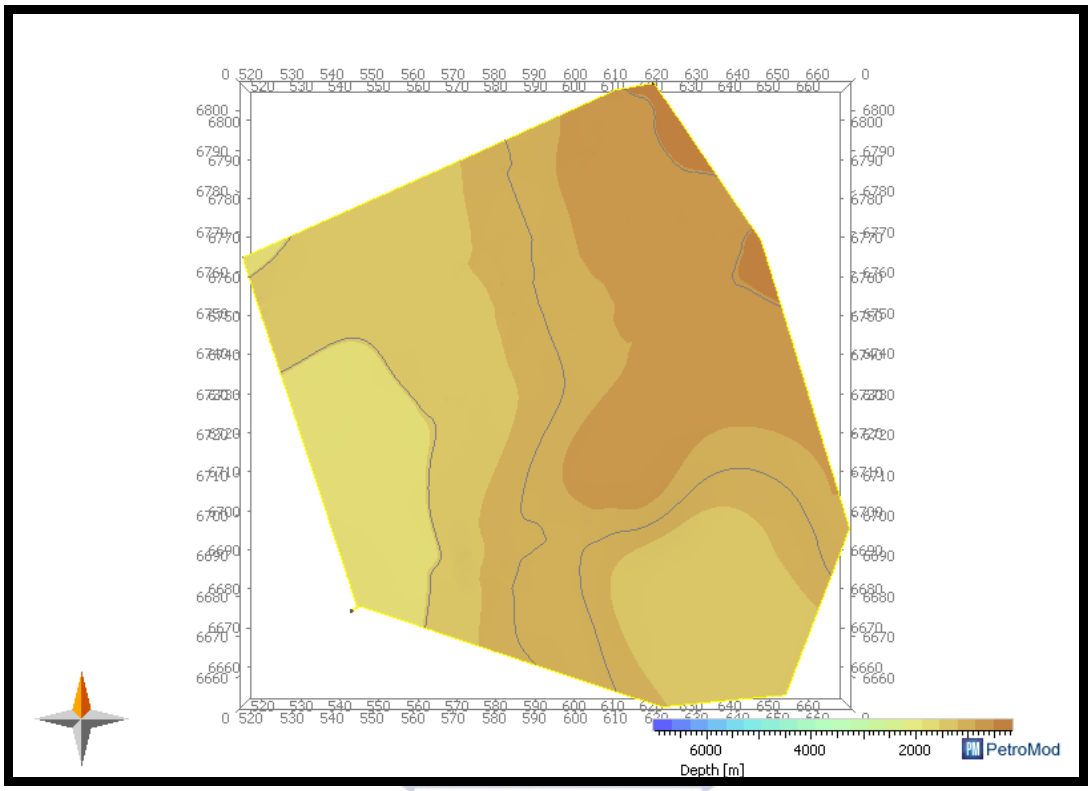

Figure 7.4G: Depth Map of Maastrichtian sequence in the study area.

7.4.2.8 Sea Floor

The depth map values of the sea floor ranges from 160m to 390m. Apparently, the sea floor gently dips westward in the study area which implies the continental shelf depth increases westward in the study area (Figure 7.4H).

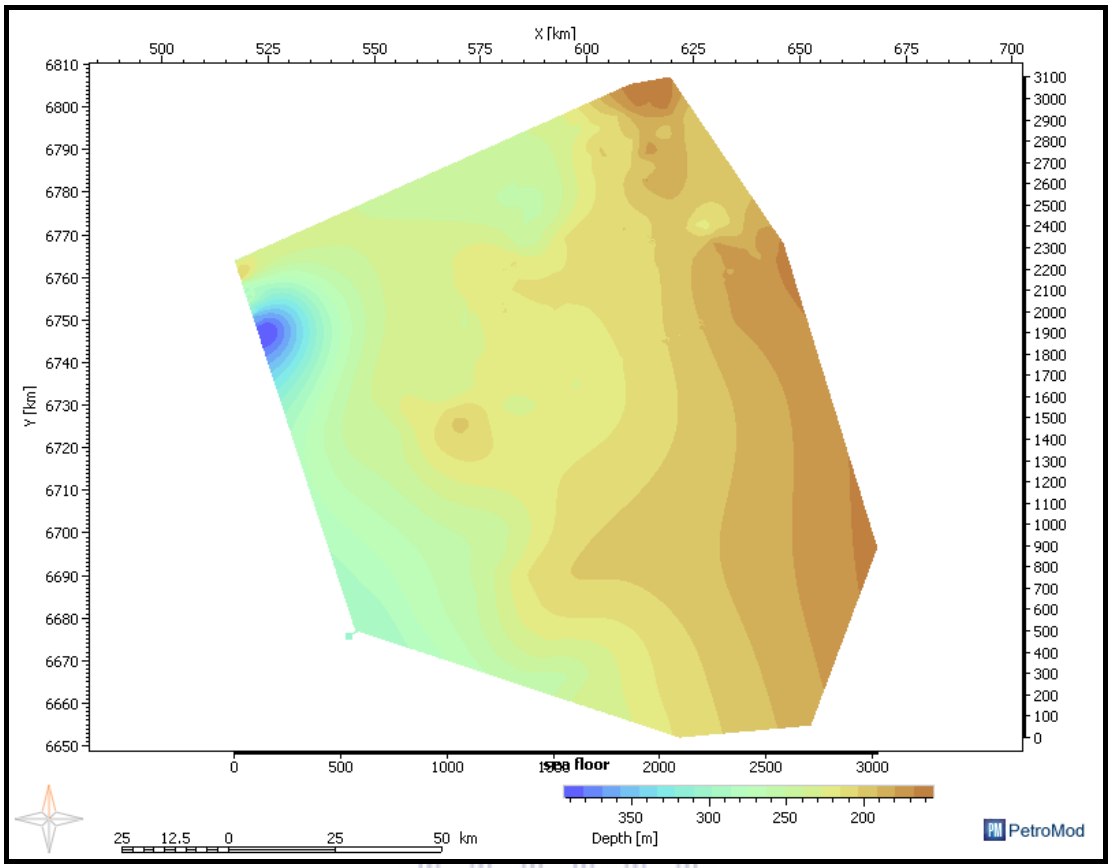

Figure 7.4H: Depth Map of Sea Floor in the study area.

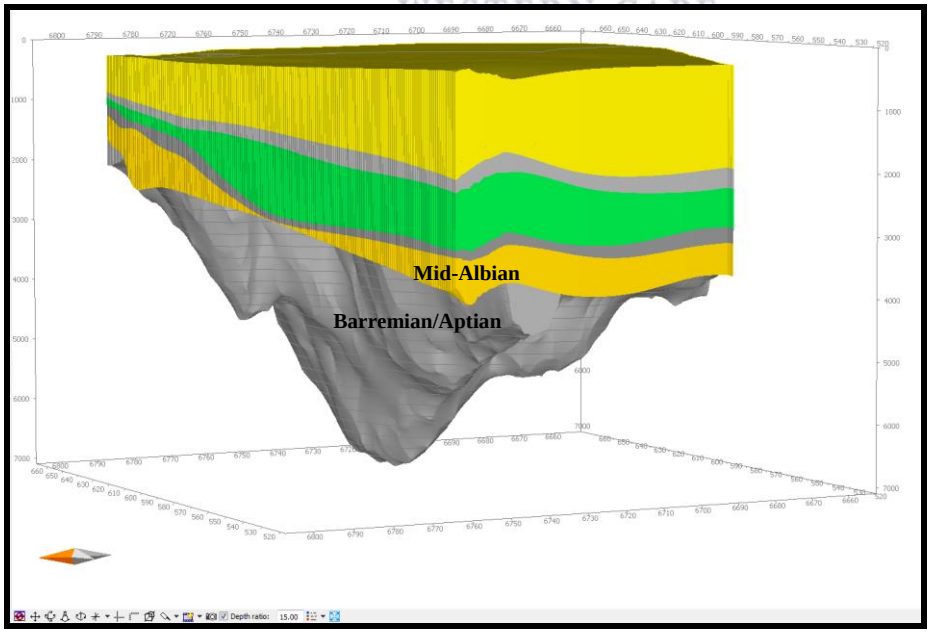

Figure 7.5. 3D Geological Model of the Study Area Comprising of different Unconformities Interpreted Above.

7.4.3 3D Primary Migration (Generation) Modeling.

The depth maps as interpreted above are used for numerical simulation of hydrocarbon-generation. The kinetics of the source rock unit which are Hydrogen Index of 290 mgHC/Gtoc and TOC of 0.6% values were taken from the geochemical well completion report and used as inputs in the simulation process. Pepper and Corvi (1995) type 111 organic matter model was used for the simulation process. The results for the Barremian /Aptian source rock generation are discussed from 120Ma, 108Ma, 95Ma to 0.0Ma below to illustrate its evolution through different geological periods.

7.4.3.1 Simulation Results for Barremian/ Aptian Source rock (120Ma)

At 120Ma, shortly after the deposition of Barremian-Aptian sequence, the average simulated temperature estimate during this period is 40ºC (Figure 7.6 A) with VR estimate of 0.2 (Figure 7.6B).

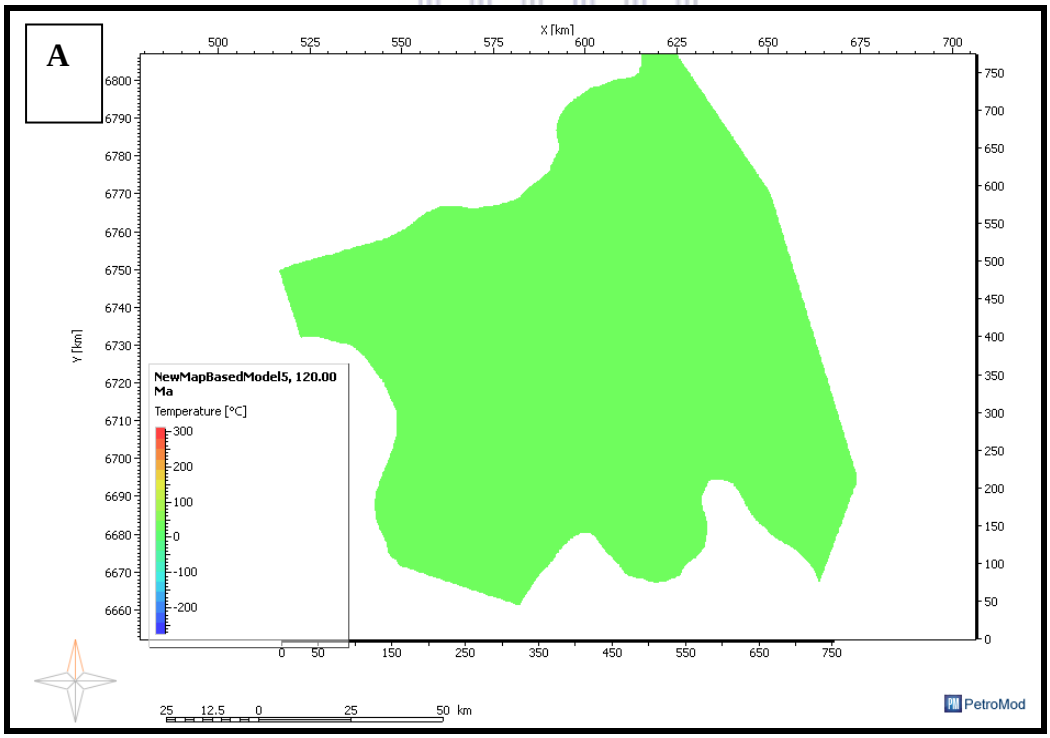

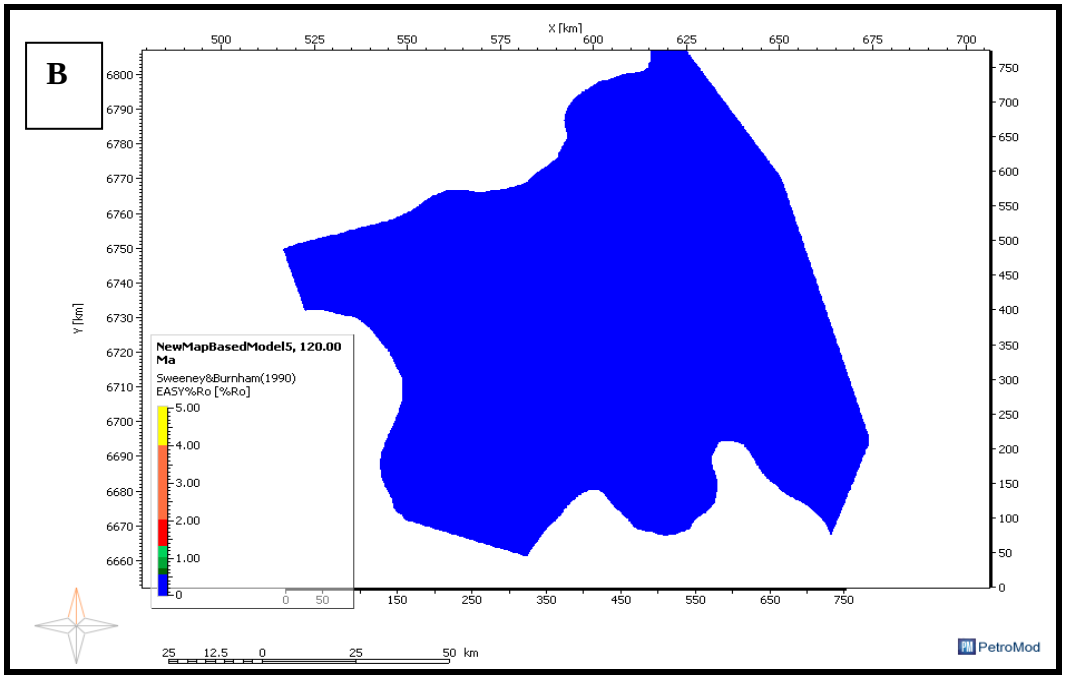

Figure 7.6 A and B: Figures showing the Temperature (A) and Vitrinite Reflectance (B) of Barremian-Aptian Source Rock at 120Ma.

7.4.3.2 Simulation Results for Barremian/Aptian Source rock (108Ma)

The source rock temperature at the depocentre increases to 80 ºC because of high thermal conductivity possibly induced by overburden thickness, while the north-eastern deposition area temperature remains around 40ºC (Figure 7.7A). The vitrinite reflectance increased to 0.5 (Figure 7.7B), however, evidence of transformation of kerogen into hydrocarbon started from 108Ma as seen from the predicted transformation ratio map (Figure 7.7C). Transformation started from the central graben-filled portion (Figure7.7C). This is not unexpected as the thicker portion of the source rock unit will attain more thermal maturity because of high thermal conductivity, compared to the thinner unit.

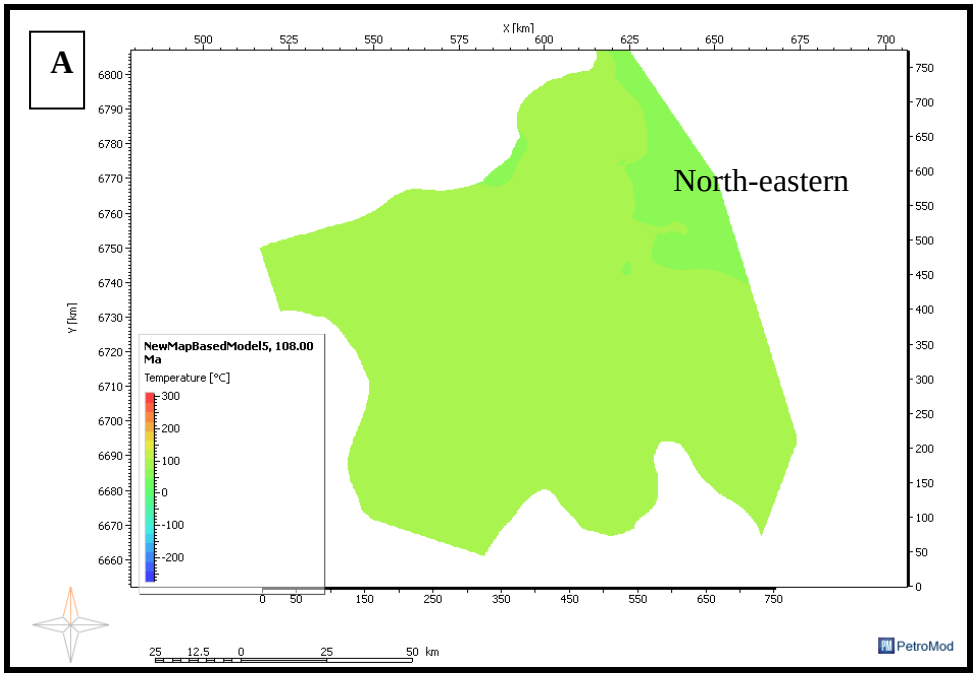

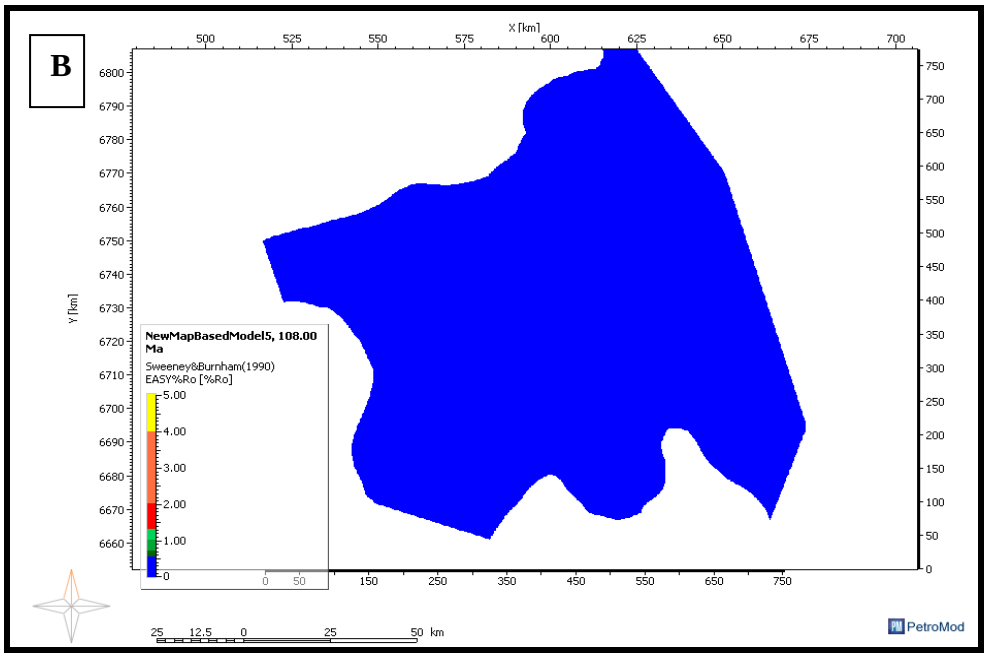

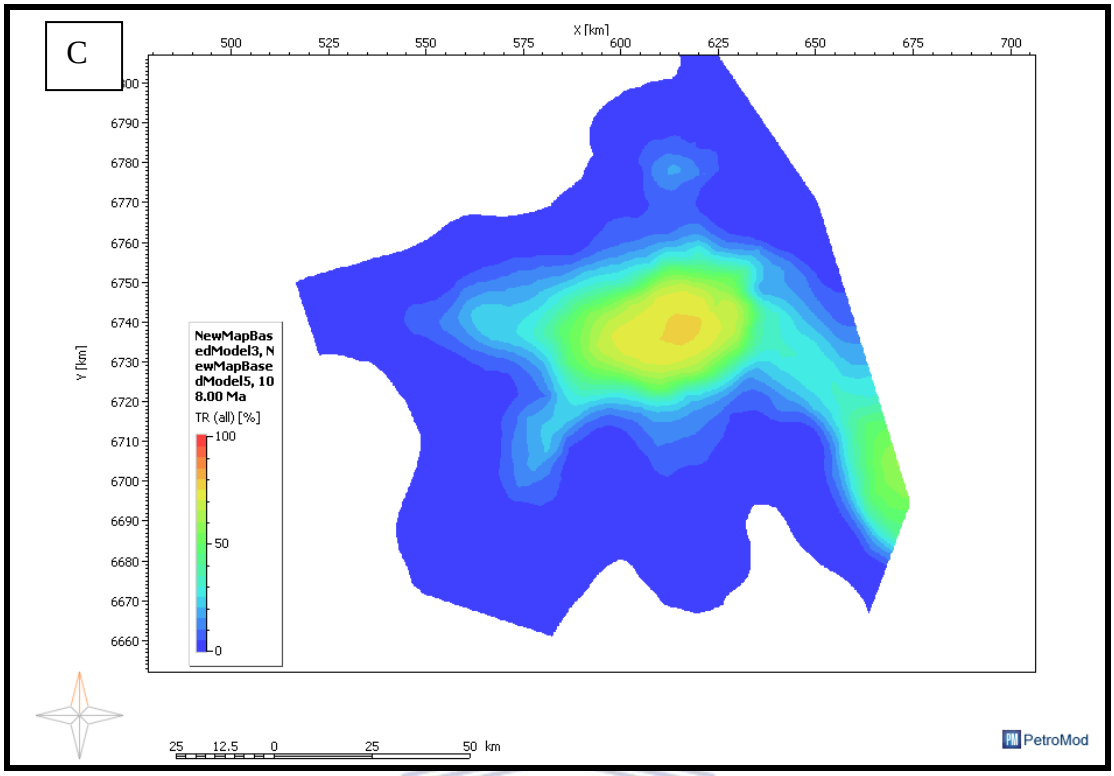

Figure 7.7 A, B and C: Figures showing the Temperature (A) Vitrinite Reflectance (B) Transformation ratio (C) of Barremian-Aptian Source Rock 108Ma. Transformation into hydrocarbon started from the central portion at 108Ma.

7.4.3.3 Simulation Results for Barremian/Aptian Source rock unit (95Ma)

The source rock attains a temperature value of 110 ºC (Figure 7.8A) in the western portion and around 80 ºC in the North-eastern portion. VR values of 0.64 and 0.72 indicate that the source rock attains oil generation potential at the central portion (graben-filled) and is more matured at the western portion (Figure 7.8B). The source rock remains organically non-matured with VR value of 0.51 at the northeastern portion of the study area (Figure 7.8B). Transformation into hydrocarbon continues during this period from the central portion, which coincidentally is the thickest portion of the source rock interval and already attained peak transformation in the deepest portion at 95Ma (Figure 7.8C)

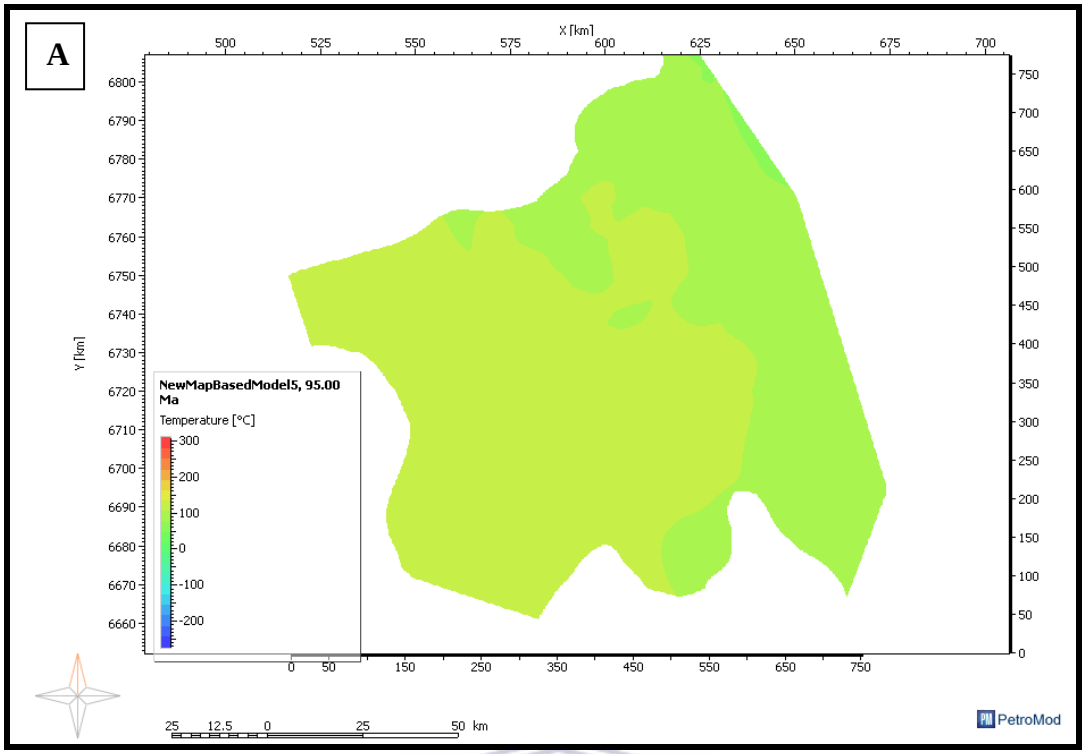

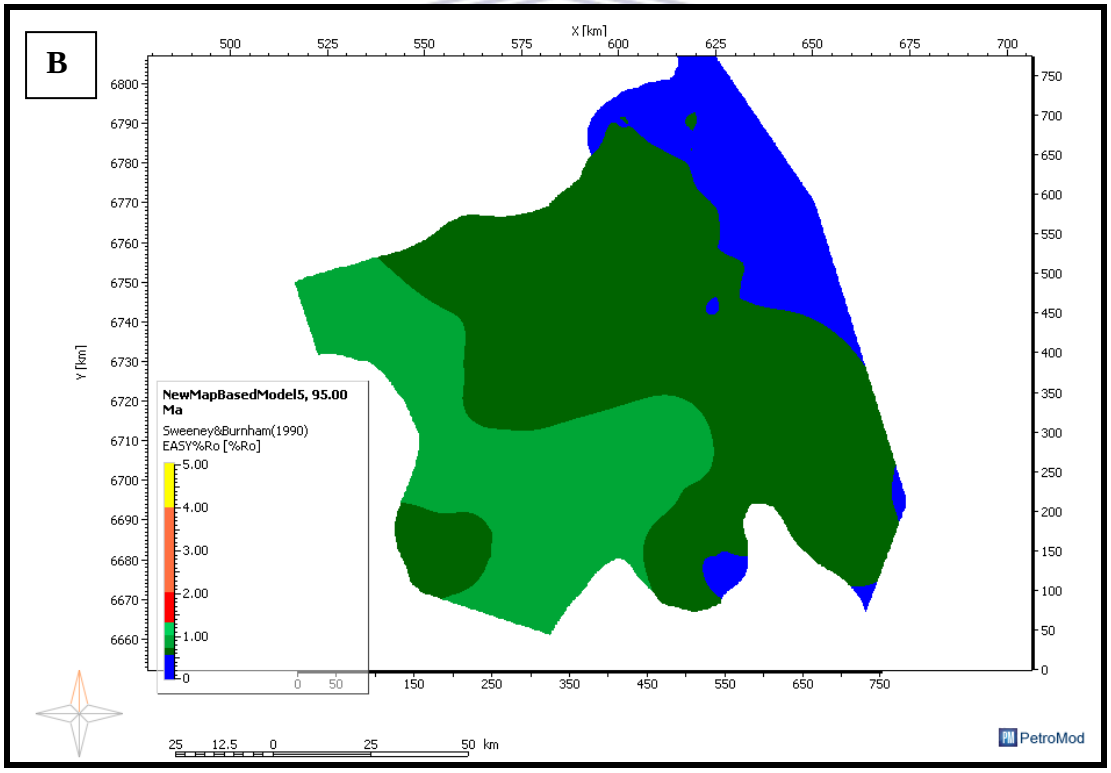

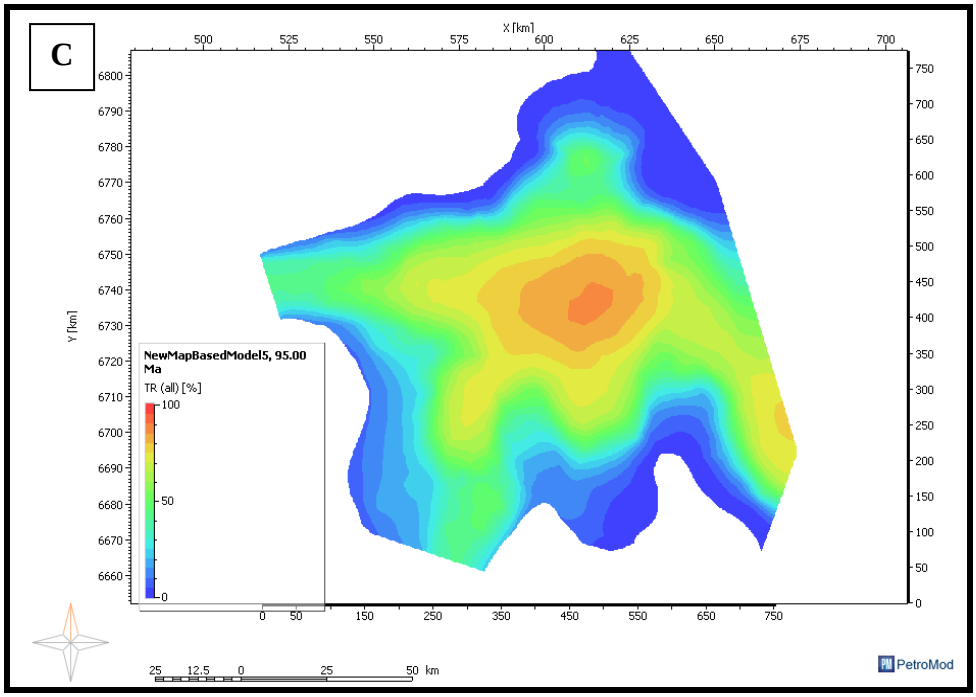

Figure 7.8 A B and C: Figures showing the Temperature (A) Vitrinite Reflectance (B) Transformation ratio (C) of Barremian-Aptian Source Rock at 95Ma.

7.4.3.4 Simulation Results for Barremian-Aptian Source rock at present day (0.0Ma)

The present day temperature modelled for the source rock is around 95 ºC in the western section of the study area and around 68 ºC in the north-eastern section (Figure 7.9A). These values represent windows for gas and oil prone generation potential in the central and eastern section respectively. However, the VR values reached a peak of 1.1 and 0.68 at the central and eastern section of the area (Figure 7.9B). These values agree well with the simulated temperature values suggesting a potential for gas and oil generation in the central and eastern section respectively. The transformation ratio map indicates 100% of the organic matter has been transformed into hydrocarbon in the central section, and no transformation yet in the most north-eastern section (Figure 7.9C).

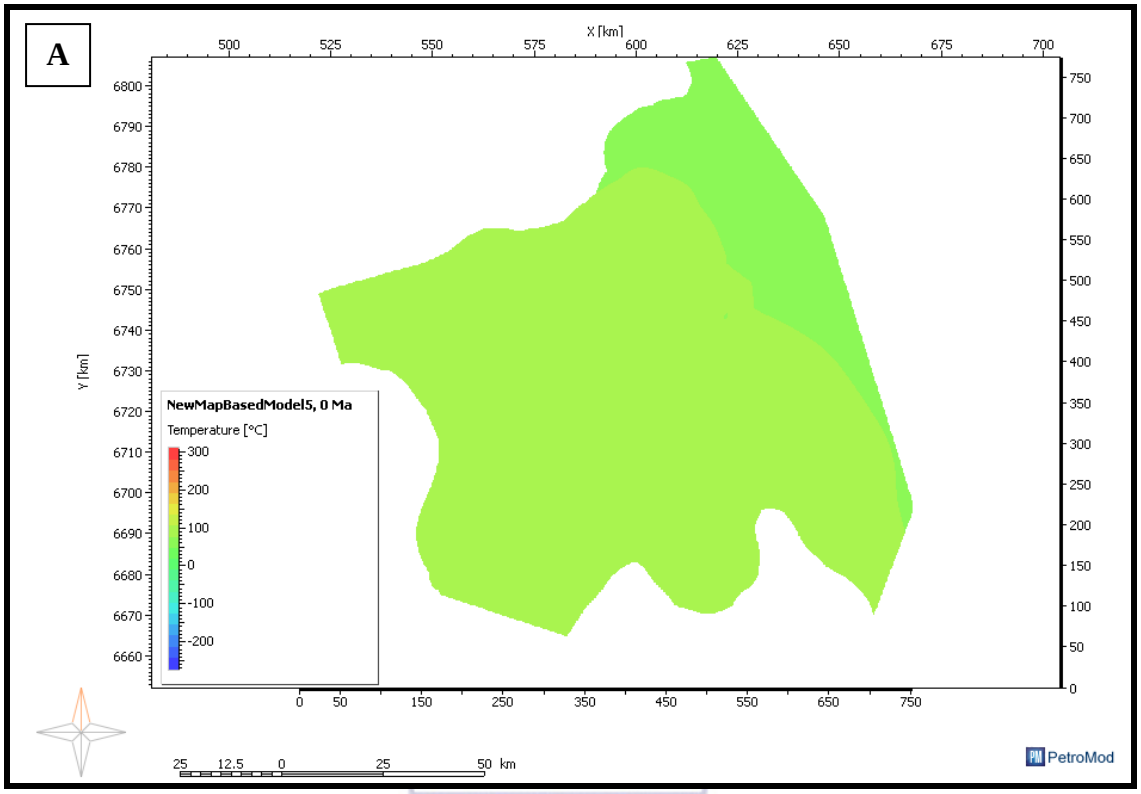

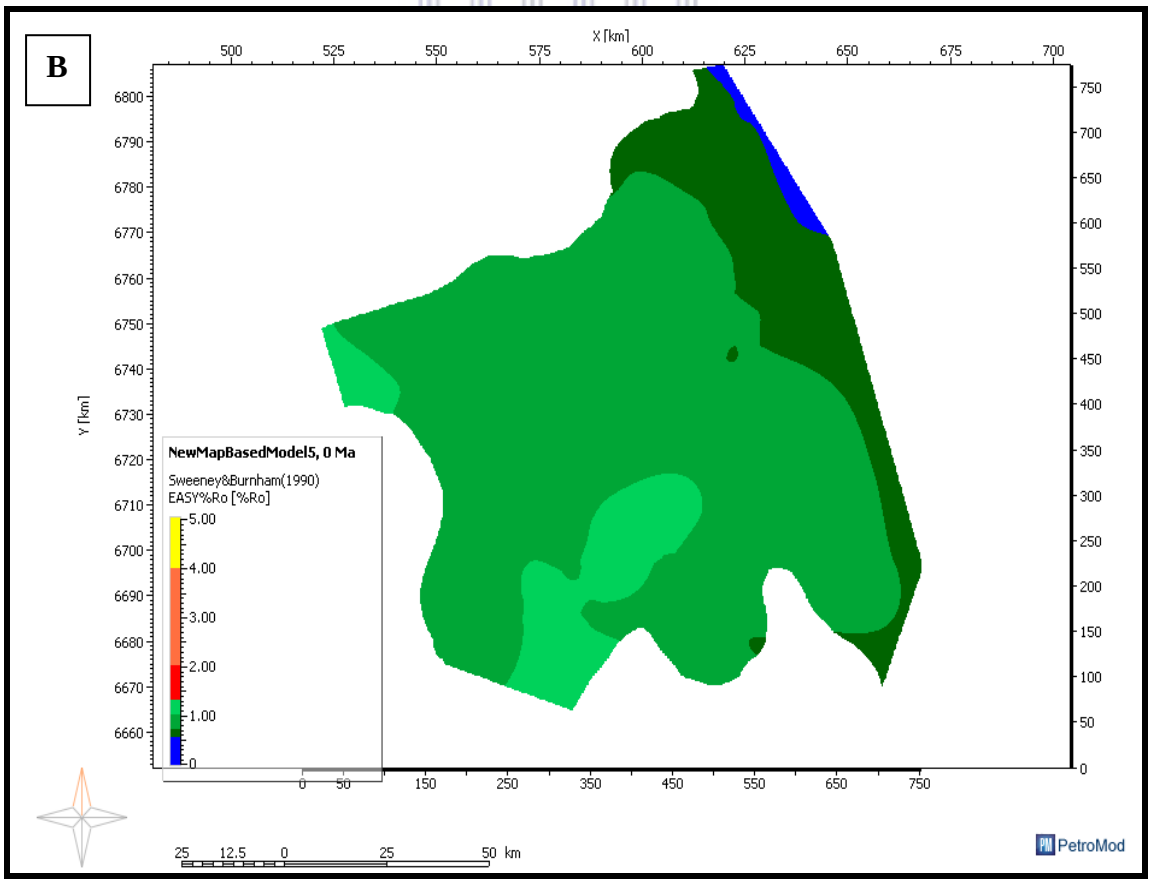

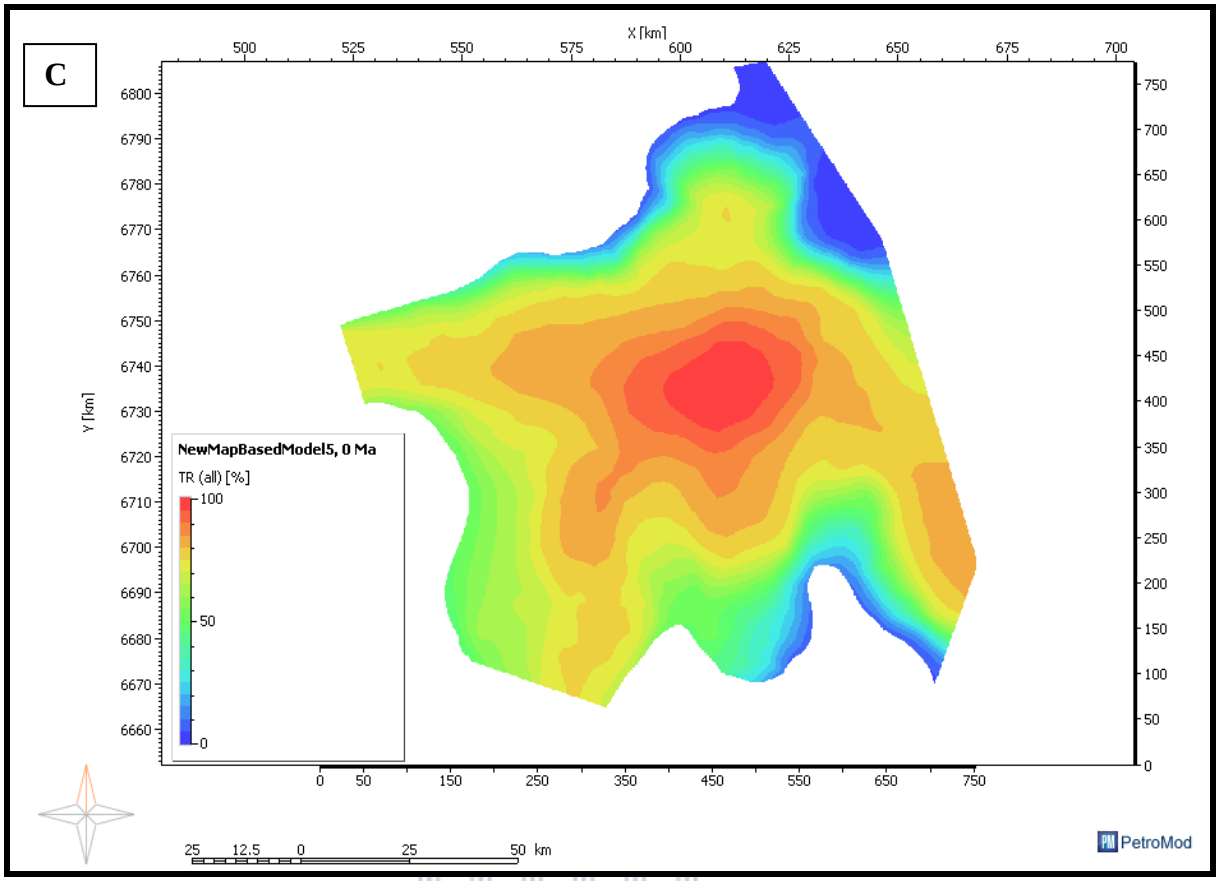

Figure 7.9 A B and C: Figures showing the Temperature (A) Vitrinite Reflectance (B) Transformation ratio (C) of Barremian-Aptian Source Rock at 0.0Ma.

7.4.4 Source Rock Hydrocarbon Generation Statistics

A comparison is made between the volume of hydrocarbon generated from the source bed at 105 Ma on the one hand and the present day (0Ma) on the other hand to evaluate the volume of hydrocarbon from primary and secondary cracking. The results are explained below.

7.4.4.1 Source Rock Generation Statistics at 105ma

The source rock entered peak generation at 105ma (Early Cenomanian) with an estimated 317985.62 Mtons oil generated from labile organic matter through primary cracking, representing 99.15% fraction of the organic matter converted into oil (Figure 7.10A). In addition, 0.85% of organic matter was converted to gas through primary cracking, representing 2724.24Mtons volume of gas (Figure 7.10A). The volume of gas generated by secondary cracking is an estimated 83161.70Mtons, representing 26.152% of the 317985.62Mtons of oil generated that was cracked into gas (Figure 7.10B).

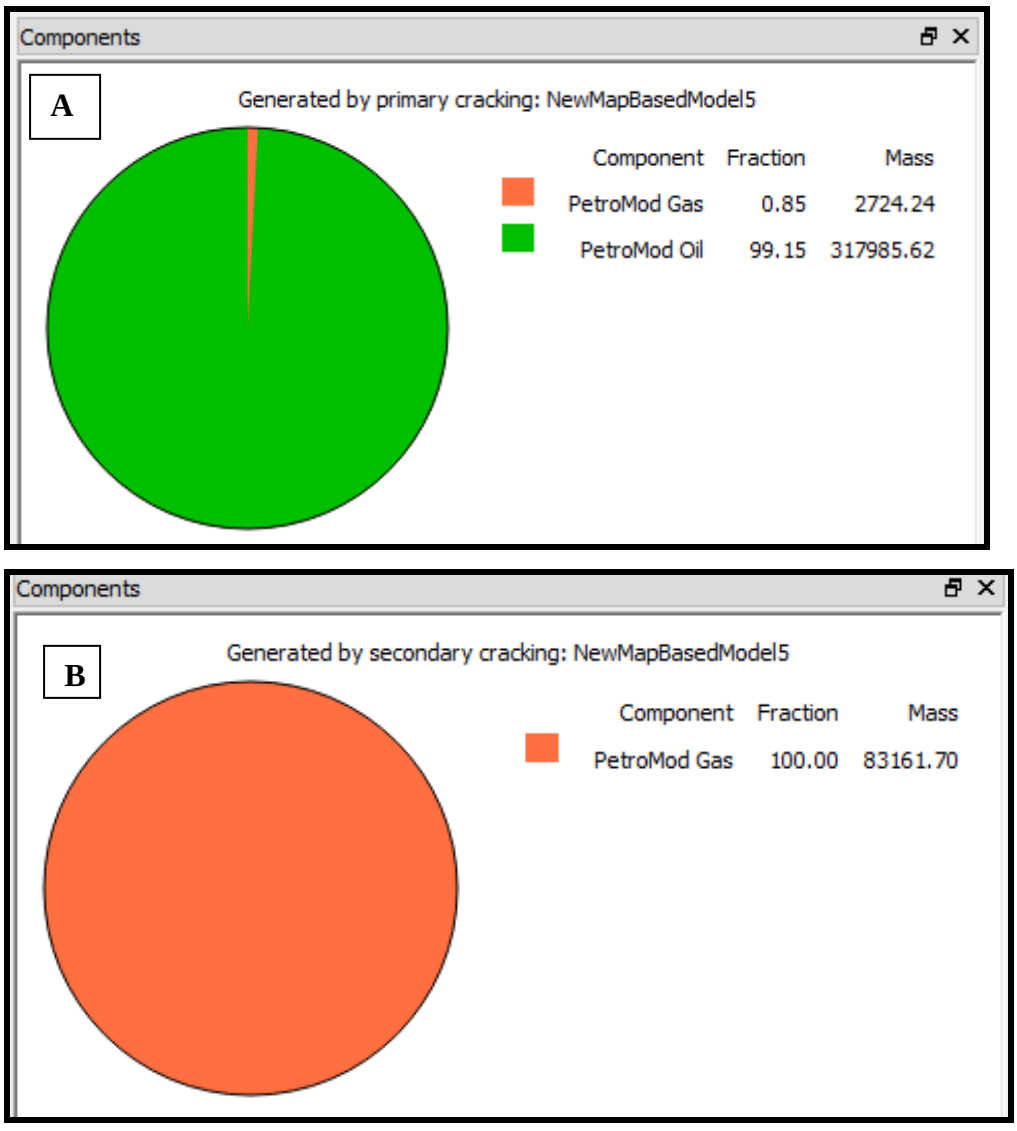

Figure 7.10 (A and B): Figures showing Primary Cracking (A) and secondary cracking (B) of Barremian-Aptian Source Rock at 105 Ma.

7.4.4.2 Source Rock Generation Statistics at 0.0 Ma

By present day an estimated amount of 633.058,70 Mtons of hydrocarbon had been by generated by primary cracking. About 584.923,68 Mtons of this value represent the volume of oil generated by primary cracking, which is an equivalent of 92.40% of the labile organic matter that was converted into oil. Similarly, the remaining 7.60% represent an equivalent of 48.135,04 Mtons of gas generated (Figure 7.11A) through primary cracking. Subsequently, out of the 584.923,68 Mtons oil generated, 382.566,89 Mtons of gas was generated by secondary cracking, representing 65.404% of the oil generated had been thermally degraded to gas (Figure 7.11B).

Figure 3Figure 7.11 A and B: Figures showing Primary Cracking (A) and secondary cracking (B) of Barremian-Aptian Source Rock at 0.0 Ma

.

7.4.4.3 Source Rock Bulk Generation and Expulsion Statistics at 0.0Ma (Present day)

At present day, bulk gas generation balance from the source rock represents the addition of the volume of gas generated by primary cracking and secondary cracking, while the bulk oil generated represents the volume that was generated but has not been thermally degraded by the process of secondary cracking. These represent total values of 430.701,94 Mtons for gas and 38.399,53 Mtons for oil which are a relative equivalent of 91.81% and 8.19% of total hydrocarbon generated respectively (Figure 7.12A). Also, the onset of expulsion started around 110 Ma and maintains a steady rate of increase in volume until the late Cretaceous when a drastic increase in expulsion rate was observed; the process reached a peak around 55Ma (Figure 7.12B).

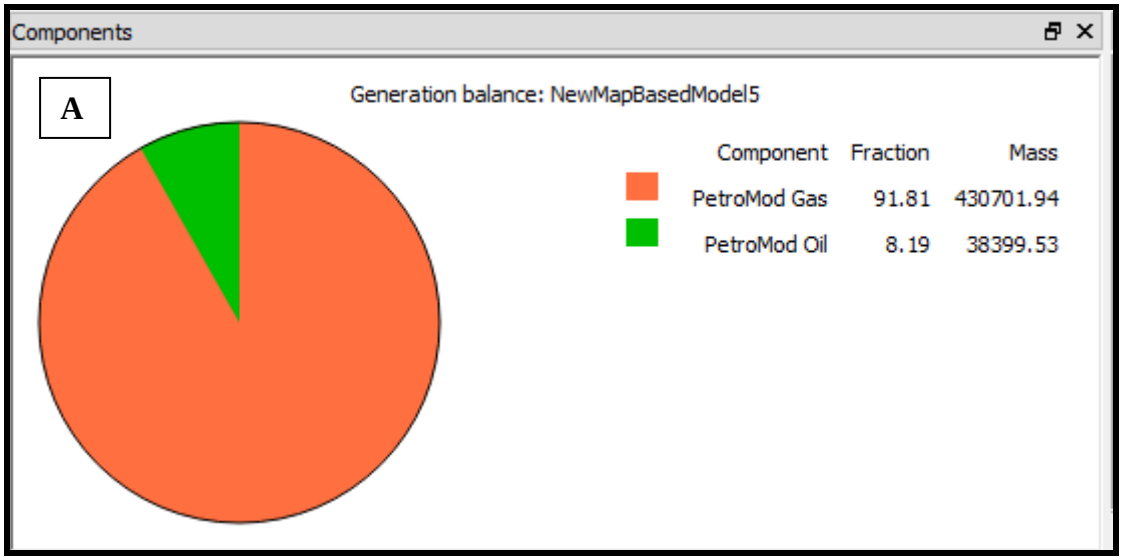

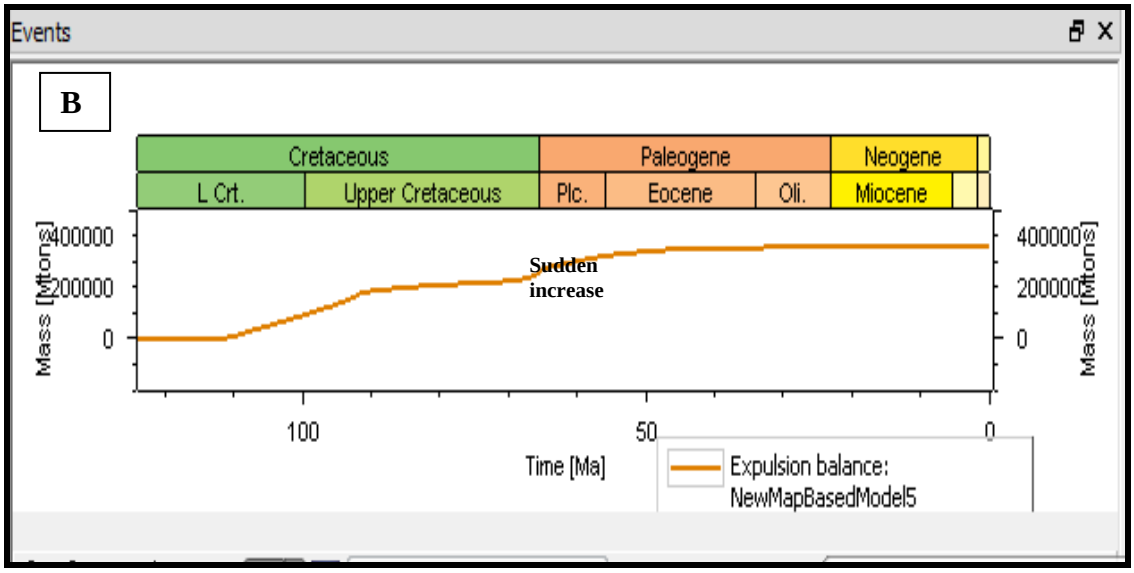

Figure 7.12 A and B: Figure showing bulk oil and gas generated from the source Rock (A) and bulk hydrocarbon expulsion over time till present day.

7.4.4.4 Timing of Hydrocarbon Generation and Expulsion.

The amount of hydrocarbon generated by a source rock is the total of the amount accumulated within it and the amount expelled from it. Figure 7.13A below indicates that the peak period of hydrocarbon-generation reached a plateau just after the end of the lower Cretaceous. Furthermore, the hydrocarbon curve approached a plateau in the upper Cretaceous (Figure 7.13A), and reached peak values during the late Cretaceous and early Cenozoic and stays on this trend till the present day. Accumulated hydrocarbon, in this case, refers to the generated hydrocarbon which has not been expelled, probably due to insufficient pressure to expel them out of the source rock. Expelled hydrocarbon refers to the hydrocarbon that leaves the source pod due to sufficient pressure (Figure 7.13B). There is a lot of accumulated hydrocarbon at the end of the lower Cretaceous with a corresponding lower expulsion, which implies that a lot of kerogen was thermally converted to hydrocarbon but with a lesser expulsion rate. As stated above, expulsion increased drastically just after the start of upper Cretaceous (Cenomanian) and reached its peak in the early Cenozoic (Figure 7.13B).

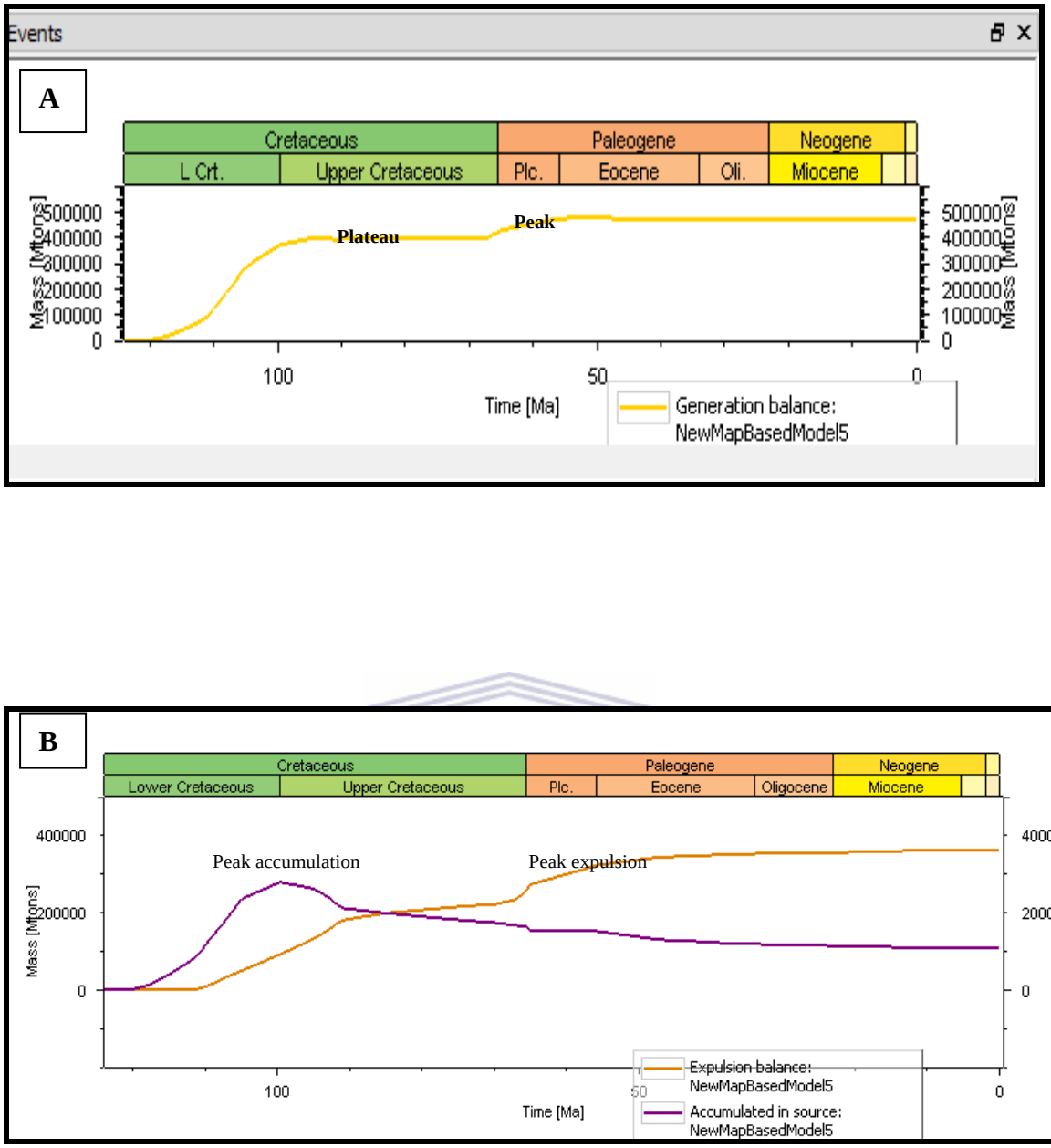

Figures 7.13 A and B: Figures showing Timing of peak Hydrocarbon-generation (A), and Accumulation plus Expulsion for the Barremian/Aptian Source rock (B).

7.4.4.5 Expulsion Efficiency

Petroleum expulsion efficiency summarises the ratio of the amount of expelled hydrocarbon to the amount of generated hydrocarbon. Commonly, the value of this expulsion efficiency ranges from 0 to 1.0 for no expulsion and complete expulsion respectively. In this study, the expulsion efficiency for the source rock stands at 0.77 with gas as the main hydrocarbon expelled. As shown earlier in figure 7.13A, there

was generation of oil which did not expel out of the source rock, probably due to insufficient pressure gradient necessary for its diffusion. Evidently, a major fraction of oil generated was thermally cracked to gas at a higher temperature as earlier shown in Figure 7.13B. This explains the higher expulsion efficiency (0.77) estimated for the source rock because gas has more expulsion efficiency than oil as it requires a lesser pressure gradient compared to oil, to expel it from the source pod.

7.4.5 3D Numerical Modeling of Hydrocarbon Migration Pathways.

Evolutions of hydrocarbon migration pathways are commonly associated with structural controls such as faults, especially when evidence manifests as seepages on the sea floor (Tryon et al., 1999). However, stratigraphy controlled migration pathways are dependent on the intrinsic lithological properties (porosity basically), bed geometry and stratigraphic erosional surfaces (Onlap, Downlap and Toplap). As earlier discussed, hydrocarbon migration pathway simulations using a hybrid model as applied here, is based on the flowpath tracing method using lithology with more than 30% porosity as carrier beds. In the absence of such lithology it switches to bed surface geometry as the flowpath tracing method. The simulation results are discussed below.

7.4.5.1 Faults Model used in the study

The different faults used for this study are formed throughout the tectono-stratigraphic evolution of the basin (Barremian-Cenozoic) in the northern part. However, in certain circumstances, there are occurrences of reactivated faults spanning across different periods. Evidence of basin inversion and associated crustal shortening is noted earlier in chapter five under the structural framework modelling.

The source of fault reactivation in an extensional regime is commonly induced seismicity as a result of drilling. Another cause of reactivation can be basin inversion which could change the dip of existing active faults (Rutqvist et al., 2013). In this study, syn-rift faults are opened while post rifts faults are closed in the model to test the controls these faults exercise on hydrocarbon migration pathways. In addition, different scenarios of open and closed faulting systems are tested to perform sensitivity analysis of the model.

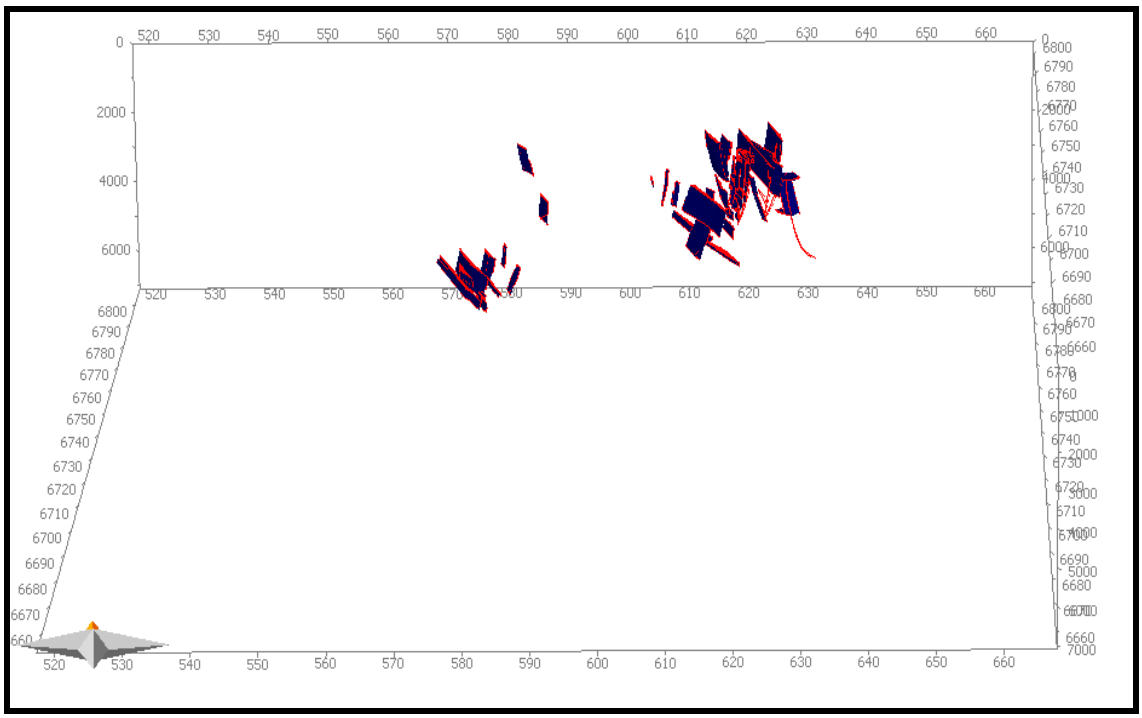

Figure 7.14: 3D View of Gridded Faults Model used in the study.

7.4.5.2 Expulsion of Hydrocarbon from the Source Rock at 108 Ma

The generation of oil (Green) and gas (Red) accompanied with water (blue) started from the source rock unit at the central part of the study area, while predominant gas migration started from the Southeastern part at 108 Ma (Figure 7.15).

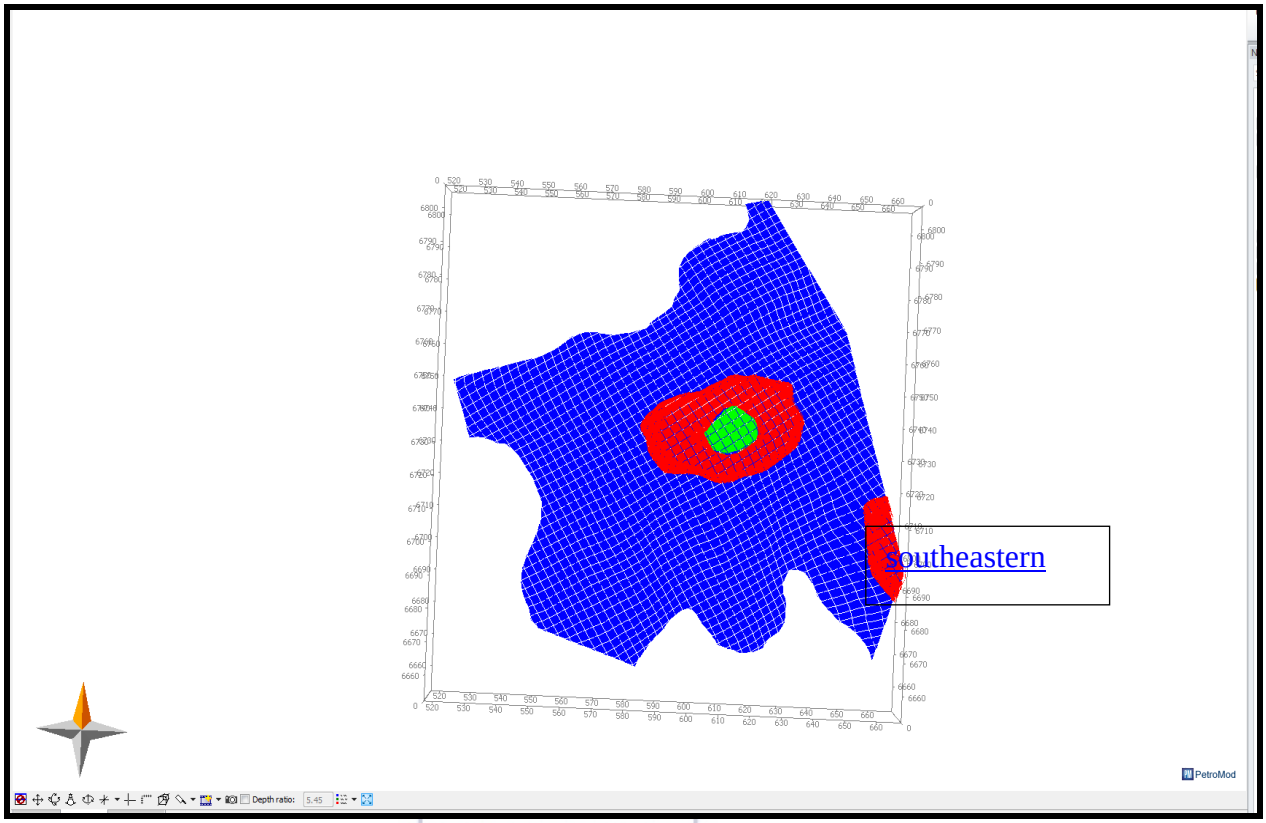

Figure 7.15: 3D generation of Hydrocarbon from the Barremian/Aptian Source Rock at 108 Mya.

7.4.5.3 Evolution of Hydrocarbon Migration Pathways in Mid-Albian Reservoirs (Vectors) .

The main reservoir in this study is of Albian- aged (112My) and sits unconformably on the Barremian Aptian source rock unit. The figures below show different migration vectors for oil and gas. At 108Ma, some of the gas (red) expelled from the Barremian-Aptian source unit has migrated into the Albian reservoir, thereby making the Albian reservoir a carrier bed for further migration. The migration vectors here indicate that gas expelled from the source rock unit migrated vertically and charged the porous Albian-aged reservoir because the expulsion pattern from the source rock in Figure 7.14 above is similar to migration pattern shown in Figure 7.15A. However, there is no evidence of oil observed in the source rock charging the reservoirs, thereby suggesting that at 108Ma, only gas migrated vertically from the source bed into the Albian. By 92My, the volume of gas expelled and migrated into the reservoir has increased tremendously spreading from the centre across to the periphery of the study area (Figure 7.15B).

By present day (Figure 7.15C), the volume of gas in the carrier bed has reduced which implies that some volume of gas has been lost during the migration process. Also, there is an oil presence (wetness) in the reservoir towards the distal portion (western part) of the study area, as seen in figure 7.15C. The presence of oil in the reservoir at present day is suggestive of late entry into the oil window of a part of Barremian-Aptian source rock which later expels oil which migrates into the reservoirs in deep waters. Another probable reason could be late expulsion of already generated oil which migrates distally of the reservoir unit.

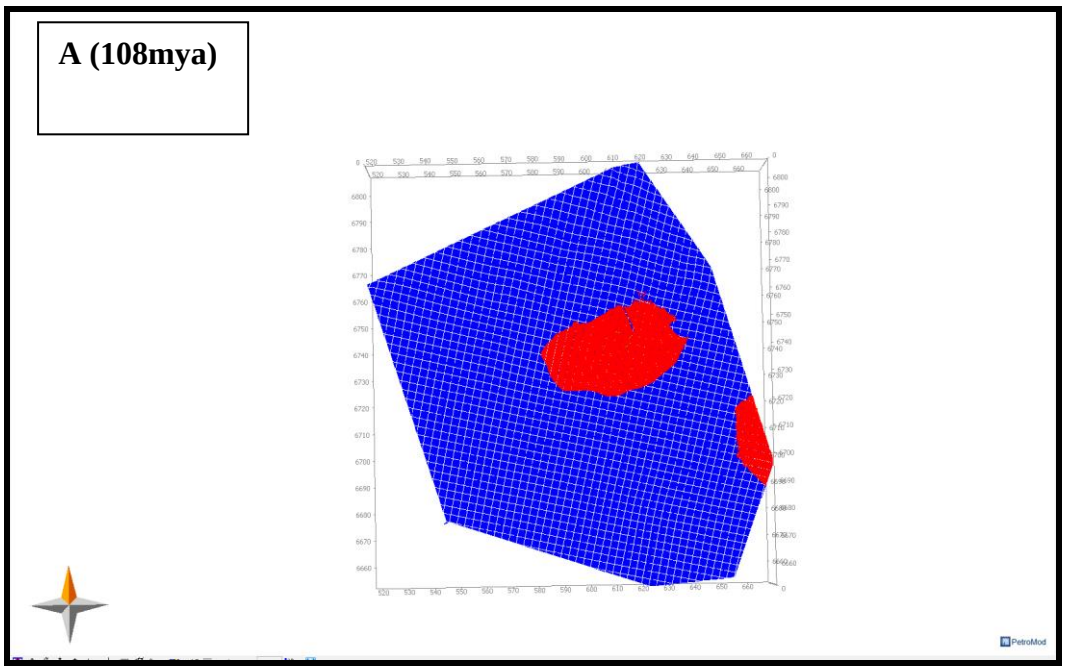

An integrated approach to understanding the geological controls on gas escape and migration pathways in offshore northern Orange Basin, South Africa.

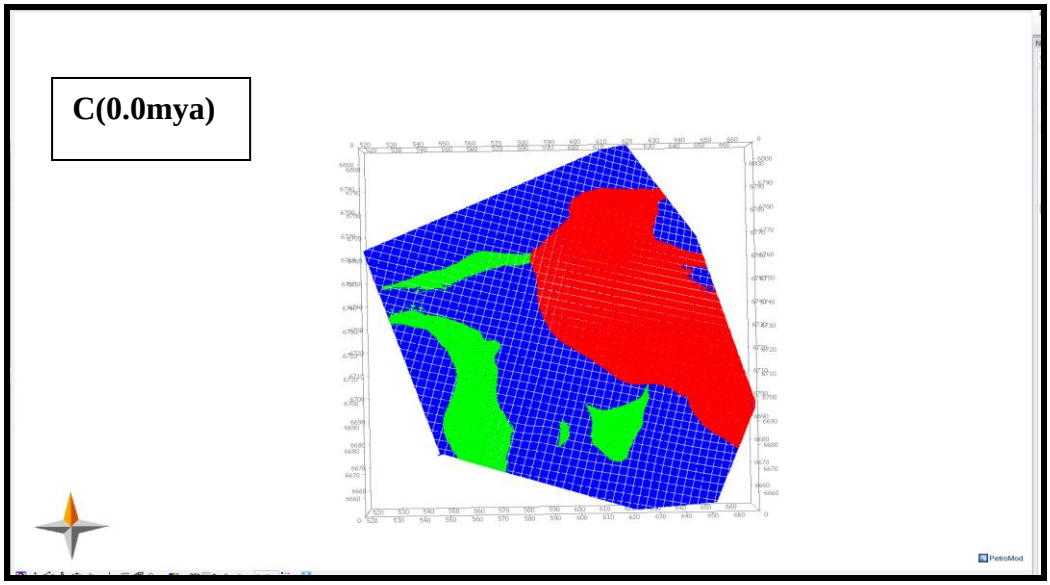

Figures 7.15 A, B, C. 3D Hydrocarbon Migration Pathways (Red-Gas, Blue-Water, Green-oil) in Albian-aged Reservoir at 108mya, 92mya and 0.0mya respectively. The present day presence of oil vector distally of the Albian reservoir suggest migration of oil into deepwater by good carrier units within the reservoir rock.

7.4.5.4 Evolution of Hydrocarbon Migration Pathways in Cenomanian Reservoirs (Vectors) .

Another potential reservoir target in the study area is the Cenomanian –aged reservoir (Figure 7.16A) which shows similarity in terms of charging pattern to the Albian aged reservoirs at 108mya (Figures 7.15A) suggesting the gas expelled from the source rock migrates vertically unconstrained and charged the overlain reservoirs. However, at present day (0mya), simulation results show that Cenomanian reservoirs are gas prone only(7.16C), which is in contrast to the result in the Albian- aged reservoirs at 0.0mya, which is oil and gas prone(7.15C).

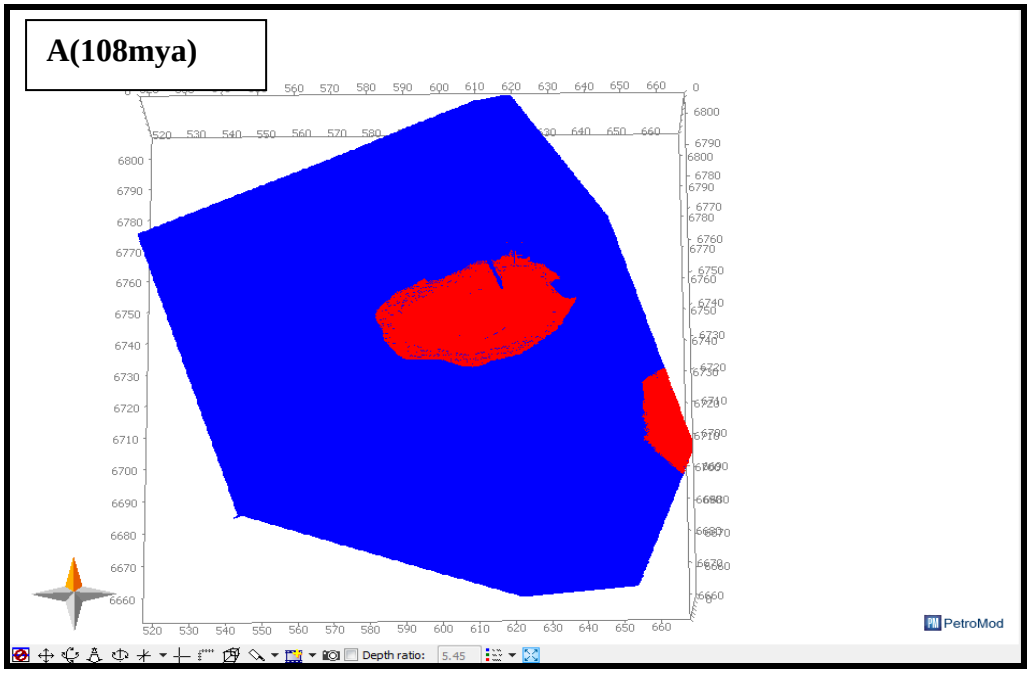

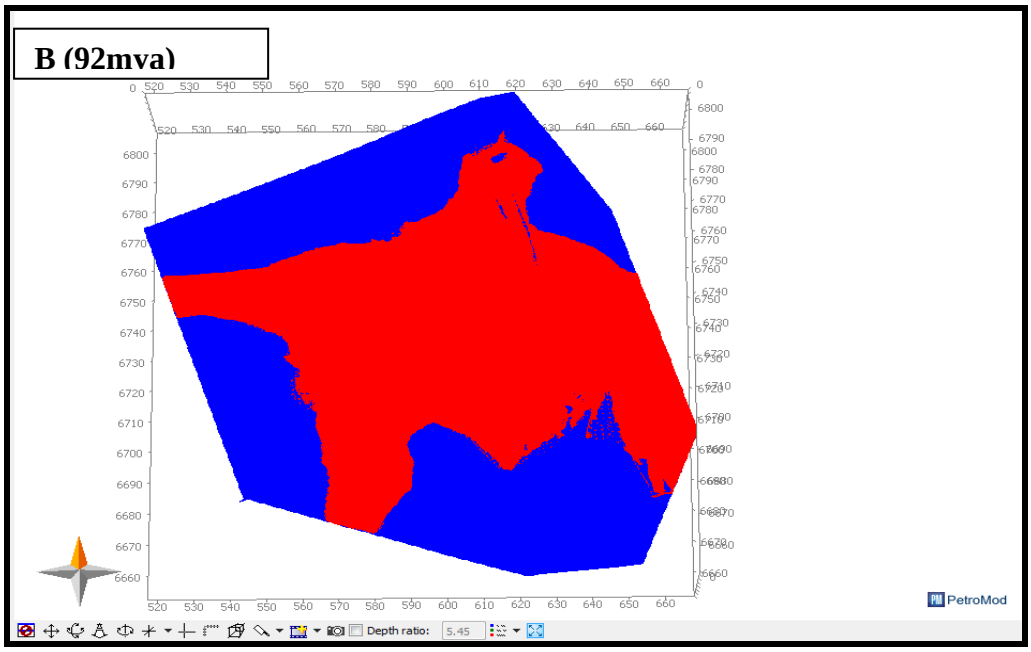

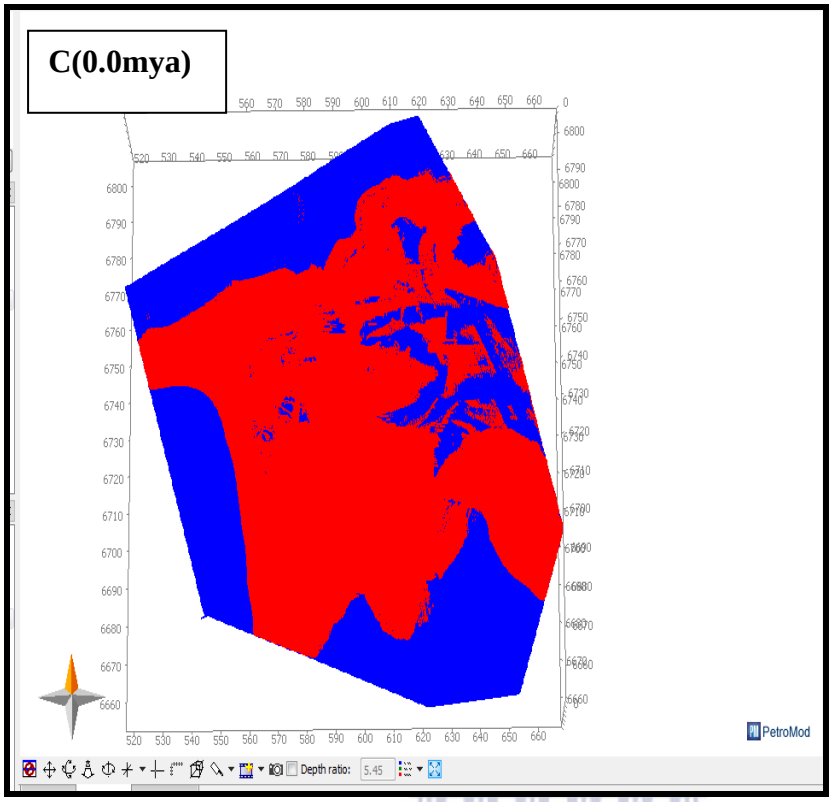

Figures 7.16 A, B, C. 3D Hydrocarbon Migration Pathways (Red-Gas, Blue-Water, Green-oil) in Albian-aged Reservoir at 108Ma, 92Ma and 0.0Ma respectively. Present day result shows Cenomanian reservoir to be gas-prone in contrast to the Albian reservoir unit which is oil and gas prone as seen in figure 7.15C above.

7.4.6 Fault Controls on hydrocarbon Migration Pathways.

The faults model for this study was tested for hydrocarbon saturation as part of the numerical simulation model to characterise their behaviour with respect to hydrocarbon migration. In the study area, sedimentary sequences older than Barremian were not deposited; individual fault inputed as part of the simulation was dated based on the age of super-sequence it is constrained to. The various faults modelled for the study date from 124Ma to the youngest Cenozoic sequence. Faults have a saturation point where further gas migration ceases and this attests to the sealing capacity of a fault due to hydraulic resistance of the fault rock. Fault rock hydraulic property does change with burial and uplift caused by different episodes of

tectonism (Cerveny et al., 2004). Age assignment of individual faults was done based on the span of ages of strata they cut across. Below are the results of faults control of gas migration pathways starting from 93Ma, 91Ma, 74Ma and 65Ma.

7.4.6.1 Faults Hydraulic Behaviours at 93Ma

The faults seen in the model below indicate the active faults during this period. However, only the listric fault already mapped, and observed with the bright spot anomaly in chapter five of this study appears to be fully saturated with gas. Other faults are not saturated. The listric fault which detached from the basement suggests it was formed during the continental rifting and breakup of the continent. It runs from the Barremian-Aptian sequence and terminates at the late Cretaceous and becomes fully saturated with gas at 93 Ma (Figure7.17A).

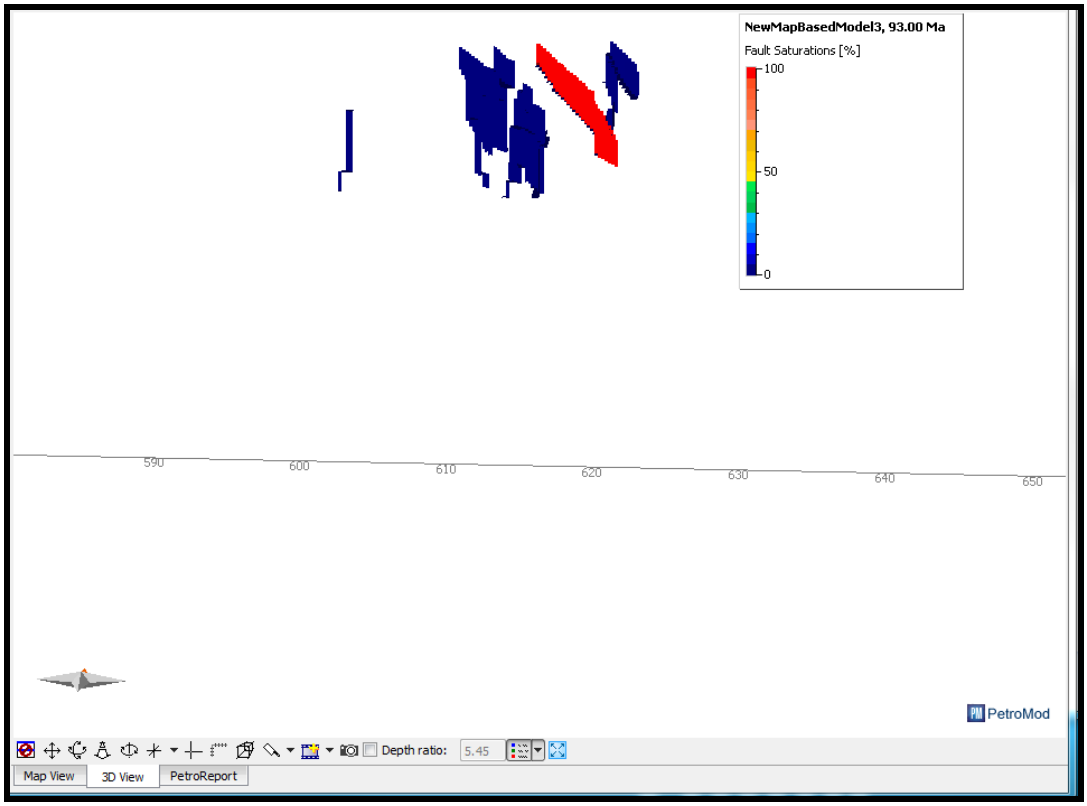

Figure 7.17A: Gas saturated Listric Fault (124-65mya) at 93mya at 625.186m by 6749.50m grid.

7.4.6.2 Faults Hydraulic Behaviours at 91Ma

At 91mya (Figure 7.17B), fault saturation with gas had drastically reduced, thereby suggesting a breakthrough path along the fault rock and a change in the hydraulic property of the fault rock which causes hydrocarbon leakage across the fault. The

saturation had reduced to almost zero percent which means the rate of leakage exceeds the rate of gas saturation along this fault and provides proof that the fault is active from time to time and leaks gas already trapped when the fault reactivates due to tectonism.

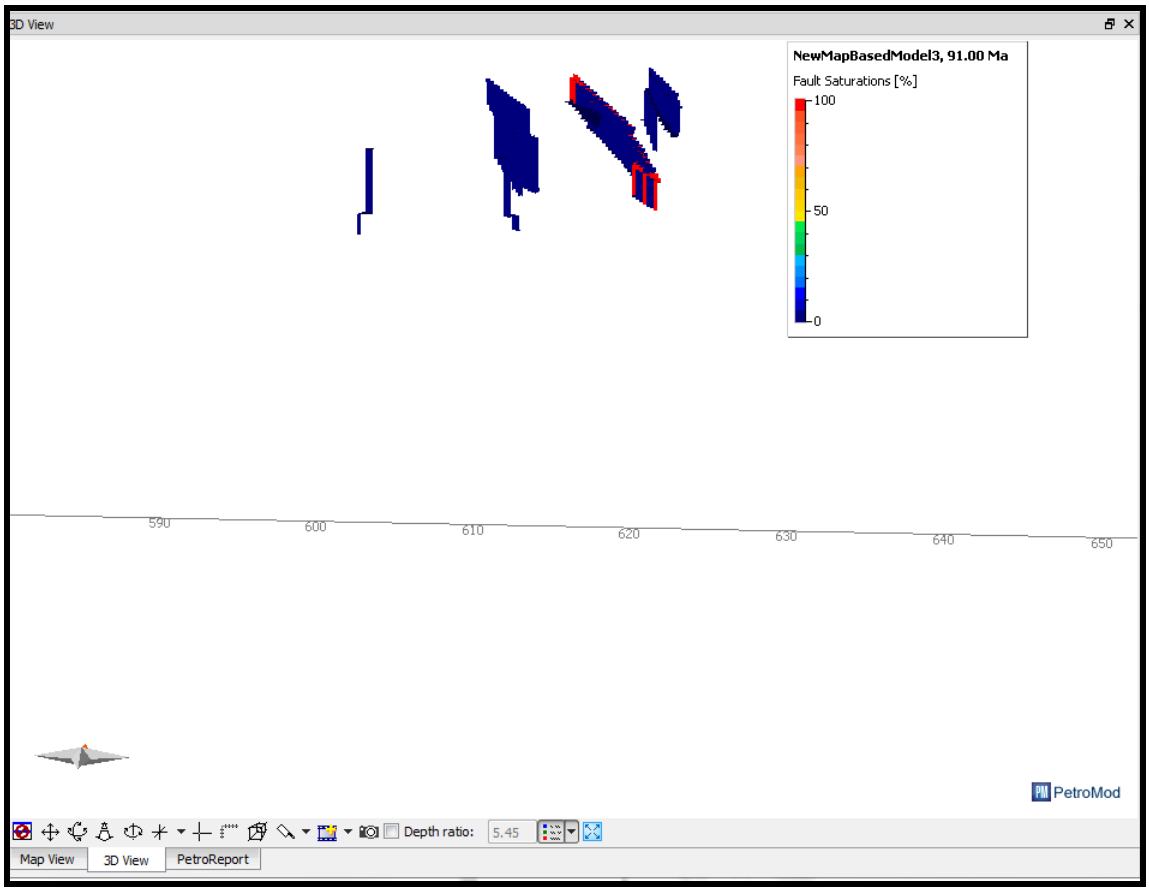

Figure7.17B: Partially saturated Listric Fault (124-65Ma) at 91Ma at 625.186km by 6749.50km grid. The listric fault has lost its saturation at 91Ma.

7.4.6.3 Faults Hydraulic Behaviours at 74Ma

In addition to the above observation, the listric fault was tested at 74Ma for hydrocarbon saturation, the geometry had increased upward and and gas stauration is limited to the upper section of the listric fault while the lower curvature had lost its saturation. This suggest that reactivation increase the permeability of the lower curvature of an older fault which let migration occurs, while newly formed fault, which is an extension of an older fault retains its sealing capacity which caused its saturation seen here (Figure 7.17C).

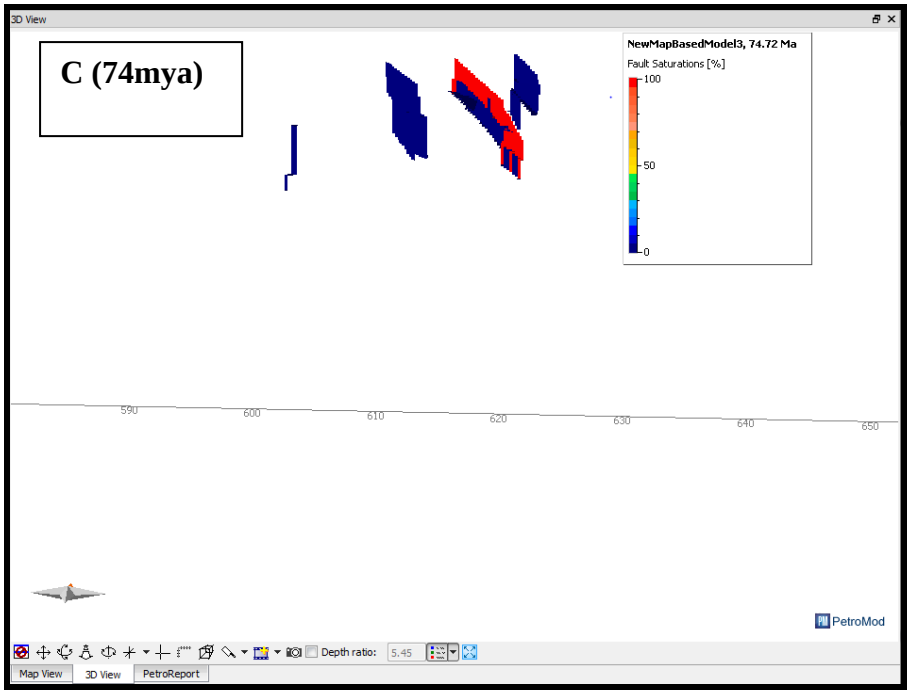

Figure 7.17 C: Partially saturated Listric Fault (124-65Ma) at 74Ma at 625.186km by 6749.50km grid. The listric fault has lost its saturation after reactivation while the younger fault which is an extension of the older listric fault, retains its sealing capacity.

Figure 7.17 C: Partially saturated Listric Fault (124-65Ma) at 74Ma at 625.186km by 6749.50km grid. The listric fault has lost its saturation after reactivation while the younger fault which is an extension of the older listric fault, retains its sealing capacity.

7.4.6.4 Faults Hydraulic Behaviours at 65Ma

At 65Ma, the listric fault could be said to be 15% gas saturated judging by partial saturation observed (Figure 7.17D). Beyond 65Ma, younger faults were observed to have no gas saturations, hence the listric fault here serves as a main control of gas migration. It also has a potential capacity to be a good trap but because of its epiosdic reactivation, already trapped hydrocarbon migrates further away from it.

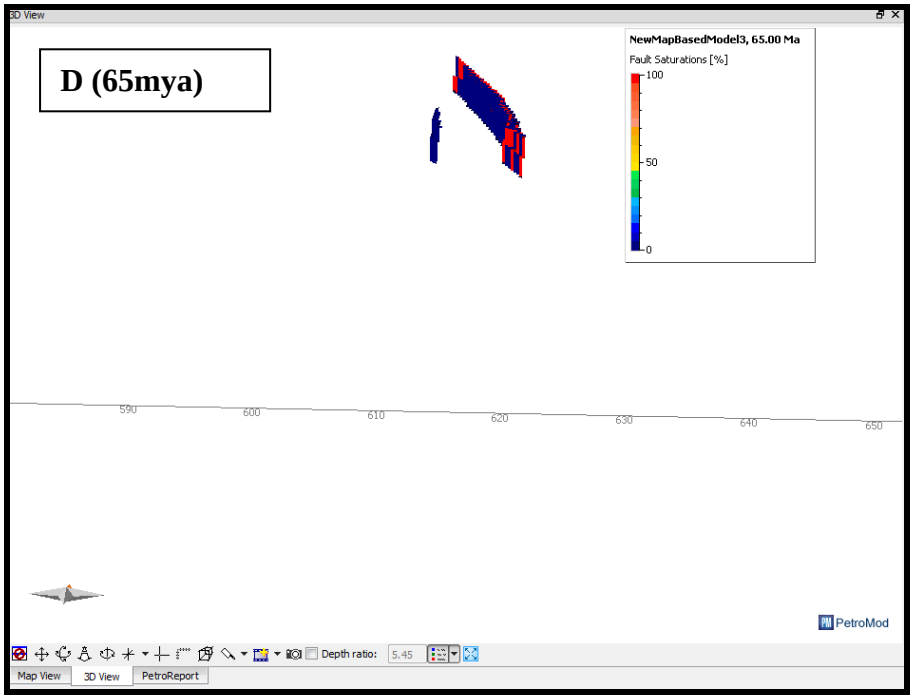

Figure 7.17D: Gas saturated Listric Fault (124-65mya) at 65Ma at 625.186km by 6749.50km grid. The listric fault has almost lost all its saturation earlier observed.

7.4.7 Evidence of Gas Escape at the Sea Floor.

3D forward numerical simulation shows the migration of gas from the source rock reaches the sea floor. The escape of gas to sea floor from deep seated source rock could be linked to the rock unit sealing capacity inconsistency in lateral geometry. In addition, reactivation of listric fault from time to time as observed here contributed significantly to escape of gas into seafloor (Figure 7.18).

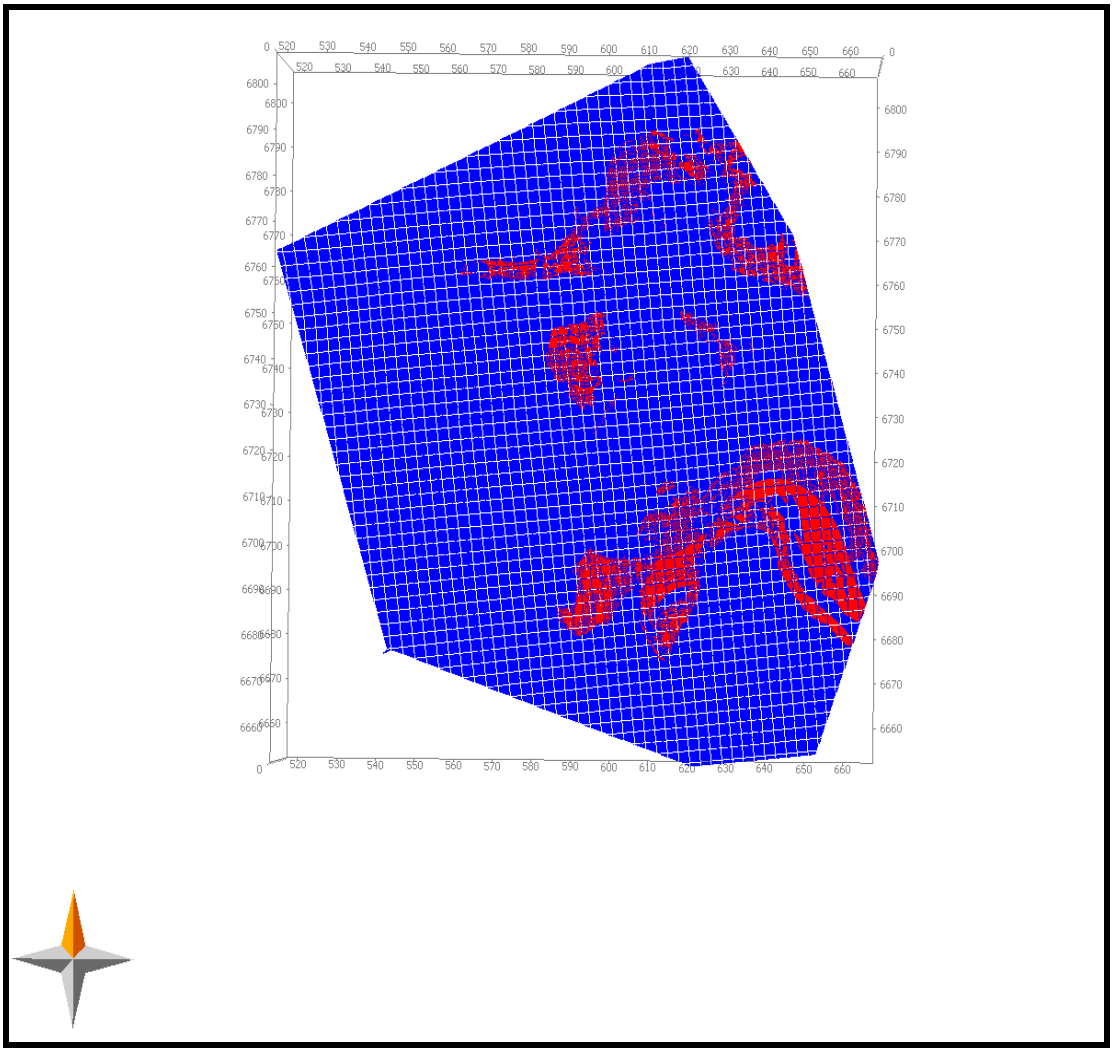

Figure 7.18: 3D Gas Migration pathways (Red) on the Sea Floor at 0.0mya.

7.4.8 Sensitivity Analysis

The sensitivity analysis of this study is based on the concept of opening up faults systems that evolved during the syn-rift and drift period while post rifts faults are closed. Reactivated listric normal fault which is the only hydrocarbon gas saturated fault among all faults modelled was initially opened and was closed to examine its hydraulic behaviour to gas saturation. However, the result on its sealing capacity remains the same through time as the fault remained saturated at 93Ma and lost its saturation at 91Ma suggesting that reactivation triggers leakage throughout the time. In addition, other reactivated faults that were kept open to observe possible saturation, were not saturated with hydrocarbon. In addition, the velocity model equation used to

generate depth maps used for the model is adequate and was corrected for, by ensuring it matched the corresponding formation tops and checkshots at each well position for the three wells used in the study. The velocity model correction is shown in Table 7.

7.5 Conclusions

The thermal (temperature) and organic maturity (Vitrinite Reflectance) evolution of source rock from 108, 95 and 0 Ma indicates the source rock reached a sufficient maturity stage just before 95 Ma, with VR values suggesting that transformation of organic matter began from the centre of the study area and expands towards the fringes of the study area around 108Ma. As at present day, 100% transformation of organic matter has generated hydrocarbon at the centre (graben fill) of the study area while the extreme fringes indicate lesser thermal maturity of organic matter compared to the centre, thereby suggesting good potential for source rock transformation into hydrocarbon at the fringes in the future. 1D calibration results in the northern part agrees with the 3D modeling that the source rock has not attained sufficient thermal maturity in the northern section of the study area (well AO-1). Source rock generation statistics reveal much of the gas was generated by secondary cracking and represents 91.8% of the bulk hydrocarbon generated. 3D modelling of hydrocarbon migration indicates that migration from the source rock is vertical as the expulsion patterns of the Barremian/Aptian source rock and Mid-Albian reservoirs are the same. In addition, the mid-Albian reservoir unit is gas prone and could be serving as carrier beds for oil in deeper parts of the basin as seen here, while the Cenomanian reservoir unit is dominantly gas prone. Evidence of gas escape at sea floor was concluded and this agrees with evidence of sea floor gas escape features that were observed in earlier chapters of this study. This study also reveals that a reactivated listric fault serves as the main control on gas migration pathways.

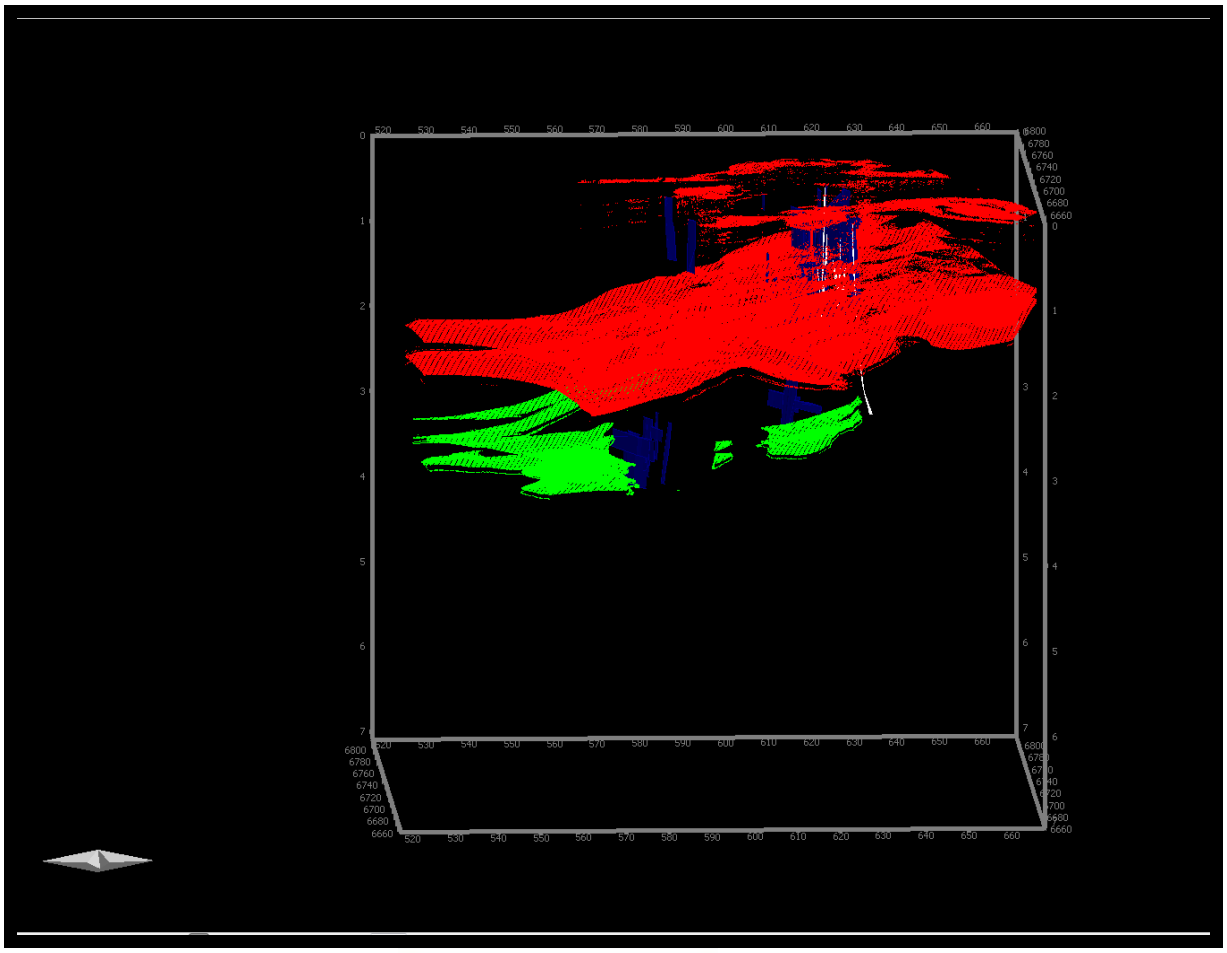

Figure 7.19: 3D Hydrocarbon Migration Model of the study area at present day with the depth horizon maps and hydrocarbon components; Gas-Red, Oil-Green but Fault Pillars-in blue. Water component has been filtered. Model grid lies between, X., 520Km and 660km and Y., 6670km by 6800km. Model size is 140km BY 130km.

Chapter Eight

Summary of Findings, Main Scientific Contributions, Conclusions and Recommendations.

8.1: Summary of Findings

a. An integrated approach was adopted using seismic stratigraphy and seismic attributes to investigate structural and stratigraphic features that could impact on migration pathways, culminating in 3D numerical simulation modelling of hydrocarbon generation and migration pathways. It is concluded that the integration of these methods proved adequate enough to meet the aim of this study which is to understand the controls on migration pathways, and the construction of a 3D hydrocarbon migration model to delineate prospective areas within the study area.

b. Litho-facies modelling indicates the presence of mouth bars and point bars within the study area, while the interpretation of gamma-ray logs signatures reveal the presence of fluvial channels and prograding delta-front sandstones deposit. Seismic stratigraphy analysis revealed three major seismic facies with internal configurations of parallel, chaotic and divergent patterns in all sequences, and the depositional environments is concluded to range between fluvial, fluvio-deltaic and shallow marine. A system of syn-rift listric, normal with antithetic faults formed due to post-rift tectonic events was seen and mapped on the seismic profiles. These sets of antithetic faults are seen within the Albian and Cenomanian sequence. The occurrence of antithetic faults points to the accommodation of an external stress with an opposite sense of shearing relative on the older fault plane, this caused the formation of younger faults dipping towards the older fault.

c. Mapping of super-sequences on seismic sections was done based on regionally correlative surfaces only across the study area. Erosional surfaces like truncation, toplap and onlap were observed. A stratigraphic pattern suggesting a prograding shelf-margin low-stand wedge was recognized. Isopach variation maps of the super-sequences show progressive thickening of the Albian sequence from North to South in the study area, while the Barremian-Aptian sequence is thicker than the Albian sequence because it occurs as graben-fill at the centre of the study area. Evidence of erosion at the flanks of the graben is apparent. In the same vein, Cenomanian and Turonian sequences thicken progressively from the North to South, coupled with westward (basinward) thickening of the sequences suggesting progradation. On the other hand, the Maastrichtian sequence also thickens from South to North, while the Cenozoic sequence thickens progressively from North to South. Progradation is evident during the Cenozoic as a result of basinward(westward) thickening of the sequence due to subsidence that followed the late Cretaceous margin uplift.

d. An attempt was made successfully to put the faulting system mapped here within the framework of stress history documented onshore in Namaqualand by Andreoli et al.,(2009) to understand the timing of formation of tectonics induced faulting. Namaqualand has been adjudged as the onshore equivalent of the Orange Basin and they both are likely to have similar structural styles. Studies reveal three bi-directional trends of faulting systems (NNW-SSE, NNE-SSW and WNW-ESE) based on dip and dip azimuths. The fault systems discovered in this study can be matched with the fault systems found on-shore by Andreoli et al., 2009 and can be dated as Cenozoic, late Cretaceous and Early Cretaceous respectively. In addition, a structural framework was constructed using major surfaces maps and faults, this revealed the occurrence of a compressional event in the late Cretaceous. This observation is similar to the one made on-shore by Andreoli et al., 2009 explaining possible compressional event associated with extensional faulting in the late Cretaceous.

e. Mapping of gas escape features which are a pointer to hydrocarbon migration pathways reveals fault- and stratigraphy-controlled gas chimneys and their sea floor expression as mud volcanoes and pock marks. In addition, a bright spot' anomaly exists on both sides of a listric fault within the Cenomanian super-sequence. The listric fault is suggested to have formed during the break-up of west Gondwanaland as it was seen detaching from the basement and dissects post-rift sequences to terminate at the top of Cenomanian sequence. The dissection of post-rifts sediments by a syn-rift fault is likely due to reactivation caused by episodic tectonic uplifts which affected the evolution of the Orange Basin.

f. A combination of seismic attributes (Impedance, Porosity and Frequency) was inversed to delineate possible carrier beds for hydrocarbon migration pathways and decipher hydrocarbon-bearing sediments. The seismic impedance inversion concept uncovers the presence of two parallel buried braided fluvial channels and calibration with a porosity cube reveals high porosity along these channels. The two parallel channels are 378m and 254m respectively. Variance attribute confirmed the observations made as regards the presence of pockmarks and mud volcanoes on the sea floor. The evidences of these are clearly seen on the horizontal variance attribute slice of the sea floor. Instantaneous frequency attribute around the listric fault reveals the presence of hydrocarbon-charged sediments on both sides of the listric fault. This point to possible leakage across the fault plane. In order to confirm this observation, a porosity calibration performed around the fault planes showed high porosity along the fault plane. This finding points to the presence of porous fault rocks along the plane. Iso-frequency was applied around the listric fault at 45 and 8Hz; while the former value shows excessive incoherency, the latter value suggests the likely presence of thin-bedded reservoir intervals based on the attenuation observed.

g. 3D numerical simulation of hydrocarbon-generation and -migration was performed using boundary conditions (SWIT, PWD and Heatflow) to get a handle on the timing of hydrocarbon generation and the formation of

migration pathways. The simulation results were calibrated with thermal and organic maturation data to test the model and sensitivity analysis was performed. The simulation results reveal that the Barremian-Aptian source rock unit already attained the gas window at the central portion and remained immature at the north-eastern section of the basin at 95Ma. Transformation ratio at present day indicates the source rock had already attained 100% transformation at the central portion and zero transformation in the extreme northern section of the study area. The higher maturation of the source rock unit at the central portion is due to:

a. 1. Huge overburden thickness within the graben fill which induced more thermal conductivity leading to early maturation of organic matter present within the source rock unit.
b. Subsequent uplift caused by Shona and Buvet hotspot during the Mid Cretaceous could have increased the radiogenic heat which contributed to the maturity of the source rock unit in the central portion before the 95Ma.

h. Source rock bulk generation and expulsion statistics indicate that 430.701,94 Mtons of gas and 38.399,53Mtons of oil representing 91.81% and 8.19% of organic matter had been converted into gas and oil respectively by thermal cracking (primary and secondary) by present day. Timing of hydrocarbon generation reveals that generation and accumulation within the source rock unit reaches its peak at the beginning of Cenomanian, while expulsion from the source unit reaches its peak at the late Cretaceous/early Cenozoic. The expulsion efficiency stands at 77% with gas being the main hydrocarbon expelled. The timing of peak expulsion coincides with the period of the Campanian-Maastrichtian uplift. It can be deduced that the late Cretaceous uplift had a role in the peak expulsion of hydrocarbon from the source rock unit and had no role in the generation of hydrocarbon within the source unit because the source rock unit had reached sufficient generation stage as early as 95Ma as mentioned in paragraph g. above.

i. 1D Calibration using thermal and organic maturation data from three wells (AE-1, AF-1 and AO-1) indicates that the modelled temperature data calibrate accurately with the temperature data for all three wells. However, the vitrinite reflectance calibration data show increased value variation in the Cenomanian and late Cretaceous for all wells. This implies additional sources of heat flow into the basin, the source of which is attributed to the uplift caused by Shona/Buvet hotspot in the Cenomanian and the late Cretaceous African super plume uplift. The former is localised while the latter affected the whole African margin. The 1D transformation ratio calibration of wells confirms the observation made from the 3D model which indicates that the source rock unit in the northernmost portion of the study area had not reached sufficient thermal maturation for hydrocarbon generation to occur. Specifically, the source unit within well AO-1 (northernmost well drilled) shows no transformation of kerogen into hydrocarbon thereby confirming the precision of the 3D model.

j. Transformation ratio reveals that AF-1 source rock units have attained 100% transformation while AE-1 has attained an estimated 60% transformation; well AO-1 has however not reached the hydrocarbon generation window by present day.

k. The 3D hydrocarbon migration model using the fault model with Albian and Cenomanian aged reservoirs as input reveals vertical migration of hydrocarbon from the Barremian/Aptian source pod which charges the overlying Albian and Cenomanian reservoirs. However, migration vectors in the Albian reservoir suggest it to be gas and oil prone; oil is seen migrating westward (deepwater) and gas is seen around the outer margin section of the Albian reservoir. The Cenomanian aged reservoir is totally gas prone.

l. The model result establishes that the listric fault trapped significant amounts of gas around 93 Ma because of the 100% saturation observed there. However, the gas escapes from this trap by 91 Ma suggesting that a breakthrough path exists along the fault which makes the leakage rate to be more than the

hydrocarbon charging rate. Further observation reveals gas trapping at 74 Ma and later escape by 65 Ma. The cause of this might be attributed to the continuous reactivation of the listric fault because of uplift events of the late Cretaceous. Therefore, the loss of gas saturation can be attributed to a tertiary migration phenomenon. In addition, the observation made here can be confirmed with the observation made at paragraph f above, which suggests high porosity along the listric fault plane at the present day. This means porous fault rock along the plane and that the listric fault is non-sealing as at present day.

m. Finally, observation on the sea floor shows gas migration reached the sea floor and the model indicates no accumulation of hydrocarbon occurred within any of the reservoir units modelled in this study.

8.2 Main Scientific Contributions and Economic Significance.

Previous suggestions made on hydrocarbon migration pathways and what controls them geologically in the Orange basin have been more of speculation than reality because it is based on mapping of faults and seismic gas escape features only. Furthermore, globally, the practises of modelling hydrocarbon migration pathways have been performed based on numerical simulation only, and there have been questions raised on the uncertainty of evaluating migration pathways based on this approach only.

In order to mitigate uncertainty from utilising numerical simulation approach only, this study adopts an integrated approach to mitigate the uncertainty and proves that a combination of seismic attributes could be integrated with 3D numerical simulation in studying the controls of hydrocarbon migration processes.

The above reasons necessitate the construction of a 3D hydrocarbon migration model integrated with observations from seismic attribute analysis to de-speculate and ascertain possible migration vectors of hydrocarbon and delineate prospective areas.

In addition, the integrated approach shows that a listric fault serves as a structural control on hydrocarbon migration pathways. The study also provides information on buried braided fluvial channels and mouth bars which may serve as hydrocarbon carrier beds and good reservoirs, implying a stratigraphic control on hydrocarbon migration pathways

This dissertation also provides detailed information about the integration of litho- and seismic-stratigraphy and its reliability in inferring depositional environment. The economic significance of this dissertation is the suggestion of prospective areas for gas and oil deposits.

This study also reveals that prospecting for oil might be more feasible within the Albian sequence in the deep waters. Basin floor fans, turbidites or slope fans might be the ideal targets as the 3D migration model suggests migration of oil westward of the basin into deep waters.

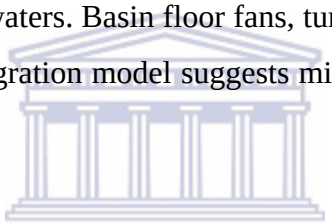

8.3 Conclusions and Recommendations

The problem statement of this research as mentioned in **Paragraph 1.6.1** stemmed from previous studies that are related to hydrocarbon migration in the Orange Basin which was done in the southern part. The previous studies focused on the mapping of gas escape features that are at close proximity to structural and stratigraphic features in order to establish any relationship or link between these features and gas escape features mapped. In addition, 3D forward numerical modelling of hydrocarbon migration vectors to investigate its interactions with faults and stratigraphic features was not performed, hence migration processes were not properly detailed.

This approach made observations from those studies more speculative than reliable as it is crucial in hydrocarbon migration studies that the timing of hydrocarbon generation and timing of regional faults formation are understood. In addition, there is a need to understand how faults and stratigraphic features interfere with the migration

pathways, as this will suggest new prospective areas and the causes of gas escape features seen. This study adopted a combination of approaches to resolve this.

In this study, it is concluded that mouth bars and braided fluvial channels as interpreted from log signatures and seismic facies, and as observed in **figures 4.9E and F, figures 6A and B** respectively might be serving as carrier beds thus exerting stratigraphic control for hydrocarbon migration. Many fluvio- deltaic depositions like mouth bars commonly display complex spatial patterns with resultant variability in connectivity and tortuosity. Poor connectivity and variable tortuosity could inhibit hydrocarbon migration, thereby exerting additional pressure within the pore spaces. This could result in hydrostatic pressure compartmentalization as seen within the Cenomanian sequence **(Appendix 1).** The study also suggested that most regional faults could have been formed during the breakup of the west Gondwana in the late Jurassic/early cretaceous, during late Cretaceous associated with crustal uplift and in the Miocene uplift of the Cenozoic. The late Cretaceous uplift led to the mild basin inversion in the study area, as seen from the structural framework **Figures 5.26 (A-D),** this coincides with the period of peak of hydrocarbon expulsion from the source rock as seen in **Figures 7.13 A and B**. This suggests increased heat flow during this period. This increase in heat flow could have been either as a result of African super plume upwelling during this period which affected the whole African continental margin, or due to high confining pressure caused by overburden thickness occasioned by high sedimentary rates or concentration of high thermally conductive rock forming minerals within the source unit. Since the late Cretaceous uplift affected the whole African continental margin, the increased heat flow is probably sourced from it. The high heat flow is deduced to have increased the expulsion efficiency of the Barremian/Aptian source rock and this is equally evident with the 1D vitrinite reflectance calibration in **Figures 7.1A, 7.2A and 7.3A**. The VR calibrated values (in cross points+) indicates higher thermal maturity than the modelled VR (straight line) during the late Cretaceous period. The study also resolved, by integrating all methods mentioned, that reactivation of the listric fault serves as the main control on gas leakages in the study area. The listric fault shows a bright spot anomaly on either side of the plane as observed in **Figure 5.18 A and B,** also, instantaneous frequency attenuation was observed on either side of the same fault as seen in **figure 6.5A and**

B. In addition, numerical simulation shows 100% gas saturation of the same listric fault at 93Ma as seen in **figure 7.16A.** The breakthrough path along the listric fault is modelled to have occurred at 91Ma as seen in **figure 7.16 B**, thereby concluding that the occurrence of gas escape features on the sea floor and the subsurface could have been sourced from the continuous listric fault reactivation. This study recommends that deep-water reservoirs within the Albian sequence are targeted for oil prone reservoirs because of the westward migration of oil as seen from the model (**Figures 7.14 A, B and C)**. In addition, Cenomanian reservoirs should be targeted for gas prospects as seen in **Figures 7.16 A,B and C** while a regional Petrophysical evaluation of Cenomanian reservoirs is also recommended to delineate better potential gas play with higher accumulation chance. The 3D model, however, revealed no accumulation of hydrocarbon within the study area.

References

Adekola, S.A., 2010. Integrated Approach to solving Reservoir problems and Evaluations using Sequence Stratigraphy, Geological Structures and diagenesis in Orange basin, South Africa. Unpublished PhD thesis, University of the Western Cape, South Africa, 203pp.

Aki, K. and Richards, P. G., 1980. Quantitative seismology: Theory and methods (Eds.), W. H. Freeman and co., New York, 1, 557pp.

Aldrich, J., Zilinski, R., Edman, J., Leu, W., Berge, T. and Corbett, K., 2003. Documentation of a new petroleum system in the South Atlantic (Abstract). American Association of Petroleum Geologists Annual Convention, May, 11 – 14, 2003.

Allen, J.L. and Peddy, C.P., 1993. Amplitude variation with offset: gulf coast case studies. In: Geophysical Developments Series, (Ed. by F.K.Levin). Journal of the Society of Exploration Geophysicist, 4, 126 pp.

Andreoli, M.A.G., Scheepers, J., Stengel, I., Viola, G., Kounov, A., Cloete, M. and McCarthy, T.S., 2009. Intraplate stress, seismicity and neotectonics in western southern Africa: a link to the African Super plume: 10th SAGA Biennial Technical meeting and Exhibition, Wild Coast 24-26 October 2009, 1-4., Okhlahoma, United States.

Anderson, E.M., 1951. The Dynamics of Faulting and Dyke Formation with Application to Britain, 2nd ed., 206 pp., Oliver and Boyd, Edinburgh.

Anka, Z., Ondrak, R. and Clausen, L.F. 2009. Modelling hydrocarbon generation, migration and present-day hydrocarbon seepage from the deep offshore slope of Angola. American Association of Petroleum Geologists Search and Discovery Article #90090. Web accessed 25th August 2011.

Athy, L. F., 1930. Density, porosity, and compaction of sedimentary rocks, American Association of Petroleum Geologists Bulletin., 14, 1–22.

Avseth, P., 2011. Explorational rock physics - the link between geological processes and geophysical observables. In Petroleum Geoscience: From Sedimentary Environments to Rock Physics. Springer-Verlag Berlin Heidelberg 2011.

Badley, M.E., 1985. Practical Seismic Interpretation: International Human Resources Development Corporation, Boston, 266 pp.

Bally, A.W., 1982. Atlas of Seismic Stratigraphy, American Association of Petroleum Geologists Studies in Geology no. 27, 300 p.

Barton, K.R., Muntingh, A. and Noble, R.D.P., 1993. Geophysical and Geological Studies Applied to the Hydrocarbon Exploration on the West Coast Margin of South Africa, Extended Abstracts of the third International Congress of the Brazilian Geological Society, Rio De Janeiro, 1993.

Barton,P., and Wood,R., 1984. Tectonic evolution of the North Sea Basin: Crustal Stretching and subsidence: Royal Astronomical Society Geophysical Journal, 79, p 987-1022.

Bortfield, R., 1961. Approximations to the reflection and transmission coefficients of plane wave longitudinal and transverse waves: Journal of Geophysical Prospecting. 9, 485-502.

Boyd, D., Anka, Z., Di primio, R., Kuhlmann, G., and De wit, M.J., 2011. Passive margin evolution and controls on natural gas leakage in the orange basin, South Africa. South African Journal of Geology,114, 415-432.

Broad, D.S., Jungslager, E.H.A., Mclachlan, I.R. and Roux, J., 2007. Offshore Mesozoic Basins. In M.R Johnson, C.R Anhaeusser and R.J. Thomas (Editors), the Geology of South Africa/Council for Geoscience, 553-565.

Brown, L.F., Brown, L.F, Jr., Benson, J.M., Brink, G.J., Doherty, S., Jollands, A., Jungslager, E.H.A., Keenan, J.H.G., Muntingh, A. and Van Wyk, N.J.S., 1996. Sequence stratigraphy in offshore South Africa divergent basins. An atlas on exploration for cretaceous lowstand traps by SQEKOR (Pty) Ltd. American Association Petroleum. Geologists Study. In Geology. 41, pp 184.

Bubb, J.N. and Hartlelid, W.G., 1978. Seismic stratigraphy and global changes of Sea level, Part 10: Seismic Recognition of Carbonate build ups. American Association of Petroleum Geologists Bulletin.

Buck, W.R., 1988. Flexural rotation of normal faults: Tectonics. 7, 959–973.

Bush, D. C. F., Flanagan, G. C. and George, F. 1972. Geometry of Sandstone Reservoir Bodies. Shell Oil Internal Reports, 1972.

Butler, R.W.H. and Paton, D.A., 2010. Evaluating lateral compaction in deepwater fold and thrust belts: How much are we missing from "nature's sandbox"? Geological Society of South Africa, 20, 4–10.

Campher, C., 2009. Geological Modelling of the offshore Orange Basin, west coast of South Africa. Unpublished M.sc thesis, University of the Western Cape. 199pp

Cartwright,J., Haddock,R., and Pinheiro, R., 1993. The lateral extent of sequence boundaries, in Williams, G., and Dobb, A., eds., Tectonics and Sequence Stratigraphy: Geological Society of London, Special Publication 71, p.15-34

Castagna, J., Sun, S. and Siegfried, R., 2003. Instantaneous spectral analysis: Detection of low-frequency shadows associated with hydrocarbons. The Leading Edge, February 2003.

Castagna, J.P., Swan, H.W. and Foster, D.J., 1998. Framework for Amplitude Versus Offset gradient and intercept interpretation. Journal of Geophysics, 63, 948-956.

Castagna, J. P. and Swan, H. W. 1997. Principles of AVO cross plotting. The leading edge. 16, 4: 337-334.

Catuneanu, O., and Eriksson, P.G., 2007. Sequence stratigraphy of the Precambrian. Journal of Gondwana Research 12, 4: 560-565.

Cerveny, K., Davies, R., Dudley, G., Fox, R., Kaufman, P., Knipe, R.J. and Krantz, B., 2004. Reducing uncertainty with Fault-Seal analysis. Oilfield Review, 16, 4: 38-51.

Chambers, R. L. and Yarus, J. M., 2002: Quantitative use of seismic attributes for reservoir characterization. Canadian Society Exploration Geophysics Recorder. 6, 15 –25.

Chen, G., Matteucci, G., Fahmi, B. and Finn, Ch., 2008. Spectral-Decomposition response to reservoir fluids from a deepwater West Africa reservoir. Journal of Geophysics 73, 23-30.

Chiburis, E.F., 1987. Studies of amplitude versus offset in Saudi Arabia: 57th Annual International Meeting. Society of Exploration Geophysics. Expanded Abstract, 614-616.

Chopra, S. and Marfurt, K. 2006. Seismic Attributes–a promising aid for geologic prediction. Canadian Society Exploration Geophysics Recorder. 31, 110-120.

Christie-Blick, N., Mountain, G.S. and Miller, K.G., 1990. Seismic stratigraphic record of sea level change: in Sea-Level change. National Academy of Sciences studies in Geophysics: Washington, D.C., National Academy Press. 116–140

Clemson, J., Cartwright, J., Booth, J., 1997. Structural segmentation and the influence of basement structure on the Namibian passive margin. Journal of the Geological Society of Namibia. 154, 477–482.

Cooke, D and Cant, J. 2010 .Model-based Seismic Inversion: Comparing deterministic and probabilistic approaches. Canadian Society of Exploration Geophysicsts. 35, 4.

Consentino, L., 2001. Integrated Reservoir Studies. Technip, Paris, 310p

Cross, T. A. and Lessenger M.A., 1988 "Seismic stratigraphy." Annual Review of Earth and Planetary Sciences.16, p.319.

Davis, A.M., 1992. Shallow gas: an overview. In: Davis, A.M. (ed.) Methane in marine sediments, Continental Shelf Research 12,1077-1079.

de Vera, J., Granado, P. and McClay, K., 2010. Structural evolution of the Orange Basin gravity-driven system, offshore Namibia. Journal of Marine and Petroleum Geology, 27, 223-237.

Dingle, R.V.,1993. Structural and sedimentary development of the continental margin off southwestern Africa Community. Geological Survey Namibia., 8, 35–43.

Dingle, R.V., Siesser, W.G., Newton, A.R., 1983. Mesozoic and Tertiary Geology of Southern Africa. A.A. Balkema, Rotterdam, 355 pp.

Elnady, M., Ramadan, F,S., Hammad, M.M. and Lotfy, N.M., 2015. Evaluation of organic matters, hydrocarbon potential and thermal maturity of source rocks based on geochemical and statistical methods: Case study of source rocks in Ras Gharib oilfield, central Gulf of Suez, Egypt. Egyptian Journal of Petroleum Geology. 24, 2: 203-211

Emery, K.O. and Uchupi, E. 1984. The Geology of the Atlantic Ocean. Springer-Verlag, New York Incorporation.

Eppelbaum, L. V., Katz, Y. I. and Ben-Avraham, Z. 2012. Israel-Petroleum Geology and Prospective Provinces. American Association of Petroleum Geologist European Newsletter, 4, 4-9

Fader, G.B.J., 1991. Gas-related sedimentary features from the eastern Canadian Continental Shelf. Journal of Continental Shelf Research, 11, 1123-1153.

Farfour, M., Yoon, W.J. and Kim, J. 2015. Seismic attributes and acoustic impedance inversion in interpretation of complex hydrocarbon reservoirs. Journal of Applied Geophysics, 114, 68-80.

Fatti, J.L., Smith, G.C., Vail, P.J., Strauss, P.J., and Levitt, P.R. 1994. Detection of gas in sandstone reservoirs using AVO analysis: A 3D seismic case history using the Geostack technique. Journal of Applied Geophysics, 59, 9: 1362-1376.

Field, M.E. and Jennings, A.E. 1987. Seafloor gas seeps triggered by a northern California earthquake. Marine Geology, 77, 39-51.

Francis, A., 2006a, Limitations of deterministic and advantages of stochastic Seismic inversion: Recorder, 30, 5–11.2006a,

Futalan, K., Mitchell, A., Amos, K. and Backe, G., 2012. Seismic Facies Analysis and Structural Interpretation of the Sandakan Sub-basin, Sulu Sea, Philippines. American Association of Petroleum Geologists Search and Discovery Article #30254 (2012).

Gerrard, I., Smith, G.C., 1982. Post-Paleozoic succession and structure of the south-western African continental margin. In: Watkins, J.S., Drake, C.L. (Eds.), Studies in Continental Margin Geology: American Association of Petroleum Geologists Memoir, 34, 49-74.

Granado, P., de Vera, J. and McClay, K.R., 2009. Tectonostratigraphic evolution of the Orange Basin, South-West Africa. Works of Geology, University of Oviedo, 29; 321-328 (2009).

Guiraud, R. and Bosworth, W., 1997. Senonian Basin inversion and rejuvenation of rifting in Africa and Arabia; synthesis and implications to plate-scale tectonics. Journal of Tectonophysics, 282, 39-82.

Guiraud, R., Bosworth, W., Thierry, J., Delplangue, A., 2005. Phanerozoic geological evolution of northern and central Africa: an overview. Journal of African Earth Sciences, 43, 83-143.

Gusterhuber, J., Hinsch, R., Linzer, H-G., and Sachsenhofer, R., 2013. Hydrocarbon generation and migration from sub-thrust source rocks to foreland reservoirs: The Austrian Molasse Basin. Austrian Journal of Earth Sciences. 106, 115-136

Hantschel, T., Kauerauf, A. and Wygrala, B., 2000. Finite Element analysis and ray tracing modelling of petroleum migration. Journal of Marine and Petroleum Geology.17, 815-820.

Hardage, B.A., Carr, D.L., Lancaster, D.E., Simmons, J.L., Hamilton, D.S., Elphick, R.Y., Oliver, K.L. and Johns, R.A., 1996 . 3D seismic imaging and seismic attribute analysis of genetic sequences deposited in low accommodation conditions. Journal of Geophysics 61, 1351–1362.

Hartwig, A., Anka, Z., and Di primio, R., 2012. Evidence of a widespread paleo-pockmarks field in the Orange Basin: An indication of an early Eocene massive fluid escape event. Journal of Marine Geology, 332–334, 222-234.

Hirsch, K.K., Scheck-Wenderoth, M., Paton, D.A., Bauer, K., 2007. Crustal structure beneath the Orange Basin, South Africa. South African Journal of Geology 110 (2-3), 249–260.

Jasinki, J.A., 1957. In Cartwright, J. A., Haddock, R. C., and Pinheiro, L. M. 1993. The lateral extent of sequence boundaries. Geological Society of London, Special Publications, 71(1), 15-34.

Jikelo, A.N. 1999. Oil and Gas potentials of the South African offshore basins. Journal of Africa Earth Sciences, GSA 11, abstracts 33. (PRI 49).

Judd, A.G., 1990. Shallow gas and gas seepages: a dynamic process? In: Ardus, D.A. & Green, C.D. (eds) Safety in offshore drilling – the role of shallow gas surveys. Advances in Underwater Technology, Ocean Science and Engineering 25, 27-50.

Judd, A.G. and Hovland, M. 1992. The evidence of shallow gas in marine sediments. Journal of Continental Shelf Research, 12, 1081-1095.

Jungslager, E.H.A., 1999 Petroleum habitat of the Atlantic margin of South Africa. In: Cameron, N.R; Bate, R.H; Clure, V.S; (Eds). The oil and gas habitat of South Atlantic. Geological Society of London. 153-168pp.

Kamp. J.J. and Turner, G.M.,1990. Pleistocene unconformity-bounded shelf Sequences (Wanganui Basin, New Zealand), correlated with global isotope record. Journal of Sedimentary Geology, 68, 4421-4436.

Kauerauf, A.I. and Hantschel, T. 2009. Fundamentals of Basin and Petroleum Systems modelling, 245pp.

Khilyuk, L. 2000. Gas migration: events preceding earthquakes. Houston, Texas.: Gulf Publishing 2000. ISBN 10: 0884154300 / ISBN 13: 9780884154303.

King, L.H. and Maclean, B., 1970. Pockmarks on Scotian Shelf: Geological Society of America Bulletin, 81, 3141-3148.

Klerkx, J., De Batist M., Poort ,J., Hus R., Van Rensbergen, P., Khlystov, O. and Granin, N., 2006.Tectonically controlled methane escape in Lake Baikal. In: Lombardi S, Altunina LK, Beaubien SE (eds) Advances in the geological storage of carbon dioxide. Springer, Dordrecht, pp 203–219.

Kopf, A.J., 2003. Global methane emission through mud volcanoes and its past and present impact on the Earth's climate. International Journal of Earth Sciences. 92, 806– 816.

Knott, C.G., 1899. Reflection and refraction of elastic waves with seismological applications: Phil. Mag., 48, 64-97.

Krumbein, W.C. and Sloss, L.L., 1963. Stratigraphy and Sedimentation, Freeman and Co. San Francisco.

Kuhlmann, G., Adams, S., Campher, C., van der Spuy, D., di Primio, R. and Horsfield, B., 2010. Passive margin evolution and its controls on natural gas leakage in the southern Orange Basin, block ¾, offshore South Africa. Journal of Marine and Petroleum Geology, 27, 973–992.

Lampe, C., Song, G., Cong, L. and Mu, X. 2012. Fault control on hydrocarbon migration and accumulation in the Tertiary Dongying depression, Bohai Basin, China. American Association of Petroleum Geologists Bulletin 96, 6: 983-1000.

Lindseth, R. O., 1979, Synthetic sonic logs : a process for stratigraphic interpretation: Journal of Geophysics, 44. 1; 3, 26.

Light, M. P. R., Maslanyj, M. P., Greenwood, R. J. And Banks, N. L. 1993: Seismic sequence stratigraphy and tectonics offshore Namibia. In: G. D. WILLIAMS and A. DOBB (eds): Tectonics and seismic sequence stratigraphy. Geological Society of London Special Publications, 71, 163-191.

Lowell, J. D., 1970. Antithetic faults in upthrusting. America Association of Petroleum Geologists Bulletin, 54, 1946-1950.

Macdonald, D., Gomez-Perez, I., Franzeze, J., Spalletti, L., Lawver, L.,Gahangan, L, Dalziel, I., Thomas, C., Trewin, N, Hole, M. and Paton, D., 2003. Mesozoic Break-up of SW Gondwana: Implication for Regional Hydrocarbon Potential of Southern \

South Atlantic. Journal of Marine and Petroleum Geology, 20, 287–308.

Madiba, G.B. and Mcmechan, G.A., 2003. Seismic Impedance inversion and interpretation of a gas carbonate reservoir in the Alberta Foothills. Western Canada. Journal of Applied Geophysics, 68, 5; 1460-1469

Magoon, L.B., and Beaumont, E.A., 1999. Petroleum system, in Beaumont, E.A.and Foster, N.H., eds., Exploring for oil and gas traps: American Association of Petroleum Geologists Treatise of Petroleum Geology, 3, 3.1-3.34.

Magoon, L. B., and Dow, W.G. 1994. The petroleum system, in Magoon, L. B, and W. G. Dow, eds., The petroleum system—from source to trap: America Association of Petroleum Geologist Memoir, 60, 3-24.

Mahieux G., Proust J.-N., Tessier B. and DeBatist M., 1998. Comparison between high-resolution seismic and sequence stratigraphic approaches applied to the Upper Jurassic deposits of the Dover Strait area (Northern France). Journal of Marine and Petroleum Geology, 15 (4), 329-342.

Martel, T., 2013. Pitfalls in Assessing Lacustrine Shale versus Marine Shale Prospects. Adapted from oral presentation given at American Association of Petroleum Geologists Annual Convention and Exhibition, Pittsburgh, Pennsylvania, May 19-22.

Mayorgal, T., Calle-Andrés E., Freddy, M. N., and Jorge, R., 2012. Seismic-Structural Interpretation, on the Identification of Possible Causes in the Formation of Gas Chimneys in Colombia's Offshore Adapted from poster presentation at America Association of Petroleum Geologists Annual Convention and Exhibition, Long Beach, California, April 22-25, 2012.

McKenzie, D., 1978. Some remarks on the development of sedimentary basins: Earth and Planetary Science Letters, 40, 1; 25–32.

McMillan, I.K., 2003. Foraminiferally defined biostratigraphic episodes and sedimentation pattern of the Cretaceous drift succession (Early Barremian to Late Maastrichtian) in seven basins on the South African and southern Namibian continental margin. South African Journal of Science 99, 537–576

McQuillin, R. and Fannin, N.G.T., 1979. Explaining the North Seafloor. New Scientist 1163, 90-92.

Menzies, M.A., Klemperer, S.L., Ebinger, C.J., Baker, J., 2002. Characteristics of volcanic rifted margins, in: Menzies, M.A., Klemperer, S.L., Ebinger, C.J., Baker, J. (Eds.), Volcanic Rifted Margins. Geological Society of America Special issue, Boulder, Colorado, 1-14.

Miller, K. G., Kopp, R. E., Horton, B. P., Browning, J. V., and Kemp, A. C. 2013. A geological perspective on sea-level rise and its impacts along the US mid-Atlantic coast. Journal of Earth's Future, 1(1), 3-18.

Mitchum Jr., R.M., Vail, P.R. and Thompson III, S., 1977. Seismic stratigraphy and global changes of sea-level. Part 2: the depositional sequence as a basic unit for stratigraphic analysis. In: Payton, C.E. (Ed.), Seismic Stratigraphy—Applications to Hydrocarbon Exploration Memoir, 26, American Association of Petroleum Geologists, 48–62

Morgan, W.J., 1971. Convection plumes in the lower mantle. Journal of Nature, 230, 42-43.

Nurnberg, D. and Muller, R.D., 1991. The tectonic evolution of the South Atlantic from Late Jurassic to present. Journal of Tectonophysics 191, 27–53

O'Brien, G. W., Lawrence, G. M., Williams, A. K., Glenn, K., Barrett, A. G., Lech, M. and Summons, R. E., 2005. Yampi Shelf, Browse Basin, North-West Shelf, Australia: A test-bed for constraining hydrocarbon migration and seepage rates using

combinations of 2D and 3D seismic data and multiple, independent remote sensing technologies, Journal of Marine and Petroleum Geology, 22, 4: 517-549.

Onyekuru, S. O., Ibelegbu, E. C., Iwuagwu, J. C., Essien, A. G., & Akaolisa C. (2012), "Sequence Stratigraphic Analysis of XB Field, Central Swamp Depobelt, Niger Delta Basin, Southern Nigeria." International Journal of Geoscience, 3,237-257.

Ostrander, W.J., 1984. Plane-wave reflection coefficients for gas sands at non normal angles of incidence: Journal of Geophysics, 49, 1637-1648.

Paton, D.A., Van der Spuy, D., Di Primio, R. and Horsfield, B., 2008. Tectonically Induced adjustment of passive-margin accommodation space; influence on the hydrocarbon potential of the Orange Basin, South Africa. American Association of Petroleum Geologists Bulletin, 92, 5: 589-609.

Partridge, T.C., 1997. Late Neogene uplift in eastern and southern Africa and its paleo climatic implications .W.F. Ruddiman (Ed.), Tectonic Uplift and Climate Change, Plenum Press, New York (1997), pp. 63–86

Partyka , G., Gridley, J., Lopez, J.A., 1999.Interpretational applications of spectral decomposition in reservoirs characterization. Leading Edge 18, 353-360.

Pegrum, R.M., Ødegård, T., Bonde, K. and Hamann, N.E., 2001.Exploration in the Fylla area, SW Greenland (abstract). UNIGRA/American Association of Petroleum Geologists International Conference, St. Petersburg, Russia, 15–18 July 2001.

Peters, K. E., Curry, D.J. and Kacewicz, M., 2012. An overview of basin and petroleum system modeling: Definitions and Concepts, in K. E. Peters, D. J.Curry, and M. Kacewicz, eds., Basin Modeling: New Horizons in Research and Applications: American Association of Petroleum Geologists Hedberg Series, 4, 1–16.

Pepper, A. S. and Corvi, P.J., 1995. Simple kinetic models of petroleum formation. Part I: Oil and Gas generation from kerogen. Journal of Marine and Petroleum Geology, 12, 3: 291-319.

Petroleum Agency South Africa Report. 2006. Petroleum Exploration Information and Opportunities: Petroleum Agency Brochure, 32pp.

Pollack, H. N. and Chapman, D. S.,1977. The flow of heat from the Earth's interior: Scientific American, 237, 2: p. 60–76

Prasad, M., Mukerji, T., Reinstaedtler, M., Bosch, R., Arnold, W. 2009. Acoustic Signatures, Impedance Microstructure, Textural Scales, and Anisotropy of Kerogen-rich Shale. Society of Petroleum Engineers Annual Technical Conference and Exhibition, New Orleans, LA, 4–7.

Qi Pang, X., Xi Li, Yu. and Xue jiang, Z., 2003. Key geological controls on migration and accumulation for hydrocarbons derived from mature source rocks in Qaidam basin. Journal of Petroleum Science and Engineering 41, 79-95.

Ramana, M.V., Ramprasad , T., Kamesh Raju , K.A., and Desa , M., 2007. Occurrence of gas hydrates along the continental margins of India, particularly the Krishna-Godavari offshore basin. International Journal of Environmental Studies, 64, 6.

Ramsayer, G.R., 1979. Seismic stratigraphy, a fundamental exploration tool: 11th Annual Offshore Technology Conference Proceedings, 101-109.

Reeves, C., and de wit, M., 2000. Making ends meet in Gondwana: retracing the transforms of the Indian Ocean and reconnecting continental shear zones. Terra Nova, 12, 272-280.

Rice, D.D. and Claypool, G.E., 1981. Generation, accumulation, and resource potential of biogenic gas. Bulletin of the American Association of Petroleum Geologists 65, 5-25.

Richards, M.A., Duncan, R.A. and Courtillot, V.E., 1989. Flood Basalts and Hot-Spot Tracks: Plume Heads and Tails. Journal of Science 246, 103-107.

Rider, M.H., 1986. The Geological Interpretation of Well Logs: John Wiley and Sons, New York, NY, 175 pp

Roberts, H. H., Kohl, B., Menzies, D., and Humphrey, G. D. 1999. Acoustic Wipe-Out Zones - A Paradox for Interpreting Seafloor Geologic/Geotechnical Characteristics. An Example from Garden Banks 161. Offshore Technology Conference. doi:10.4043/10921-MS

Roux, J., van der Spuy, D. and Singh, V., 2004, Deepwater drilling on the way off South Africa. Offshore, February 2004.

Rowan, M.G., Peel, F.J. and Vendeville, B.C., 2004. Gravity-driven fold belts on passive margins. In: McClay, K.R. (Ed.), Thrust Tectonics and Hydrocarbon Systems. American Association of Petroleum Geologists Memoir 82, 157–182.

Rutherford, S. R., and Williams, R. H. 1989. Amplitude-versus-offset variations in gas sands: Journal of Applied Geophysics, 54, 680–688.

Rutqvist, J., Rinaldi, A. P., Cappa, F and Moridis, G.J. 2013. Modelling of fault reactivation and induced seismicity during hydraulic fracturing of shale-gas reservoirs, J. Pet. Sci. Eng., 107, 31–44, doi:10.1016/j.petrol.2013.04.023.

Salomon,E., Koehn, D., Passchier, C., Hackspacher, P.C. and Glasmacher, U.A. 2014. Contrasting Stress fields on correlating margins of the South Atlantic. Gondwana Research 28, 1152-1167.

Sangree, J.B. and Widmier, J.M., 1979. Interpretation of depositional facies from seismic data. Geophysics, 44, 2,131-160.

Sangree, J. B. and Widmier, J. M., 1977. Seismic interpretation of clastic depositional facies. American Association of Petroleum Geologist Memoir, 26, 165-184.

Schmidt, S., 2004. The Petroleum Potential of the Passive Continental Margin of South-Western Africa – A Basin Modelling Study. Unpublished PhD thesis, RWTH Aachen, 161 pp.

Schneider, F., Potdevin, J.L., Wolf, S. and Faille, I., 1996. Mechanical and Chemical Compaction model for Sedimentary basin simulators. Journal of Tectonophysics, 263, 307-317.

Schroot, B.M. and Schüttenhelm R.T.E., 2003. Expressions of shallow gas in the Netherlands North Sea Netherlands Journal of Geosciences / Geologie en Mijnbouw 82(1): 91.

Sekiguchi, H. and Ohta H., 1977. Induced anisotropy and time dependency in clays. In: Murayama S, Schofield AN, editors. Proceedings of the 9th ICSMFE 1977; Specialty Session 9, p. 229.

Séranne, M. and Anka, Z. 2005: South Atlantic continental margins of Africa: a comparison of the tectonic vs. climate inter-play on the evolution of Equatorial West Africa and SW Africa margins. Journal of Africa Earth Sciences. 43, 283-300.

Schlumberger, 2009. Schlumberger Oil Field Glossary: Basin and Petroleum System Modelling. URL https://www.slb.com/~/media/Files/resources/oilfield_review/ors09/sum09/basin_petroleum.ashx

Sinha, S., Routh, P.S., Anno, P.D., and Castagna, J.P.,2005. Spectral Decomposition of Seismic Data with Continuous-wavelet transforms. Journal of Geophysics, 70, 19-25.

Sloss, L.L., 1963. Sequence in the cratonic interior of North America. Geological Society of America Bulletin 74, 93–114.

Snedden, J. W. and Sarg, J.F., 2008. Seismic Stratigraphy-A Primer on Methodology, American Association of Petroleum Geology Search and Discovery Article #40270 (2008).

Spencer, J.E., 1984. The role of tectonic denudation in the warping and uplift of low-angle normal faults: Geology, v. 12, p. 95–98, doi: 10.1130/0091-7613 (1984).

Stoker, M.S., Pheasant, J.B. and Josenans, H., 1997. Seismic methods and interpretation. In, T.A. Davies, T. Bell, A.K. Cooper, H. Josenhans, L. Polyak, A. Solheim, M.S. Stoker, J.A. Stravers (Eds.), Glaciated Continental margins: An atlas of acoustic images, pp. 9-19

Subrahmanyam, D. and Rao, P.H., 2008. Seismic Attributes-A Review. 7th International Conference and Exposition of Petroleum Geophysics. P398.

Sweeney, J.J and Burnham, A.K. 1990. Evaluation of a simple model of vitrinite reflectance based on chemical kinetics. American Association of Petroleum Geologists Bulletin 74 (10), 1559-1570.

Tainter, P.A., 1984, Stratigraphic and Paleostructural controls on hydrocarbon migration in Cretaceous D and J sandstones of the Denver Basin, in Woodward, J.F., Meissner, F.F., and Clayton, J.L., eds., Hydrocarbon source rocks of the greater Rocky Mountain region: Rocky Mountain Association of Geologists, p. 339–354

Taner, M. T., Schuelke, J.S., O'Doherty, R. and Baysal, E. 1994. Seismic attributes Revisited (abstract). 64th Annual International Meeting, Society of Exploration Geophysicists Expanded 1104-1106.

Tinker, T., de Wit, M. and Brown, R., 2008. Linking source and sink: Evaluating the balance between onshore erosion and offshore sediment accumulation since Gondwana break-up, South Africa. Tectonophysics, 455, 94–103.

Tinivella, U. and Giustiniani M., 2012. An overview of mud volcanoes associated to gas hydrate system. Book title: Volcanology (ISBN 980-953-307-547-6).

Tryon, M. D., Brown, K., Torres, M.E., Trehu, M., McManus, J. and Collier, R.W., 1999. Measurements of transience and downward fluid flow near episodic methane gas vents, Hydrate Ridge, Cascadia: Geology, 27, 1075 – 1078.

Vail, P. R., 1987. Seismic stratigraphy interpretation procedure, in Bally, A.W. (ed.), Atlas of seismic stratigraphy: AAPG Studies in Geology No. 27, Vol. 1, p. 1-10.

Vail, P.R., Mitchum Jr., R.M. and Thompson III, S., 1977. Seismic stratigraphy and global changes of sea level, part 3: relative changes of sea level from coastal onlap. In: Payton, C.E. (Ed.), Seismic of Petroleum Geologists, Pp. 63–81.

Vail, P.R., 1975. Eustatic cycles from seismic data for global stratigraphic analysis (abstract). American Association of Petroleum Geologists Bulletin 59, 2198–2199

Van Dyke, S., 2011. Basic Concepts of Hydrocarbon Indicators (DHIs). Van Dyke Geosciences, Houston, Texas. United States.

Van Der Spuy, D., 2003. Aptian source rocks in some South African Cretaceous Basins. Geological Society of London Special Publications, 207, 185-202.

Van Wagoner, J.C., Mitchum R.M., Campion K.M. and Rahmanina, V.D., 1990. Siliciclastic Sequence Stratigraphy in Well Logs, Cores, and Outcrops: Concepts for High-Resolution of Correlation of Time and Facies: American Association of Petroleum Geologists Methods in Exploration Series.7, pp55

Veeken, P., 2013. Seismic Stratigraphy and Depositional Facies Models. Academic Press, 2013.

Viola, G., Kounov,A., Andreoli,M., Matilla,J., 2012. Brittle Tectonic evolution along the western margin of South Africa: More than 500Ma of continued reactivation. Tectonophysics 514-517, 5, 93-114.

Visher, G.S., 1987. Unconformities: Key to Hydrocarbon Migration and Entrapment. AAPG Search and Discovery Article #91039, American Association Petroleum Geologists Mid-Continent Section Meeting, Tulsa, Oklahoma, September 27-29, 1987. Web accessed 1st February 2016.

Visser, D. J. L.,1998. The geotectonic evolution of South Africa and offshore areas: Explanation of structure map, scale 1:1000 000. Council for Geoscience. Pretoria.

Wang Y., 2015. Generalized Seismic Wavelets. Geophysical Journal International, 203, 2: 1172-1178.

Waples, D.H. and Waples, J.S. 2004. A Review and Evaluation of Specific Heat Capacities of Rocks, Minerals, and Subsurface Fluids. Fluids and Porous Rocks, Natural Resources Research. 2: 1573-8981.

Welte, D.H., Horsfield, B. and Baker, D.R. (Eds). 1997. Petroleum and Basin Evolution, Insights from Petroleum Geochemistry, Geology and Basin Modelling, Springer.

Wilhelms, A., Larter, S. R., Head, I., Farrimond, P., di Primio, R. and Zwach, C. 2001b. Biodegradation of oil in uplifted basins prevented by deep-burial sterilization: Journal of Nature, 411, 1034-1037.

Wu, K., Paton, D. and Zha, M.,2012. Unconformity structures controlling stratigraphic reservoirs in the north-west margin of Junggar basin, North-west China. Higher Education Press and Springer-Verlag Berlin Heidelberg 2012

Wygrala, B.P., 1989. Integrated study of an oil field in the southern Po basin, northern Italy: Ph.D. dissertation, Köln University: Jülich, Research Centre Jülich, Jul-Rep. 2313, ISSN 0366-0885, 217p.

Yu, X., and Li, X., 2012 .Future Control and Automation, LNEE 173, pp. 111-118 In W. Deng(Ed): Springer-Verlag Berlin Heidelberg 2012.

Zhang, H F., and Fang, C. L., 2002. A primary study on oil and gas accumulation dynamics in basin-a new theory about oil and gas geological exploration in the 21st century. Acta Petrol Sin, 23(4): 7–12.

Zoeppritz, K. 1919 .On the reflection and penetration of seismic waves through unstable layers. Erdbebenwellen Viii B, (Goettinger Nachr, Ed.), Pp. 66-84.

Internet Reference

http://science.dodlive.mil/2013/06/16/nrl-reveals-absence-of-greenhouse-gas-emissions

Appendix

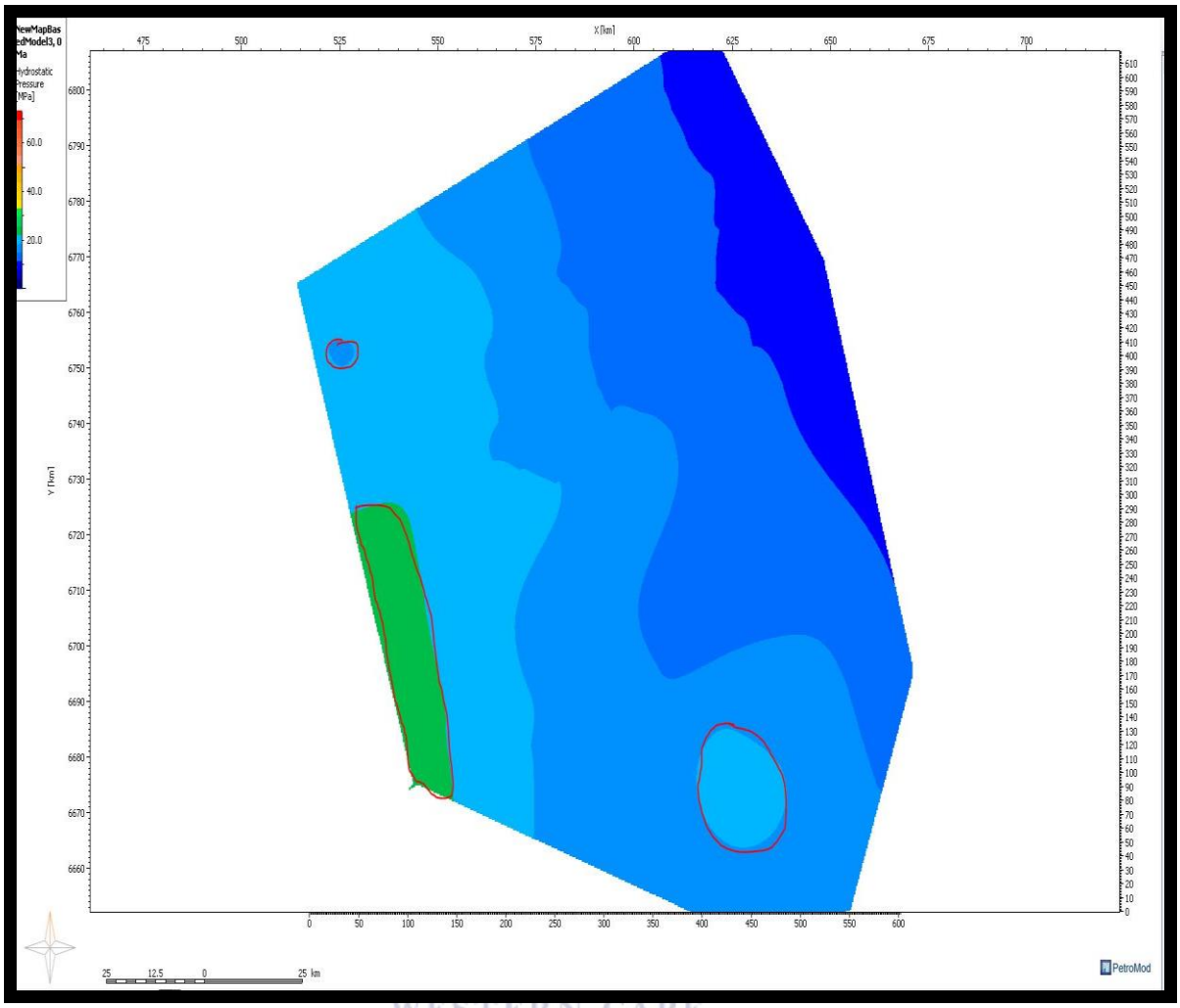

Appendix 1: Hydrostatic Pressure compartmentalization in red circles within the Cenomanian Sequence.